Engineering and Science Contracts Group
Houston, Texas

ESCG-4460-06-LODY-DOC-0216

Pretest Analysis for the Alpha Magnet Spectrometer (AMS-02) Vacuum Case Sine Sweep Test

Prepared by

Jacobs Engineering
Houston, TX

For

National Aeronautics and Space Administration
Lyndon B. Johnson Space Center

November, 2006

Pretest Analysis for the Alpha Magnet Spectrometer (AMS-02) Vacuum Case Sine Sweep Test

Prepared by:

Carl Lauritzen
AMS-02 Dynamics Lead
Loads and Dynamics Analysis Section
Jacobs Engineering

Reviewed by:

Chris Tutt
AMS-02 Chief Systems Engineer
Special Projects Section
Jacobs Engineering

Approval:

Paul Nemeth
AMS-02 Division Technical Manager
Jacobs Engineering

Preface

This pretest report was prepared by the Loads and Dynamics Analysis Group of the Engineering and Science Contract Group (ESCG) in support of the Alpha Magnetic Spectrometer – 02 (AMS-02) Project under contract NNJ05HI05C for the National Aeronautics and Space Administration (NASA).

This report presents the modeling and analysis approach for generating the pretest predictions of loads and dynamic response of the test article and test fixture during the sine sweep test. This pretest analysis is the basis for the preparation of the "Test Plan for the Sine Sweep Test of the Alpha Magnetic Spectrometer 02 (AMS-02) Vacuum Case and Magnet System", JSC-63594.

Table of Contents

SECTION PAGE

PREFACE iii
LIST OF FIGURES v
LIST OF TABLES vi
REFERENCES vi

1. Introduction 1
2. Overview 1
3. Math Models 1
4. Mass Properties 20
5. Static Load Conditions 20
6. System Modal Characteristics 20
7. Dynamic Load Conditions 27
8. Verification of Measurement Locations for the Sine Sweep Test 29
9. Predicted Dynamic Response of the Magnet Support Straps 31
10. Predicted Dynamic Response at the CMR Accelerometer Locations 299

List of Figures

FIGURE PAGE

3-1 Stress-strain data for magnet support straps in warm environment 3

3-2 Force-displacement data for magnet support straps in warm environment 4

3-3 Cut-away view of vacuum case showing cold mass replica attached to upper and lower rings by sixteen support straps 6

3-4 Top view of CMR showing strap layout (only eight upper straps are visible) 7

3-5 Isometric view of the baseline finite element model of the VCTF for the x-axis test configuration 9

3-6 Isometric view of the baseline finite element model of the VCTF for the y-axis test configuration 10

3-7 Isometric view of the baseline finite element model of the VCTF for the z-axis test configuration 11

3-8 Isometric view of the finite element model of the vacuum case 12

3-9 Top view of the finite element model of the magnet and helium tank 12

3-10 Isometric view of the finite element model of the test article in the VCTF for the x-axis sine sweep test 14

3-11 Isometric view of the finite element model of the test article in the VCTF for the y-axis sine sweep test 15

3-12 Isometric view of the finite element model of the test article in the VCTF for the z-axis sine sweep test 16

3-13 Excerpts from NASTRAN showing strain energy checks for the x-axis configuration 17

3-14 Excerpts from NASTRAN showing strain energy checks for the y-axis configuration 18

3-15 Excerpts from NASTRAN showing strain energy checks for the z-axis configuration 19

5-1 Stress-strain offset curve for strap 1in x-axis test configuration 26

8-1 Location of single-axis accelerometers on cold mass replica 30

8-2 Mounting block for accelerometers on CMR 32

8-3 Location of the eight tri-axial accelerometers on the VCTF interface blocks 33

8-4 Location of accelerometer on the transition frame for the x-axis and y-axis test configurations 34

List of Figures (continued)

FIGURE PAGE

8-5 Location of accelerometer on the transition frame for the z-axis test configuration 35

8-6 Location of reference accelerometers on the slip table 36

8-7 Location of the reference accelerometer on the spherical coupling 37

9-1 Strap 1 displacement response for x-axis configuration with 0.05 g sweep up 47

9-2 Strap 1 force response for x-axis configuration with 0.05 g sweep up 48

9-3 Strap 1 force-displacement curve for x-axis configuration with 0.05 g sweep up 49

9-4 Strap 4 displacement response for x-axis configuration with 0.05 g sweep up 50

9-5 Strap 4 force response for x-axis configuration with 0.05 g sweep up 51

9-6 Strap 4 force-displacement curve for x-axis configuration with 0.05 g sweep up 52

9-7 Strap 1 displacement response for x-axis configuration with 0.05 g sweep down 53

9-8 Strap 1 force response for x-axis configuration with 0.05 g sweep down 54

9-9 Strap 1 force-displacement curve for x-axis configuration with 0.05 g sweep down 55

9-10 Strap 4 displacement response for x-axis configuration with 0.05 g sweep down 56

9-11 Strap 4 force response for x-axis configuration with 0.05 g sweep down 57

9-12 Strap 4 force-displacement curve for x-axis configuration with 0.05 g sweep down 58

9-13 Strap 7 displacement response for x-axis configuration with 0.28 g sweep up 59

9-14 Strap 7 force response for x-axis configuration with 0.28 g sweep up 60

9-15 Strap 7 force-displacement curve for x-axis configuration with 0.28 g sweep up 61

9-16 Strap 16 displacement response for x-axis configuration with 0.28 g sweep up 62

9-17 Strap 16 force response for x-axis configuration with 0.28 g sweep up 63

9-18 Strap 16 force-displacement curve for x-axis configuration with 0.28 g sweep up 64

List of Figures (continued)

FIGURE PAGE

9-19 Strap 15 displacement response for x-axis configuration with 0.28 g sweep down....65

9-20 Strap 15 force response for x-axis configuration with 0.28 g sweep down....66

9-21 Strap 15 force-displacement curve for x-axis configuration with 0.28 g sweep down....67

9-22 Strap 16 displacement response for x-axis configuration with 0.28 g sweep down....68

9-23 Strap 16 force response for x-axis configuration with 0.28 g sweep down....69

9-24 Strap 16 force-displacement curve for x-axis configuration with 0.28 g sweep down....70

9-25 Strap 7 displacement response for x-axis configuration with 0.35 g sweep up....71

9-26 Strap 7 force response for x-axis configuration with 0.35 g sweep up....72

9-27 Strap 7 force-displacement curve for x-axis configuration with 0.35 g sweep up....73

9-28 Strap 16 displacement response for x-axis configuration with 0.35 g sweep up....74

9-29 Strap 16 force response for x-axis configuration with 0.35 g sweep up....75

9-30 Strap 16 force-displacement curve for x-axis configuration with 0.35 g sweep up....76

9-31 Strap 15 displacement response for x-axis configuration with 0.35 g sweep down....77

9-32 Strap 15 force response for x-axis configuration with 0.35 g sweep down....78

9-33 Strap 15 force-displacement curve for x-axis configuration with 0.35 g sweep down....79

9-34 Strap 16 displacement response for x-axis configuration with 0.35 g sweep down....80

9-35 Strap 16 force response for x-axis configuration with 0.35 g sweep down....81

9-36 Strap 16 force-displacement curve for x-axis configuration with 0.35 g sweep down....82

9-37 Strap 5 displacement response for y-axis configuration with 0.05 g sweep up....83

9-38 Strap 5 force response for y-axis configuration with 0.05 g sweep up....84

List of Figures (continued)

FIGURE PAGE

9-39 Strap 5 force-displacement curve for y-axis configuration with 0.05 g sweep up....85

9-40 Strap 3 displacement response for y-axis configuration with 0.05 g sweep up....86

9-41 Strap 3 force response for y-axis configuration with 0.05 g sweep up....87

9-42 Strap 3 force-displacement curve for y-axis configuration with 0.05 g sweep up....88

9-43 Strap 3 displacement response for y-axis configuration with 0.05 g sweep down....89

9-44 Strap 3 force response for y-axis configuration with 0.05 g sweep down....90

9-45 Strap 3 force-displacement curve for y-axis configuration with 0.05 g sweep down....91

9-46 Strap 7 displacement response for y-axis configuration with 0.05 g sweep down....92

9-47 Strap 7 force response for y-axis configuration with 0.05 g sweep down....93

9-48 Strap 7 force-displacement curve for y-axis configuration with 0.05 g sweep down....94

9-49 Strap 2 displacement response for y-axis configuration with 0.24 g sweep up....95

9-50 Strap 2 force response for y-axis configuration with 0.24 g sweep up....96

9-51 Strap 2 force-displacement curve for y-axis configuration with 0.24 g sweep up....97

9-52 Strap 3 displacement response for y-axis configuration with 0.24 g sweep up....98

9-53 Strap 3 force response for y-axis configuration with 0.24 g sweep up....99

9-54 Strap 3 force-displacement curve for y-axis configuration with 0.24 g sweep up....100

9-55 Strap 12 displacement response for y-axis configuration with 0.24 g sweep down....101

9-56 Strap 12 force response for y-axis configuration with 0.24 g sweep down....102

9-57 Strap 12 force-displacement curve for y-axis configuration with 0.24 g sweep down....103

9-58 Strap 15 displacement response for y-axis configuration with 0.24 g sweep down....104

List of Figures (continued)

FIGURE PAGE

9-59 Strap 15 force response for y-axis configuration with 0.24 g sweep down.....105

9-60 Strap 15 force-displacement curve for y-axis configuration with 0.24 g sweep down.....106

9-61 Strap 12 displacement response for y-axis configuration with 0.37 g sweep up.....107

9-62 Strap 12 force response for y-axis configuration with 0.37 g sweep up.....108

9-63 Strap12 force-displacement curve for y-axis configuration with 0.37 g sweep up.....109

9-64 Strap 3 displacement response for y-axis configuration with 0.37 g sweep up.....110

9-65 Strap 3 force response for y-axis configuration with 0.37 g sweep up.....111

9-66 Strap3 force-displacement curve for y-axis configuration with 0.37 g sweep up.....112

9-67 Strap 12 displacement response for y-axis configuration with 0.37 g sweep down.....113

9-68 Strap 12 force response for y-axis configuration with 0.37 g sweep down.....114

9-69 Strap 12 force-displacement curve for y-axis configuration with 0.37 g sweep down.....115

9-70 Strap 14 displacement response for y-axis configuration with 0.37 g sweep down.....116

9-71 Strap 14 force response for y-axis configuration with 0.37 g sweep down.....117

9-72 Strap 14 force-displacement curve for y-axis configuration with 0.37 g sweep down.....118

9-73 Strap 11 displacement response for z-axis configuration with 0.05 g sweep down.....119

9-74 Strap 11 force response for z-axis configuration with 0.05 g sweep down.....120

9-75 Strap 11 force-displacement curve for z-axis configuration with 0.057 g sweep down.....121

9-76 Strap 7 displacement response for z-axis configuration with 0.05 g sweep up.....122

9-77 Strap 7 force response for z-axis configuration with 0.05 g sweep up.....123

9-78 Strap 7 force-displacement curve for z-axis configuration with 0.05 g sweep up.....124

List of Figures (continued)

FIGURE PAGE

9-79 Strap 9 displacement response for z-axis configuration with 0.05 g sweep down....125

9-80 Strap 9 force response for z-axis configuration with 0.05 g sweep down....126

9-81 Strap 9 force-displacement curve for z-axis configuration with 0.05 g sweep down....127

9-82 Strap 5 displacement response for z-axis configuration with 0.05 g sweep down....128

9-83 Strap 5 force response for z-axis configuration with 0.05 g sweep down....129

9-84 Strap 5 force-displacement curve for z-axis configuration with 0.05 g sweep down....130

9-85 Strap 9 displacement response for z-axis configuration with 0.40 g sweep up....131

9-86 Strap 9 force response for z-axis configuration with 0.40 g sweep up....132

9-87 Strap 9 force-displacement curve for z-axis configuration with 0.40 g sweep up....133

9-88 Strap 16 displacement response for z-axis configuration with 0.40 g sweep up....134

9-89 Strap 16 force response for z-axis configuration with 0.40 g sweep up....135

9-90 Strap 16 force-displacement curve for z-axis configuration with 0.40 g sweep up....136

9-91 Strap 9 displacement response for z-axis configuration with 0.40 g sweep up....137

9-92 Strap 9 force response for z-axis configuration with 0.40 g sweep up....138

9-93 Strap 9 force-displacement curve for z-axis configuration with 0.40 g sweep up....139

9-94 Strap 16 displacement response for z-axis configuration with 0.40 g sweep down....140

9-95 Strap 16 force response for z-axis configuration with 0.40 g sweep down....141

9-96 Strap 16 force-displacement curve for z-axis configuration with 0.40 g sweep down....142

9-97 Strap 8 displacement response for z-axis configuration with 0.68 g sweep up....143

9-98 Strap 8 force response for z-axis configuration with 0.68 g sweep up....144

List of Figures (continued)

FIGURE PAGE

9-99 Strap 8 force-displacement curve for z-axis configuration with 0.68 g sweep up....145

9-100 Strap 10 displacement response for z-axis configuration with 0.68 g sweep up....146

9-101 Strap 10 force response for z-axis configuration with 0.68 g sweep up....147

9-102 Strap 10 force-displacement curve for z-axis configuration with 0.68 g sweep up....148

9-103 Strap 8 displacement response for z-axis configuration with 0.68 g sweep down....149

9-104 Strap 8 force response for z-axis configuration with 0.68 g sweep down....150

9-105 Strap 8 force-displacement curve for z-axis configuration with 0.68 g sweep down....151

9-106 Strap 16 displacement response for z-axis configuration with 0.68 g sweep down....152

9-107 Strap 16 force response for z-axis configuration with 0.68 g sweep down....153

9-108 Strap 16 force-displacement curve for z-axis configuration with 0.68 g sweep down....154

9-109 Strap 1 frequency response envelope for x-axis 0.05 g excitation....155

9-110 Strap 2 frequency response envelope for x-axis 0.05 g excitation....156

9-111 Strap 3 frequency response envelope for x-axis 0.05 g excitation....157

9-112 Strap 4 frequency response envelope for x-axis 0.05 g excitation....158

9-113 Strap 5 frequency response envelope for x-axis 0.05 g excitation....159

9-114 Strap 6 frequency response envelope for x-axis 0.05 g excitation....160

9-115 Strap 7 frequency response envelope for x-axis 0.05 g excitation....161

9-116 Strap 8 frequency response envelope for x-axis 0.05 g excitation....162

9-117 Strap 9 frequency response envelope for x-axis 0.05 g excitation....163

9-118 Strap 10 frequency response envelope for x-axis 0.05 g excitation....164

9-119 Strap 11 frequency response envelope for x-axis 0.05 g excitation....165

9-120 Strap 12 frequency response envelope for x-axis 0.05 g excitation....166

9-121 Strap 13 frequency response envelope for x-axis 0.05 g excitation....167

9-122 Strap 14 frequency response envelope for x-axis 0.05 g excitation....168

List of Figures (continued)

FIGURE PAGE

9-123 Strap 15 frequency response envelope for x-axis 0.05 g excitation 169
9-124 Strap 16 frequency response envelope for x-axis 0.05 g excitation 170
9-125 Strap 1 frequency response envelope for x-axis 0.28 g excitation 171
9-126 Strap 2 frequency response envelope for x-axis 0.28 g excitation 172
9-127 Strap 3 frequency response envelope for x-axis 0.28 g excitation 173
9-128 Strap 4 frequency response envelope for x-axis 0.28 g excitation 174
9-129 Strap 5 frequency response envelope for x-axis 0.28 g excitation 175
9-130 Strap 6 frequency response envelope for x-axis 0.28 g excitation 176
9-131 Strap 7 frequency response envelope for x-axis 0.28 g excitation 177
9-132 Strap 8 frequency response envelope for x-axis 0.28 g excitation 178
9-133 Strap 9 frequency response envelope for x-axis 0.28 g excitation 179
9-134 Strap 10 frequency response envelope for x-axis 0.28 g excitation 180
9-135 Strap 11 frequency response envelope for x-axis 0.28 g excitation 181
9-136 Strap 12 frequency response envelope for x-axis 0.28 g excitation 182
9-137 Strap 13 frequency response envelope for x-axis 0.28 g excitation 183
9-138 Strap 14 frequency response envelope for x-axis 0.28 g excitation 184
9-139 Strap 15 frequency response envelope for x-axis 0.28 g excitation 185
9-140 Strap 16 frequency response envelope for x-axis 0.28 g excitation 186
9-141 Strap 1 frequency response envelope for x-axis 0.35 g excitation 187
9-142 Strap 2 frequency response envelope for x-axis 0.35 g excitation 188
9-143 Strap 3 frequency response envelope for x-axis 0.35 g excitation 189
9-144 Strap 4 frequency response envelope for x-axis 0.35 g excitation 190
9-145 Strap 5 frequency response envelope for x-axis 0.35 g excitation 191
9-146 Strap 6 frequency response envelope for x-axis 0.35 g excitation 192
9-147 Strap 7 frequency response envelope for x-axis 0.35 g excitation 193
9-148 Strap 8 frequency response envelope for x-axis 0.35 g excitation 194
9-149 Strap 9 frequency response envelope for x-axis 0.35 g excitation 195
9-150 Strap 10 frequency response envelope for x-axis 0.35 g excitation 196
9-151 Strap 11 frequency response envelope for x-axis 0.35 g excitation 197

List of Figures (continued)

FIGURE PAGE

9-152 Strap 12 frequency response envelope for x-axis 0.35 g excitation 198
9-153 Strap 13 frequency response envelope for x-axis 0.35 g excitation 199
9-154 Strap 14 frequency response envelope for x-axis 0.35 g excitation 200
9-155 Strap 15 frequency response envelope for x-axis 0.35 g excitation 201
9-156 Strap 16 frequency response envelope for x-axis 0.35 g excitation 202
9-157 Strap 1 frequency response envelope for y-axis 0.05 g excitation 203
9-158 Strap 2 frequency response envelope for y-axis 0.05 g excitation 204
9-159 Strap 3 frequency response envelope for y-axis 0.05 g excitation 205
9-160 Strap 4 frequency response envelope for y-axis 0.05 g excitation 206
9-161 Strap 5 frequency response envelope for y-axis 0.05 g excitation 207
9-162 Strap 6 frequency response envelope for y-axis 0.05 g excitation 208
9-163 Strap 7 frequency response envelope for y-axis 0.05 g excitation 209
9-164 Strap 8 frequency response envelope for y-axis 0.05 g excitation 210
9-165 Strap 9 frequency response envelope for y-axis 0.05 g excitation 211
9-166 Strap 10 frequency response envelope for y-axis 0.05 g excitation 212
9-167 Strap 11 frequency response envelope for y-axis 0.05 g excitation 213
9-168 Strap 12 frequency response envelope for y-axis 0.05 g excitation 214
9-169 Strap 13 frequency response envelope for y-axis 0.05 g excitation 215
9-170 Strap 14 frequency response envelope for y-axis 0.05 g excitation 216
9-171 Strap 15 frequency response envelope for y-axis 0.05 g excitation 217
9-172 Strap 16 frequency response envelope for y-axis 0.05 g excitation 218
9-173 Strap 1 frequency response envelope for y-axis 0.24 g excitation 219
9-174 Strap 2 frequency response envelope for y-axis 0.24 g excitation 220
9-175 Strap 3 frequency response envelope for y-axis 0.24 g excitation 221
9-176 Strap 4 frequency response envelope for y-axis 0.24 g excitation 222
9-177 Strap 5 frequency response envelope for y-axis 0.24 g excitation 223
9-178 Strap 6 frequency response envelope for y-axis 0.24 g excitation 224
9-179 Strap 7 frequency response envelope for y-axis 0.24 g excitation 225
9-180 Strap 8 frequency response envelope for y-axis 0.24 g excitation 226

List of Figures (continued)

FIGURE PAGE

9-181 Strap 9 frequency response envelope for y-axis 0.24 g excitation 227
9-182 Strap 10 frequency response envelope for y-axis 0.24 g excitation 228
9-183 Strap 11 frequency response envelope for y-axis 0.24 g excitation 229
9-184 Strap 12 frequency response envelope for y-axis 0.24 g excitation 230
9-185 Strap 13 frequency response envelope for y-axis 0.24 g excitation 231
9-186 Strap 14 frequency response envelope for y-axis 0.24 g excitation 232
9-187 Strap 15 frequency response envelope for y-axis 0.24 g excitation 233
9-188 Strap 16 frequency response envelope for y-axis 0.24 g excitation 234
9-189 Strap 1 frequency response envelope for y-axis 0.37 g excitation 235
9-190 Strap 2 frequency response envelope for y-axis 0.37 g excitation 236
9-191 Strap 3 frequency response envelope for y-axis 0.37 g excitation 237
9-192 Strap 4 frequency response envelope for y-axis 0.37 g excitation 238
9-193 Strap 5 frequency response envelope for y-axis 0.37 g excitation 239
9-194 Strap 6 frequency response envelope for y-axis 0.37 g excitation 240
9-195 Strap 7 frequency response envelope for y-axis 0.37 g excitation 241
9-196 Strap 8 frequency response envelope for y-axis 0.37 g excitation 242
9-197 Strap 9 frequency response envelope for y-axis 0.37 g excitation 243
9-198 Strap 10 frequency response envelope for y-axis 0.37 g excitation 244
9-199 Strap 11 frequency response envelope for y-axis 0.37 g excitation 245
9-200 Strap 12 frequency response envelope for y-axis 0.37 g excitation 246
9-201 Strap 13 frequency response envelope for y-axis 0.37 g excitation 247
9-202 Strap 14 frequency response envelope for y-axis 0.37 g excitation 248
9-203 Strap 15 frequency response envelope for y-axis 0.37 g excitation 249
9-204 Strap 16 frequency response envelope for y-axis 0.37 g excitation 250
9-205 Strap 1 frequency response envelope for z-axis 0.05 g excitation.....251
9-206 Strap 2 frequency response envelope for z-axis 0.05 g excitation.....252
9-207 Strap 3 frequency response envelope for z-axis 0.05 g excitation.....253
9-208 Strap 4 frequency response envelope for z-axis 0.05 g excitation.....254
9-209 Strap 5 frequency response envelope for z-axis 0.05 g excitation.....255

List of Figures (continued)

FIGURE PAGE

9-210 Strap 6 frequency response envelope for z-axis 0.05 g excitation.....256
9-211 Strap 7 frequency response envelope for z-axis 0.05 g excitation.....257
9-212 Strap 8 frequency response envelope for z-axis 0.05 g excitation.....258
9-213 Strap 9 frequency response envelope for z-axis 0.05 g excitation.....259
9-214 Strap 10 frequency response envelope for z-axis 0.05 g excitation.....260
9-215 Strap 11 frequency response envelope for z-axis 0.05 g excitation.....261
9-216 Strap 12 frequency response envelope for z-axis 0.05 g excitation.....262
9-217 Strap 13 frequency response envelope for z-axis 0.05 g excitation.....263
9-218 Strap 14 frequency response envelope for z-axis 0.05 g excitation.....264
9-219 Strap 15 frequency response envelope for z-axis 0.05 g excitation.....265
9-220 Strap 16 frequency response envelope for z-axis 0.05 g excitation.....266
9-221 Strap 1 frequency response envelope for z-axis 0.40 g excitation.....267
9-222 Strap 2 frequency response envelope for z-axis 0.40 g excitation.....268
9-223 Strap 3 frequency response envelope for z-axis 0.40 g excitation.....269
9-224 Strap 4 frequency response envelope for z-axis 0.40 g excitation.....270
9-225 Strap 5 frequency response envelope for z-axis 0.40 g excitation.....271
9-226 Strap 6 frequency response envelope for z-axis 0.40 g excitation.....272
9-227 Strap 7 frequency response envelope for z-axis 0.40 g excitation.....273
9-228 Strap 8 frequency response envelope for z-axis 0.40 g excitation.....274
9-229 Strap 9 frequency response envelope for z-axis 0.40 g excitation.....275
9-230 Strap 10 frequency response envelope for z-axis 040 g excitation.....276
9-231 Strap 11 frequency response envelope for z-axis 0.40 g excitation.....277
9-232 Strap 12 frequency response envelope for z-axis 0.40 g excitation.....278
9-233 Strap 13 frequency response envelope for z-axis 0.40 g excitation.....279
9-234 Strap 14 frequency response envelope for z-axis 0.40 g excitation.....280
9-235 Strap 15 frequency response envelope for z-axis 0.40 g excitation.....281
9-236 Strap 16 frequency response envelope for z-axis 0.40 g excitation.....282
9-237 Strap 1 frequency response envelope for z-axis 0.68 g excitation.....283
9-238 Strap 2 frequency response envelope for z-axis 0.68 g excitation.....284

List of Figures (continued)

FIGURE PAGE

9-239 Strap 3 frequency response envelope for z-axis 0.68 g excitation.....285
9-240 Strap 4 frequency response envelope for z-axis 0.68 g excitation.....286
9-241 Strap 5 frequency response envelope for z-axis 0.68 g excitation.....287
9-242 Strap 6 frequency response envelope for z-axis 0.68 g excitation.....288
9-243 Strap 7 frequency response envelope for z-axis 0.68 g excitation.....289
9-244 Strap 8 frequency response envelope for z-axis 0.68 g excitation.....290
9-245 Strap 9 frequency response envelope for z-axis 0.68 g excitation.....291
9-246 Strap 10 frequency response envelope for z-axis 0.68 g excitation.....292
9-247 Strap 11 frequency response envelope for z-axis 0.68 g excitation.....293
9-248 Strap 12 frequency response envelope for z-axis 0.68 g excitation.....294
9-249 Strap 13 frequency response envelope for z-axis 0.68 g excitation.....295
9-250 Strap 14 frequency response envelope for z-axis 0.68 g excitation.....296
9-251 Strap 15 frequency response envelope for z-axis 0.68 g excitation.....297
9-252 Strap 16 frequency response envelope for z-axis 0.68 g excitation.....298
10-1 Channel 1 accelerometer response for the x-axis configuration with 0.35 g excitation.....301
10-2 Channel 2 accelerometer response for the x-axis configuration with 0.35 g excitation.....302
10-3 Channel 3 accelerometer response for the x-axis configuration with 0.35 g excitation.....303
10-4 Channel 4 accelerometer response for the x-axis configuration with 0.35 g excitation.....304
10-5 Channel 5 accelerometer response for the x-axis configuration with 0.35 excitation.....305
10-6 Channel 6 accelerometer response for the x-axis configuration with 0.35 g excitation.....306
10-7 Channel 7 accelerometer response for the x-axis configuration with 0.35 g excitation.....307
10-8 Channel 8 accelerometer response for the x-axis configuration with 0.35 g excitation.....308
10-9 Channel 9 accelerometer response for the x-axis configuration with 0.35 g excitation.....309

List of Figures (continued)

FIGURE PAGE

10-10 Channel 10 accelerometer response for the x-axis configuration with 0.35 g excitation....310

10-11 Channel 11 accelerometer response for the x-axis configuration with 0.35 g excitation....311

10-12 Channel 12 accelerometer response for the x-axis configuration with 0.35 g excitation....312

10-13 Channel 13 accelerometer response for the x-axis configuration with 0.35 g excitation....313

10-14 Channel 14 accelerometer response for the x-axis configuration with 0.35 g excitation....314

10-15 Channel 15 accelerometer response for the x-axis configuration with 0.35 g excitation....315

10-16 Channel 16 accelerometer response for the x-axis configuration with 0.35 g excitation....316

10-17 Channel 1 accelerometer response for the y-axis configuration with 0.37 g excitation....317

10-18 Channel 2 accelerometer response for the y-axis configuration with 0.37 g excitation....318

10-19 Channel 3 accelerometer response for the y-axis configuration with 0.37 g excitation....319

10-20 Channel 4 accelerometer response for the y-axis configuration with 0.37 g excitation....320

10-21 Channel 5 accelerometer response for the y-axis configuration with 0.37 excitation....321

10-22 Channel 6 accelerometer response for the y-axis configuration with 0.37 g excitation....322

10-23 Channel 7 accelerometer response for the y-axis configuration with 0.37 g excitation....323

10-24 Channel 8 accelerometer response for the y-axis configuration with 0.37 g excitation....324

10-25 Channel 9 accelerometer response for the y-axis configuration with 0.37 g excitation....325

10-26 Channel 10 accelerometer response for the y-axis configuration with 0.37 g excitation....326

List of Figures (continued)

FIGURE PAGE

10-27 Channel 11 accelerometer response for the y-axis configuration with 0.37 g excitation....327

10-28 Channel 12 accelerometer response for the y-axis configuration with 0.37 g excitation....328

10-29 Channel 13 accelerometer response for the y-axis configuration with 0.37 g excitation....329

10-30 Channel 14 accelerometer response for the y-axis configuration with 0.37 g excitation....330

10-31 Channel 15 accelerometer response for the y-axis configuration with 0.37 g excitation....331

10-32 Channel 16 accelerometer response for the y-axis configuration with 0.37 g excitation....332

10-33 Channel 1 accelerometer response for the z-axis configuration with 0.68 g excitation....333

10-34 Channel 2 accelerometer response for the z-axis configuration with 0.68 g excitation....334

10-35 Channel 3 accelerometer response for the z-axis configuration with 0.68 g excitation....335

10-36 Channel 4 accelerometer response for the z-axis configuration with 0.68 g excitation....336

10-37 Channel 5 accelerometer response for the z-axis configuration with 0.68 excitation....337

10-38 Channel 6 accelerometer response for the z-axis configuration with 0.68 g excitation....338

10-39 Channel 7 accelerometer response for the z-axis configuration with 0.68 g excitation....339

10-40 Channel 8 accelerometer response for the z-axis configuration with 0.68 g excitation....340

10-41 Channel 9 accelerometer response for the z-axis configuration with 0.68 g excitation....341

10-42 Channel 10 accelerometer response for the z-axis configuration with 0.68 g excitation....342

10-43 Channel 11 accelerometer response for the z-axis configuration with 0.68 g excitation....343

List of Figures (continued)

FIGURE PAGE

10-44 Channel 12 accelerometer response for the z-axis configuration with 0.68 g excitation....344

10-45 Channel 13 accelerometer response for the z-axis configuration with 0.68 g excitation....345

10-46 Channel 14 accelerometer response for the z-axis configuration with 0.68 g excitation....346

10-47 Channel 15 accelerometer response for the z-axis configuration with 0.68 g excitation....347

10-48 Channel 16 accelerometer response for the z-axis configuration with 0.68 g excitation....348

List of Tables

TABLE PAGE

3-1 Baseline Stress-Strain and Force-Displacement Data for the Magnet Support Straps....2

4-1 Mass Properties for the X-axis Test Configuration (slip table, test fixture, and test article)....21

4-2 Mass Properties for the Y-axis Test Configuration (slip table, test fixture, and test article)....22

4-3 Mass Properties for the Z-axis Test Configuration (slip table, test fixture, and test article)....23

4-4 Comparison of Predicted and Measured Weights for the Sine Sweep Test Hardware....24

5-1 Preload Offset Data for Magnet Support Straps for X-axis....24

5-2 Preload Offset Data for Magnet Support Straps for Y-axis....25

5-3 Preload Offset Data for Magnet Support Straps for Z-axis....25

6-1 Modal Frequencies for X-axis Test Configuration (shaker interface constrained in x)....28

6-2 Modal Frequencies for Y-axis Test Configuration (shaker interface constrained in y)....28

6-3 Modal Frequencies for Z-axis Test Configuration (shaker interface constrained in z)....28

8-1 Modal Assurance Criteria Calculations for the X-axis Test Configuration (VCTF with test article)....38

8-2 Modal Assurance Criteria Calculations for the Y-axis Test Configuration (VCTF with test article)....39

8-3 Modal Assurance Criteria Calculations for the Y-axis Test Configuration (VCTF with test article)....40

8-4 Modal Assurance Criteria Calculations for the Empty (VCTF only) X-axis Test Configuration....41

8-5 Modal Assurance Criteria Calculations for the Empty (VCTF only) Z-axis Test Configuration....41

9-1 Maximum Responses of the Magnet Support Straps for the X-axis Test Configuration....44

List of Tables (continued)

TABLE PAGE

9-2 Maximum Responses of the Magnet Support Straps for the Y-axis Test Configuration 45

9-3 Maximum Responses of the Magnet Support Straps for the Z-axis Test Configuration 46

10-1 Description of Math Model Nodes Used to Represent Accelerometer Locations 299

References

(1) NASA, JSC, Houston, Texas. *Alpha Magnetic Spectrometer – 02 Structural Verification Plan for the Space Transportation and the International Space Station,* (JSC-28792, Revision E) September, 2006.

(2) NASA, JSC, Houston, Texas. *Alpha Magnetic Spectrometer – 02 Structural Assembly and Testing Integration Plan,* (JSC-63123) February 21, 2006.

(3) NASA, JSC, Houston, Texas. *Test Plan for the Sine Sweep Test of the Alpha Magnetic Spectrometer 02 (AMS-02) Vacuum Case and Magnet System*, (JSC-63594) October, 2006.

1.0 Introduction

The AMS-02 vacuum case sine sweep test is a portion of the overall structural verification plan for the AMS-02 payload that has been defined in JSC 28792, Revision E. The test will be performed on a test article consisting of the vacuum case (VC) structural test article (STA) with a mass replica of the cryogenic magnet and helium tank. A set of sixteen, flight-like strap assemblies will support the magnet and helium tank replica inside the vacuum case.

The force versus displacement response for the magnet support straps has a distinct nonlinear characteristic. The sine sweep test will be performed at excitation levels that are sufficient to induce a measurable nonlinear response for the magnet support straps. The results of this test will be used to correlate the nonlinear mathematical model of the vacuum case assembly.

2.0 Overview

For the previous tests using the two-strap, in-line configuration, the pretest response predictions were made using a closed-form solution. For this test of the full system that uses sixteen straps, the pretest response predictions have been made using a finite element simulation.

3.0 Math Models

The AMS-02 design group develops and maintains the CAD model and the engineering drawings used for manufacturing of the VCTF hardware. The AMS-02 design group provided the required geometry information for the hardware in the form of Parasolid (*.x_t) files that were output from their CAD model. These geometry files were imported into FEMAP and used to generate a finite element model for use by MSC NASTRAN to perform the structural analyses. Detailed finite element models were developed for all of the major components that affect the structural response. These components are:

(1) vacuum case structural test article
(2) mass replica of the magnet and helium tank
(3) vacuum case test fixture
(4) slip table
(5) sixteen flight-like magnet support strap assemblies

The math models for the first four components were generated using standard MSC Nastran element types (CBEAM, CQUAD4, CTRIA3, CHEXA, CPENTA, CTETRA) with linear material properties. A separate math model of the VCTF was built for each of the three sine sweep test configurations (i.e. x-axis, y-axis, and z-axis). The magnet support straps are represented by CROD elements with nonlinear stress dependent material properties. The force-displacement relationship for individual straps has been measured during several previous tests. This test data was used to generate correlated stress-strain curves for analytical assessments. The baseline stress-strain curves for the magnet support straps are shown in Table 3-1 and Figure 3-1. The corresponding force-displacement curves are shown in Figure 3-2. The straps are only capable of reacting tension loads so the curves in Figure 3-1 only show data in the positive quadrant. When the NASTRAN inputs are defined for the baseline strap curves, negative strain is defined to have zero stress.

Table 3-1 Baseline Stress-Strain and Force-Displacement Data for the Magnet Support Straps

	Condition	Strain	Stress		Force		Deflection	
			(N/mm^2)	(psi)	(kN)	(lbf)	(mm)	(inch)
C1W1	Cold	0.0	0.0	0.0	0.00	0	0.0	0.0
		0.02479	88.5	12836	8.85	1990	22.345	0.8797
		0.02628	195.67	28380	19.57	4399	23.683	0.9324
		0.03356	1200	174046	120.00	26977	30.243	1.1907
	Warm	0.0	0.0	0.0	0.00	0	0.0	0.0
		0.01630	58.0	8408	5.80	1303	14.69	0.5783
		0.02468	88.5	12836	8.85	1990	22.237	0.8755
		0.03335	1200	174046	120.00	26977	30.051	1.1831

	Condition	Strain	Stress		Force		Deflection	
			(N/mm^2)	(psi)	(kN)	(lbf)	(mm)	(inch)
C2W2	Cold	0.0	0.0	0.0	0.00	0	0.0	0.0
		0.0269	88.5	12836	8.85	1990	22.418	0.8826
		0.02786	148.66	21561	14.87	3342	23.219	0.9141
		0.03615	1200	174046	120.00	26977	30.131	1.1863
	Warm	0.0	0.0	0.0	0.00	0	0.0	0.0
		0.00949	31.1	4509	3.11	699	7.909	0.3114
		0.02651	88.5	12836	8.85	1990	22.093	0.8698
		0.03594	1200	174046	120.00	26977	29.955	1.1793

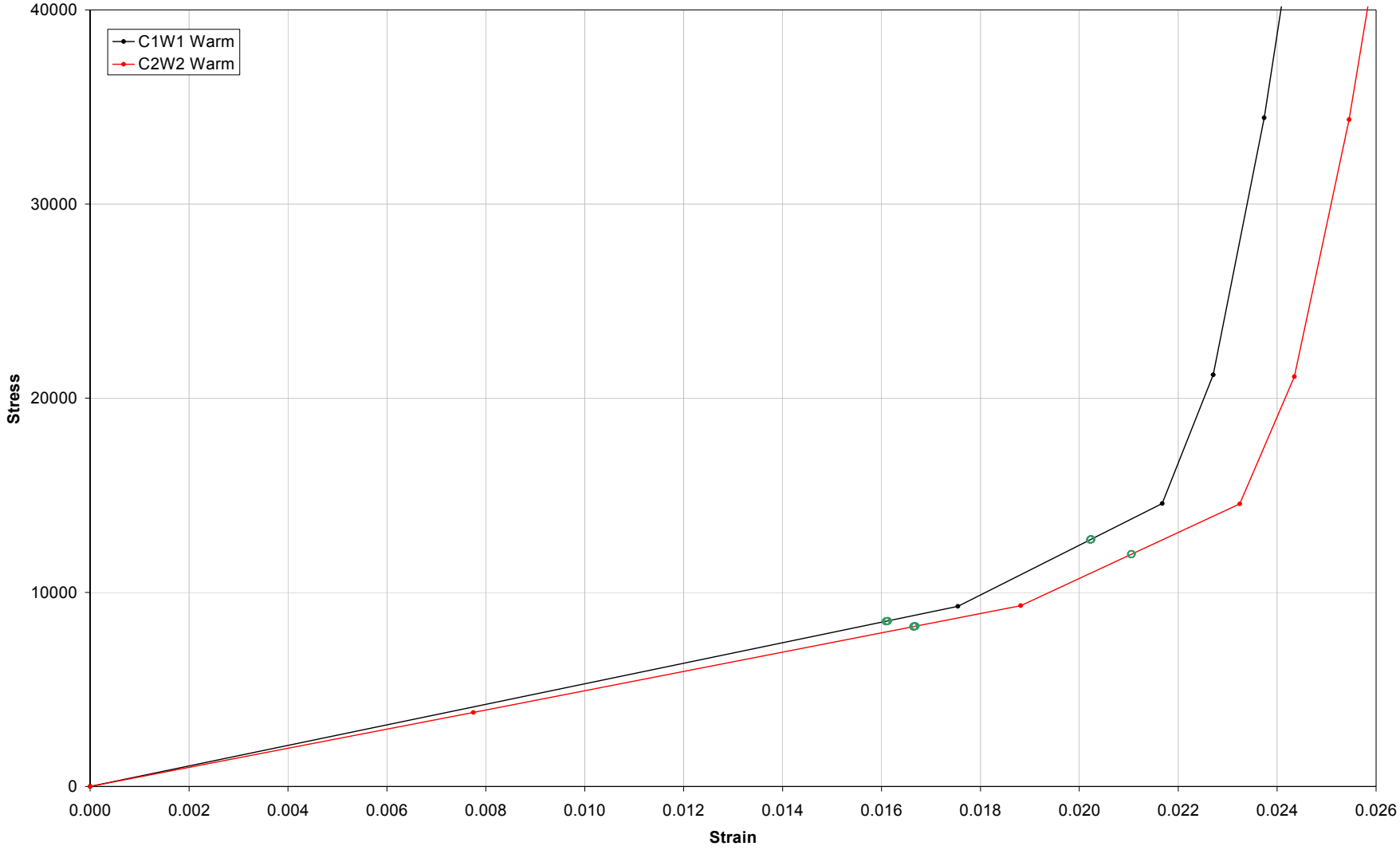

Figure 3-1 Stress-strain data for magnet support straps in warm environment
(Note: x-axis preload values indicated by green circles)

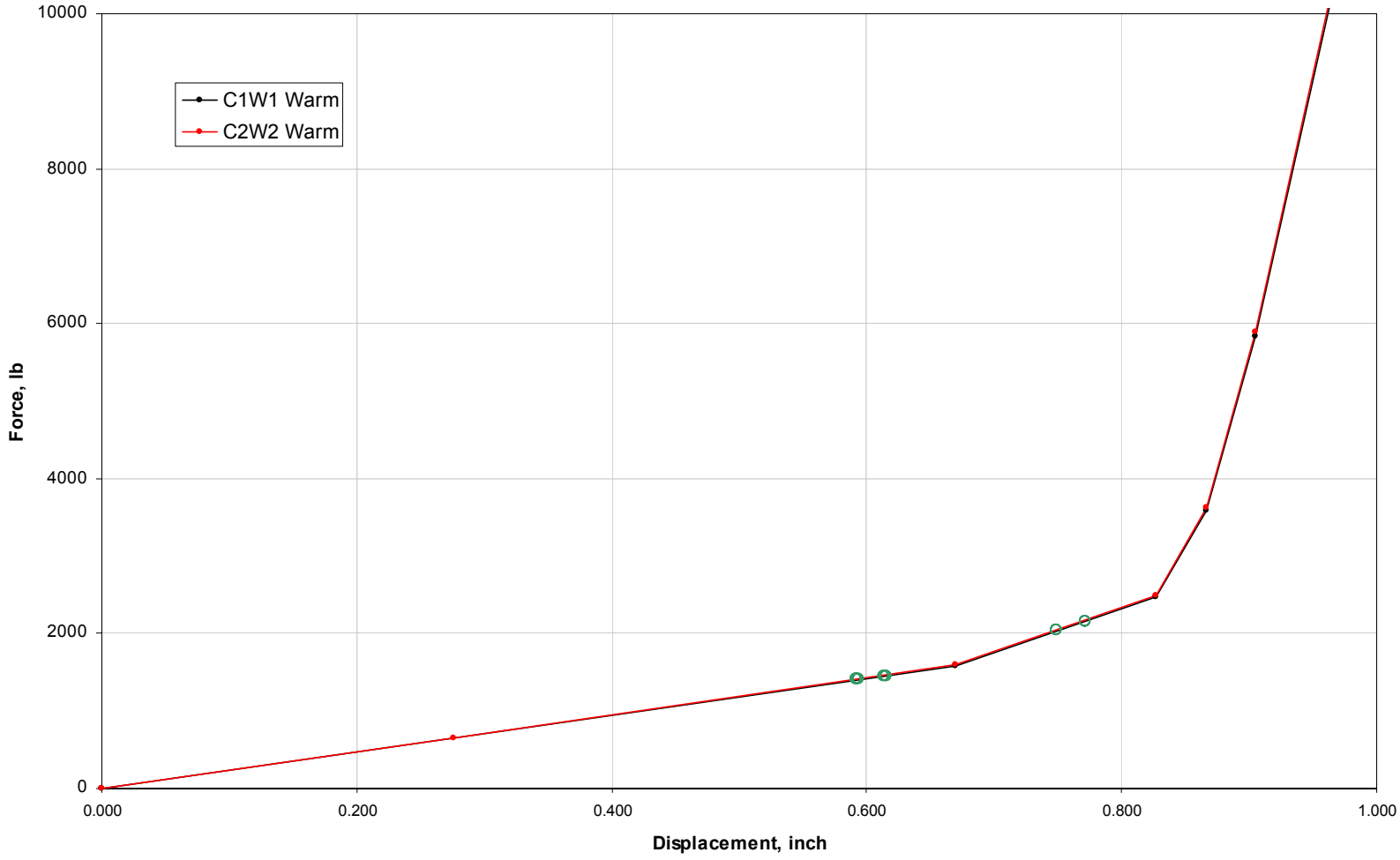

Figure 3-2 Force-displacement data for magnet support straps in warm environment
(Note: x-axis preload values indicated by green circles)

The baseline stress-strain and force-displacement curves for the magnet support straps provide a simplified representation of the expected behavior. They do not account for the variation that occurs during vibration that involves successive loading and unloading. Although the straps exhibit elastic behavior by unloading back to the initial stress-strain state, they also exhibit a typical hysteresis loop due to material damping that is not represented by the baseline curves. In addition, the baseline curves do not account for any differences between straps due to material or manufacturing variations. These effects of these factors on the strap response will be accounted for through the post-test correlation process.

The nomenclature C1W1 refers to the straps that are oriented along the x-axis of the magnet (relative to the AMS-02 reference coordinate system) and C2W2 refers to the straps that are oriented along the y-axis. Figure 3-3 shows the layout of the magnet support straps with the cold mass replica (CMR) and the vacuum case rings. Figure 3-4 shows the numbering designation for the straps that is used in the math model and analyses. The odd numbered straps are the C1W1 straps and the even numbered straps are the C2W2 straps.

For static and modal analyses, NASTRAN bulk data was used directly to represent the models. For transient analyses, the NASTRAN bulk data was used to generate superelement models in a component mode format.

The VCTF frame is manufactured primarily from aluminum tubes. A four-inch, square tube with 0.25 inch wall thickness is the basic component. These tubes are welded together to form beams with various cross sections. The beams are then welded to form an upper frame assembly, a lower frame assembly, and four column assemblies. The upper and lower frames have corner blocks that are machined from aluminum. The columns are completed by welding the tubes to a machined aluminum blocks that form the interface for the vacuum case. The upper and lower frame assemblies are bolted to the four columns to form the completed frame assembly.

The portions of the VCTF frame that are built up from the four-inch square tubes are modeled using CBEAM elements with PBEAM entries to provide the cross-section details. The eight corner blocks and the eight interface blocks are modeled using solid elements (CHEXA, CPENTA, and CTETRA). At the eight locations where the column assemblies bolt to the upper and lower frame assemblies, the bolt pattern is represented by single CBUSH element at the center of the pattern. One node of the CBUSH is connected to elements that form the bolt holes in the corner block and the other node of the CBUSH is connected to the elements that form the bolt holes in interface block. These connections between the CBUSH and the solid elements are made using rigid elements (RBE2).

Two sections of aluminum plate are welded to the bottom face of the lower frame assembly. These plates serve as the interface for bolting the VCTF to the slip table. This slip table interface plate is modeled using CQUAD4 and CTRIA3 elements. The bolts that connect the interface plate to the slip table are modeled using a single CBUSH element for each individual bolt.

The transition frame that connects the VCTF frame to the spherical coupler is composed of four round, steel tubes. One end of each tube is welded to a central interface block and a plate that is bolted to the spherical coupler. The other end of each tube is welded to a corner block that is

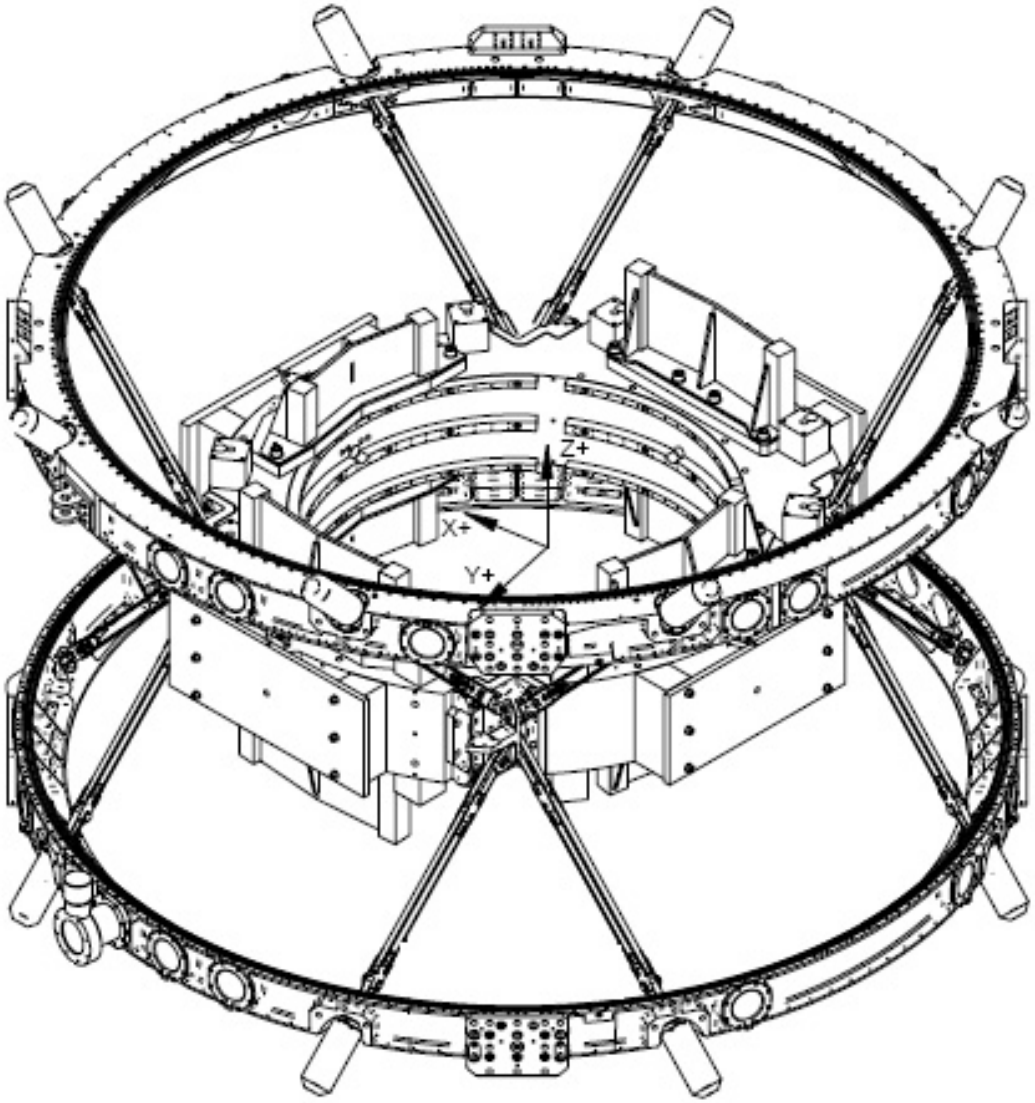

Figure 3-3 Cut-away view of vacuum case showing cold mass replica attached to upper and lower rings by sixteen support straps

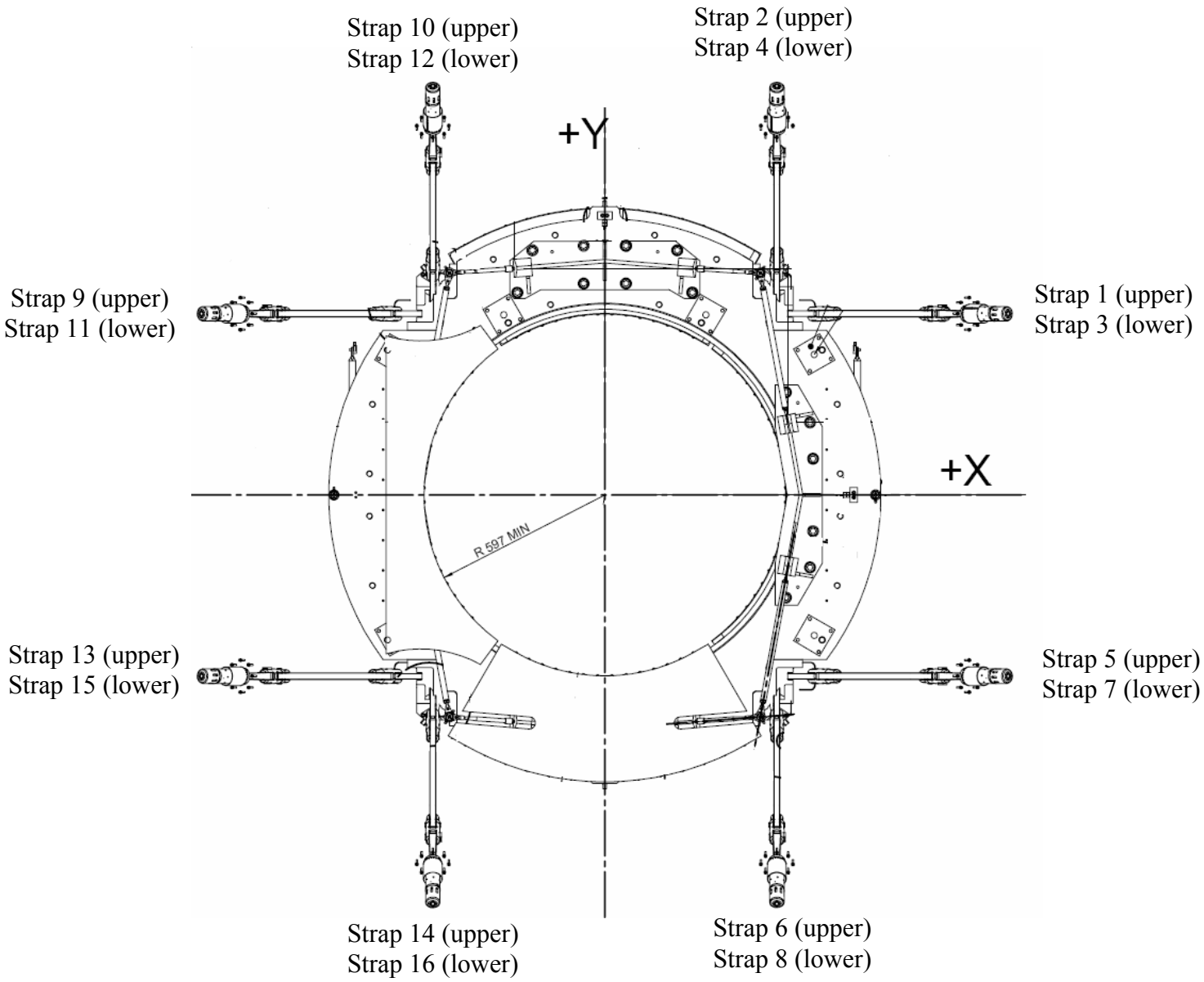

Figure 3-4 Top view of CMR showing strap layout (only eight upper straps are visible)

machined from steel. The four corner blocks provide the interface for bolting the transition frame to the primary frame. A fifth tube is welded between the two upper tubes of the frame to provide a means of lifting the frame assembly. The x/y configuration transition frame has for additional steel bars that are welded between the four corner blocks to provide additional stiffness. The tubes and bars of the transition frame are modeled using CBEAM elements. The corner blocks and the interface to the spherical coupler are modeled using solid elements. The joints where the transition frame bolts to the four corner blocks of the frame are modeled with CBUSH elements. A single CBUSH is used to represent the bolt pattern at each joint. The CBUSH elements are connected to the solid elements of the corner blocks using RBE elements.

The standoff assembly for the z-axis test configuration consists of a large, horizontal plate that bolts to the slip plate. A set of eight box-like structures are welded the upper face of the horizontal plate. The upper surface of these box-like structures provides an interface for bolting to the VCTF frame. The standoff plates are modeled using CQUAD4 and CTRIA3 elements. The bolts that connect the VCTF frame to the standoff structure are modeled using a CBUSH element for each bolt. In the locations where the standoff connects to the corner blocks of the frame, an RBE2 element is used to connect multiple CBUSH elements to a single beam node.

The entire VCTF assembly bolts to a slip table that is in turn mounted on a set of linear bearings. The slip table is modeled using CQUAD4 and CTRIA3 elements. The connection the VCTF assembly is modeled using CBUSH elements for the individual bolts. The connection to the linear bearings is also modeled using CBUSH elements for the individual bolts. The other end of the CBUSH that represents the connection to the linear bearings is constrained in the math model. The constraints are selected to correspond to the single-axis motion of the linear bearings and slip table.

Gusset plates attach to the lower sides of the frame to increase the stiffness. These plates are manufactured from half-inch aluminum plate. The gusset plates bolt to the frame and interface plate. The gusset plates are modeled using CQUAD4 and CTRIA3 elements. The bolts are represented by individual CBUSH elements.

The finite element models of the VCTF consist of the following:

(1) 45854 nodes and 42353 elements for the x-axis test configuration
(2) 45810 nodes and 42306 elements for the y-axis test configuration
(3) 60174 nodes and 57388 elements for the z-axis test configuration

These math models are shown in Figures 3-5 through 3-7.

When the analyses are performed for each of the sine sweep test configurations, the VCTF model is combined with a model of the test article. The test article model consists of finite element representations of the following components:

(1) STA vacuum case (19050 nodes and 31597 elements)
(2) cold mass replica of the magnet and helium tank (13543 nodes and 18902 elements)
(3) magnet support straps (32 nodes and 16 elements)

Math models of the flight hardware for each of these components were modified to represent the test article. These math models of the test article components are shown in Figures 3-8 and 3-9.

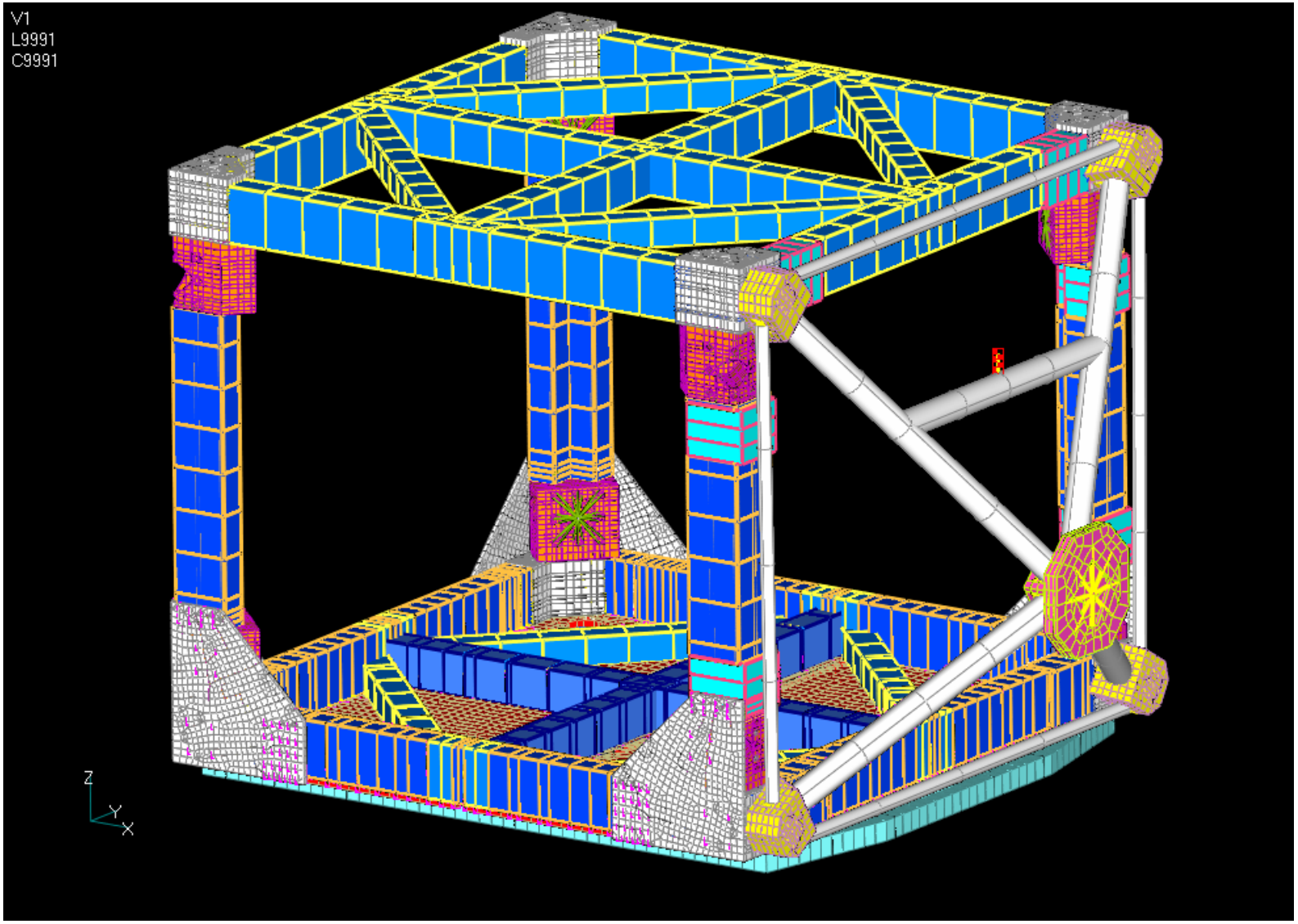

Figure 3-5 Isometric view of the baseline finite element model of the VCTF for the x-axis test configuration

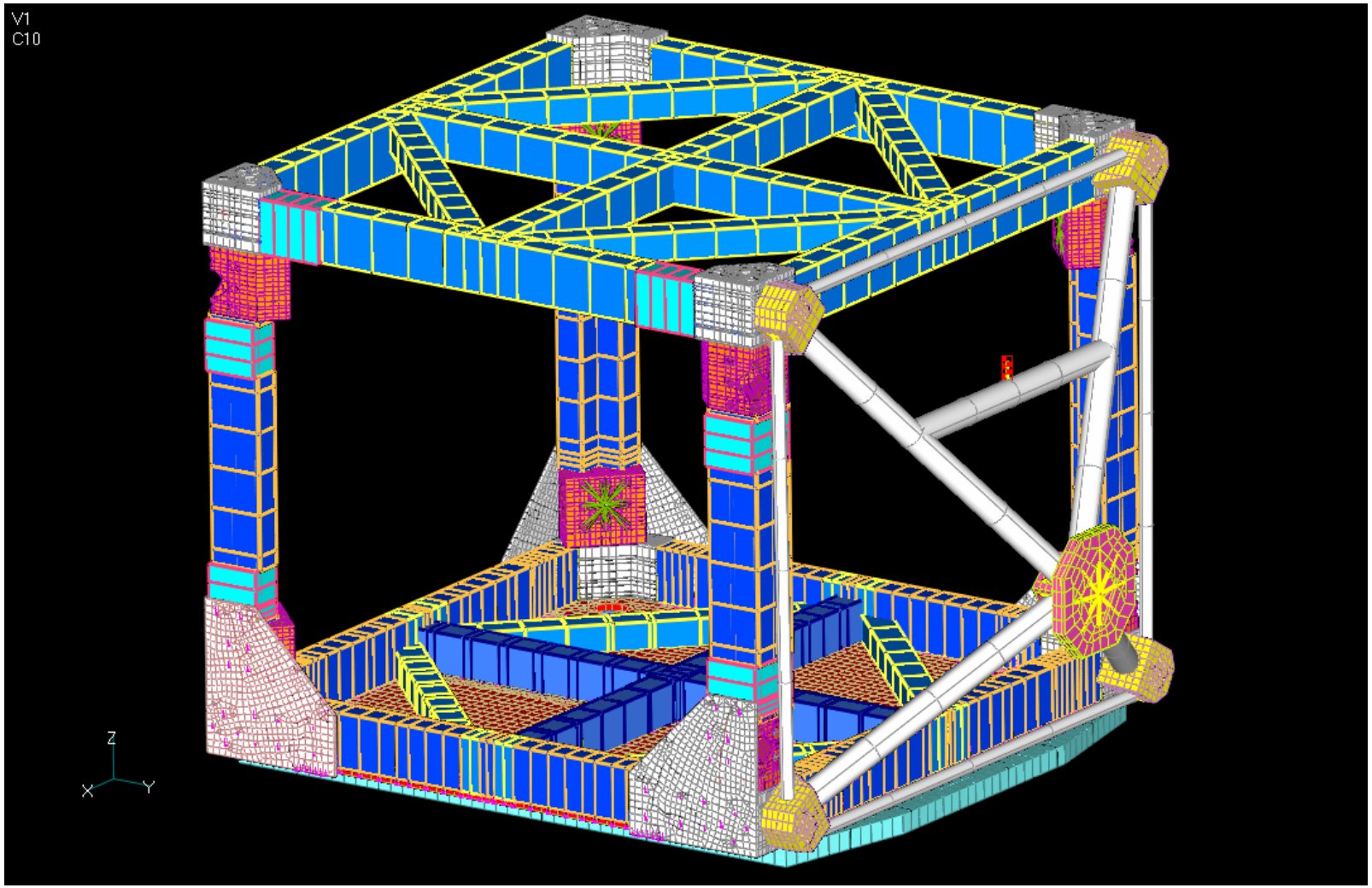

Figure 3-6 Isometric view of the baseline finite element model of the VCTF for the y-axis test configuration

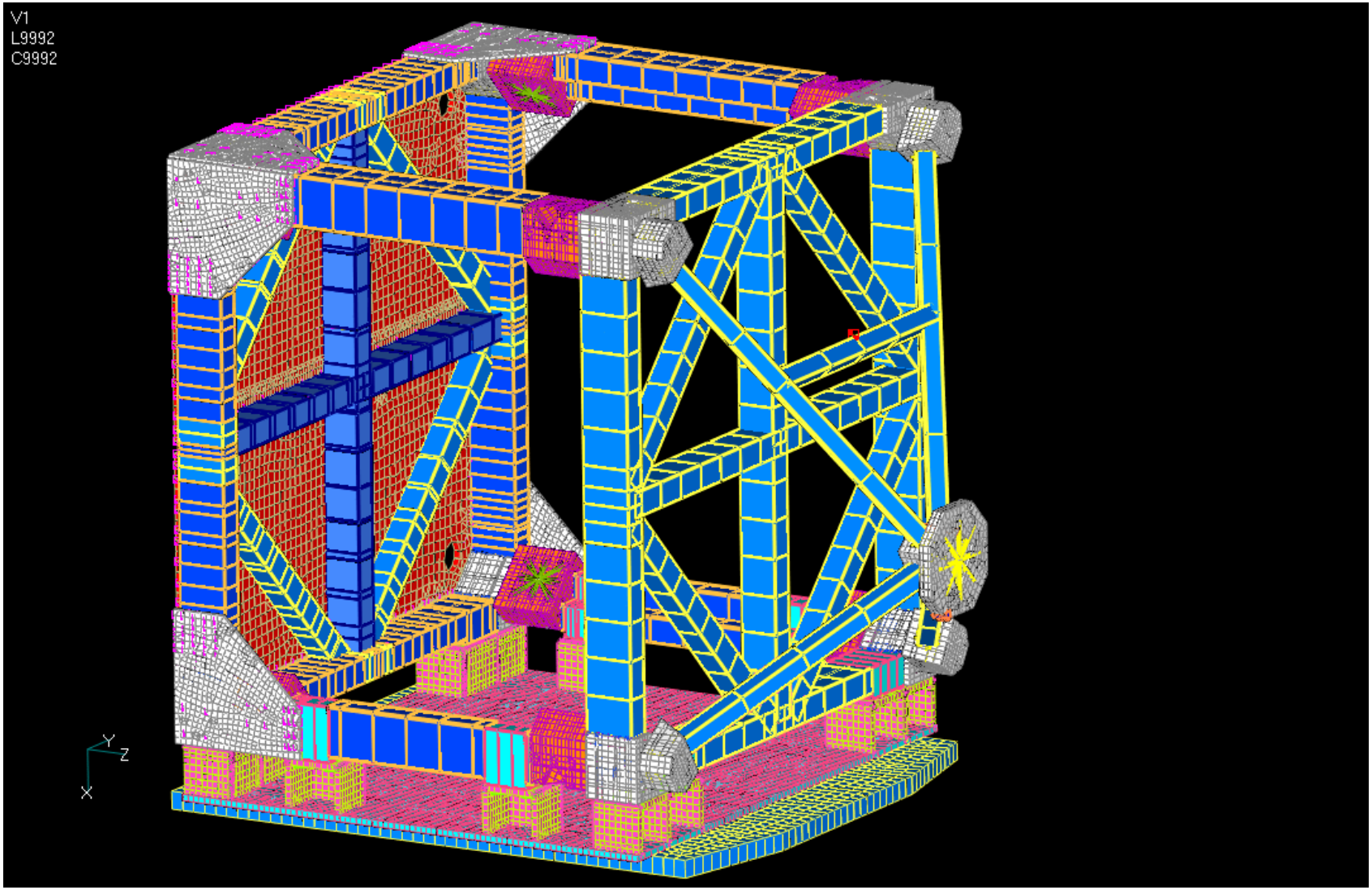

Figure 3-7 Isometric view of the baseline finite element model of the VCTF for the z-axis test configuration

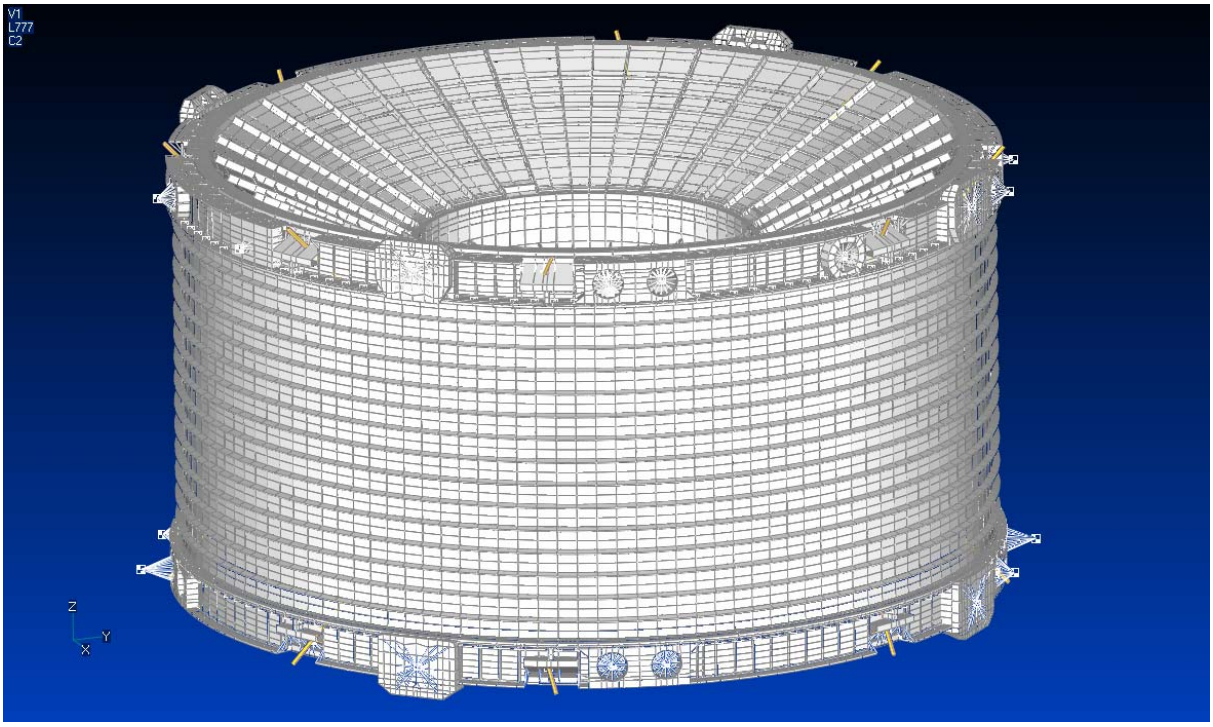

Figure 3-8 Isometric view of the finite element model of the vacuum case

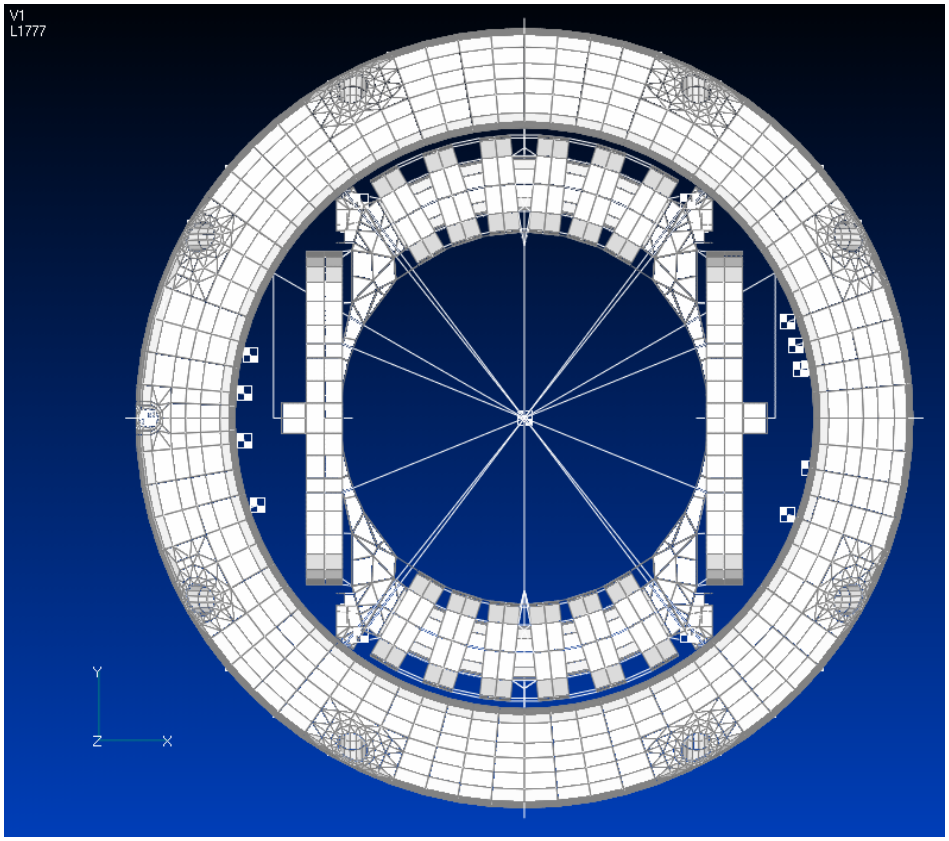

Figure 3-9 Top view of the finite element model of the magnet and helium tank

The simulation of the sine sweep test was performed using integrated models of the VCTF and test article. Figures 3-10 through 3-12 show the test article mounted in the VCTF for the x-axis, y-axis, and z-axis sine sweep test configurations, respectively.

The finite element models of the components comprising the test article and test fixture for the AMS-02 vacuum case sine sweep test have undergone a series of checks that verify that the math models are adequate for use in the structural assessment of the hardware. The integrated models of the test article and VCTF have undergone the same checks. These model checks include the following:

(1) Visual checks were performed make sure that the geometric shape (dimensions), material properties, and structural details conform to the engineering drawings. Visual checks were also made to verify the placement of the loads and boundary conditions.
(2) Element distortion checks were performed using FEMAP to verify that the taper, skew angle and aspect ratio for each element is acceptable.
(3) Mass property checks were performed using FEMAP and NASTRAN. The results from both programs match the measured inertia properties of the hardware within a reasonable accuracy.
(4) Strain energy checks were performed at the G-set, N-set, F-set, and A-set levels. The results show that there are no grounding or singularity issues.
(5) Unit gravity loads were used to compute displaced shapes of the structure. The results showed reasonable displacements and appropriate boundary conditions.

Excerpts from the NASTRAN jobs used to check the math models are shown in Figure 3-13 through Figure 3-15 for the x-axis, y-axis, and z-axis test configurations, respectively.

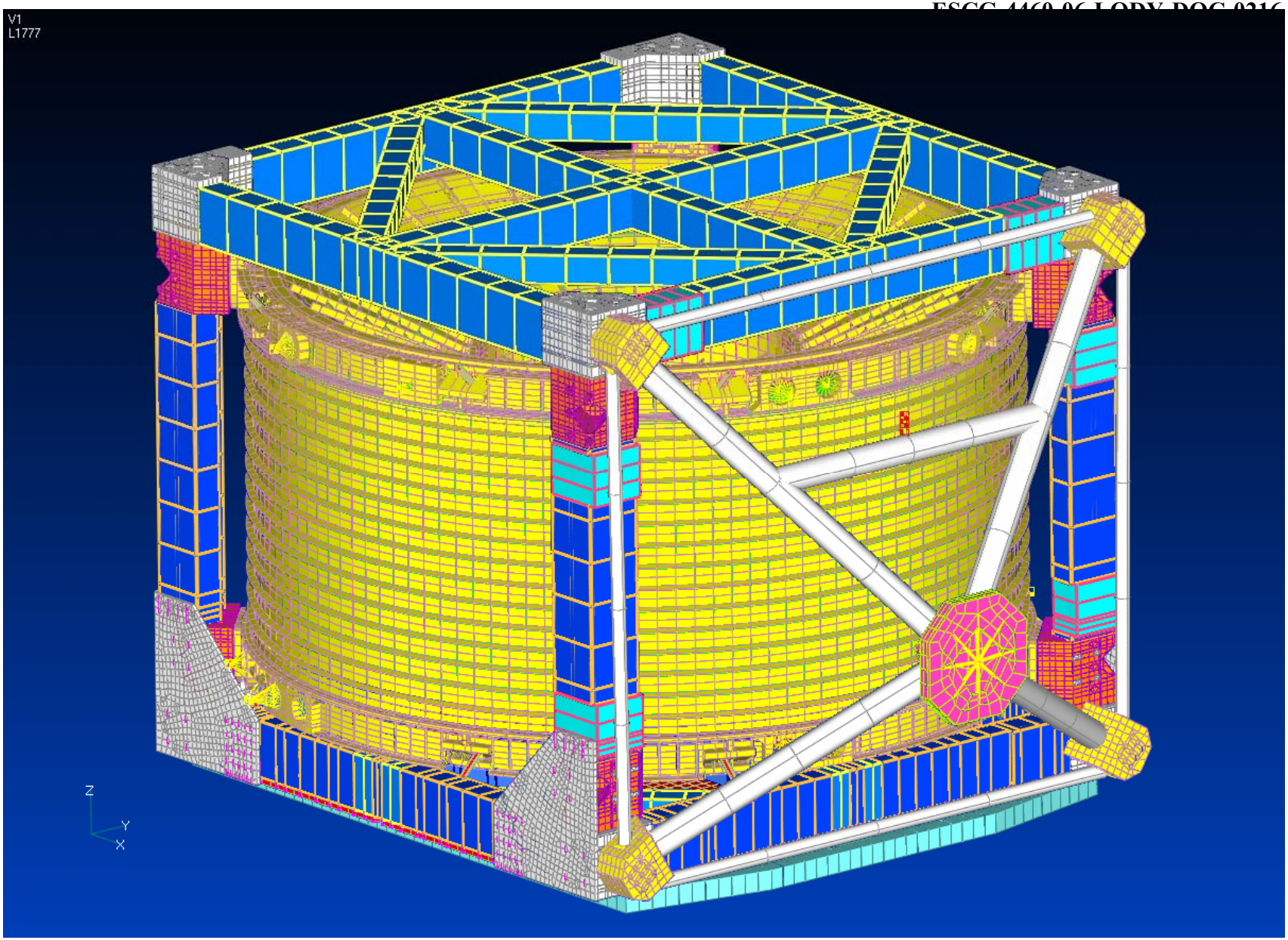

Figure 3-10 Isometric view of the finite element model of the test article in the VCTF for the x-axis sine sweep test

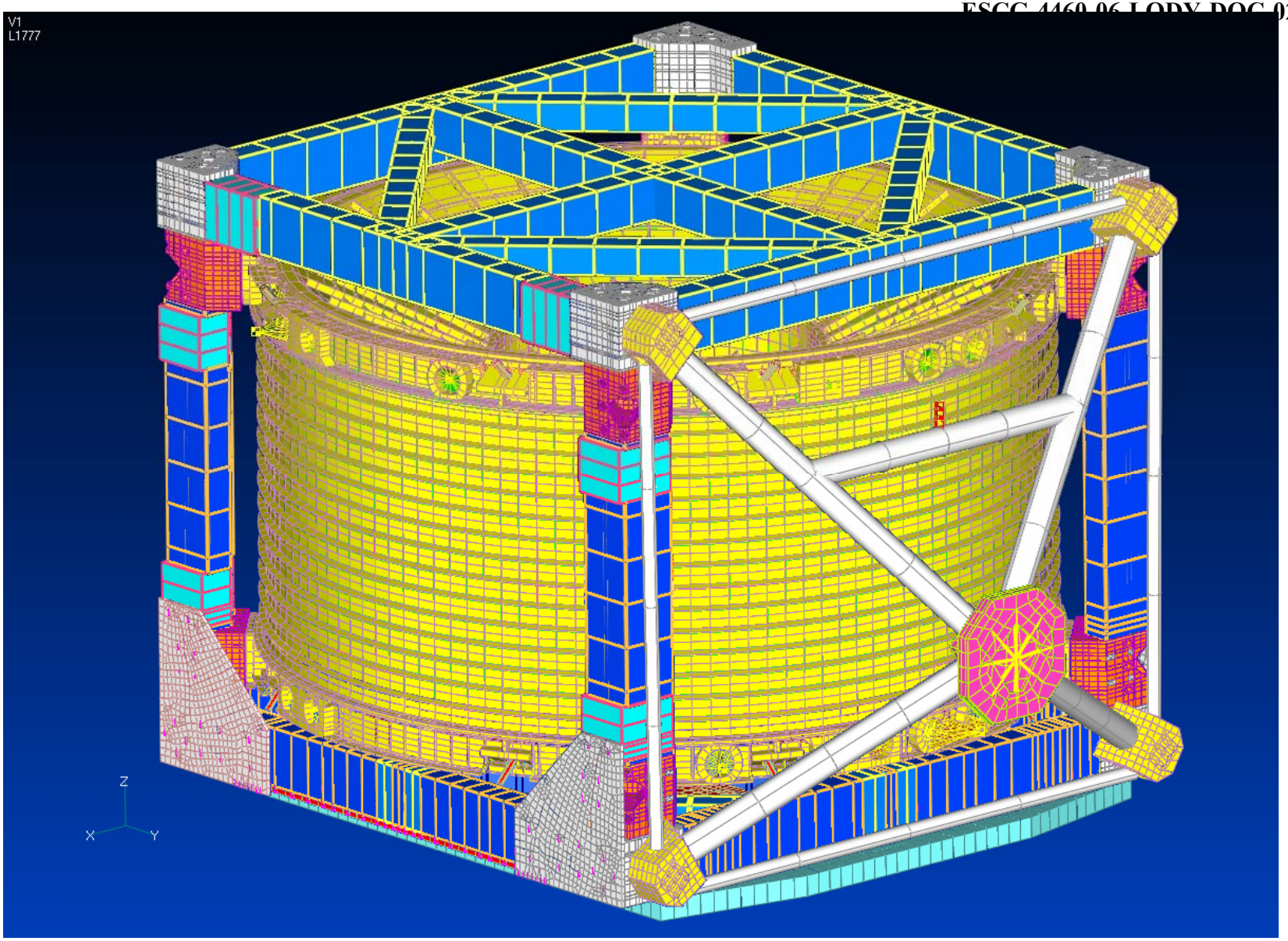

Figure 3-11 Isometric view of the finite element model of the test article in the VCTF for the y-axis sine sweep test

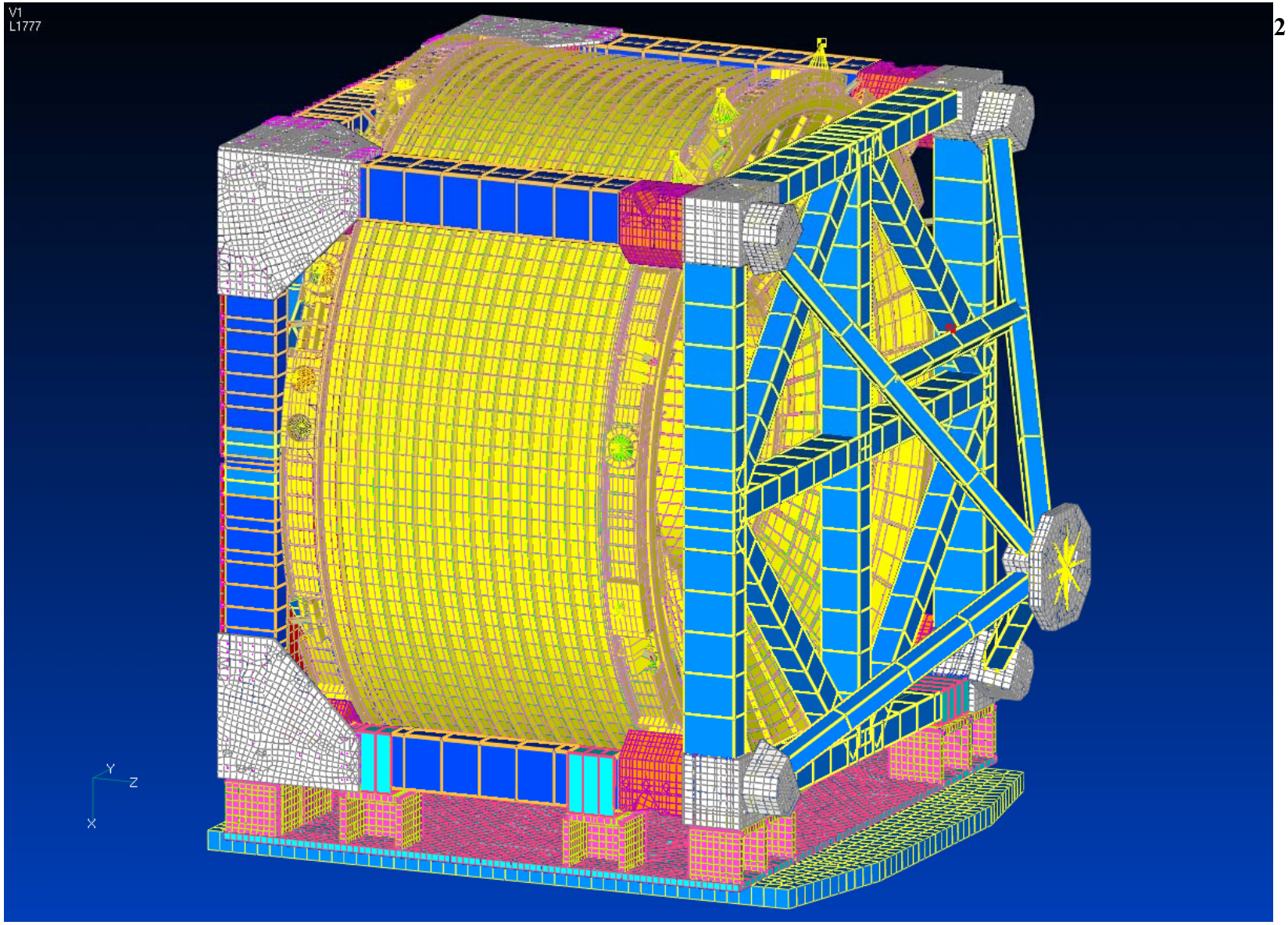

Figure 3-12 Isometric view of the finite element model of the test article in the VCTF for the z-axis sine sweep test

Figure 3-13 Excerpts from NASTRAN showing strain energy checks for the x-axis configuration

```
-------------------------------------------------------------------------------------
*** USER INFORMATION MESSAGE 7570 (GPWG1D)
     RESULTS OF RIGID BODY CHECKS OF MATRIX KGG      (G-SET)  FOLLOW:
     PRINT RESULTS IN ALL SIX DIRECTIONS AGAINST THE LIMIT OF   1.007892E+00
           DIRECTION        STRAIN ENERGY        PASS/FAIL
           ---------        -------------        ---------
             1               3.062964E-05          PASS
             2               1.753130E-05          PASS
             3               2.624711E-08          PASS
             4               1.699020E-02          PASS
             5               3.936280E-02          PASS
             6               4.663097E-02          PASS
     SOME POSSIBLE REASONS MAY LEAD TO THE FAILURE:
       1. CELASI ELEMENTS CONNECTING TO ONLY ONE GRID POINT;
       2. CELASI ELEMENTS CONNECTING TO NON-COINCIDENT POINTS;
       3. CELASI ELEMENTS CONNECTING TO NON-COLINEAR DOF;
       4. IMPROPERLY DEFINED DMIG MATRICES

-------------------------------------------------------------------------------------
*** USER INFORMATION MESSAGE 7570 (GPWG1D)
     RESULTS OF RIGID BODY CHECKS OF MATRIX KNN      (N-SET)  FOLLOW:
     PRINT RESULTS IN ALL SIX DIRECTIONS AGAINST THE LIMIT OF   4.986746E+01
           DIRECTION        STRAIN ENERGY        PASS/FAIL
           ---------        -------------        ---------
             1               1.564894E-05          PASS
             2               2.875445E-05          PASS
             3               1.550976E-05          PASS
             4               1.133142E-02          PASS
             5               1.530689E-02          PASS
             6               4.533274E-02          PASS
     SOME POSSIBLE REASONS MAY LEAD TO THE FAILURE:
       1. MULTIPOINT CONSTRAINT EQUATIONS WHICH DO NOT SATISFY RIGID-BODY MOTION;
       2. RBE3 ELEMENTS FOR WHICH THE INDEPENDENT DEGREE-OF-FREEDOM CANNOT DESCRIBE
          ALL POSSIBLE RIGID-BODY MOTIONS.

-------------------------------------------------------------------------------------
*** USER INFORMATION MESSAGE 7570 (GPWG1D)
     RESULTS OF RIGID BODY CHECKS OF MATRIX KFF      (F-SET)  FOLLOW:
     PRINT RESULTS IN ALL SIX DIRECTIONS AGAINST THE LIMIT OF   4.986746E+01
           DIRECTION        STRAIN ENERGY        PASS/FAIL
           ---------        -------------        ---------
             1               1.564894E-05          PASS
             2               2.875445E-05          PASS
             3               1.550976E-05          PASS
             4               1.133142E-02          PASS
             5               1.530689E-02          PASS
             6               4.533274E-02          PASS
     SOME POSSIBLE REASONS MAY LEAD TO THE FAILURE:
       1.  CONSTRAINTS WHICH PREVENT RIGID-BODY MOTION.

-------------------------------------------------------------------------------------
*** USER INFORMATION MESSAGE 7570 (GPWG1D)
     RESULTS OF RIGID BODY CHECKS OF MATRIX KAA1     (A-SET)  FOLLOW:
     PRINT RESULTS IN ALL SIX DIRECTIONS AGAINST THE LIMIT OF   4.986746E+01
           DIRECTION        STRAIN ENERGY        PASS/FAIL
           ---------        -------------        ---------
             1               1.564894E-05          PASS
             2               2.875445E-05          PASS
             3               1.550976E-05          PASS
             4               1.133142E-02          PASS
             5               1.530689E-02          PASS
             6               4.533274E-02          PASS
     IF THE MODEL HAS PASSED THE PREVIOUS CHECKS FOR THE G-SET AND N-SET,
     THEN SOME POSSIBLE CAUSES ARE:
       1. THE MODEL IS NOT INTENDED TO BE FREE-FREE WHICH INDICATES THAT THE MODEL IS
          PROPERLY CONSTRAINED TO GROUND;
       2. THE REFERENCE GRID POINT (GRID=GID ON THE GROUNDCHECK COMMAND) IS LOCATED
          TOO FAR FROM THE MODEL'S CENTER OF GRAVITY. IT IS RECOMMENDED THAT THE
          REFERENCE GRID POINT BE LOCATED AS CLOSE AS POSSIBLE TO THE MODEL'S CENTER
          OF GRAVITY OF THE MODEL (SEE THE GRID POINT WEIGHT GENERATOR OUTPUT);
       3. PARAM,AUTOSPC,YES CONSTRAINS NEAR-SINGULAR DEGREES-OF-FREEDOM. WHEN A
          FINITE ELEMENT MODEL WITH AUTOSPC FAILS THE A-SET CHECK, IT IS NOT EVIDENT
          THAT GROUNDING HAS OCCURRED. THE USE OF PARAM,SNORM WILL NOT ELIMINATE THE
          SPURIOUS FAILURE.
```

Figure 3-14 Excerpts from NASTRAN showing strain energy checks for the y-axis configuration

```
-------------------------------------------------------------------------------------
*** USER INFORMATION MESSAGE 7570 (GPWG1D)
     RESULTS OF RIGID BODY CHECKS OF MATRIX KGG      (G-SET)  FOLLOW:
     PRINT RESULTS IN ALL SIX DIRECTIONS AGAINST THE LIMIT OF   1.007892E+00
           DIRECTION        STRAIN ENERGY        PASS/FAIL
           ---------        -------------        ---------
             1               3.253477E-05          PASS
             2               1.739526E-05          PASS
             3               5.626732E-07          PASS
             4               3.685430E-02          PASS
             5               1.800227E-03          PASS
             6               5.672927E-02          PASS
     SOME POSSIBLE REASONS MAY LEAD TO THE FAILURE:
       1. CELASI ELEMENTS CONNECTING TO ONLY ONE GRID POINT;
       2. CELASI ELEMENTS CONNECTING TO NON-COINCIDENT POINTS;
       3. CELASI ELEMENTS CONNECTING TO NON-COLINEAR DOF;
       4. IMPROPERLY DEFINED DMIG MATRICES;

-------------------------------------------------------------------------------------
*** USER INFORMATION MESSAGE 7570 (GPWG1D)
     RESULTS OF RIGID BODY CHECKS OF MATRIX KNN      (N-SET)  FOLLOW:
     PRINT RESULTS IN ALL SIX DIRECTIONS AGAINST THE LIMIT OF   4.986746E+01
           DIRECTION        STRAIN ENERGY        PASS/FAIL
           ---------        -------------        ---------
             1               1.860590E-05          PASS
             2               2.969547E-05          PASS
             3               1.678075E-05          PASS
             4               1.011117E-03          PASS
             5               5.102468E-02          PASS
             6               4.090207E-02          PASS
     SOME POSSIBLE REASONS MAY LEAD TO THE FAILURE:
       1. MULTIPOINT CONSTRAINT EQUATIONS WHICH DO NOT SATISFY RIGID-BODY MOTION;
       2. RBE3 ELEMENTS FOR WHICH THE INDEPENDENT DEGREE-OF-FREEDOM CANNOT DESCRIBE
          ALL POSSIBLE RIGID-BODY MOTIONS.

-------------------------------------------------------------------------------------
*** USER INFORMATION MESSAGE 7570 (GPWG1D)
     RESULTS OF RIGID BODY CHECKS OF MATRIX KFF      (F-SET)  FOLLOW:
     PRINT RESULTS IN ALL SIX DIRECTIONS AGAINST THE LIMIT OF   4.986746E+01
           DIRECTION        STRAIN ENERGY        PASS/FAIL
           ---------        -------------        ---------
             1               1.860590E-05          PASS
             2               2.969547E-05          PASS
             3               1.678075E-05          PASS
             4               1.011117E-03          PASS
             5               5.102468E-02          PASS
             6               4.090207E-02          PASS
     SOME POSSIBLE REASONS MAY LEAD TO THE FAILURE:
       1. CONSTRAINTS WHICH PREVENT RIGID-BODY MOTION.

-------------------------------------------------------------------------------------
*** USER INFORMATION MESSAGE 7570 (GPWG1D)
     RESULTS OF RIGID BODY CHECKS OF MATRIX KAA1     (A-SET)  FOLLOW:
     PRINT RESULTS IN ALL SIX DIRECTIONS AGAINST THE LIMIT OF   4.986746E+01
           DIRECTION        STRAIN ENERGY        PASS/FAIL
           ---------        -------------        ---------
             1               1.860590E-05          PASS
             2               2.969547E-05          PASS
             3               1.678075E-05          PASS
             4               1.011117E-03          PASS
             5               5.102468E-02          PASS
             6               4.090207E-02          PASS
     IF THE MODEL HAS PASSED THE PREVIOUS CHECKS FOR THE G-SET AND N-SET,
     THEN SOME POSSIBLE CAUSES ARE:
       1. THE MODEL IS NOT INTENDED TO BE FREE-FREE WHICH INDICATES THAT THE MODEL IS
          PROPERLY CONSTRAINED TO GROUND;
       2. THE REFERENCE GRID POINT (GRID=GID ON THE GROUNDCHECK COMMAND) IS LOCATED
          TOO FAR FROM THE MODEL'S CENTER OF GRAVITY. IT IS RECOMMENDED THAT THE
          REFERENCE GRID POINT BE LOCATED AS CLOSE AS POSSIBLE TO THE MODEL'S CENTER
          OF GRAVITY OF THE MODEL (SEE THE GRID POINT WEIGHT GENERATOR OUTPUT);
       3. PARAM,AUTOSPC,YES CONSTRAINS NEAR-SINGULAR DEGREES-OF-FREEDOM. WHEN A
          FINITE ELEMENT MODEL WITH AUTOSPC FAILS THE A-SET CHECK, IT IS NOT EVIDENT
          THAT GROUNDING HAS OCCURRED. THE USE OF PARAM,SNORM WILL NOT ELIMINATE THE
          SPURIOUS FAILURE.
```

Figure 3-15 Excerpts from NASTRAN showing strain energy checks for the z-axis configuration

```
-----------------------------------------------------------------------------------------
*** USER INFORMATION MESSAGE 7570 (GPWG1D)
     RESULTS OF RIGID BODY CHECKS OF MATRIX KGG      (G-SET)  FOLLOW:
     PRINT RESULTS IN ALL SIX DIRECTIONS AGAINST THE LIMIT OF   1.007892E+00
           DIRECTION        STRAIN ENERGY        PASS/FAIL
           ---------        -------------        ---------
             1               3.211922E-05          PASS
             2               1.847137E-05          PASS
             3               8.297759E-07          PASS
             4               1.971177E-01          PASS
             5               1.470380E-01          PASS
             6               7.050720E-02          PASS
     SOME POSSIBLE REASONS MAY LEAD TO THE FAILURE:
       1. CELASI ELEMENTS CONNECTING TO ONLY ONE GRID POINT;
       2. CELASI ELEMENTS CONNECTING TO NON-COINCIDENT POINTS;
       3. CELASI ELEMENTS CONNECTING TO NON-COLINEAR DOF;
       4. IMPROPERLY DEFINED DMIG MATRICES;

-----------------------------------------------------------------------------------------
*** USER INFORMATION MESSAGE 7570 (GPWG1D)
     RESULTS OF RIGID BODY CHECKS OF MATRIX KNN      (N-SET)  FOLLOW:
     PRINT RESULTS IN ALL SIX DIRECTIONS AGAINST THE LIMIT OF   4.986746E+01
           DIRECTION        STRAIN ENERGY        PASS/FAIL
           ---------        -------------        ---------
             1               1.786499E-05          PASS
             2               3.050529E-05          PASS
             3               1.755207E-05          PASS
             4               1.197325E-01          PASS
             5               1.058514E-01          PASS
             6               4.278465E-02          PASS
     SOME POSSIBLE REASONS MAY LEAD TO THE FAILURE:
       1. MULTIPOINT CONSTRAINT EQUATIONS WHICH DO NOT SATISFY RIGID-BODY MOTION;
       2. RBE3 ELEMENTS FOR WHICH THE INDEPENDENT DEGREE-OF-FREEDOM CANNOT DESCRIBE
          ALL POSSIBLE RIGID-BODY MOTIONS.

-----------------------------------------------------------------------------------------
*** USER INFORMATION MESSAGE 7570 (GPWG1D)
     RESULTS OF RIGID BODY CHECKS OF MATRIX KFF      (F-SET)  FOLLOW:
     PRINT RESULTS IN ALL SIX DIRECTIONS AGAINST THE LIMIT OF   4.986746E+01
           DIRECTION        STRAIN ENERGY        PASS/FAIL
           ---------        -------------        ---------
             1               1.786499E-05          PASS
             2               3.050529E-05          PASS
             3               1.755207E-05          PASS
             4               1.197325E-01          PASS
             5               1.058514E-01          PASS
             6               4.278465E-02          PASS
     SOME POSSIBLE REASONS MAY LEAD TO THE FAILURE:
       1. CONSTRAINTS WHICH PREVENT RIGID-BODY MOTION.

-----------------------------------------------------------------------------------------
*** USER INFORMATION MESSAGE 7570 (GPWG1D)
     RESULTS OF RIGID BODY CHECKS OF MATRIX KAA1     (A-SET)  FOLLOW:
     PRINT RESULTS IN ALL SIX DIRECTIONS AGAINST THE LIMIT OF   4.986746E+01
           DIRECTION        STRAIN ENERGY        PASS/FAIL
           ---------        -------------        ---------
             1               1.786499E-05          PASS
             2               3.050529E-05          PASS
             3               1.755207E-05          PASS
             4               1.197325E-01          PASS
             5               1.058514E-01          PASS
             6               4.278465E-02          PASS
     IF THE MODEL HAS PASSED THE PREVIOUS CHECKS FOR THE G-SET AND N-SET,
     THEN SOME POSSIBLE CAUSES ARE:
       1. THE MODEL IS NOT INTENDED TO BE FREE-FREE WHICH INDICATES THAT THE MODEL IS
          PROPERLY CONSTRAINED TO GROUND;
       2. THE REFERENCE GRID POINT (GRID=GID ON THE GROUNDCHECK COMMAND) IS LOCATED
          TOO FAR FROM THE MODEL'S CENTER OF GRAVITY. IT IS RECOMMENDED THAT THE
          REFERENCE GRID POINT BE LOCATED AS CLOSE AS POSSIBLE TO THE MODEL'S CENTER
          OF GRAVITY OF THE MODEL (SEE THE GRID POINT WEIGHT GENERATOR OUTPUT);
       3. PARAM,AUTOSPC,YES CONSTRAINS NEAR-SINGULAR DEGREES-OF-FREEDOM. WHEN A
          FINITE ELEMENT MODEL WITH AUTOSPC FAILS THE A-SET CHECK, IT IS NOT EVIDENT
          THAT GROUNDING HAS OCCURRED. THE USE OF PARAM,SNORM WILL NOT ELIMINATE THE
          SPURIOUS FAILURE.
```

4.0 Mass Properties

The mass properties for each test configuration are provided in this section. This data has been extracted from a NASTRAN analysis using the math models of the test fixture and test article. The x-axis, y-axis, and z-axis test configurations are shown in Tables 4-1 through 4-3, respectively.

Most of the individual components of the test hardware have been weighed and a comparison of the measured weight and the predicted weight is shown in Table 4-4.

5.0 Static Load Conditions

Due to the tension-only characteristic of the support straps, the static load condition prior to the dynamic excitation must be simulated. When the magnet system is installed in the vacuum case, the C1W1 support straps are mechanically tensioned to 1750 pounds and the C2W2 straps are tensioned to 1650 pounds. These values for the mechanical preload represent the nominal value and were used in the simulation. For the actual hardware, the preload for each strap may deviate as much as 25% from the nominal. These deviations will be accounted for through the post-test analysis and correlation process.

The weight of the cold mass replica increases the preload in the upper straps and reduces the preload in the lower straps. In addition, the vacuum induced in the vacuum case causes deformations of the support rings that also affect the strap preload forces. There is also deformation of the vacuum case and the VCTF due to these preload conditions. The total preload offset data for the x-axis, y-axis, and z-axis test configurations are provided in Table 5-1, Table 5-2, and Table 5-3, respectively.

Due to limitations of the MSC NASTRAN nonlinear transient solution, there is no simple method of directly accounting for all of these static preload effects. The deformation of the vacuum case and VCTF has a second order effect that is omitted during the transient solution; however, the loads due to deformation of the vacuum case and VCTF are added to the transient loads during the post-processing phase. The strap preload, however, must be accounted for during the transient solution. The easiest method to accomplish this is by offsetting the origin of the strap stress-strain curves by the amount of the static preload value. For each of the sixteen straps, the baseline curve (Figure 3-1) is offset by the preload value (Table 4-1) to generate a unique stress-strain curve for each strap. Figure 5-1 provides an example, showing the offset curve for strap 1 in the x-axis test configuration.

6.0 System Modal Characteristics

Determining the modal characteristics for the sine sweep configurations is complicated by the nonlinear nature of the magnet support straps. The static preload condition produces a set of frequencies that exist prior to application of the shaker excitation. As the magnitude of the external load is increased, the tension load of each strap changes and this change in strap load causes the frequency of the system to also change.

Table 4-1 Mass Properties for the X-axis Test Configuration (slip table, test fixture, and test article)

```
     O U T P U T   F R O M   G R I D   P O I N T   W E I G H T   G E N E R A T O R
                                REFERENCE POINT =       0
                                          M O
*  3.265507E+01  2.775558E-17  3.794708E-17  7.105427E-15  1.242941E+04 -3.534007E+00 *
*  2.775558E-17  3.265507E+01 -1.734723E-17 -1.242941E+04  2.842171E-14  1.604771E+02 *
*  3.794708E-17 -1.734723E-17  3.265507E+01  3.534007E+00 -1.604771E+02  1.776357E-15 *
*  7.105427E-15 -1.242941E+04  3.534007E+00  4.786671E+06 -1.186189E+02 -6.219678E+04 *
*  1.242941E+04  2.842171E-14 -1.604771E+02 -1.186189E+02  4.791589E+06 -1.310071E+03 *
* -3.534007E+00  1.604771E+02  1.776357E-15 -6.219678E+04 -1.310071E+03  6.810280E+04 *
                                           S
                    *  1.000000E+00  0.000000E+00  0.000000E+00 *
                    *  0.000000E+00  1.000000E+00  0.000000E+00 *
                    *  0.000000E+00  0.000000E+00  1.000000E+00 *
         DIRECTION
    MASS AXIS SYSTEM (S)     MASS              X-C.G.        Y-C.G.        Z-C.G.
            X            3.265507E+01      2.175903E-16  1.082223E-01  3.806273E+02
            Y            3.265507E+01      4.914310E+00  8.703613E-16  3.806273E+02
            Z            3.265507E+01      4.914310E+00  1.082223E-01  5.439758E-17
                                          I(S)
                    *  5.569656E+04  1.012517E+02  1.114795E+03 *
                    *  1.012517E+02  5.982514E+04 -3.506841E+01 *
                    *  1.114795E+03 -3.506841E+01  6.731379E+04 *
                                          I(Q)
                    *  6.742006E+04                             *
                    *                5.982712E+04               *
                    *                             5.558831E+04 *
                                           Q
                    *  9.479824E-02 -2.234270E-02  9.952458E-01 *
                    * -5.857185E-03  9.997183E-01  2.300101E-02 *
                    * -9.954793E-01 -8.009793E-03  9.464066E-02 *
```

Table 4-2 Mass Properties for the Y-axis Test Configuration (slip table, test fixture, and test article)

```
     O U T P U T   F R O M   G R I D   P O I N T   W E I G H T   G E N E R A T O R
                                 REFERENCE POINT =       0
                                            M O
*  3.265507E+01  2.775558E-17  3.859760E-17  1.065814E-14  1.242941E+04 -1.592519E+02 *
*  2.775558E-17  3.265507E+01 -3.469447E-17 -1.242941E+04  2.131628E-14  2.807215E+00 *
*  3.859760E-17 -3.469447E-17  3.265507E+01  1.592519E+02 -2.807215E+00  2.220446E-16 *
*  1.065814E-14 -1.242941E+04  1.592519E+02  4.793800E+06 -1.134774E+02 -1.026675E+03 *
*  1.242941E+04  2.131628E-14 -2.807215E+00 -1.134774E+02  4.784240E+06 -6.171536E+04 *
* -1.592519E+02  2.807215E+00  2.220446E-16 -1.026675E+03 -6.171536E+04  6.788334E+04 *
                                             S
                     *  1.000000E+00  0.000000E+00  0.000000E+00 *
                     *  0.000000E+00  1.000000E+00  0.000000E+00 *
                     *  0.000000E+00  0.000000E+00  1.000000E+00 *
          DIRECTION
      MASS AXIS SYSTEM (S)     MASS             X-C.G.        Y-C.G.        Z-C.G.
              X            3.265507E+01      3.263855E-16  4.876788E+00  3.806273E+02
              Y            3.265507E+01      8.596568E-02  6.527710E-16  3.806273E+02
              Z            3.265507E+01      8.596568E-02  4.876788E+00  6.799698E-18
                                            I(S)
                     *  6.204892E+04  9.978722E+01 -4.182769E+01 *
                     *  9.978722E+01  5.326548E+04  1.099740E+03 *
                     * -4.182769E+01  1.099740E+03  6.710645E+04 *
                                            I(Q)
                     *  6.719377E+04                             *
                     *                6.204949E+04               *
                     *                               5.317760E+04 *
                                             Q
                     *  9.631888E-03  9.998949E-01  1.084162E-02 *
                     * -7.881548E-02 -1.004926E-02  9.968386E-01 *
                     *  9.968427E-01 -1.045593E-02  7.871040E-02 *
```

Table 4-3 Mass Properties for the Z-axis Test Configuration (slip table, test fixture, and test article)

```
     O U T P U T   F R O M   G R I D   P O I N T   W E I G H T   G E N E R A T O R
                                REFERENCE POINT =       0
                                          M O
*  3.465529E+01  2.775558E-17  3.621235E-17  3.552714E-15  1.361196E+04 -3.533966E+00 *
*  2.775558E-17  3.465529E+01 -2.428613E-17 -1.361196E+04  3.552714E-14  4.971205E+02 *
*  3.621235E-17 -2.428613E-17  3.465529E+01  3.533966E+00 -4.971205E+02  1.665335E-15 *
*  3.552714E-15 -1.361196E+04  3.533966E+00  5.407838E+06 -1.186314E+02 -1.968936E+05 *
*  1.361196E+04  3.552714E-14 -4.971205E+02 -1.186314E+02  5.428313E+06 -1.310037E+03 *
* -3.533966E+00  4.971205E+02  1.665335E-15 -1.968936E+05 -1.310037E+03  8.669629E+04 *
                                           S
                    *  1.000000E+00  0.000000E+00  0.000000E+00 *
                    *  0.000000E+00  1.000000E+00  0.000000E+00 *
                    *  0.000000E+00  0.000000E+00  1.000000E+00 *
         DIRECTION
    MASS AXIS SYSTEM (S)     MASS             X-C.G.        Y-C.G.        Z-C.G.
            X            3.465529E+01      1.025158E-16  1.019748E-01  3.927815E+02
            Y            3.465529E+01      1.434472E+01  1.025158E-15  3.927815E+02
            Z            3.465529E+01      1.434472E+01  1.019748E-01  4.805427E-17
                                          I(S)
                    *  6.131270E+04  6.793761E+01  1.633841E+03 *
                    *  6.793761E+01  7.465635E+04 -7.803938E+01 *
                    *  1.633841E+03 -7.803938E+01  7.956487E+04 *
                                          I(Q)
                    *  7.971136E+04                             *
                    *                7.465523E+04               *
                    *                                6.116733E+04 *
                                           Q
                    *  8.844857E-02 -3.021868E-03  9.960762E-01 *
                    * -1.656410E-02  9.998527E-01  4.504167E-03 *
                    * -9.959430E-01 -1.689749E-02  8.838548E-02 *
```

Table 4-4 Comparison of Predicted and Measured Weights for the Sine Sweep Test Hardware

Component	Math Model	Actual Weight	Delta Weight
Frame assembly (upper, lower, columns)	2173.	3080.	118.
Interface Plate (welded to frame for x/y config)	789.		
Gussets (x/y config)	338.		
Gussets (z config)	343.		
Transition frame (x/y config)	1062.	1050.	-12.
Transition frame (z config)	803	800.	-3.
Standoff for z-axis config	1026.		

NOTE: The weight of the bolts was not modeled.

Table 5-1 Preload Offset Data for Magnet Support Straps for X-axis

Strap ID	Strain Offset (in/in)	Stress Offset (psi)	Displace Offset (inch)	Force Offset (lb)
1	0.02023796	12730.2	0.7720	2159.4
2	0.02105367	11963.9	0.7489	2050.7
3	0.0160981	8505.9	0.6141	1442.8
4	0.01664626	8230.8	0.5922	1410.8
5	0.02023911	12731.6	0.7720	2159.7
6	0.02104511	11953.8	0.7486	2049.0
7	0.01608867	8500.9	0.6137	1442.0
8	0.01668904	8252.1	0.5937	1414.5
9	0.02023201	12722.5	0.7718	2158.1
10	0.02105704	11967.9	0.7491	2051.4
11	0.01613325	8524.4	0.6154	1446.0
12	0.0166708	8243.0	0.5930	1412.9
13	0.0202169	12703.1	0.7712	2154.8
14	0.02105759	11968.6	0.7491	2051.5
15	0.01612184	8518.4	0.6150	1445.0
16	0.01664721	8231.3	0.5922	1410.9

Table 5-2 Preload Offset Data for Magnet Support Straps for Y-axis

Strap ID	Strain Offset (in/in)	Stress Offset (psi)	Displace Offset (inch)	Force Offset (lb)
1	0.02023516	12726.6	0.7719	2158.8
2	0.02105803	11969.1	0.7491	2051.6
3	0.01609595	8504.7	0.6140	1442.7
4	0.01665059	8233.0	0.5923	1411.2
5	0.02024317	12736.9	0.7722	2160.6
6	0.02104094	11948.9	0.7485	2048.2
7	0.01609244	8502.9	0.6139	1442.3
8	0.01668399	8249.6	0.5935	1414.1
9	0.02023482	12726.1	0.7719	2158.7
10	0.02105462	11965.1	0.7490	2050.9
11	0.01613683	8526.3	0.6156	1446.3
12	0.0166689	8242.1	0.5930	1412.8
13	0.0202144	12699.9	0.7711	2154.3
14	0.02106023	11971.7	0.7492	2052.1
15	0.01611803	8516.4	0.6148	1444.6
16	0.01664856	8232.0	0.5922	1411.0

Table 5-3 Preload Offset Data for Magnet Support Straps for Z-axis

Strap ID	Strain Offset (in/in)	Stress Offset (psi)	Displace Offset (inch)	Force Offset (lb)
1	0.01438702	7601.8	0.5488	1289.5
2	0.01886046	9367.7	0.6709	1605.7
3	0.01439533	7606.1	0.5491	1290.2
4	0.01885822	9365.1	0.6708	1605.3
5	0.01438957	7603.1	0.5489	1289.7
6	0.01885474	9361.0	0.6707	1604.6
7	0.01438019	7598.1	0.5486	1288.9
8	0.01889808	9412.3	0.6723	1613.4
9	0.02191848	16154.6	0.8361	2740.3
10	0.01891115	9427.7	0.6727	1616.0
11	0.02192354	16186.8	0.8363	2745.8
12	0.01888205	9393.3	0.6717	1610.1
13	0.02191037	16103.0	0.8358	2731.5
14	0.01890866	9424.8	0.6726	1615.5
15	0.02191406	16126.5	0.8359	2735.5
16	0.01885035	9355.8	0.6706	1603.7

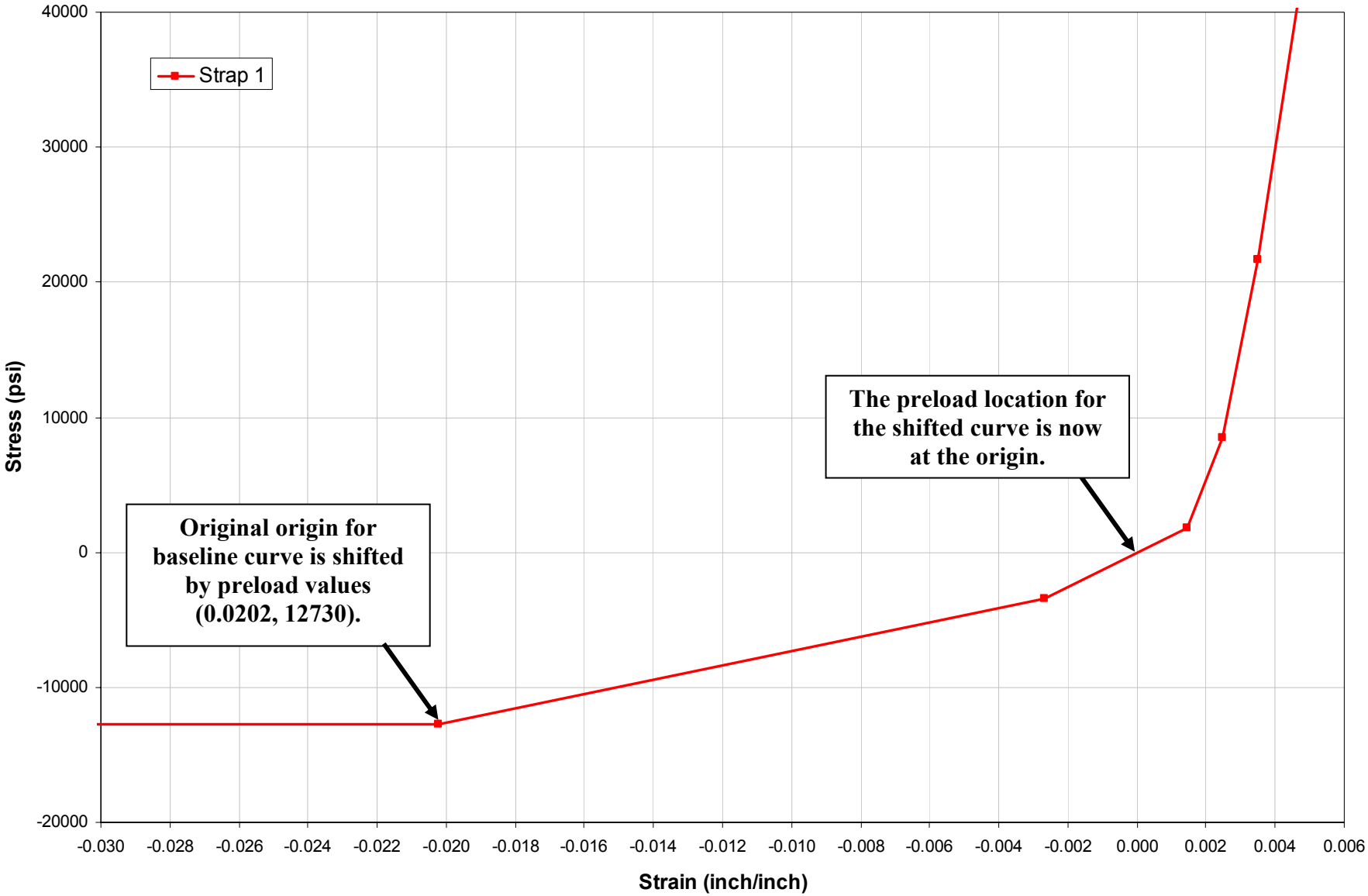

Figure 5-1 Stress-strain offset curve for strap 1 in x-axis test configuration

Baseline analyses were performed for each test configuration to identify the frequencies and modes assuming that the straps were loaded to the static preload condition and the first ten system modes are shown in Tables 6-1 through 6-3. These results show that for the strap stiffness values associated with the preload conditions, the frequency range associated with motion of the CMR ranges from 5 to 15 Hertz.

When the strap~~s~~ loads increase due to dynamic excitation, the frequencies that correspond to the resonance response shift to a larger frequency value.

Another aspect of the math model that influences the system modal characteristics is the method used to simulate the shaker interface constraint. For the physical hardware, the VCTF is attached to the shaker by a spherical coupler. In the simulation, the spherical coupler and shaker are not modeled. Modal assessments were made with the shaker interface unconstrained and compared to results for various combinations of constraints. The characteristics of the modes associated with the straps and CMR did not change when constraints were added at the shaker interface. However, applying constraints to the shaker interface introduces a flexure mode of the VCTF that is lower in frequency than the lowest VCTF flexure mode for the unconstrained case. It is anticipated that the actual frequency for the first VCTF flexure mode will be between the constrained and unconstrained frequencies.

7.0 Dynamic Load Conditions

The dynamic excitation for the sine sweep test will be applied using an electro-dynamic shaker manufactured by Ling (model 335). The shaker has a maximum force capability of approximately 18000 pounds. The excitation will be a sinusoidal force with a frequency that varies between 5 and 25 hertz at a linear rate of 0.5 hertz per second. The total duration of the excitation is 40 seconds for each test case. Sweep up cases will be performed with the frequency increasing from 5 to 25 hertz. Sweep down cases will also be performed with the frequency decreasing from 25 to 5 hertz.

Initially, test cases were developed with the objective of inducing forces in the straps that approximated the flight-level loads. Unfortunately, subsequent assessments of the VCTF showed that it does not have adequate strength to withstand the external loads that are required to induce these forces in the straps. As a result, the limiting criterion for the shaker excitation levels is the strength capability of the VCTF. This is not a significant issue, because the nonlinear response characteristics of the straps are observed at reduced excitation levels and correlation of these responses is the primary goal of the test.

Extensive pretest analyses have been performed to determine the maximum shaker excitation level that can be achieved for each test configuration and still have acceptable margins for the VCTF. Based on these pretest analyses a set of five load cases were identified as design cases for assessing structural margins:

(1) x-axis configuration with a shaker excitation of 0.28 g's
(2) y-axis configuration with a shaker excitation of 0.24 g's
(3) z-axis configuration with a shaker excitation of 0.68 g's

Table 6-1 Modal Frequencies for X-axis Test Configuration (shaker interface constrained in x)

Mode	Frequency (Hz)	Mode Description
1	0.00	Rigid-body motion of test fixture and test article
2	5.50	Motion of the CMR in the y-z plane
3	5.52	Motion of the CMR in the x-z plane
4	5.77	Rotation of the CMR about the z-axis
5	7.74	Rotation of the CMR about the x-axis
6	8.69	Rotation of the CMR about the y-axis
7	9.13	Motion of the CMR along the z-axis
8	24.73	First VCTF flexure mode, bending of the VCTF transition frame
9	30.39	Lateral motion (y-z plane) of the VCTF
10	37.02	Twisting of the VCTF about the z-axis

Table 6-2 Modal Frequencies for Y-axis Test Configuration (shaker interface constrained in y)

Mode	Frequency (Hz)	Mode Description
1	0.00	Rigid-body motion of test fixture and test article
2	5.50	Motion of the CMR in the y-z plane
3	5.52	Motion of the CMR in the x-z plane
4	5.77	Rotation of the CMR about the z-axis
5	7.74	Rotation of the CMR about the x-axis
6	8.69	Rotation of the CMR about the y-axis
7	9.13	Motion of the CMR along the z-axis
8	24.73	First VCTF flexure mode, bending of the VCTF transition frame
9	30.39	Lateral (x-z plane) motion of the VCTF
10	37.02	Twisting of the VCTF about the z-axis

Table 6-3 Modal Frequencies for Z-axis Test Configuration (shaker interface constrained in z)

Mode	Frequency (Hz)	Mode Description
1	0.00	Rigid-body motion of test fixture and test article
2	7.12	Lateral motion (x-y plane) of the CMR
3	8.54	Motion of the CMR in the x-z plane
4	9.22	Rotation of the CMR about the z-axis
5	11.46	Motion of the CMR along the x-axis
6	11.54	Rotation of the CMR about the x-axis
7	14.77	Rotation of the CMR about the y-axis
8	23.24	First VCTF flexure mode, bending of the VCTF transition frame
9	29.42	Lateral motion of the VCTF (x-y plane)
10	35.92	Twisting of the VCTF about the x-axis

(4) x-axis configuration with a shaker excitation of 0.35 g's
(5) y-axis configuration with a shaker excitation of 0.37 g's

Load cases 1 to 3 produce the maximum loads that can be sustained by all components of the VCTF. Load cases 4 and 5 produce the maximum loads that can be sustained by the VCTF with positive margins for all locations except for several welds. Stated in another way, the limit loads for the low-margin welds are defined by cases 1, 2, and 3, and the limit loads for the remainder of the structure are defined by cases 3, 4, and 5.

The procedures for conducting the test are intended to ensure that the limit loads at each critical location are not exceeded. The sine sweep test will be conducted as a series of runs with each run incrementally increasing the shaker input. The critical weld areas have the lowest margins and are predicted to reach their limit load at a lower excitation level. Therefore, strain gages will be used to monitor the loads at these locations and ensure that the limit loads are not exceeded. The limit loads for the remainder of the structure are closely correlated to the load levels in the magnet support straps; therefore, the loads in the straps will also be monitored during the test and used to limit the excitation to acceptable levels.

Nonlinear transient analyses were performed using math models for the x-axis, y-axis, and z-axis test configurations. A series of cases were assessed with sweep up and sweep down sinusoidal loading conditions and the excitation levels described above. The internal loads for the VCTF, magnet support straps, and the interface to the vacuum case were recovered for subsequent assessment of the stress margins. The results of the stress assessment for the test hardware are documented in ESCG-4450-05-STAN-DOC-0125, "Stress Analysis of the AMS-02 Vacuum Case Test Fixture".

8.0 Verification of Measurement Locations for the Sine Sweep Test

To allow for correlation between analysis and test, the response of the system will be measured and recorded as a function of time during the sine sweep test. The sixteen magnet support straps are instrumented with strain gage bridges to measure the axial force in the straps.

There is no practical method for measuring the displacement of the straps or the CMR; therefore, the motion of the CMR will be determined from acceleration measurements. Since the CMR is extremely rigid and does not have any flexure modes within the range of interest, the objective is to measure and characterize the rigid-body motion of the CMR. Theoretically, this can be accomplished with six properly located accelerometers; however, the vacuum case will be sealed and evacuated prior to the test, and replacement of faulty instrumentation will not be possible. Therefore, a redundant set of sixteen single-axis accelerometers have been installed on the CMR. The locations of the accelerometers are shown in Figure 8-1. Aluminum mounting blocks are used to attach the accelerometers to the CMR. Each block has two accelerometers — one is mounted to sense acceleration in the vertical (z-axis) direction and the other is mounted to sense

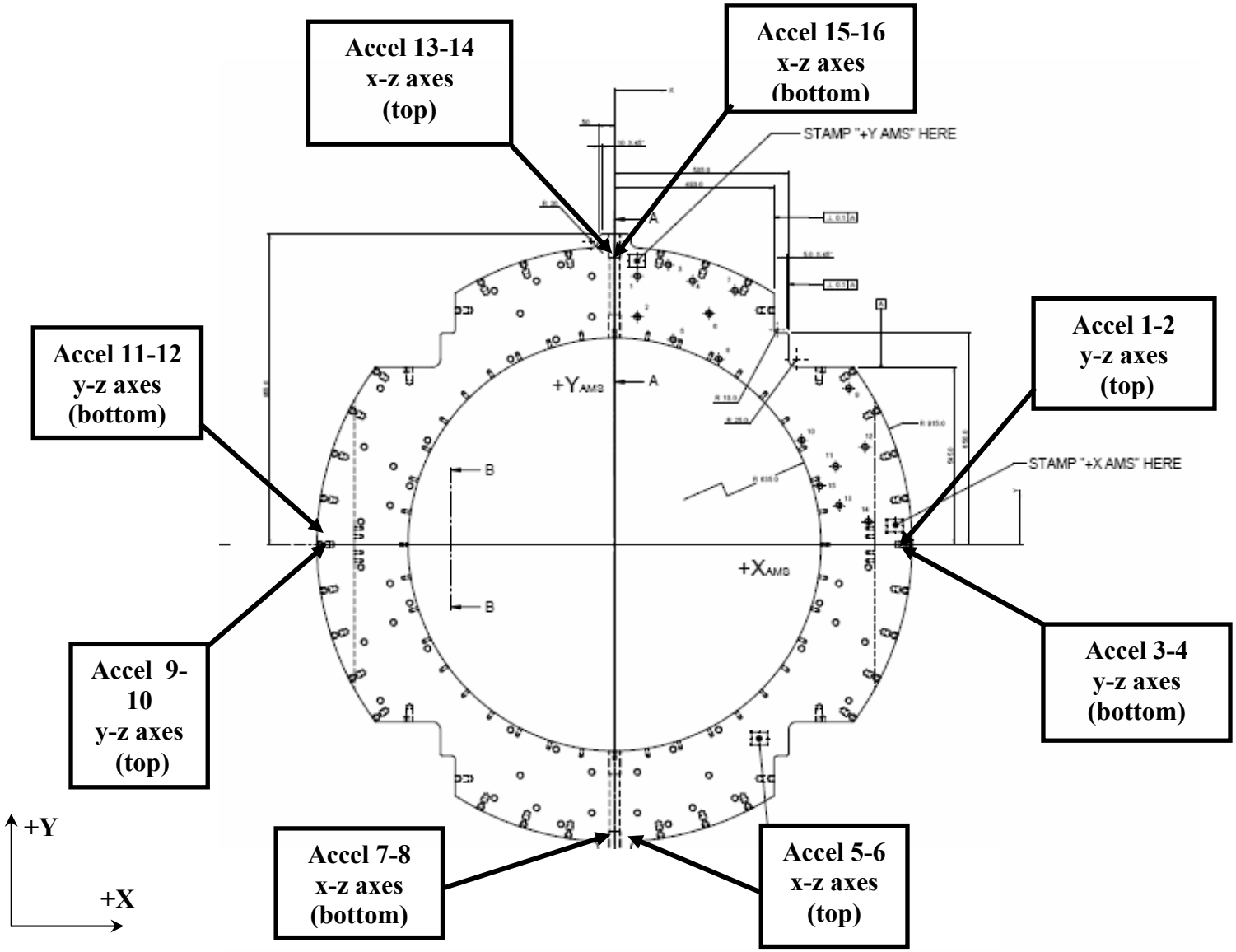

Figure 8-1 Location of single-axis accelerometers on cold mass replica

acceleration in the tangential direction. A photograph of a mounting block is shown in Figure 8-2.

The modal analysis of the test hardware predicts that the resonance frequency of the first flexural mode of the VCTF is slightly less than 25 Hertz when the test article is installed. Since there is the potential for vibration of the VCTF that may affect the measurements for the CMR, accelerometers have been mounted on the VCTF to measure this vibration. Figure 8-3 shows the locations of eight tri-axial accelerometers on the VCTF primary frame. Accelerometers will also be mounted on the VCTF transition frame (both x/y and z configurations) as shown in Figures 8-4 and 8-5 to provide feedback to the shaker controller. A tri-axial accelerometer will be mounted at the forward edge of the slip table to provide a reference measurement of the rigid-body motion of the entire system (refer to Figure 8-6). An accelerometer will also be mounted to the spherical coupling at the shaker interface to serve as a reference measurement (refer to Figure 8-7).

A series of modal analyses were performed to verify that the selected locations for the accelerometers are adequate for measuring the needed data. Modal assurance criteria (MAC) computations were used to determine if the accelerometer measurements were sufficient to capture the flexure motion of the VCTF. The MAC computation results for the selected set of accelerometers are shown in Tables 8-1 through 8-3 for the x-axis, y-axis, and z-axis test configurations (combined VCTF and test article). The MAC computation results for the empty VCTF configurations (x-axis and z-axis) are provided in Table 8-4 and Table 8-5. The computations use eigenvectors corresponding to the full, unreduced math model as the baseline, and compare these with eigenvectors for a reduced math model that only has DOF at the selected accelerometer locations. Values of 1.0 for the diagonal terms and 0.0 for the off-diagonal terms indicate perfect correlation between the modes of the full model and the modes based on the reduced measurement set.

Although the MAC computations show occurrences of mode swapping and cross coupling, the chosen set of accelerometers should allow the motion of the CMR to be adequately identified.

9.0 Predicted Dynamic Response of the Magnet Support Straps

The primary focus of the pre-test analysis is to predict the response of the magnet support straps when subjected to dynamic excitation. The nonlinear transient capability of MSC Nastran was used to simulate the sine sweep test. The large-mass method was used to enforce the desired acceleration at the node representing the interface to the shaker. A structural damping value of 0.14 was used for the magnet support straps and a value of 0.02 was used for the remainder of the structure.

Sweeps with the frequency increasing from 5 to 25 Hertz and sweeps with the frequency decreasing from 25 to 5 Hertz were simulated. For an excitation such as a sine sweep where the frequency changes with time, two deviations from a steady-state response will

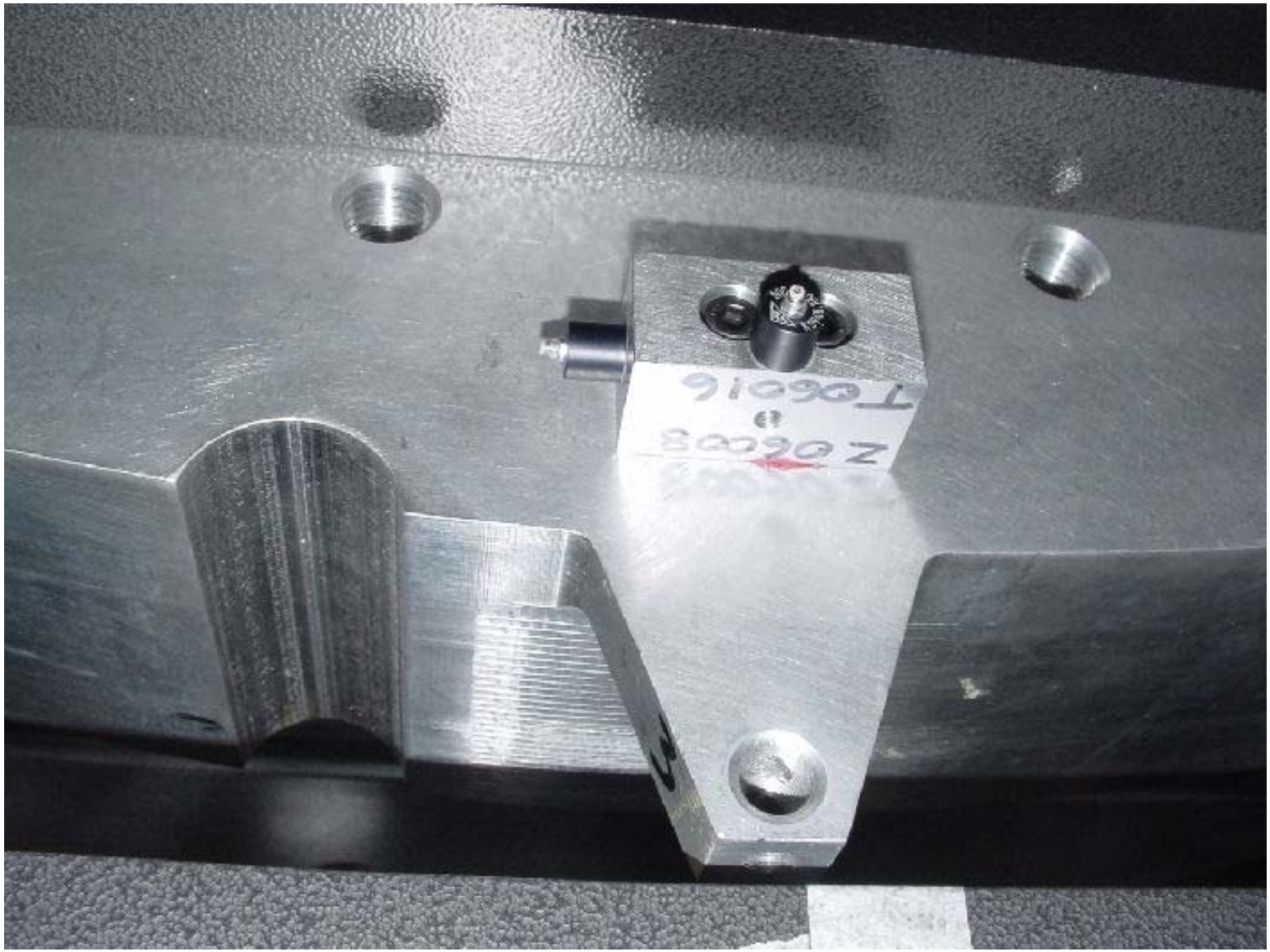

Figure 8-2 Mounting block for accelerometers on CMR

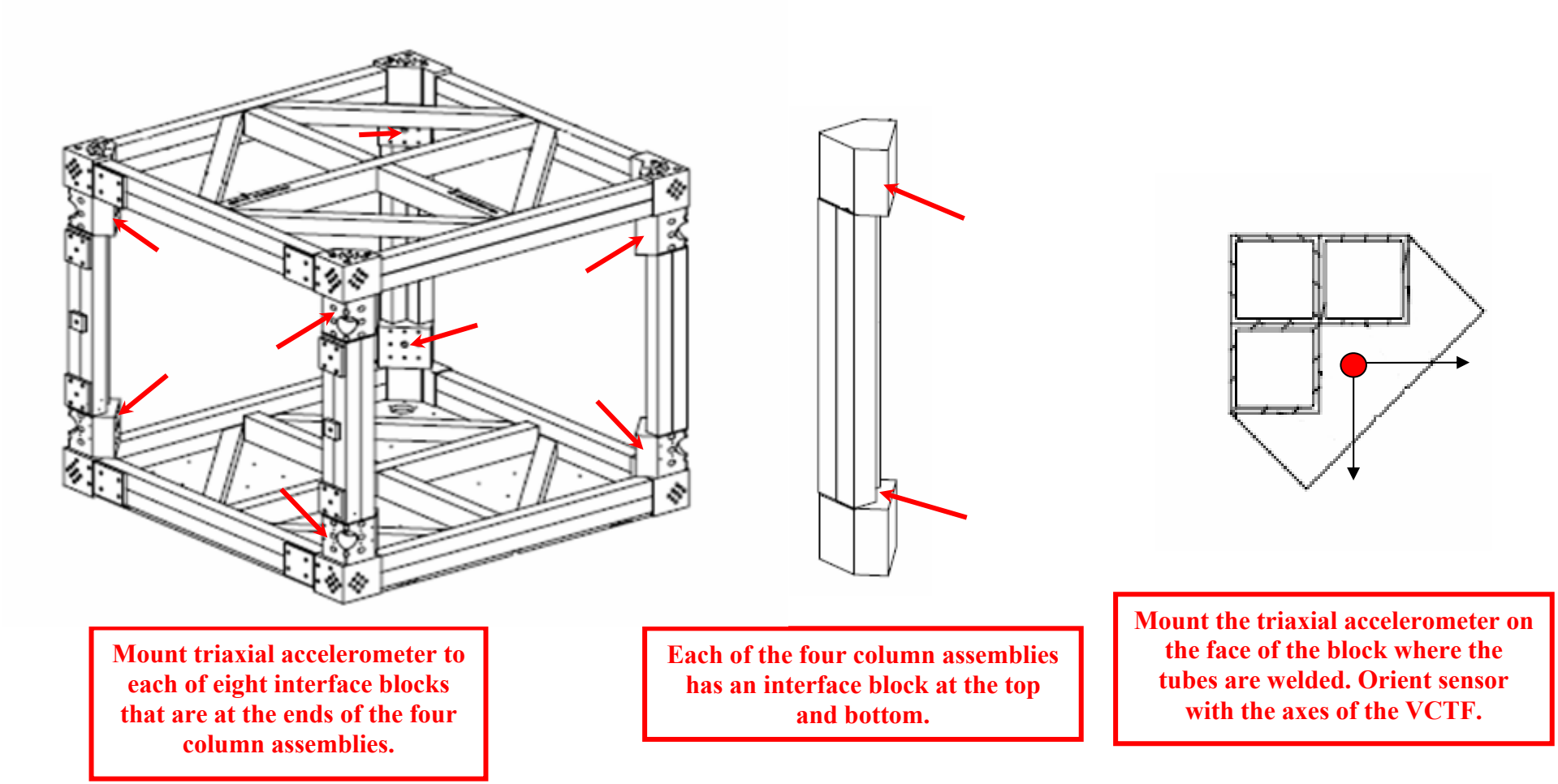

Figure 8-3 Location of the eight tri-axial accelerometers on the VCTF interface blocks

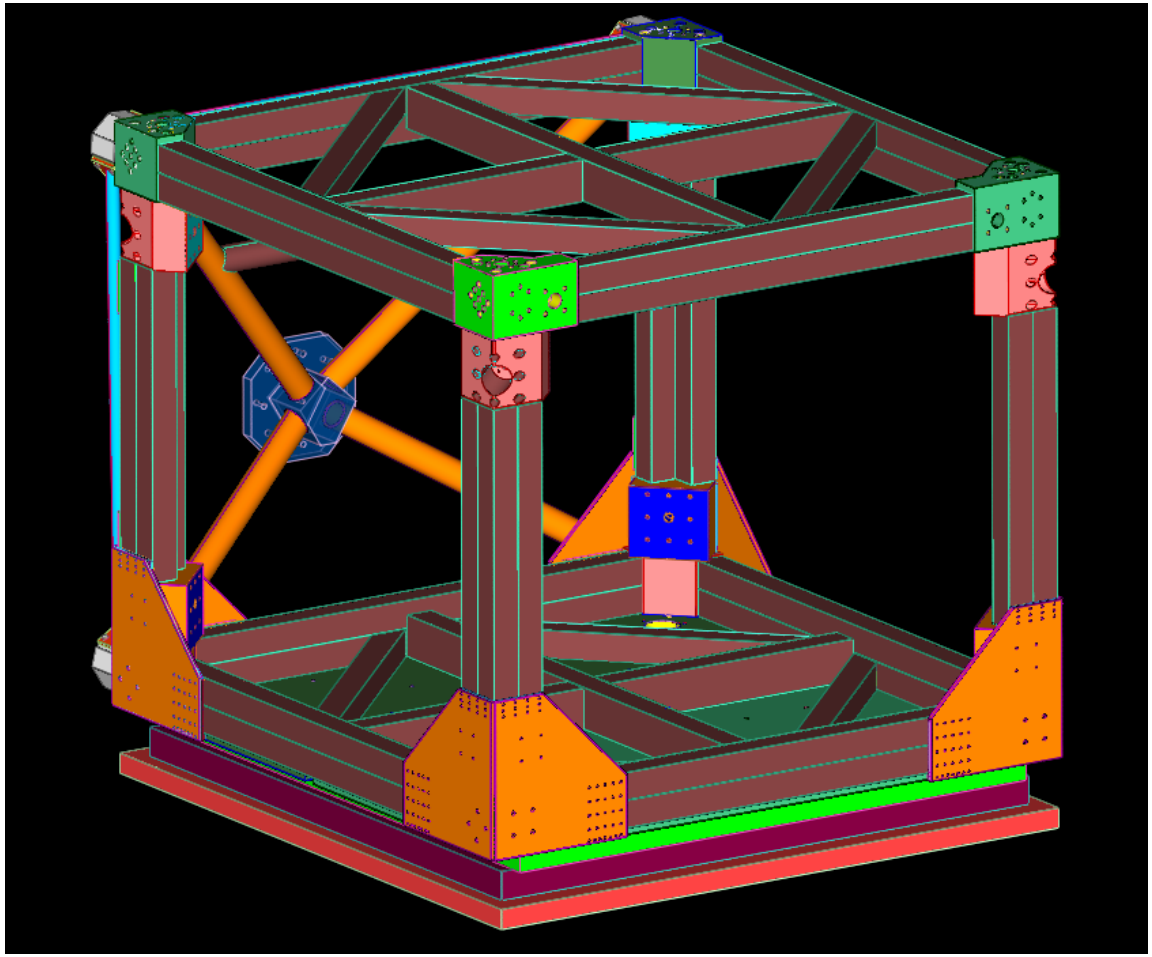

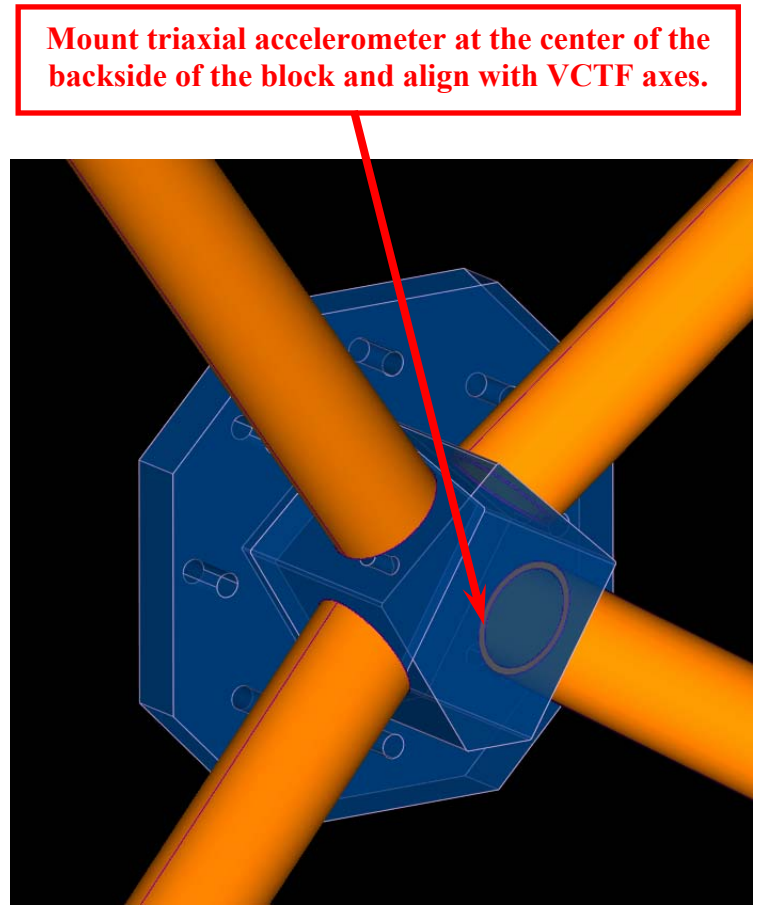

Figure 8-4 Location of accelerometer on the transition frame for the x-axis and y-axis test configurations

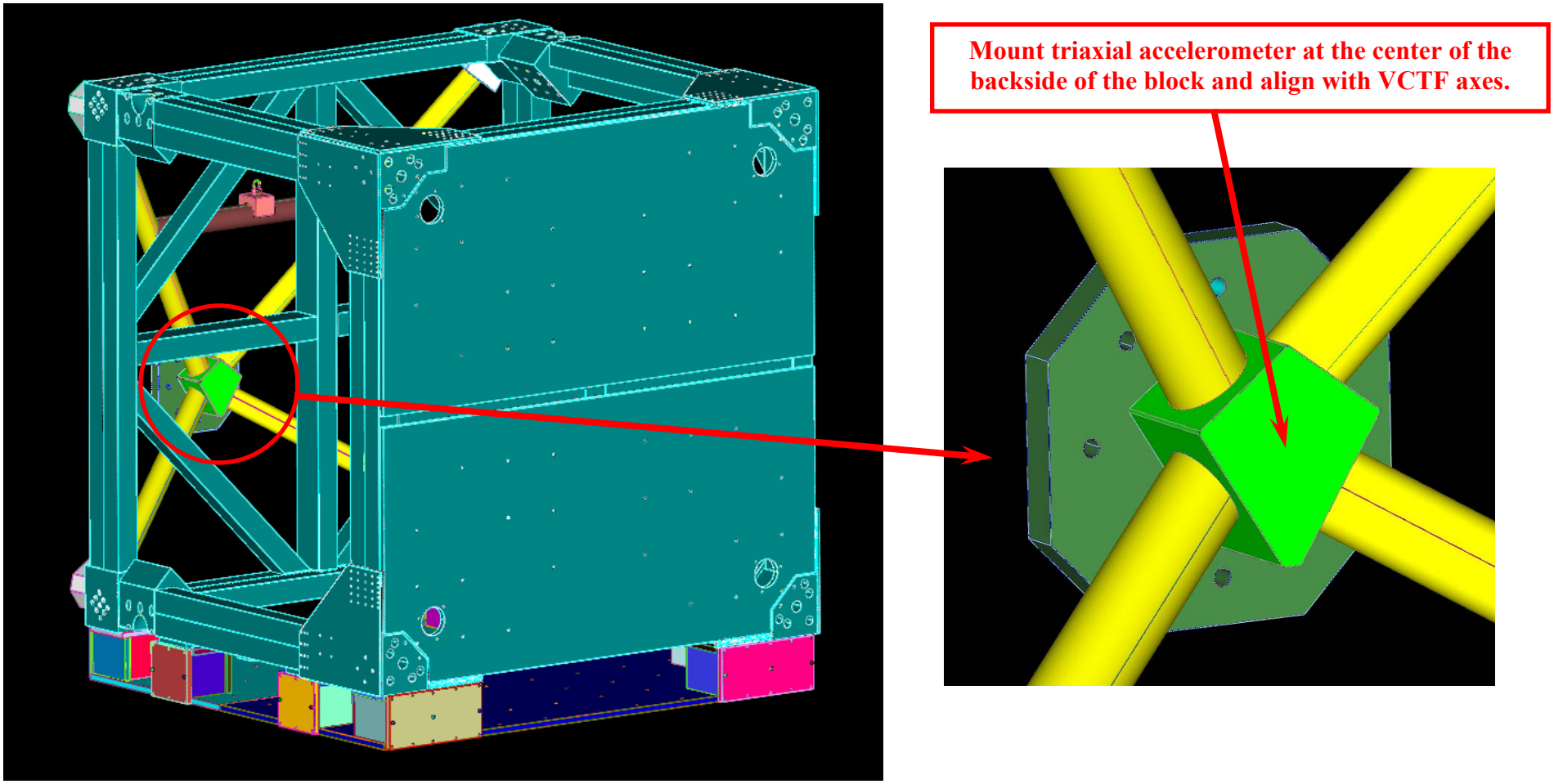

Figure 8-5 Location of accelerometer on the transition frame for the z-axis test configuration

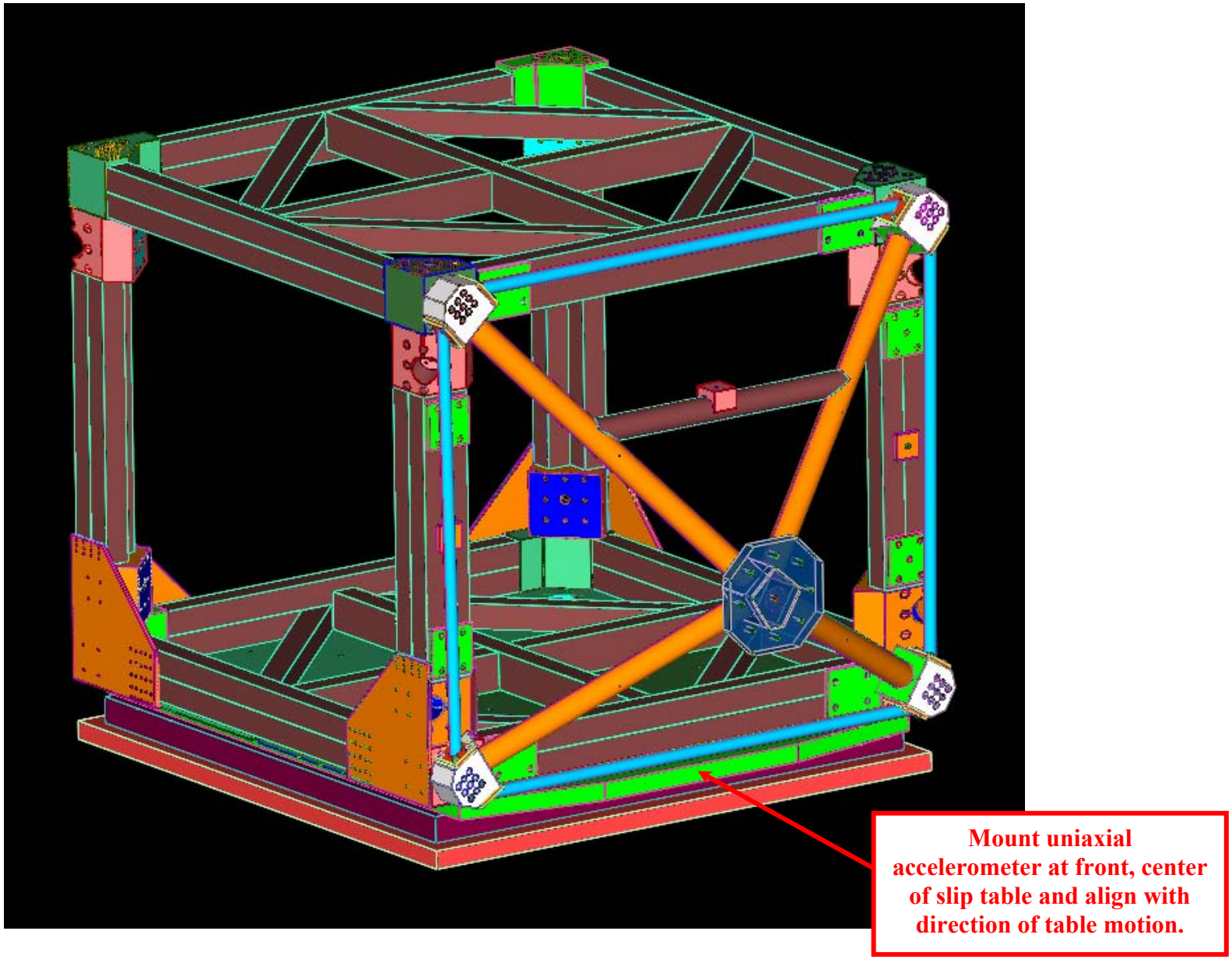

Figure 8-6 Location of reference accelerometer on the slip table

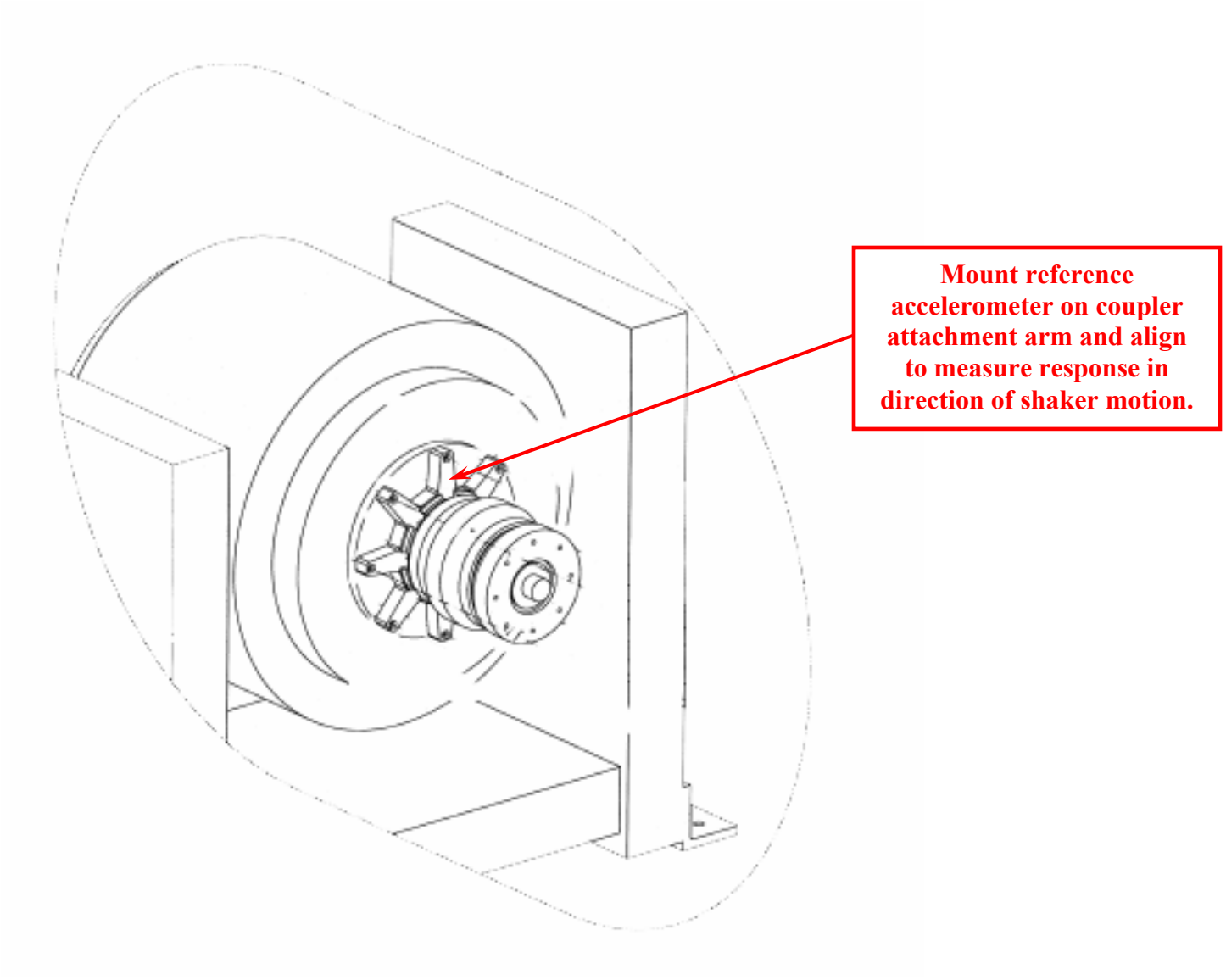

Figure 8-7 Location of the reference accelerometer on the spherical coupling

Table 8-1 Modal Assurance Criteria Calculations for the X-axis Test Configuration (VCTF with test article)

	FREQ	Description	1	2	3	4	5	6	7	8	9	10	11
1	0.000	Rigid-body motion of full system	**1.000**	0.000	**0.262**	0.000	0.000	0.025	0.000	**0.597**	0.000	0.000	0.122
2	5.504	Motion of the CMR in the y-z plane	**0.262**	0.002	**0.998**	0.000	0.000	0.036	0.000	0.000	0.000	0.000	0.000
3	5.515	Motion of the CMR in the x-z plane	0.000	**0.998**	0.002	0.000	0.053	0.000	0.000	0.000	0.000	0.000	0.000
4	5.770	Rotation of the CMR about the z-axis	0.000	0.000	0.000	**1.000**	0.000	0.000	0.000	0.000	0.000	0.000	0.000
5	7.741	Rotation of the CMR about the x-axis	0.000	0.035	0.000	0.000	**0.999**	0.000	0.000	0.000	0.000	0.000	0.000
6	8.687	Rotation of the CMR about the y-axis	0.024	0.000	0.037	0.000	0.000	**1.000**	0.000	0.000	0.000	0.000	0.000
7	9.126	Motion of the CMR along the z-axis	0.000	0.000	0.000	0.000	0.000	0.000	**1.000**	0.000	0.000	0.000	0.000
8	24.730	Flexure of the transition frame	**0.597**	0.000	0.000	0.000	0.000	0.000	0.000	**1.000**	0.000	0.000	0.117
9	30.391	Lateral motion (y-z plane) of VCTF	0.000	0.000	0.000	0.000	0.000	0.000	0.000	0.000	**1.000**	0.002	0.000
10	37.019	Twisting of VCTF about z-axis	0.000	0.000	0.000	0.000	0.000	0.000	0.000	0.000	0.000	**1.000**	0.000
11	38.140	Pitching motion of VCTF in x-z plane	0.128	0.000	0.000	0.000	0.000	0.000	0.000	0.126	0.000	0.000	**1.000**

NOTE: The MAC calculations are based on a set of predicted mode shapes with 16 DOF for the CMR, 24 DOF for the VCTF interface blocks, 3 DOF at the shaker interface, and 3 DOF at the front of the slip table (total of 46 DOF)

Table 8-2 Modal Assurance Criteria Calculations for the Y-axis Test Configuration (VCTF with test article)

	FREQ	Description	1	2	3	4	5	6	7	8	9	10	11
1	0.000	Rigid motion of system	**1.000**	0.000	0.000	0.001	0.001	0.000	0.000	0.000	0.012	0.050	0.037
2	5.504	Motion of the CMR in the y-z plane	0.000	**1.000**	0.000	0.000	0.000	0.037	0.000	0.000	0.000	0.000	0.000
3	5.515	Motion of the CMR in the x-z plane	0.000	0.000	**1.000**	0.000	0.000	0.000	0.000	0.000	0.000	0.000	0.000
4	5.770	Rotation of the CMR about the z-axis	0.000	0.000	0.000	**1.000**	0.065	0.000	0.000	0.000	0.002	0.008	0.005
5	7.741	Rotation of the CMR about the x-axis	0.000	0.000	0.000	0.044	**0.998**	0.000	0.000	0.000	0.002	0.009	0.007
6	8.687	Rotation of the CMR about the y-axis	0.000	0.038	0.000	0.000	0.000	**1.000**	0.000	0.000	0.000	0.000	0.000
7	9.126	Motion of the CMR along the z-axis	0.000	0.000	0.000	0.000	0.000	0.000	**1.000**	0.000	0.000	0.000	0.000
8	24.730	Flexure of the transition frame	0.000	0.000	0.000	0.000	0.000	0.000	0.000	**1.000**	0.001	0.000	0.000
9	30.391	Lateral (x-z plane) motion of the VCTF	0.002	0.000	0.000	0.000	0.000	0.000	0.000	0.000	**0.931**	0.213	0.011
10	37.019	Twisting of the VCTF about the z-axis	0.075	0.000	0.000	0.015	0.015	0.000	0.000	0.000	0.039	**0.839**	**0.510**
11	38.140	Pitching of the VCTF on the y-z plane	0.014	0.000	0.000	0.003	0.003	0.000	0.000	0.000	0.001	0.003	0.295

NOTE: The MAC calculations are based on a set of predicted mode shapes with 16 DOF for the CMR, 24 DOF for the VCTF interface blocks, 3 DOF at the shaker interface, and 3 DOF at the front of the slip table (total of 46 DOF)

Table 8-3 Modal Assurance Criteria Calculations for the Z-axis Test Configuration (VCTF with test article)

	FREQ	Description	1	2	3	4	5	6	7	8	9	10	11
1	0.00	Rigid-body motion of full system	**1.000**	0.000	**0.277**	0.000	0.000	0.000	**0.473**	0.029	0.000	0.000	0.025
2	7.12	Lateral motion (x-y plane) of the CMR	0.000	**1.000**	0.000	0.001	0.000	0.000	0.000	0.000	0.000	0.000	0.000
3	8.54	Motion of the CMR in the x-z plane	**0.277**	0.000	**1.000**	0.000	0.000	0.000	0.000	0.010	0.000	0.000	0.000
4	9.22	Rotation of the CMR about the z-axis	0.000	0.000	0.000	**1.000**	0.000	0.000	0.000	0.000	0.000	0.000	0.000
5	11.46	Motion of the CMR along the x-axis	0.000	0.000	0.000	0.000	**1.000**	0.000	0.000	0.000	0.000	0.000	0.000
6	11.54	Rotation of the CMR about the x-axis	0.000	0.000	0.000	0.000	0.000	**1.000**	0.000	0.000	0.000	0.000	0.000
7	14.77	Rotation of the CMR about the y-axis	**0.477**	0.000	0.001	0.000	0.000	0.000	**1.000**	0.092	0.000	0.000	0.000
8	23.24	Flexure of the transition frame	0.019	0.000	0.012	0.000	0.000	0.000	0.113	**0.999**	0.000	0.000	0.029
9	29.42	Lateral motion of the VCTF (x-y plane)	0.000	0.000	0.000	0.000	0.000	0.000	0.000	0.000	**0.999**	0.006	0.000
10	35.92	Twisting of the VCTF about the x-axis	0.000	0.000	0.000	0.000	0.000	0.001	0.000	0.000	0.002	**0.999**	0.000
11	37.19	Pitching of the VCTF in the x-z plane	0.023	0.000	0.000	0.000	0.000	0.000	0.000	0.047	0.000	0.000	**0.998**

NOTE: The MAC calculations are based on a set of predicted mode shapes with 16 DOF for the CMR, 24 DOF for the VCTF interface blocks, 3 DOF at the shaker interface, and 3 DOF at the front of the slip table (total of 46 DOF)

Table 8-4 Modal Assurance Criteria Calculations for the Empty (VCTF only) X-axis Test Configuration

	FREQ	Description	1	2	3	4	5
1	0.00	rigid-body motion of VCTF	**1.000**	0.022	0.000	**0.736**	0.000
2	20.16	Pitching motion of VCTF in x-z plane	0.025	**1.000**	0.000	0.072	0.000
3	24.08	Lateral motion of VCTF in y-z plane	0.000	0.000	**1.000**	0.000	0.027
4	30.85	Pitching motion of VCTF in x-z plane	**0.722**	0.087	0.000	**1.000**	0.000
5	35.56	Lateral motion of VCTF in y-z plane	0.000	0.000	0.015	0.000	**0.999**

NOTE: The MAC calculations are based on a set of predicted mode shapes with 24 DOF for the VCTF interface blocks, 3 DOF at the shaker interface, and 3 DOF at the front of the slip table (total of 30 DOF)

Table 8-5 Modal Assurance Criteria Calculations for the Empty (VCTF only) Z-axis Test Configuration

	FREQ	Description	1	2	3	4	5
1	0.00	rigid-body motion of VCTF	**1.000**	0.007	**0.685**	0.000	0.000
2	18.68	Pitching motion of VCTF (x-z plane)	0.006	**1.000**	0.170	0.000	0.000
3	23.14	Pitching motion of VCTF (x-z plane)	**0.688**	0.166	**1.000**	0.000	0.000
4	30.99	Lateral motion (x-y plane) with twisting	0.000	0.000	0.000	**0.990**	0.007
5	35.03	Lateral motion (x-y plane) with twisting	0.000	0.000	0.000	0.028	**0.976**

NOTE: The MAC calculations are based on a set of predicted mode shapes with 24 DOF for the VCTF interface blocks, 3 DOF at the shaker interface, and 3 DOF at the front of the slip table (total of 30 DOF)

be observed. The first deviation is the magnitude of the peak response will be reduced. As the sweep rate increases the reduction in magnitude will be more prominent. The second deviation is the frequency of the response will be shifted from the steady-state resonance frequency. For sweeps with increasing frequency, the peak response will shift to a higher frequency. For sweeps with increasing frequency, the peak response will shift to a lower frequency. This shift in frequency also becomes more pronounced when the sweep rate is increased.

A magnitude of 0.05 g's was chosen as the minimum excitation level. This excitation is sufficient to produce measurable responses in the straps while maintaining a linear response for most of the straps. A series of larger excitation levels were also simulated that produce nonlinear strap response. The maximum excitation level for each test configuration is limited by the structural capability of the VCTF. As discussed previously in section 7, the maximum excitation levels for each configuration are:

(1) x-axis configuration with a shaker excitation of 0.35 g's
(2) y-axis configuration with a shaker excitation of 0.37 g's
(3) z-axis configuration with a shaker excitation of 0.68 g's

The maximum predicted responses for the magnet support straps are summarized in Tables 9-1 through 9-3 for the x-axis, y-axis, and z-axis test configurations, respectively. During the static test to failure of the magnet support strap, yielding first occurred at 28500 pounds and failure occurred at 42860 pounds. The maximum strap response during the sine sweep test is predicted to be 12730 pounds and occur at the 0.68 g excitation level for the z-axis test configuration. Thus, there is adequate protection for uncertainty in the pretest predictions.

The strap response data from the sine sweep simulations provides the axial force and displacement data for each strap as a function of time. Plots of the force and displacement as a function of time, as well as plots of force versus displacement are shown in Figures 9-1 through 9-36 for the straps with the largest peak response (yellow highlight in Table 9-1) and smallest peak response (green highlight in Table 9-1) in the x-axis configuration. The corresponding plots for the y-axis configuration are provided in Figures 9-37 through 9-72. The corresponding plots for the z-axis configuration are provided in Figures 9-73 through 9-108. Plots of all the straps for each excitation case are available upon request.

For the lowest planned excitation level of 0.05 g's, the response of each strap is such that it remains on the same linear segment of the force-displacement curve that it was preloaded to. This is illustrated in Figure 9-3 and Figure 9-6 by the response of straps 1 and 2 for the x-axis case. The y-axis and z-axis configurations have similar response characteristics at the lowest excitation level. For the increased excitation levels, the straps with the largest response magnitude are clearly in the nonlinear region of the force-displacement curve. This is illustrated in Figure 9-15 and Figure 9-27 by the response of strap 7 for the x-axis case at 0.28 and 0.35 g's excitation. The y-axis and z-axis configurations have similar response characteristics for the increased excitation levels.

Plots of the strap response data are also provided as a function of excitation frequency by converting the response data as a function of time to frequency using the following relationship: frequency(Hz) = 5 + 0.5 * time(secs). The magnitudes of the curves represent an upper bound of the time history data. The fluctuations that appear to be data drop outs in some of the envelopes are an artifact of the data post-processing and should be ignored. This data is presented in Figures 9-109 through 9-156 for the x-axis, Figures 9-157 through 9-204 for the y-axis, and Figures 9-205 through 9-252 for the z-axis. The figures show curves for both the sweep up and the sweep down cases.

As mentioned previously in this section, the frequency of resonance will shift somewhat from the resonance expected with a steady-state excitation. This phenomenon is easily observed in the frequency response plots when the sweep up and sweep down have resonances at different frequencies for the low level excitation cases. The strap response for the x-axis configuration with 0.05 g's excitation is shown in Figures 9-109 through 9-124. The primary resonance for the sweep up occurs at approximately 5.9 hertz and the primary resonance for the sweep down occurs at approximately 5.2 hertz. The modal analysis predicted that this resonance should have been at 5.5 hertz (refer to Table 6-1) which is about midway between the sweep up and sweep down peaks. This frequency shift due to sweeping will also occur for the higher excitation levels, but the difference in the sweep up and sweep down responses is then dominated by the nonlinear jump phenomenon (refer to Figure 9-237).

Table 9-1 Maximum Responses of the Magnet Support Straps for the X-axis Test Configuration

Strap ID	Sweep Up 0.05 g's	Sweep Down 0.05 g's	Sweep Up 0.28 g's	Sweep Down 0.28 g's	Sweep Up 0.35 g's	Sweep Down 0.35 g's
1	2382.3	2384.9	4714.8	4193.3	5642.6	4759.5
2	2161.3	2155.3	2777.7	2593.7	2881.4	2756.0
3	1712.7	1704.6	5959.0	5247.4	7047.8	6200.5
4	1460.9	1458.3	1780.8	1717.2	1837.5	1780.2
5	2382.0	2384.8	4679.2	4069.6	5623.4	4669.5
6	2158.8	2153.0	2769.3	2605.4	2874.7	2756.2
7	1710.0	1702.2	5961.4	5232.3	7052.2	6353.7
8	1464.9	1462.2	1791.6	1726.4	1846.8	1790.6
9	2381.2	2382.6	4679.2	4116.3	5622.9	4850.1
10	2161.1	2155.1	2741.3	2603.9	2838.1	2735.2
11	1718.0	1710.0	5929.4	5227.3	7005.4	6363.5
12	1462.6	1460.3	1784.6	1722.0	1840.1	1789.8
13	2377.1	2378.8	4640.1	4014.6	5590.9	4711.7
14	2160.6	2155.1	2762.3	2625.0	2853.0	2761.6
15	1715.1	1707.3	5918.1	5253.1	7002.3	6396.4
16	1461.0	1458.4	1771.3	1708.2	1829.6	1768.4

Table 9-2 Maximum Responses of the Magnet Support Straps for the Y-axis Test Configuration

Strap ID	Sweep Up 0.05 g's	Sweep Down 0.05 g's	Sweep Up 0.24 g's	Sweep Down 0.24 g's	Sweep Up 0.37 g's	Sweep Down 0.37 g's
1	2302.3	2294.6	4802.7	3187.7	5606.7	3369.9
2	2239.4	2249.2	5152.1	3936.4	7899.4	4873.5
3	1502.2	1498.6	1793.8	1790.9	1903.3	1887.6
4	1597.6	1599.4	4202.8	3921.3	7278.1	6046.2
5	2303.9	2294.3	3122.4	3149.3	3808.2	3322.8
6	2240.1	2246.9	3932.2	3881.2	5508.6	4756.4
7	1500.0	1497.8	2158.6	1790.2	2283.3	1904.8
8	1603.5	1607.8	4766.4	3938.8	7869.3	5945.0
9	2299.8	2292.7	3128.1	3200.0	3819.2	3460.0
10	2236.6	2249.6	3961.2	3932.0	6055.7	4688.5
11	1505.0	1501.9	2163.9	1786.8	2294.6	1872.7
12	1596.8	1603.6	4746.2	4000.2	8163.1	6361.2
13	2295.5	2289.1	4804.4	3218.5	6000.9	3489.6
14	2233.7	2248.7	5140.9	3986.9	7554.4	4789.8
15	1505.4	1501.0	1796.1	1777.6	1944.8	1855.0
16	1594.4	1599.4	4207.3	3989.6	7575.0	6324.2

Table 9-3 Maximum Responses of the Magnet Support Straps for the Z-axis Test Configuration

Strap ID	Sweep Up 0.05 g's	Sweep Down 0.05 g's	Sweep Up 0.40 g's	Sweep Down 0.40 g's	Sweep Up 0.68 g's	Sweep Down 0.68 g's
1	1357.6	1342.2	1925.1	1921.2	4191.0	2403.9
2	1769.0	1715.8	3175.2	3155.6	12684.5	7407.2
3	1358.5	1335.7	1928.3	1920.6	5703.7	2437.8
4	1767.6	1729.9	3145.7	3104.1	11092.8	7089.8
5	1357.2	1334.4	1925.7	1917.1	5695.3	2433.2
6	1766.1	1731.2	3134.0	3099.7	11122.7	7185.0
7	1357.1	1344.8	1923.0	1918.6	4339.0	2408.4
8	1777.8	1727.0	3199.6	3181.0	12729.6	7295.9
9	2943.1	2938.5	3900.0	3897.7	5547.0	4831.2
10	1657.4	1652.4	1888.1	1887.7	2077.8	2072.6
11	2946.2	2930.8	3892.7	3891.5	5574.1	4822.4
12	1651.4	1651.3	1880.9	1880.6	2174.8	2064.9
13	2934.6	2889.3	3874.9	3873.6	5539.2	4807.4
14	1656.8	1654.0	1886.4	1886.0	2077.9	2070.4
15	2937.0	2932.6	3865.9	3864.4	5585.4	4794.7
16	1644.6	1637.3	1873.5	1873.0	2156.8	2056.8

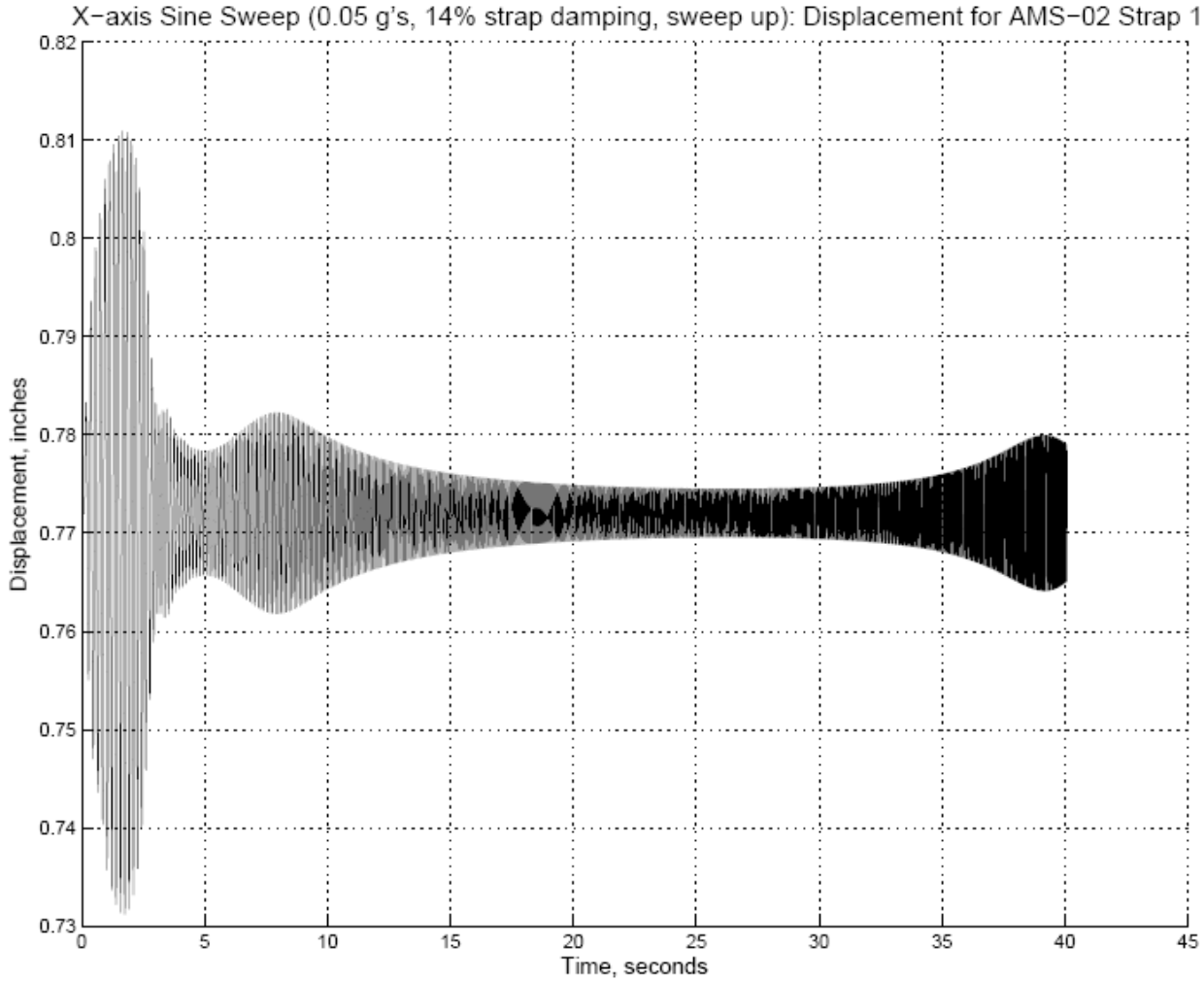

Figure 9-1 Strap 1 displacement response for x-axis configuration with 0.05 g sweep up

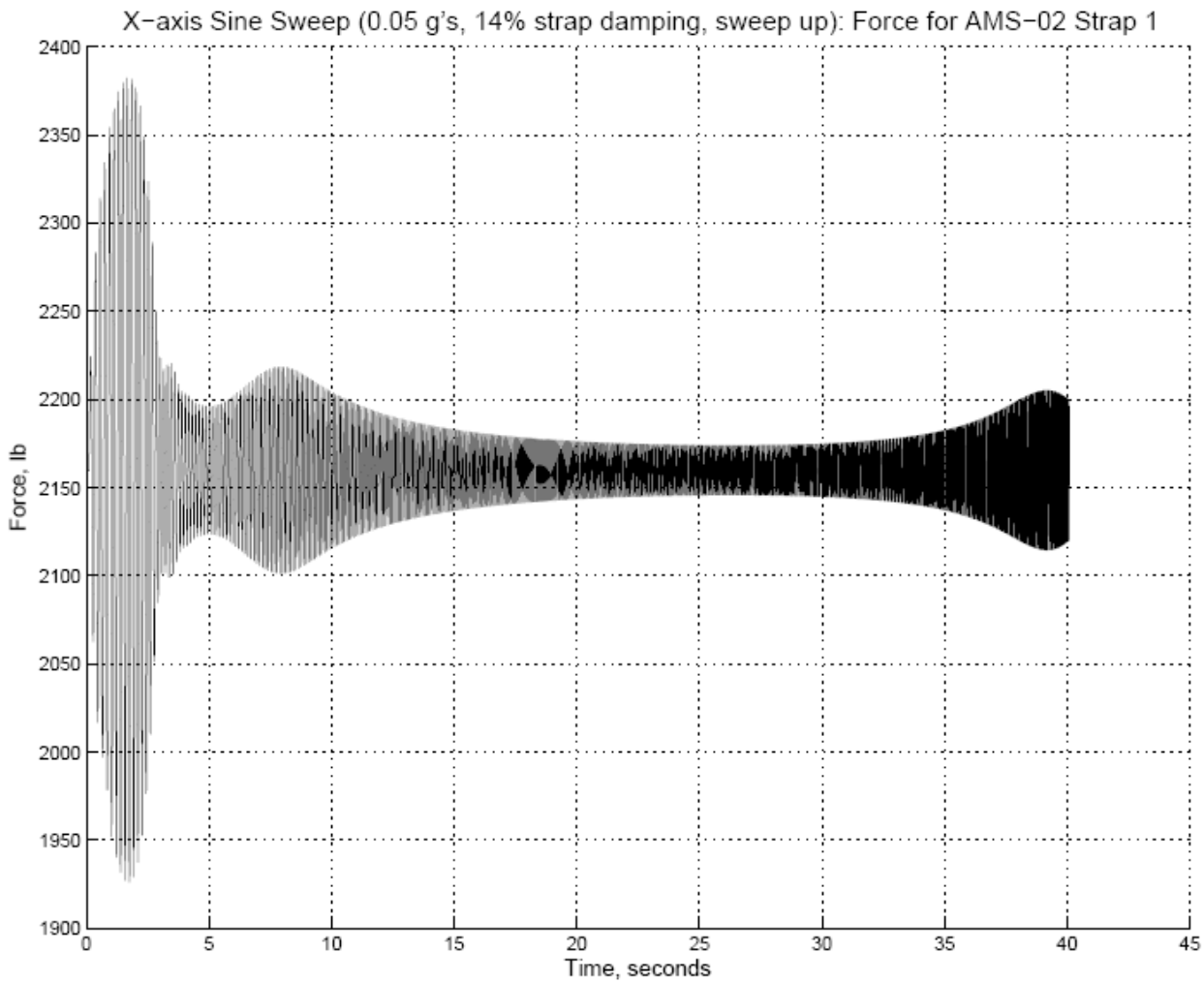

Figure 9-2 Strap 1 force response for x-axis configuration with 0.05 g sweep up

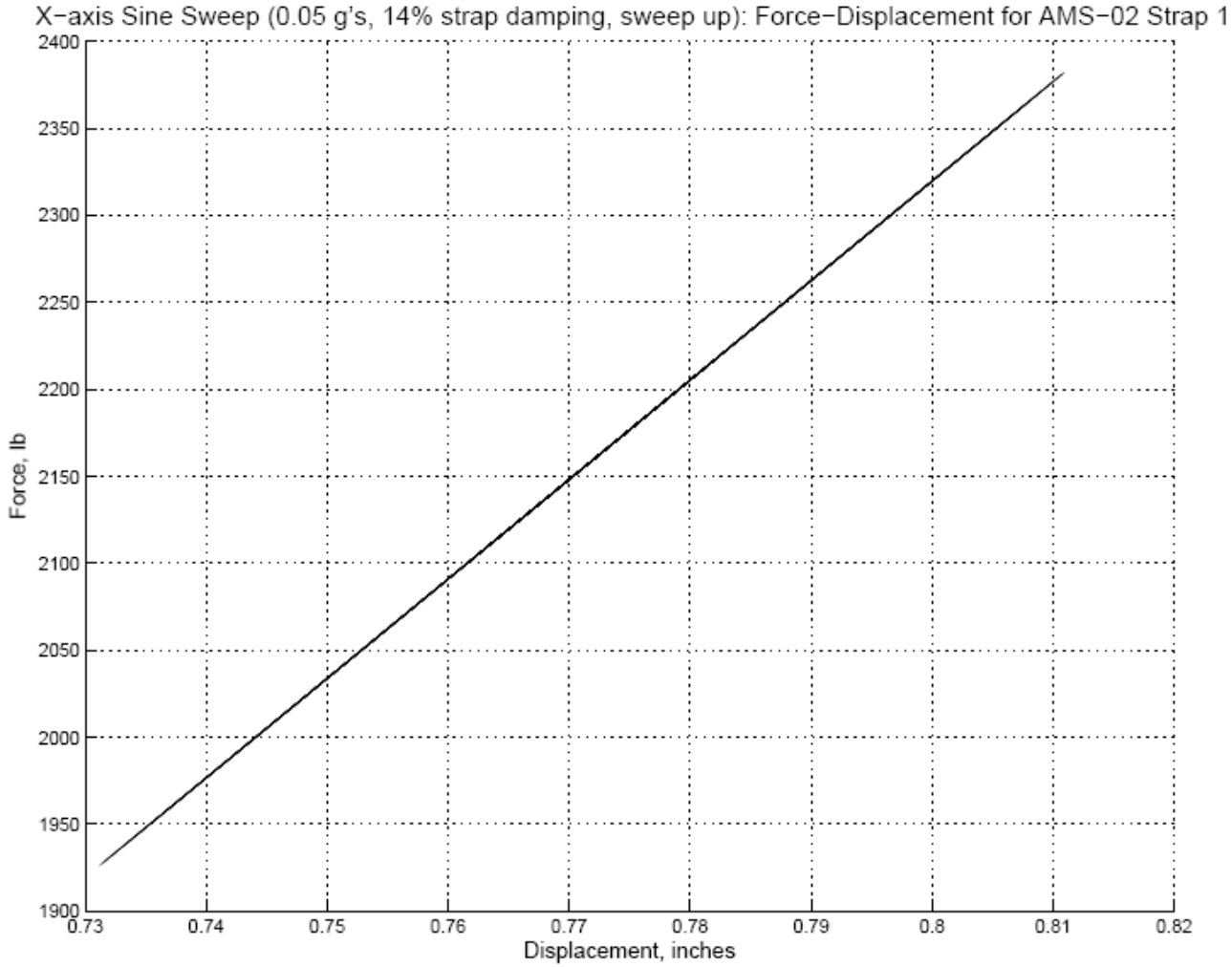

Figure 9-3 Strap 1 force-displacement curve for x-axis configuration with 0.05 g sweep up

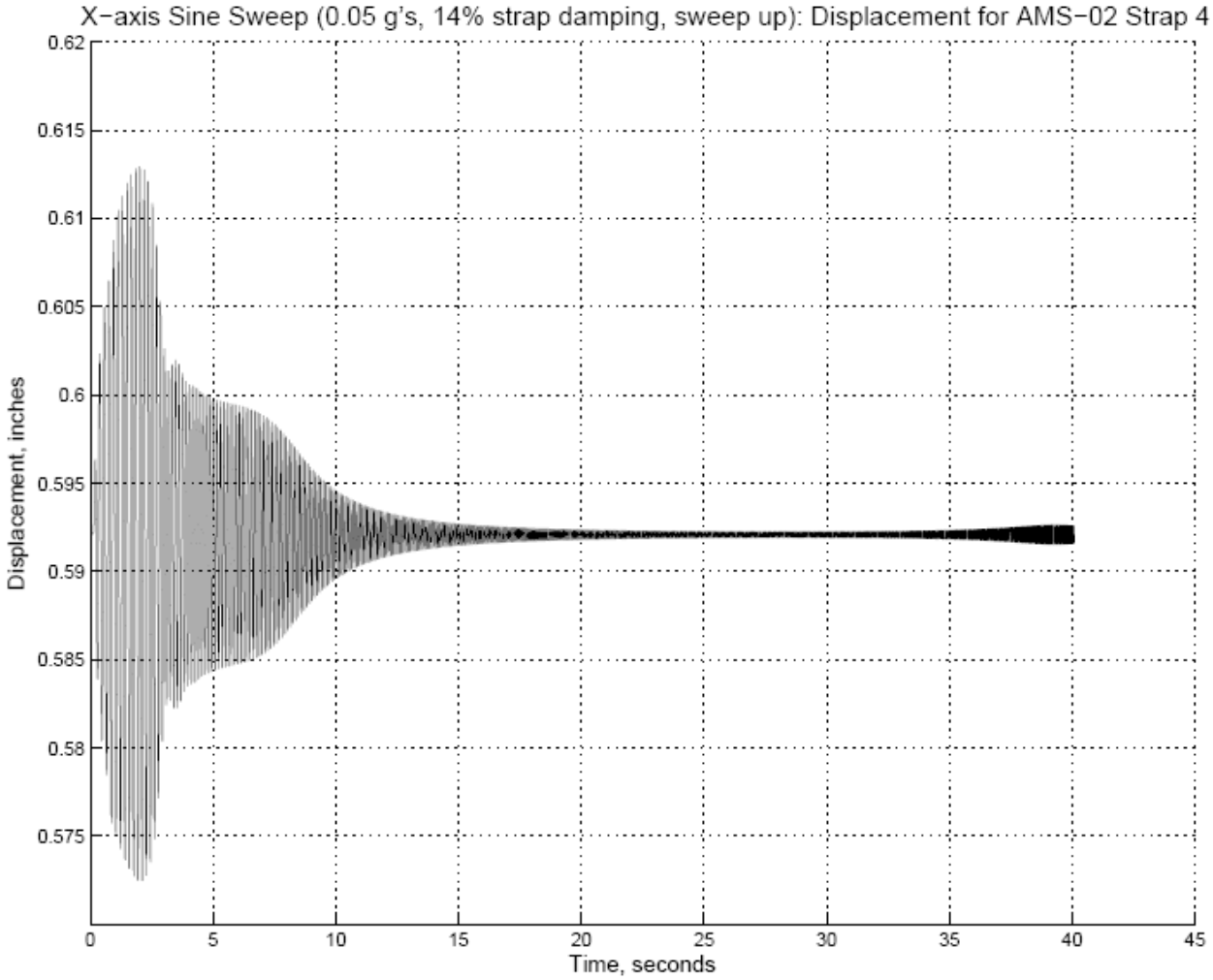

Figure 9-4 Strap 4 displacement response for x-axis configuration with 0.05 g sweep up

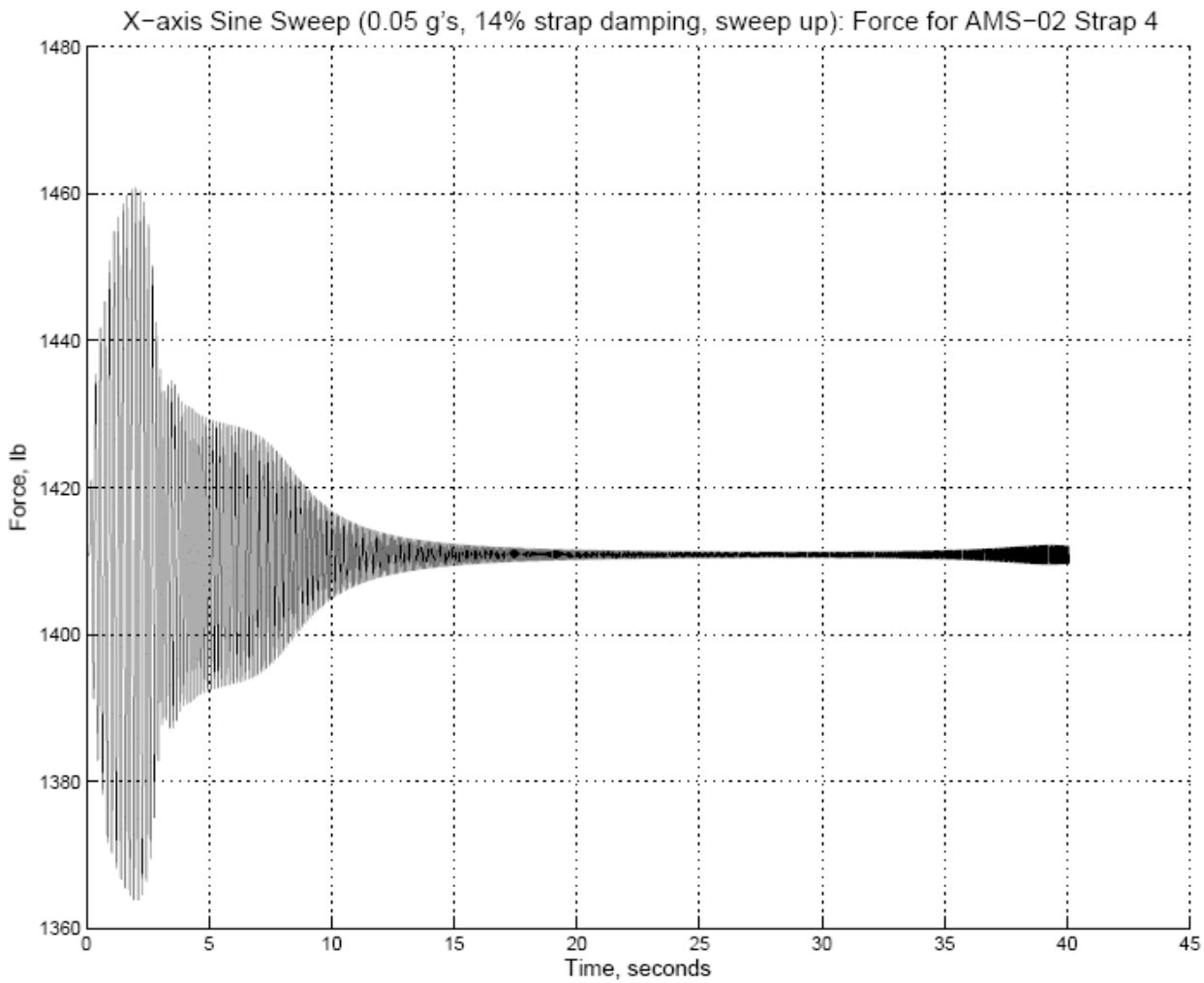

Figure 9-5 Strap 4 force response for x-axis configuration with 0.05 g sweep up

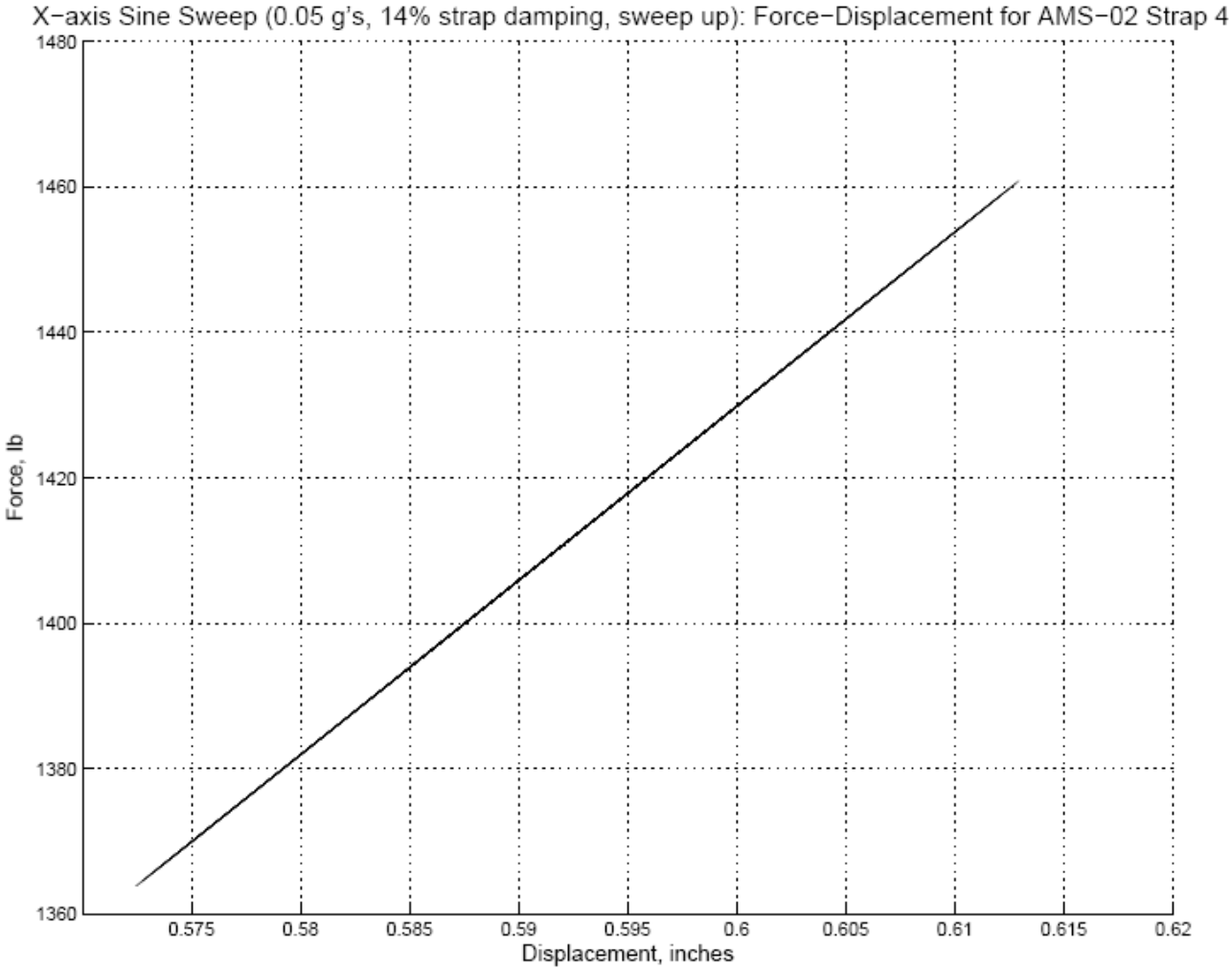

Figure 9-6 Strap 4 force-displacement curve for x-axis configuration with 0.05 g sweep up

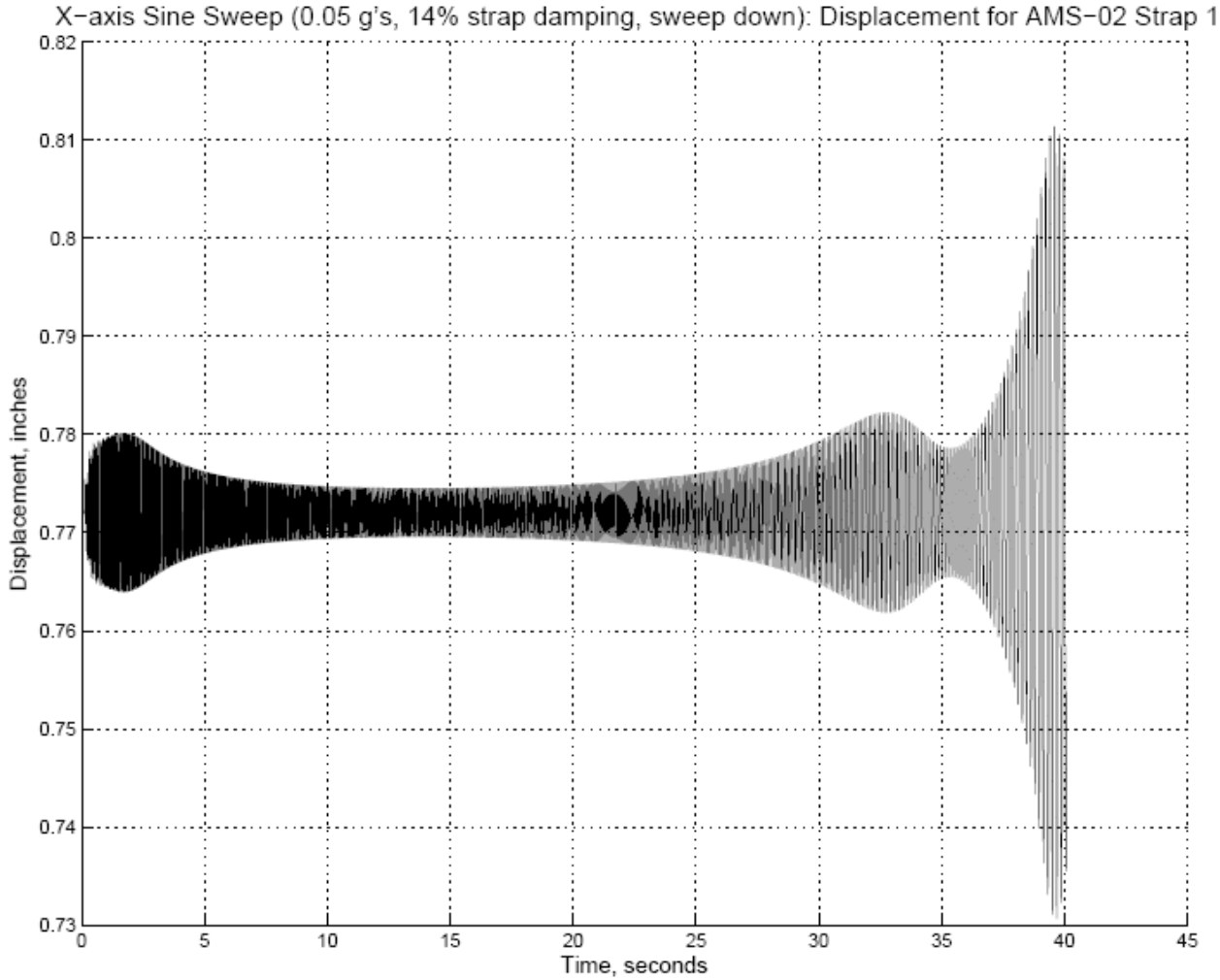

Figure 9-7 Strap 1 displacement response for x-axis configuration with 0.05 g sweep down

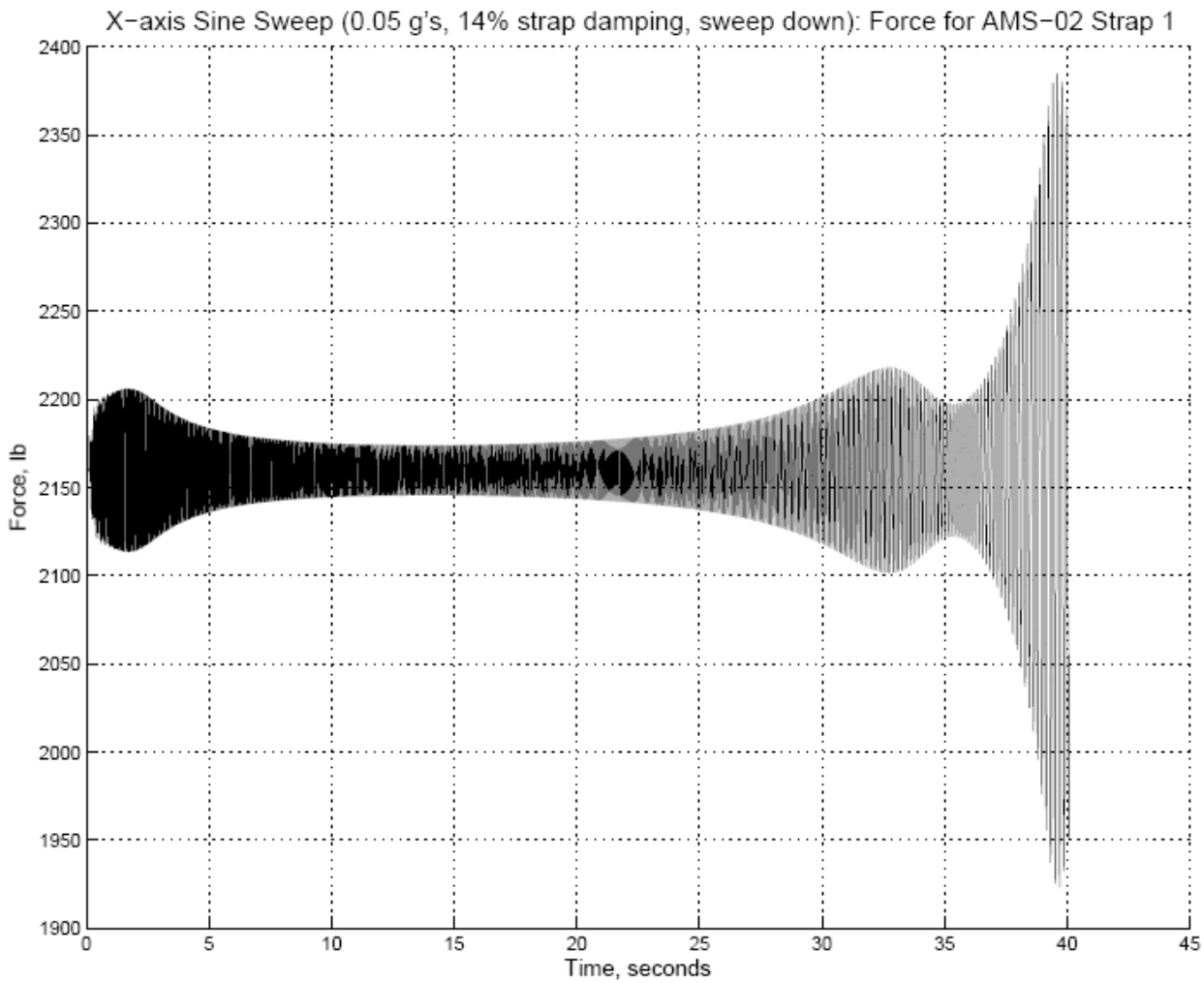

Figure 9-8 Strap 1 force response for x-axis configuration with 0.05 g sweep down

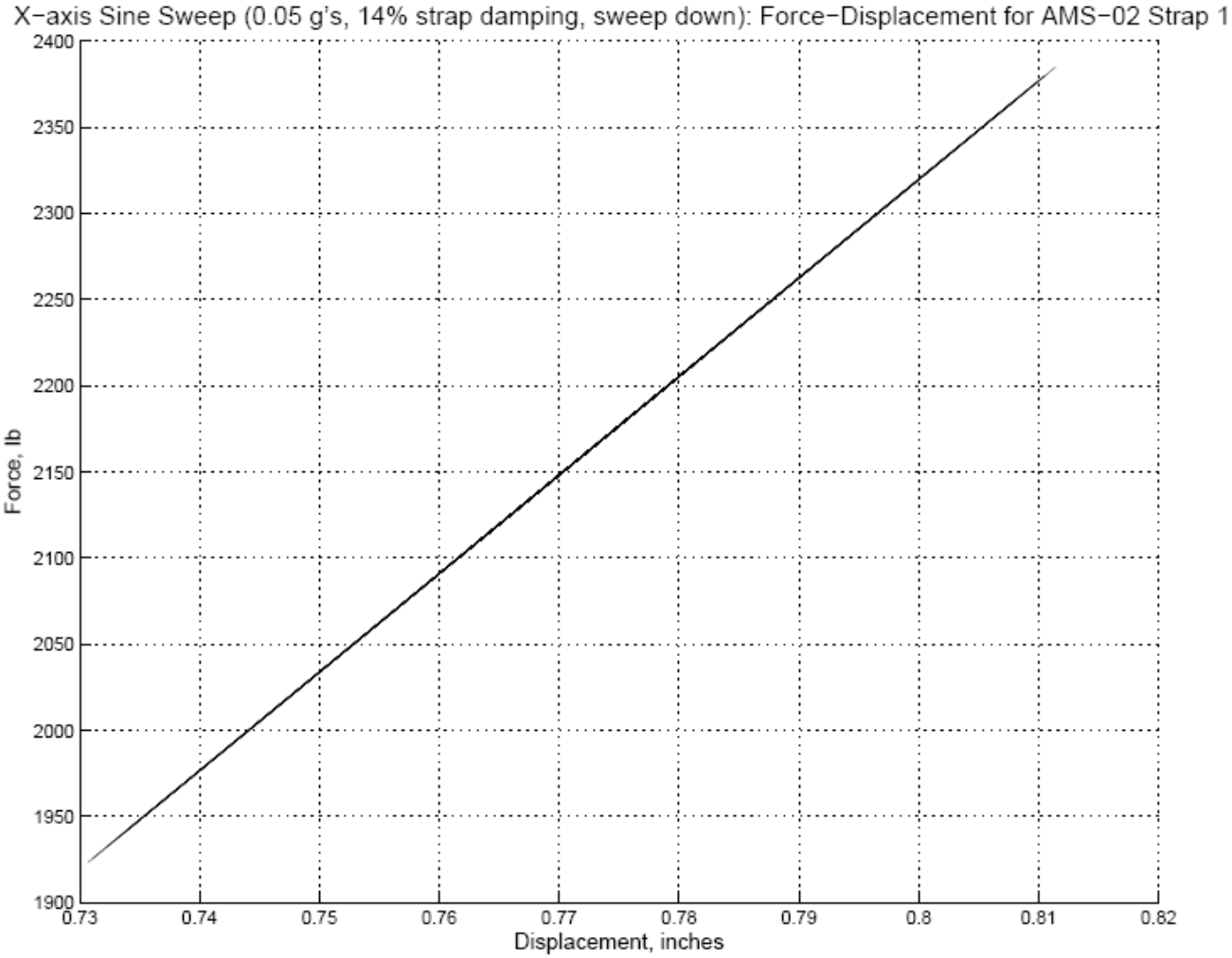

Figure 9-9 Strap 1 force-displacement curve for x-axis configuration with 0.05 g sweep down

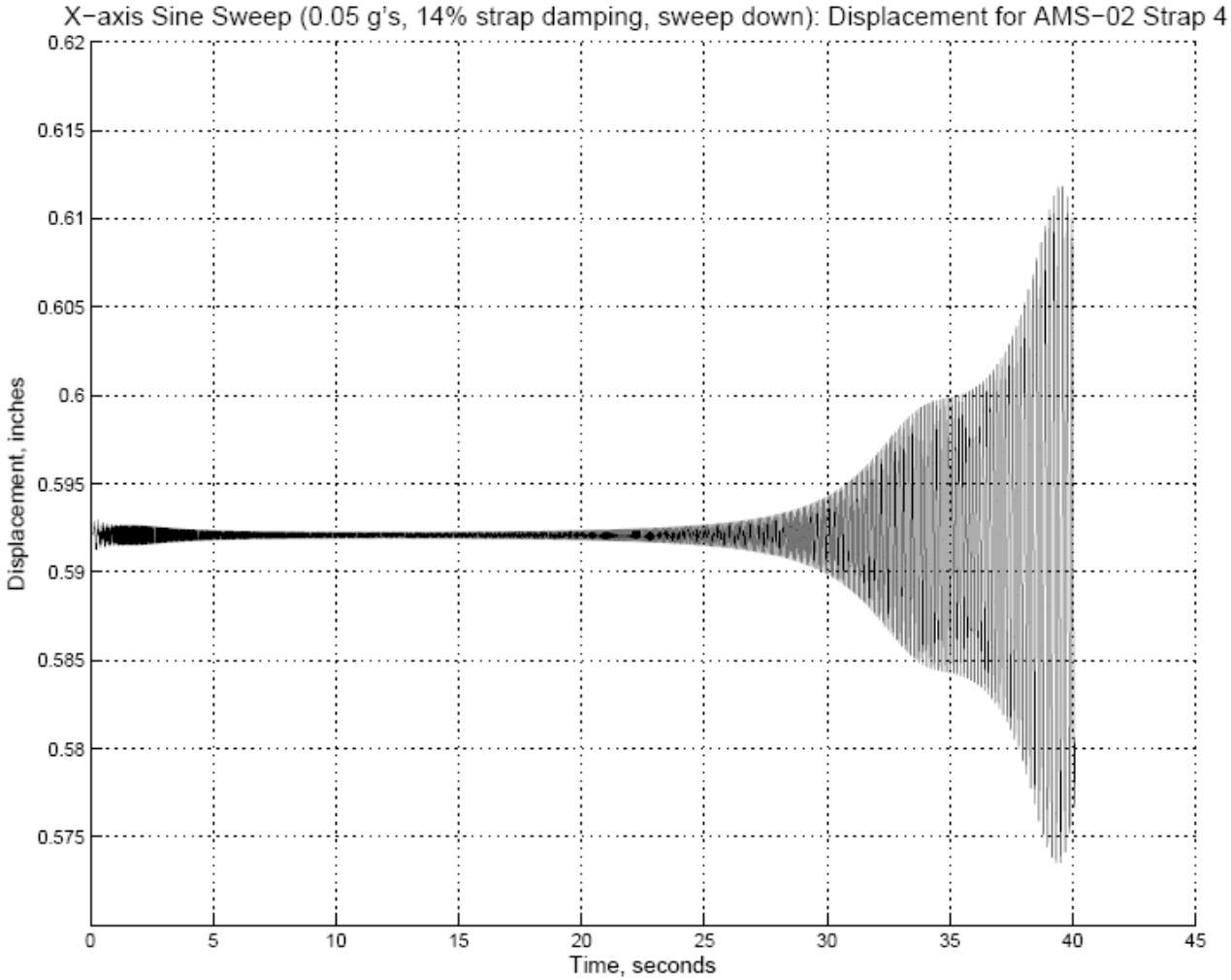

Figure 9-10 Strap 4 displacement response for x-axis configuration with 0.05 g sweep down

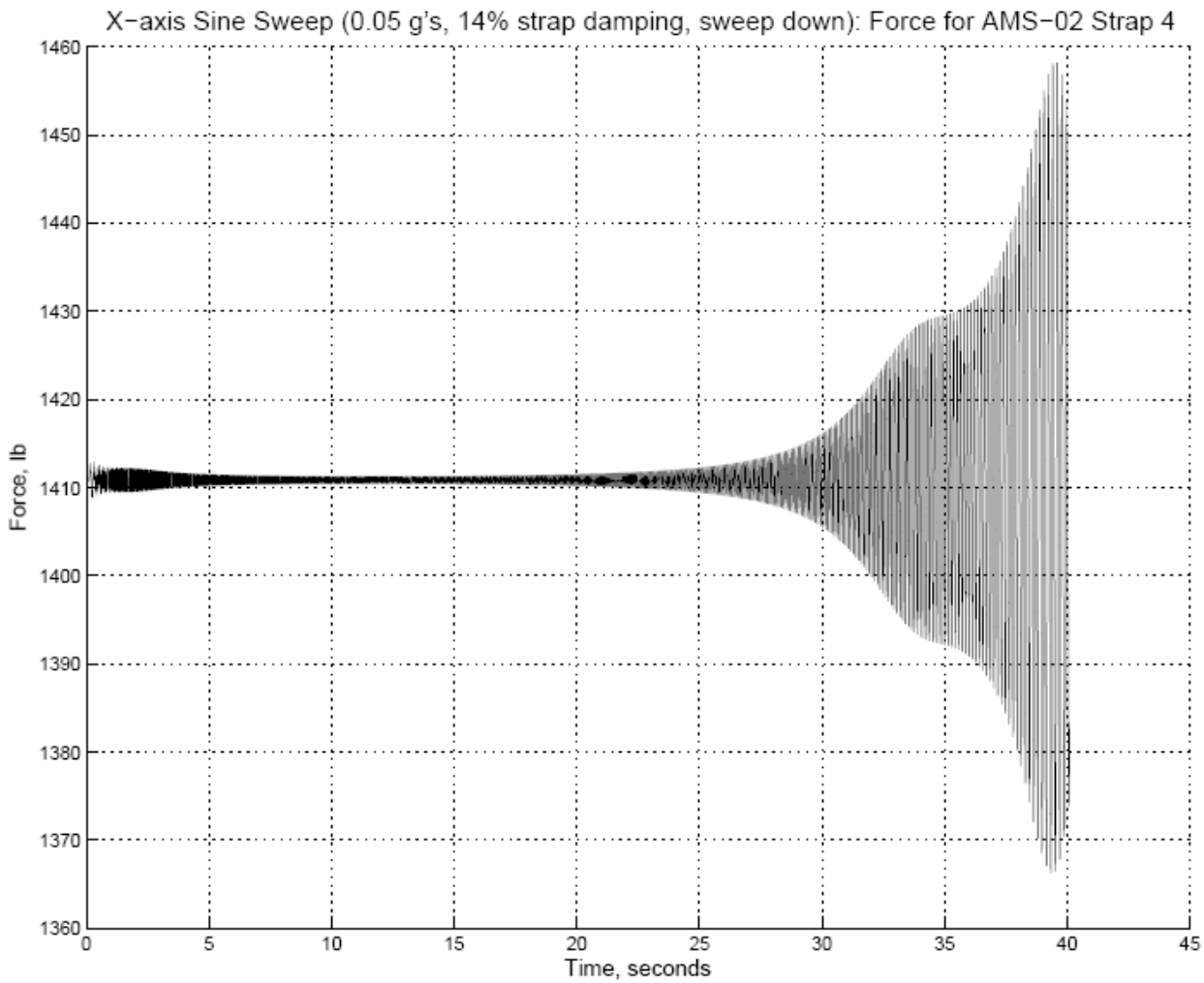

Figure 9-11 Strap 4 force response for x-axis configuration with 0.05 g sweep down

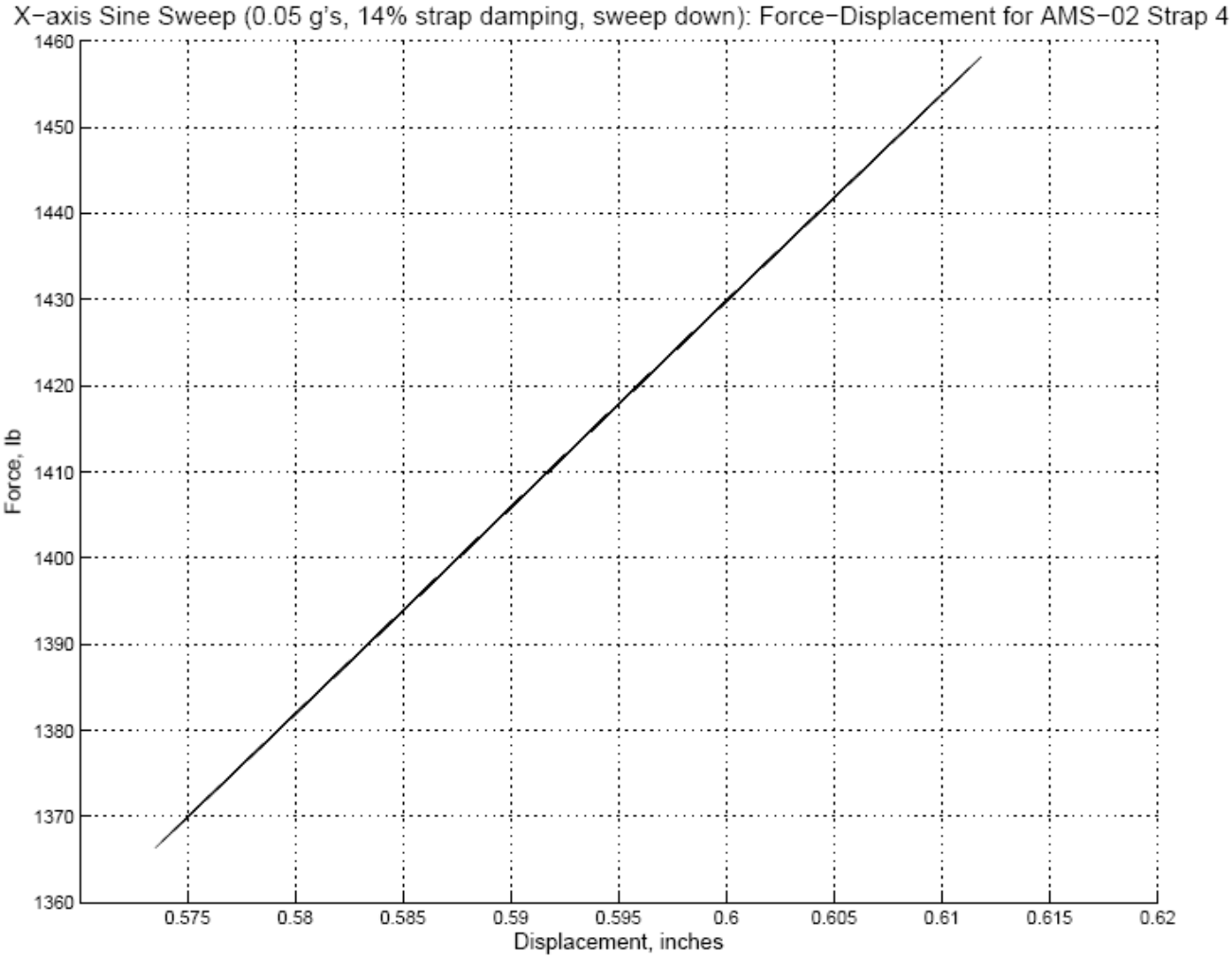

Figure 9-12 Strap 4 force-displacement curve for x-axis configuration with 0.05 g sweep down

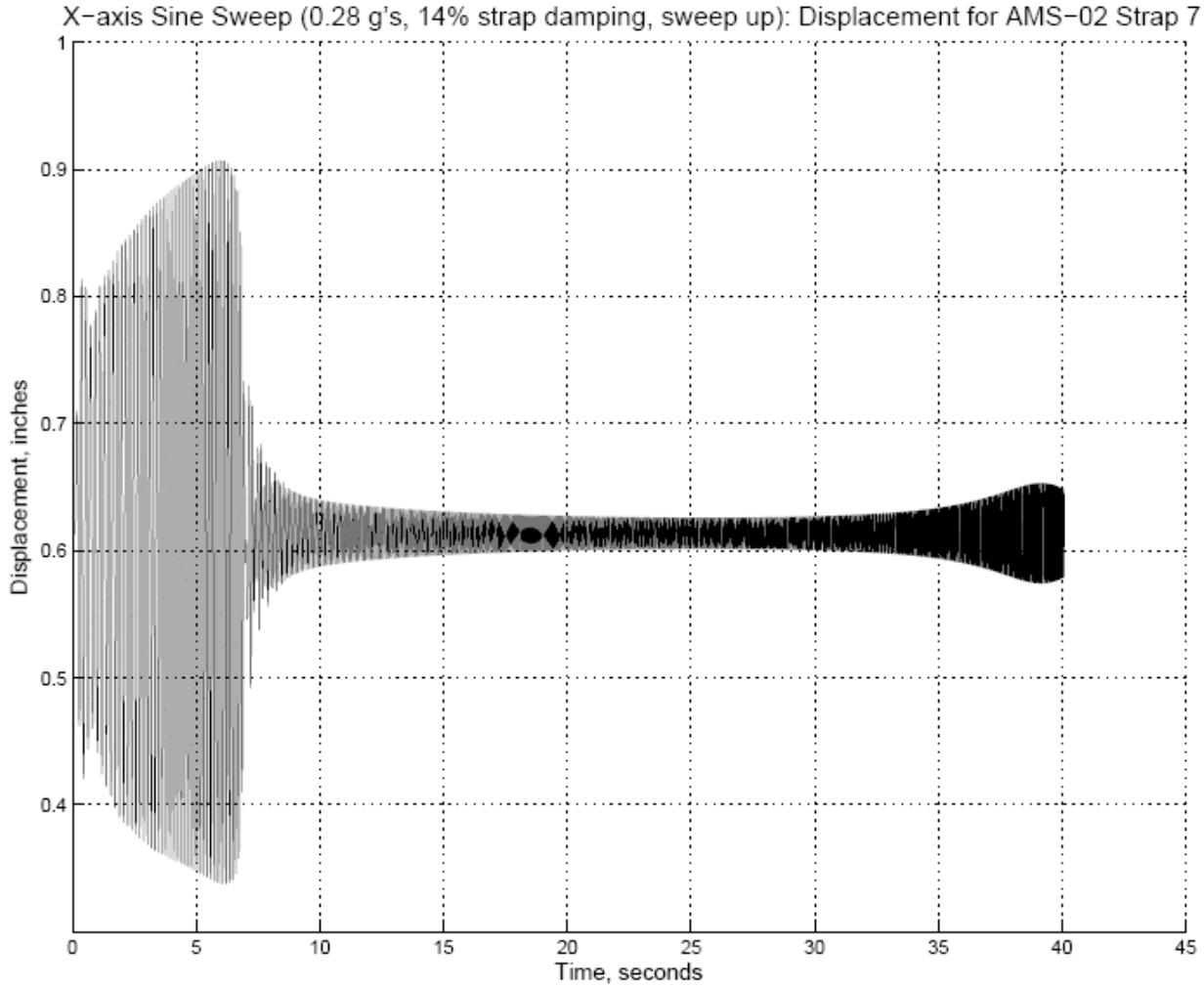

Figure 9-13 Strap 7 displacement response for x-axis configuration with 0.28 g sweep up

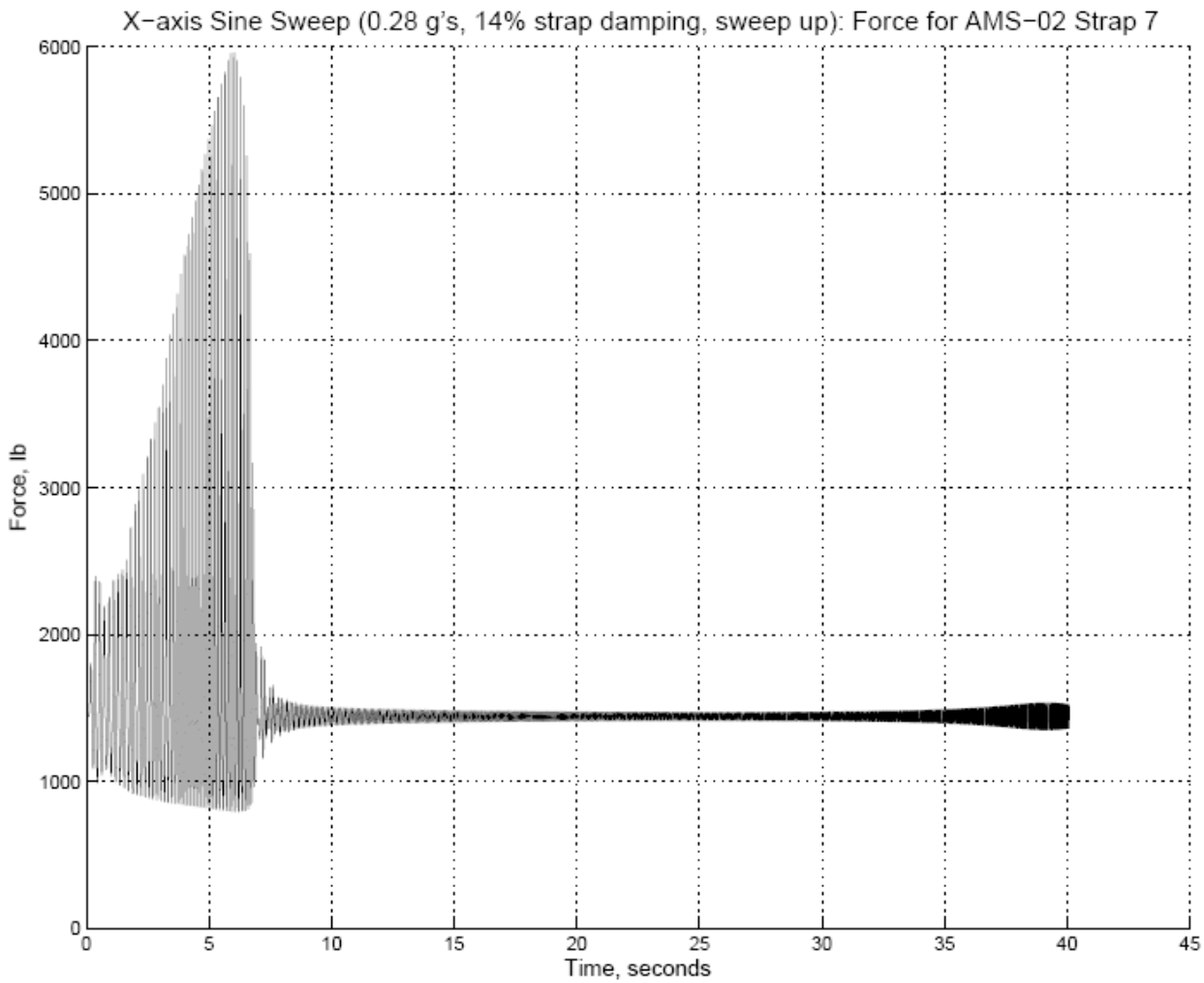

Figure 9-14 Strap 7 force response for x-axis configuration with 0.28 g sweep up

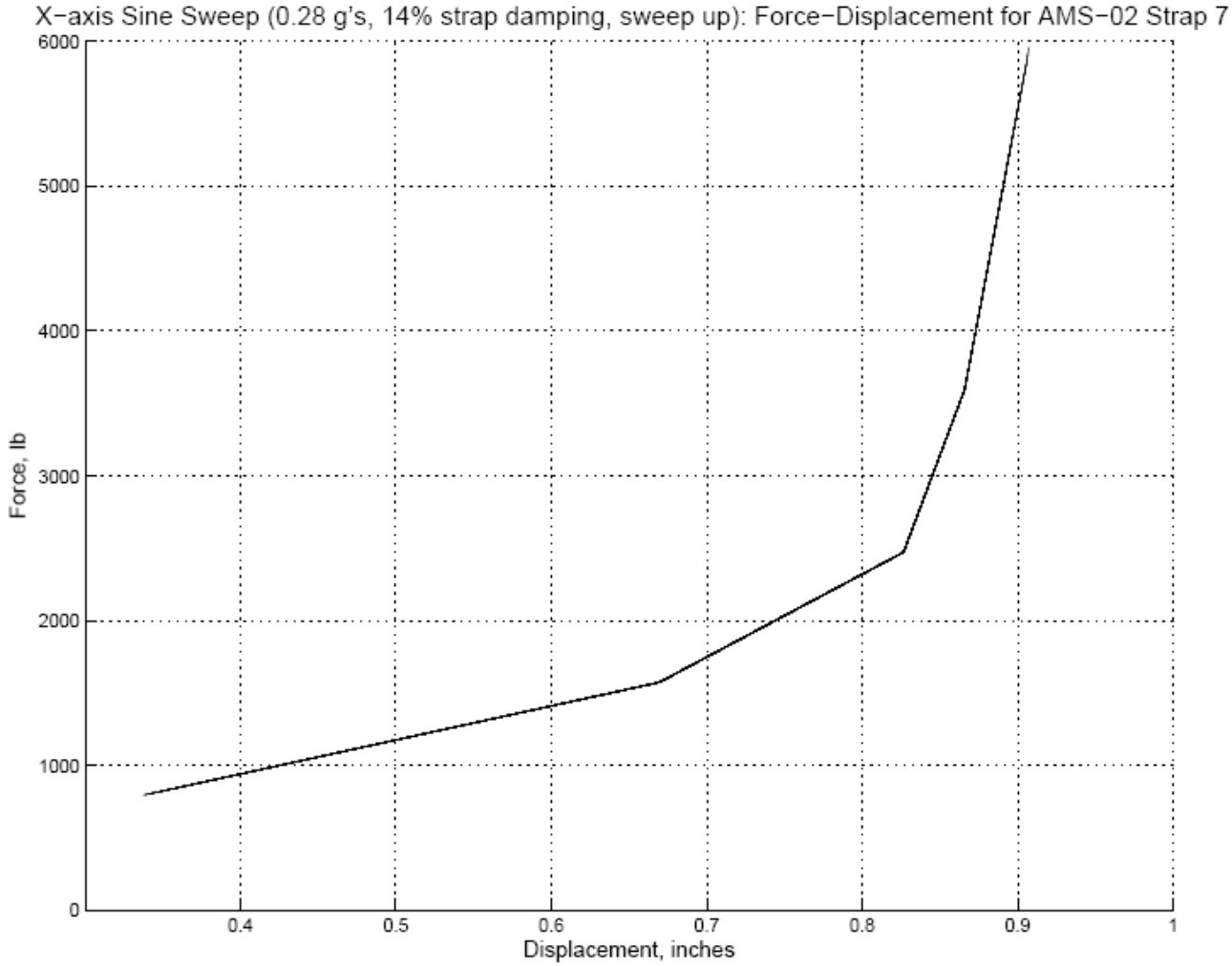

Figure 9-15 Strap 7 force-displacement curve for x-axis configuration with 0.28 g sweep up

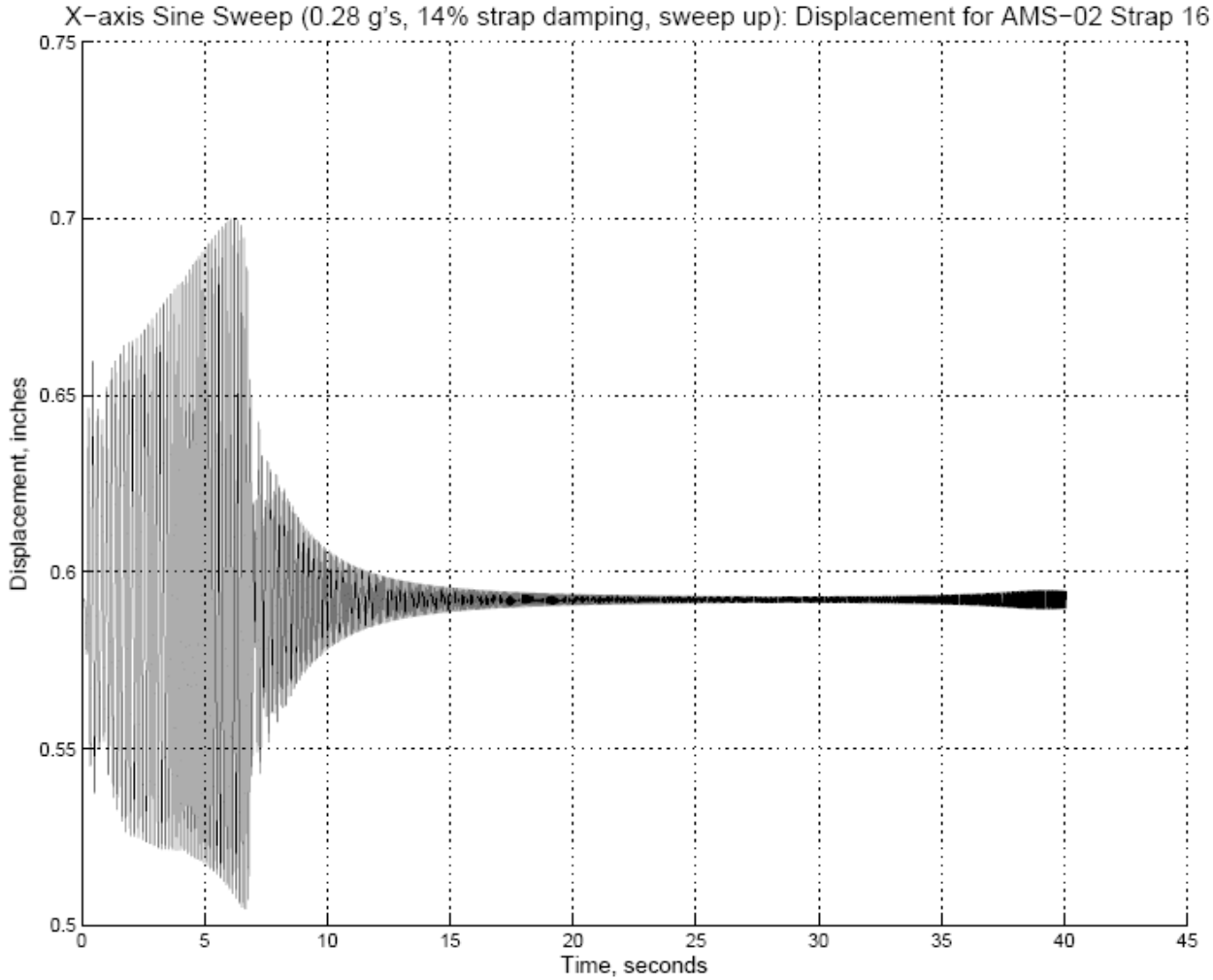

Figure 9-16 Strap 16 displacement response for x-axis configuration with 0.28 g sweep up

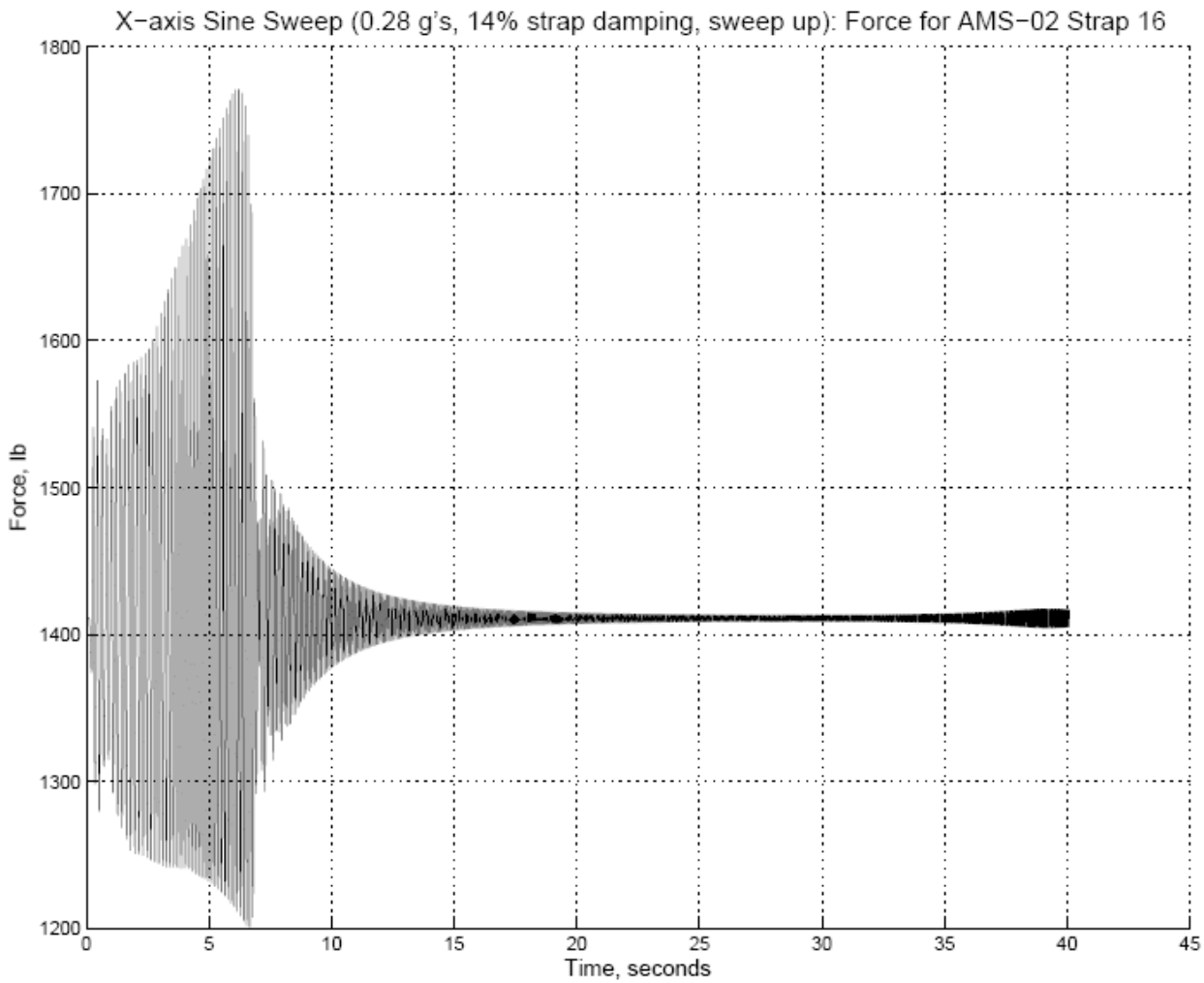

Figure 9-17 Strap 16 force response for x-axis configuration with 0.28 g sweep up

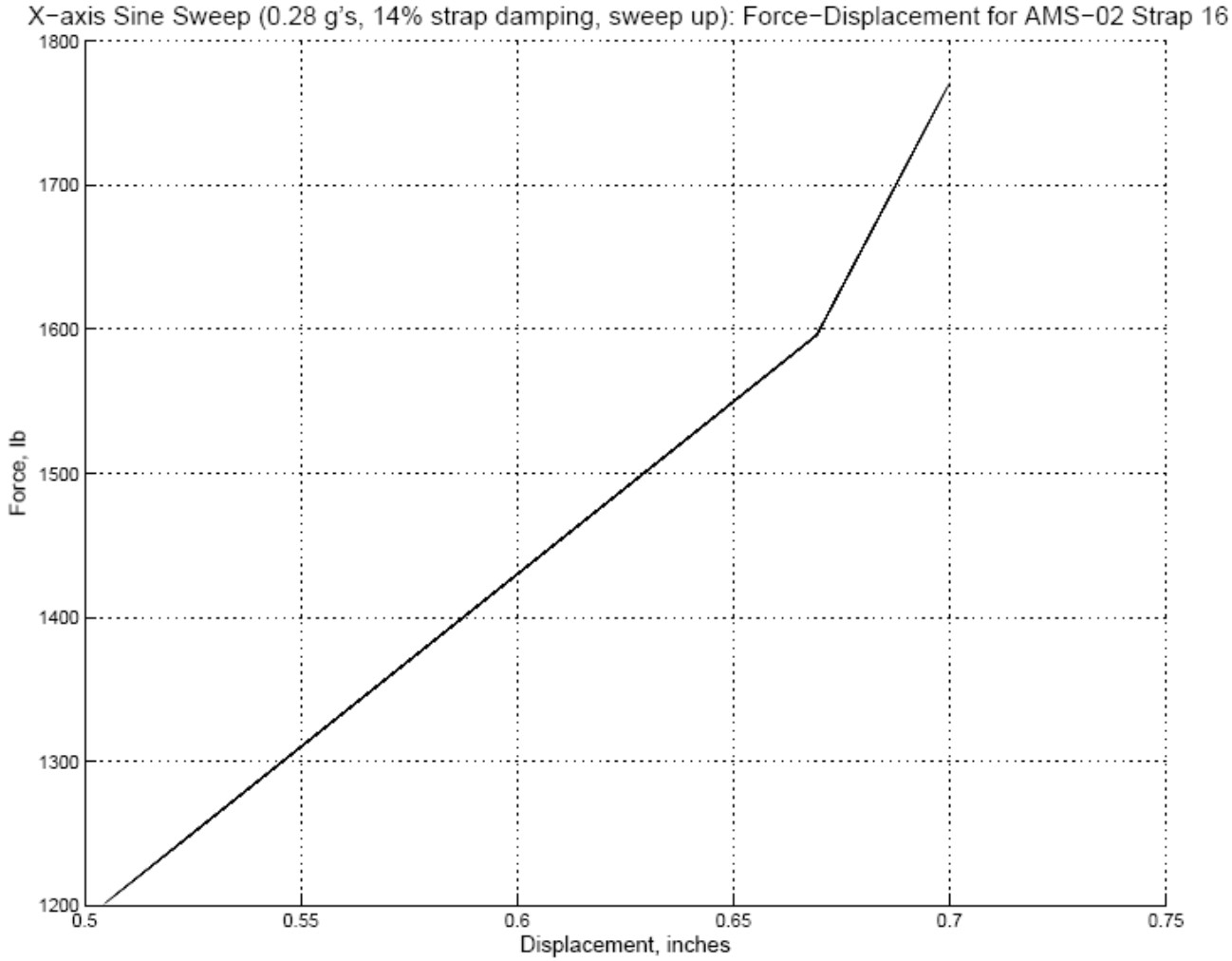

Figure 9-18 Strap 16 force-displacement curve for x-axis configuration with 0.28 g sweep up

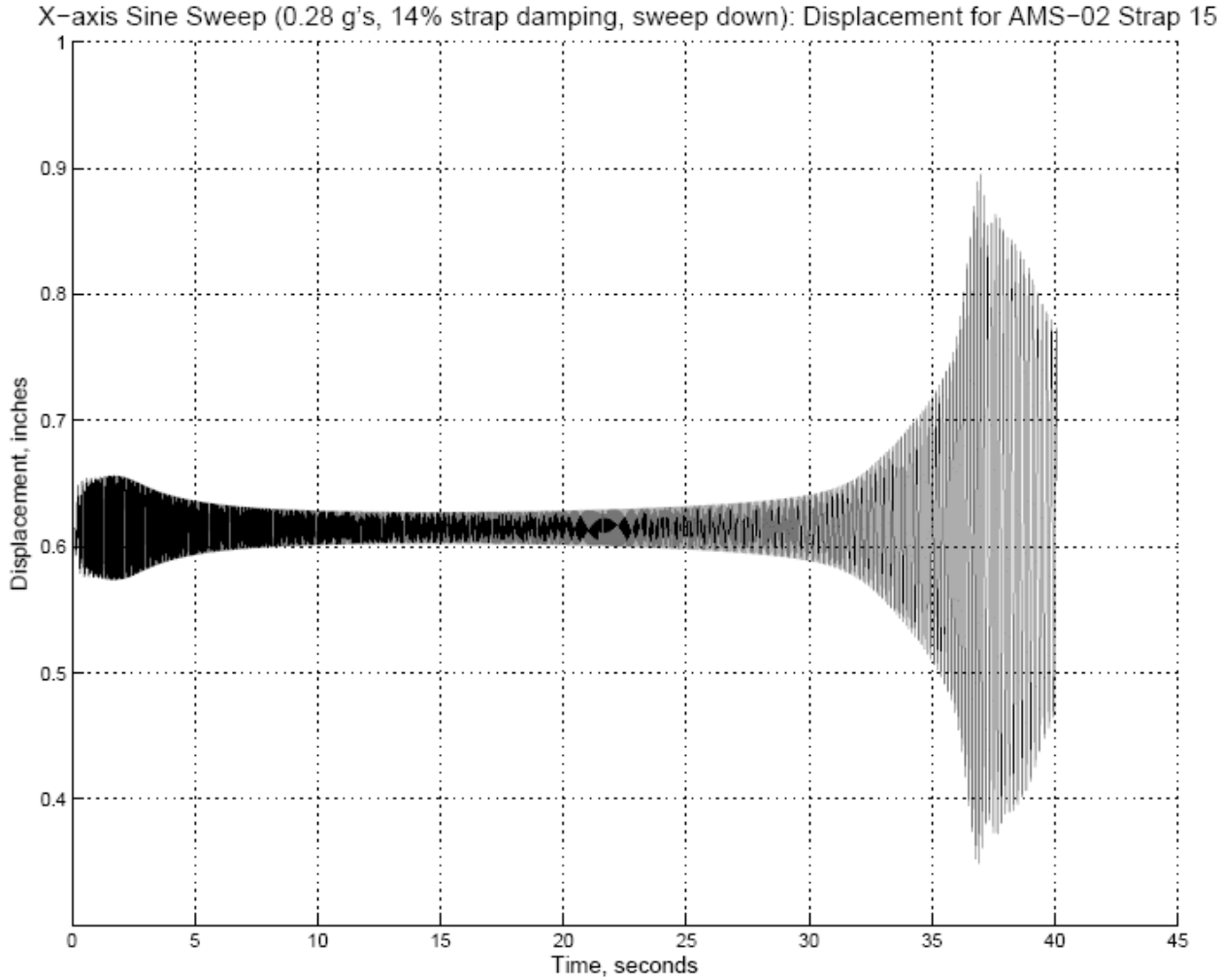

Figure 9-19 Strap 15 displacement response for x-axis configuration with 0.28 g sweep down

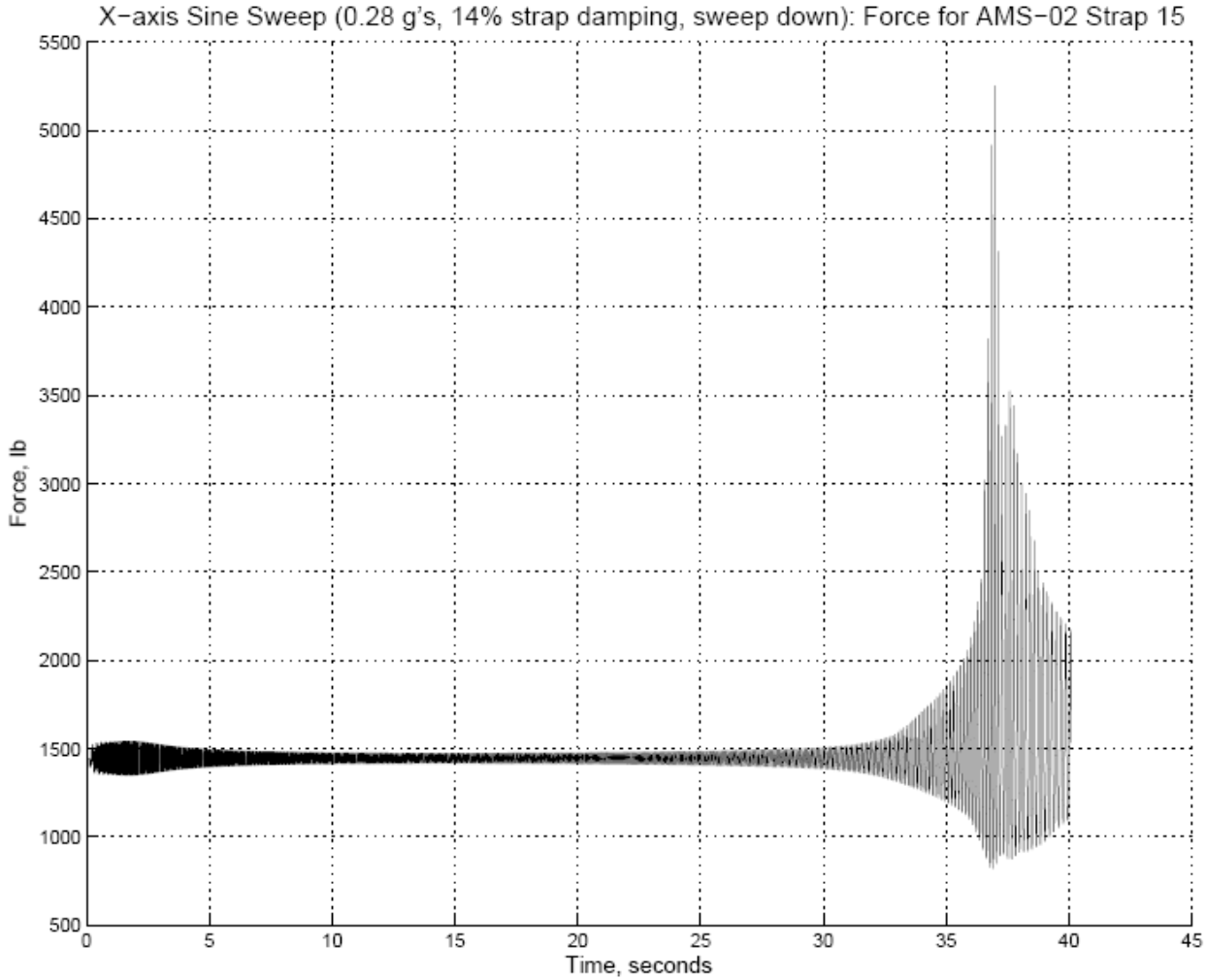

Figure 9-20 Strap 15 force response for x-axis configuration with 0.28 g sweep down

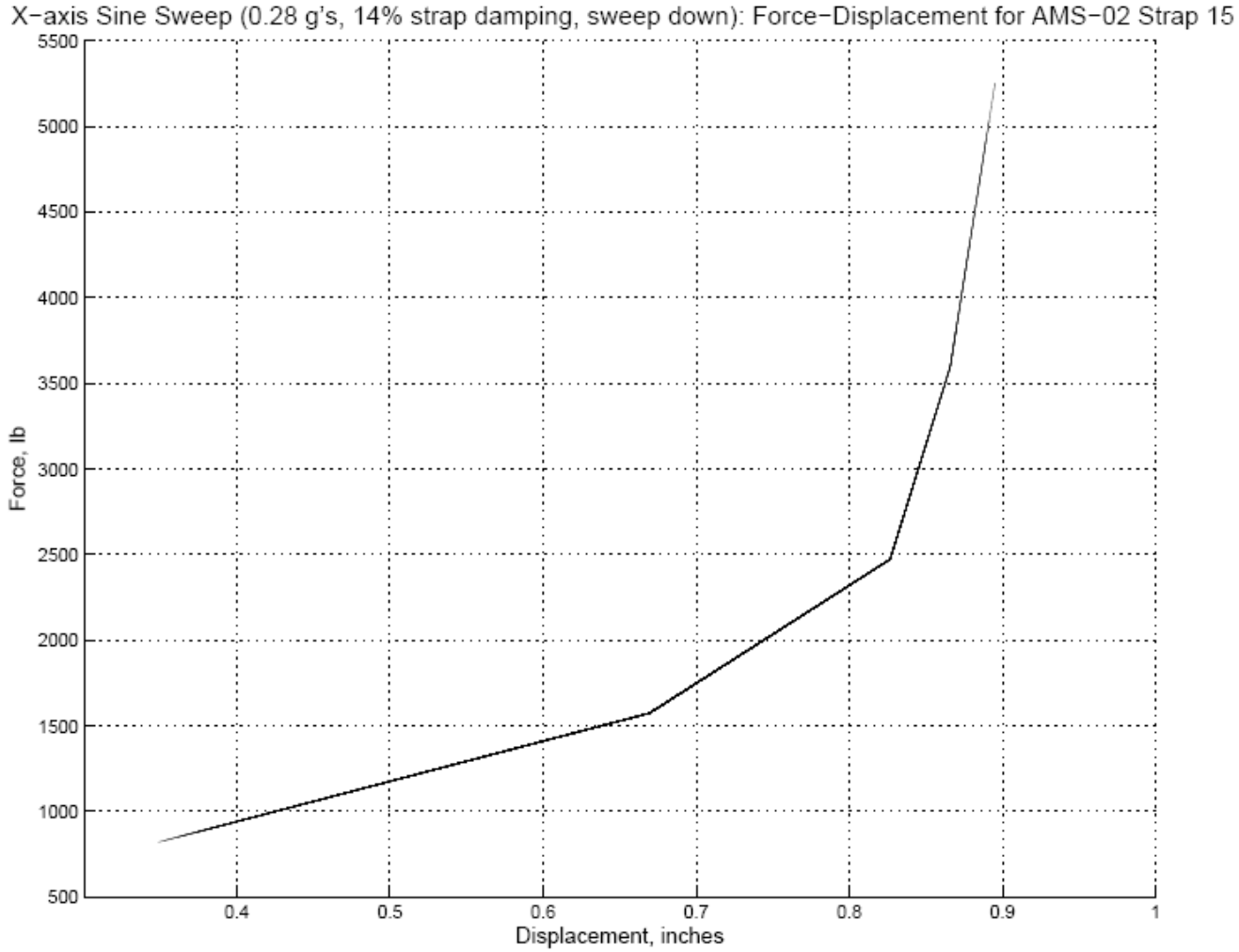

Figure 9-21 Strap 15 force-displacement curve for x-axis configuration with 0.28 g sweep down

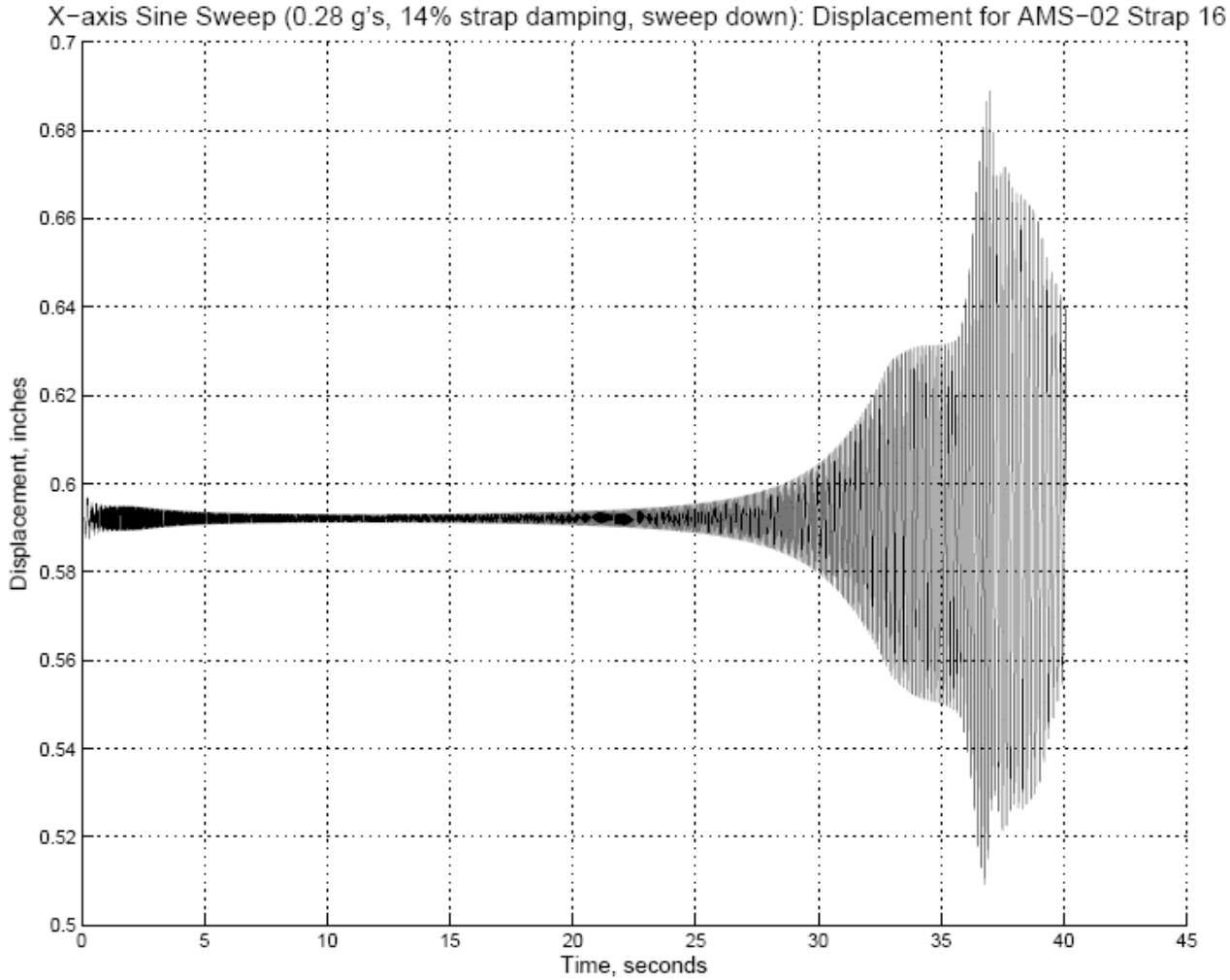

Figure 9-22 Strap 16 displacement response for x-axis configuration with 0.28 g sweep down

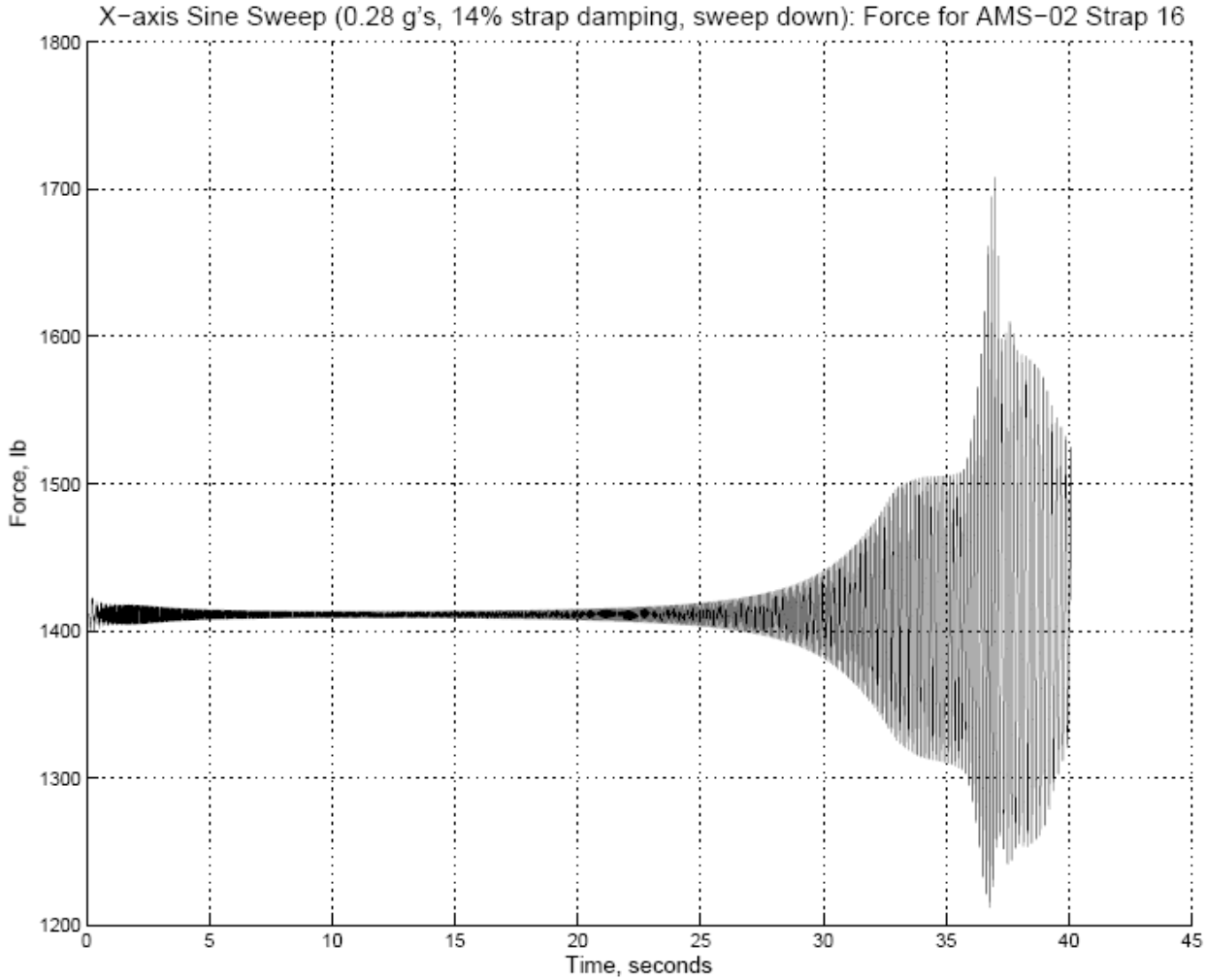

Figure 9-23 Strap 16 force response for x-axis configuration with 0.28 g sweep down

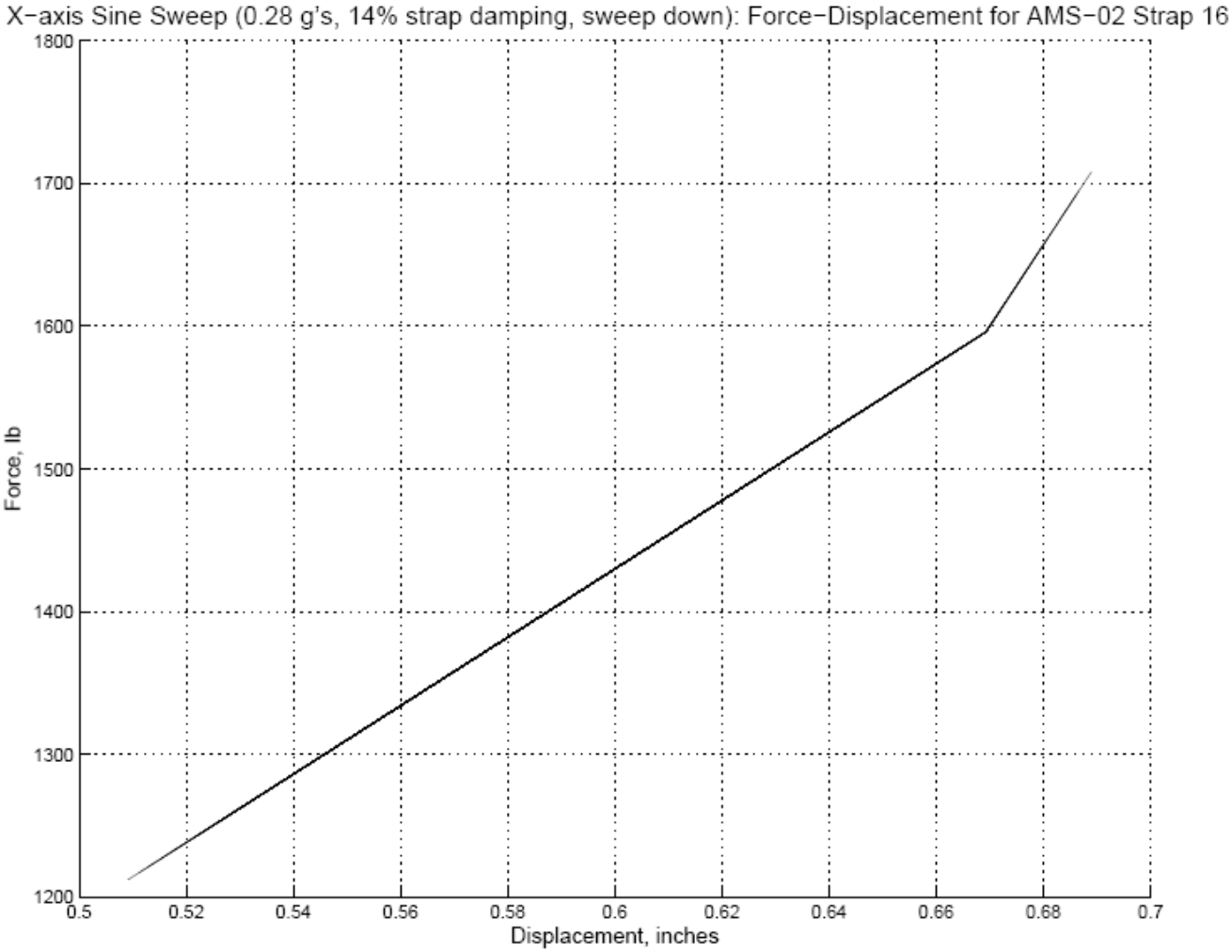

Figure 9-24 Strap 16 force-displacement curve for x-axis configuration with 0.28 g sweep down

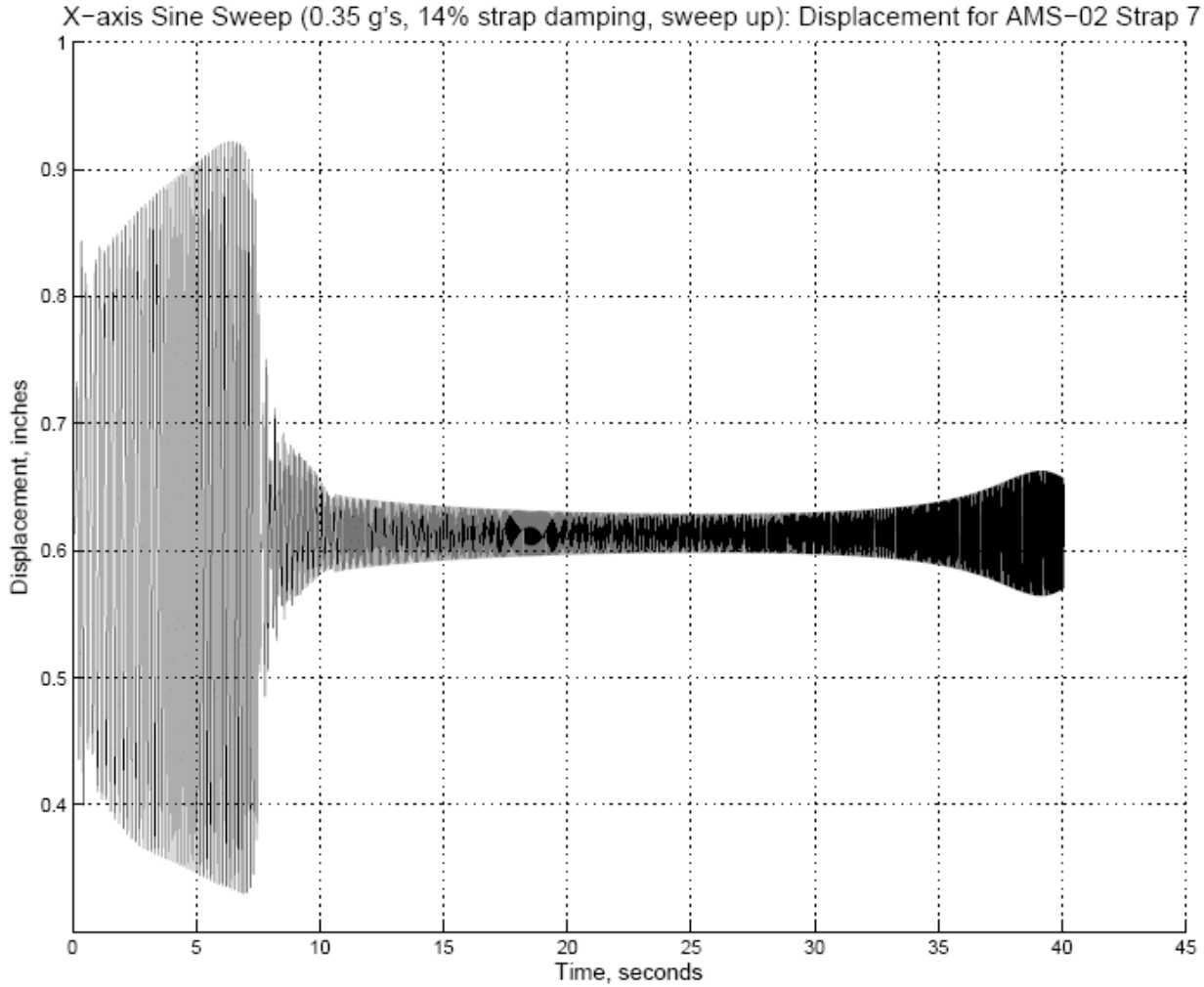

Figure 9-25 Strap 7 displacement response for x-axis configuration with 0.35 g sweep up

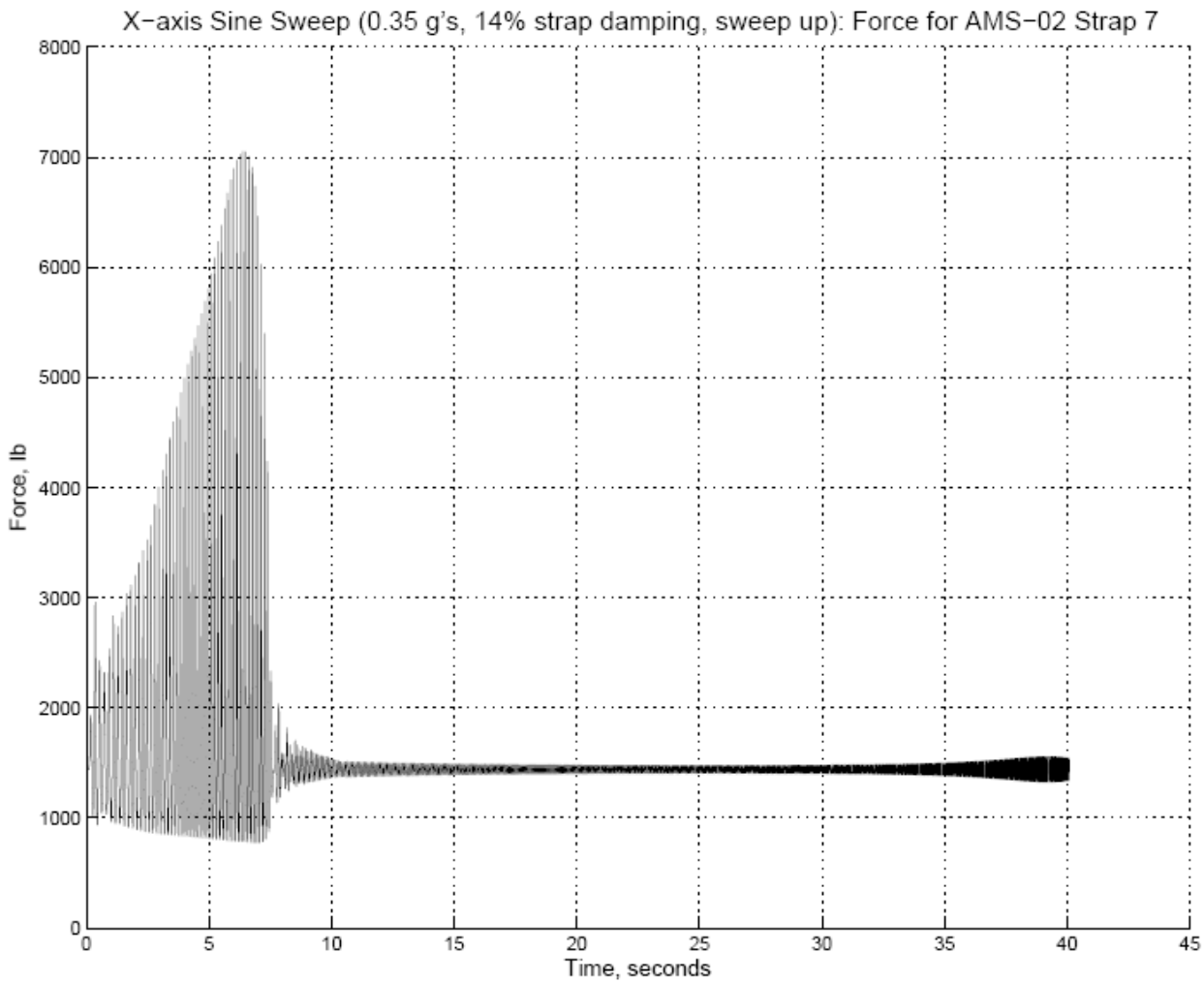

Figure 9-26 Strap 7 force response for x-axis configuration with 0.35 g sweep up

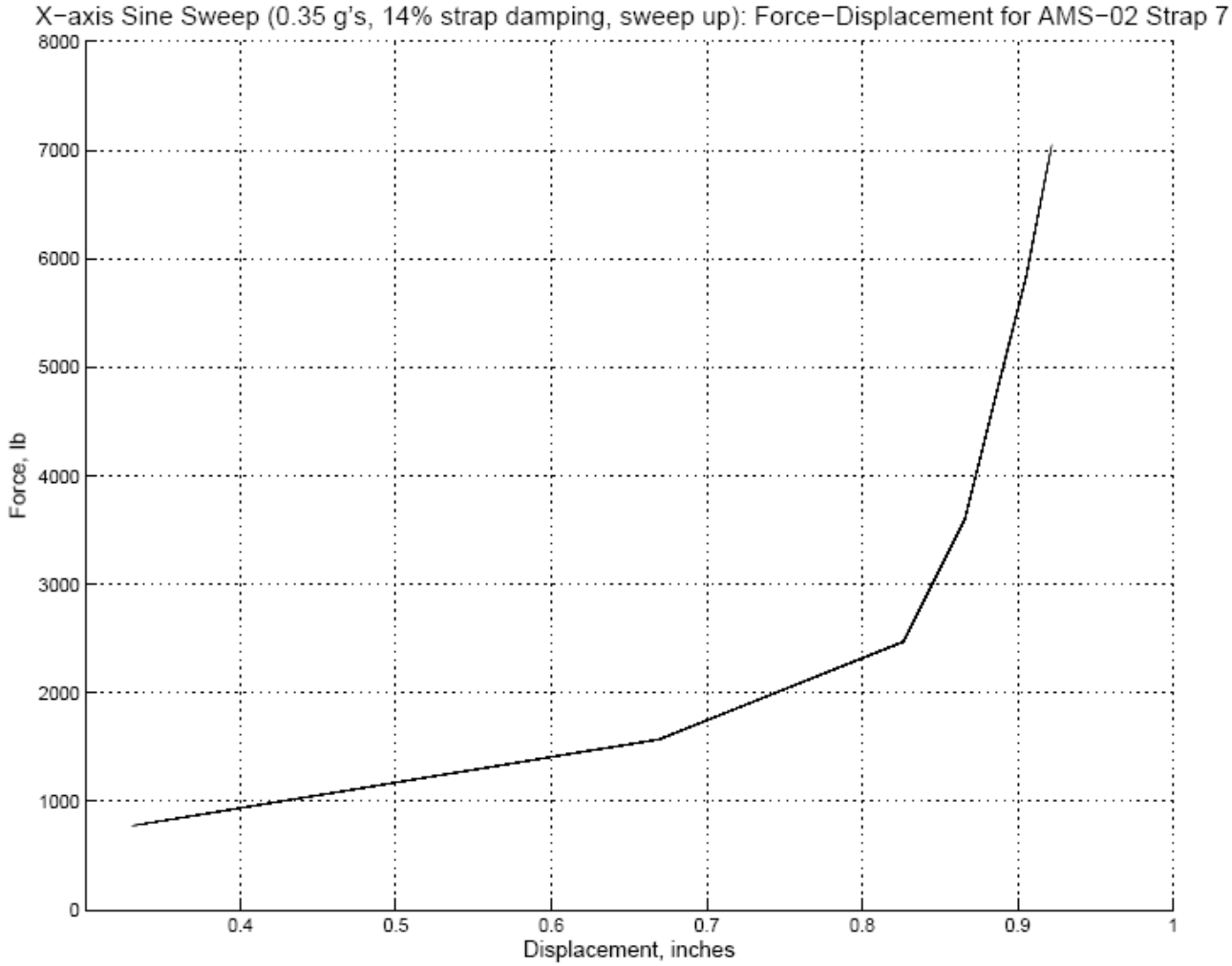

Figure 9-27 Strap 7 force-displacement curve for x-axis configuration with 0.35 g sweep up

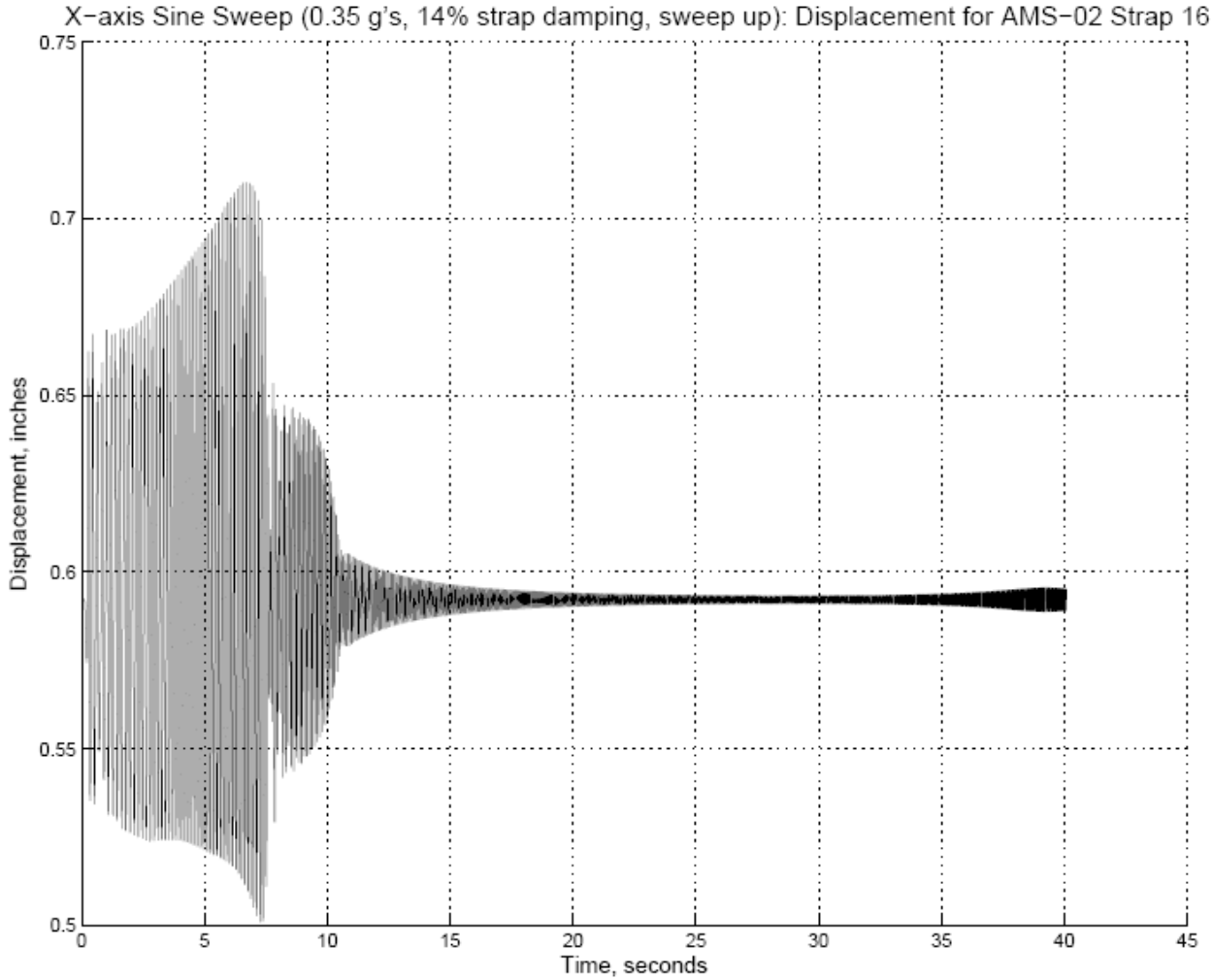

Figure 9-28 Strap 16 displacement response for x-axis configuration with 0.35 g sweep up

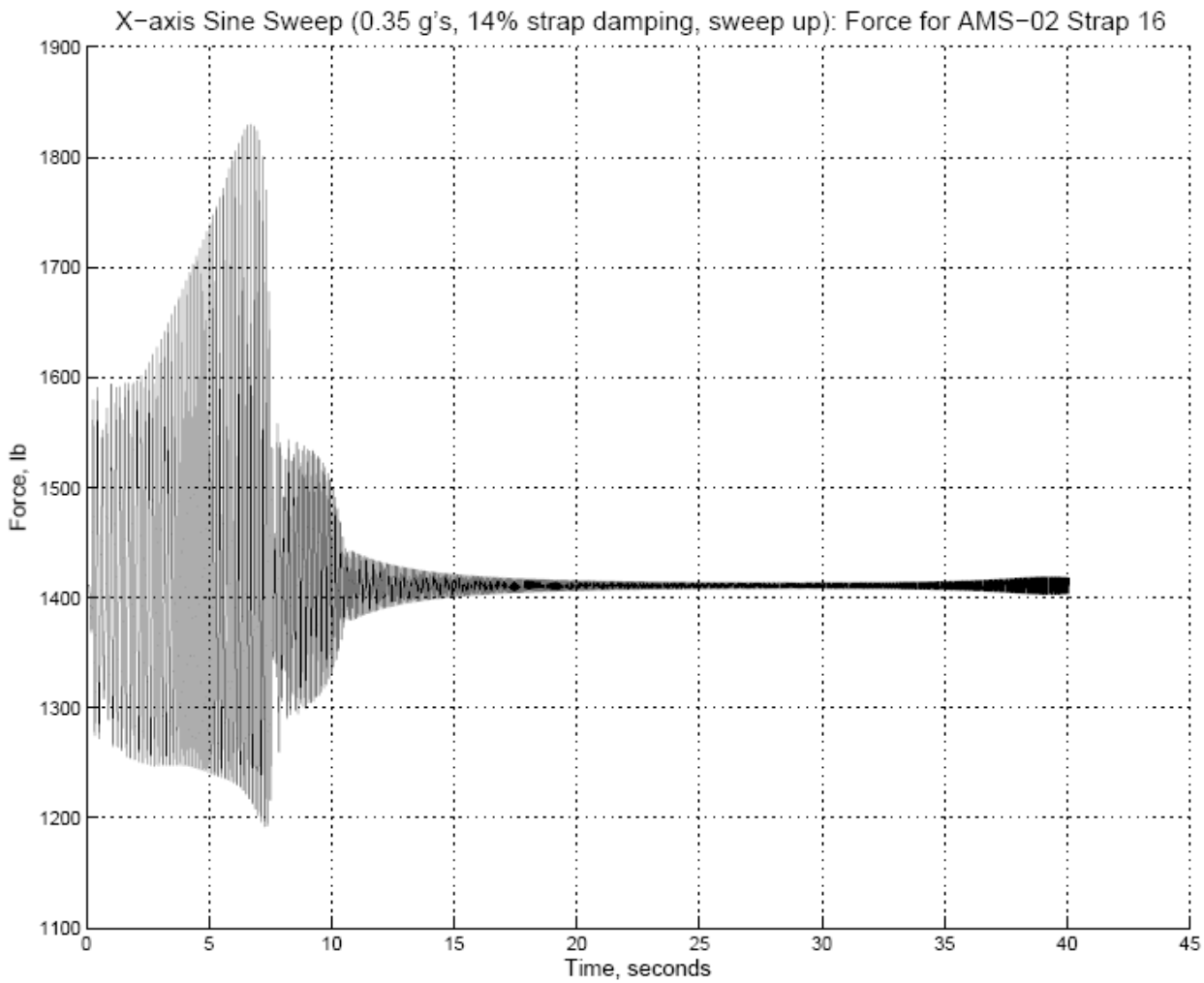

Figure 9-29 Strap 16 force response for x-axis configuration with 0.35 g sweep up

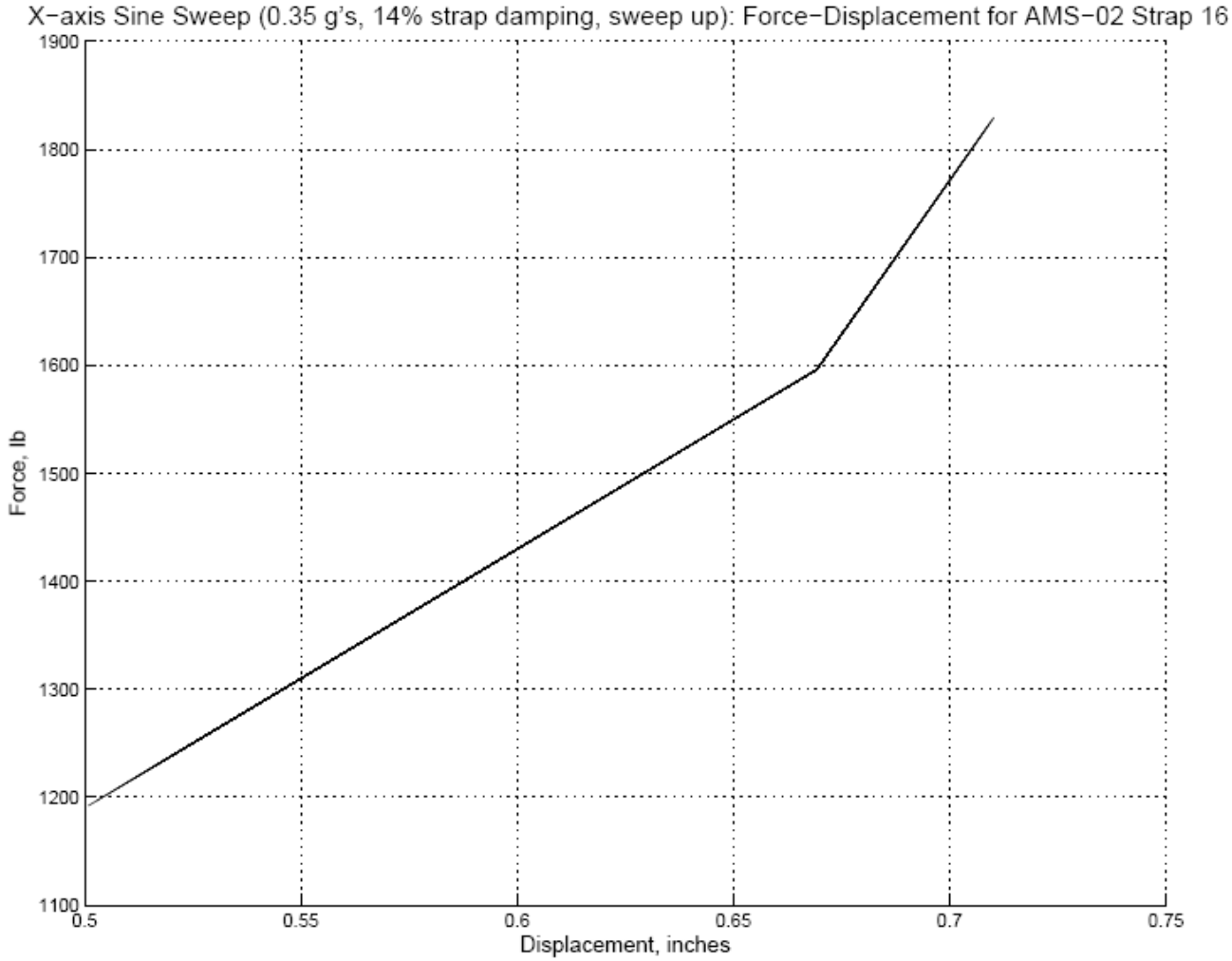

Figure 9-30 Strap 16 force-displacement curve for x-axis configuration with 0.35 g sweep up

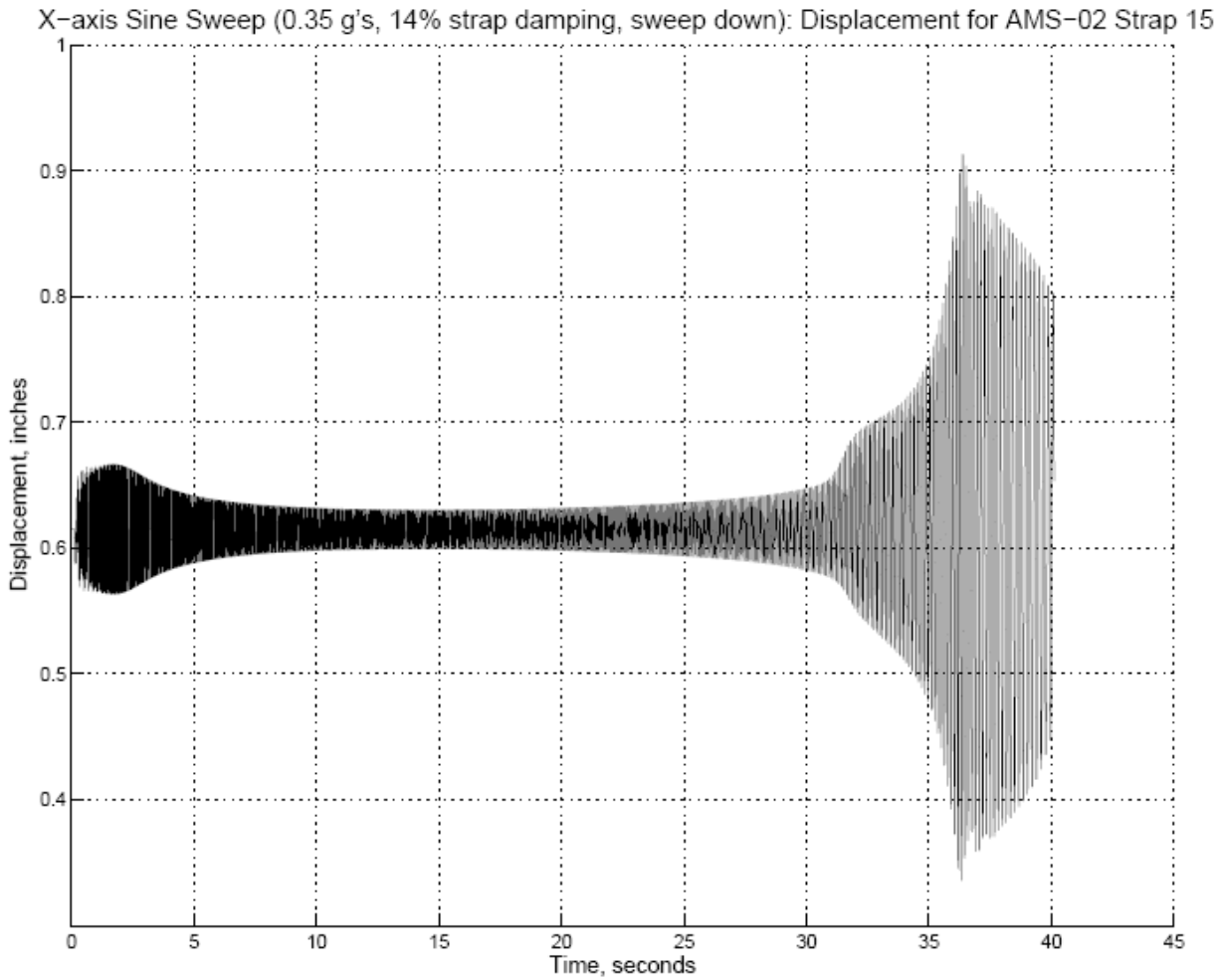

Figure 9-31 Strap 15 displacement response for x-axis configuration with 0.35 g sweep down

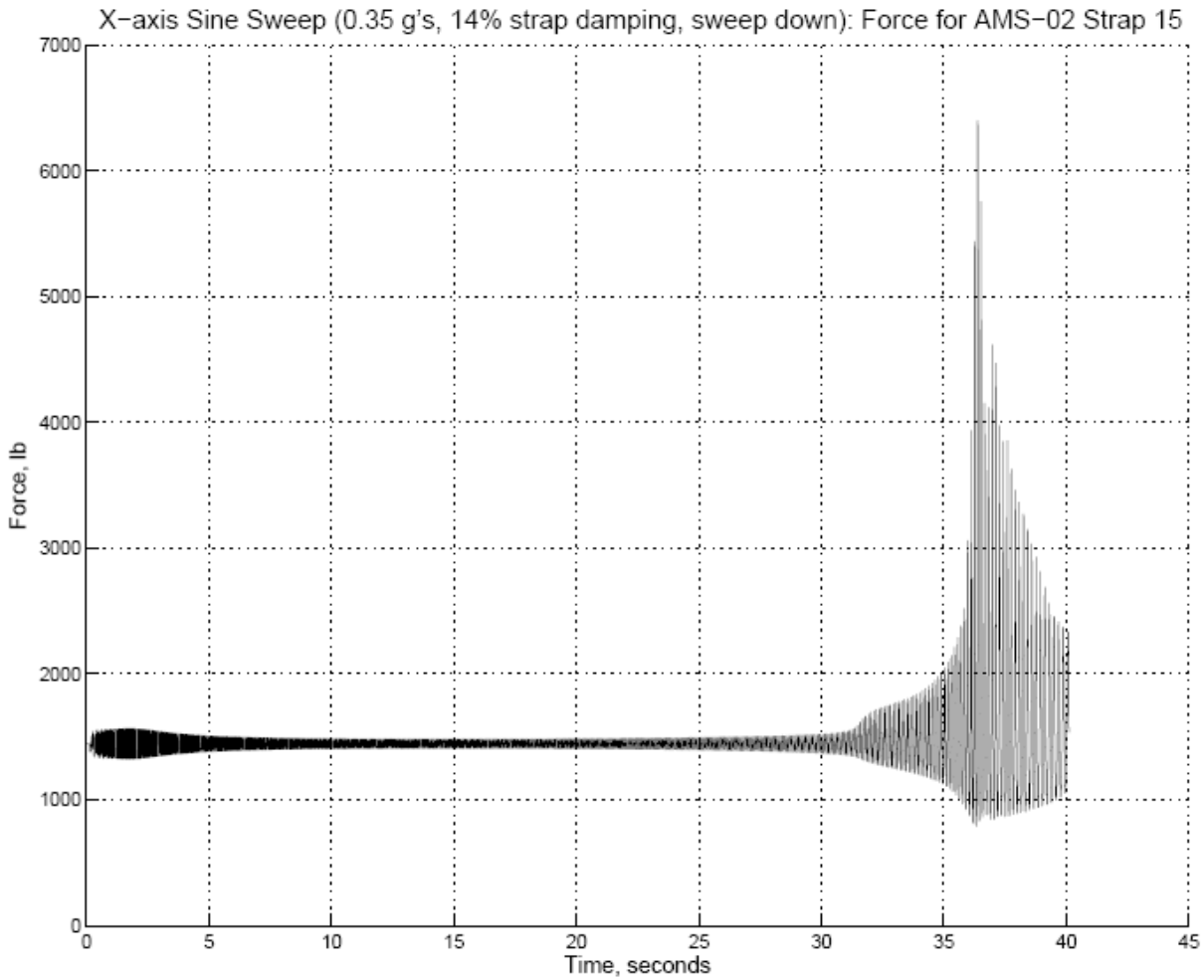

Figure 9-32 Strap 15 force response for x-axis configuration with 0.35 g sweep down

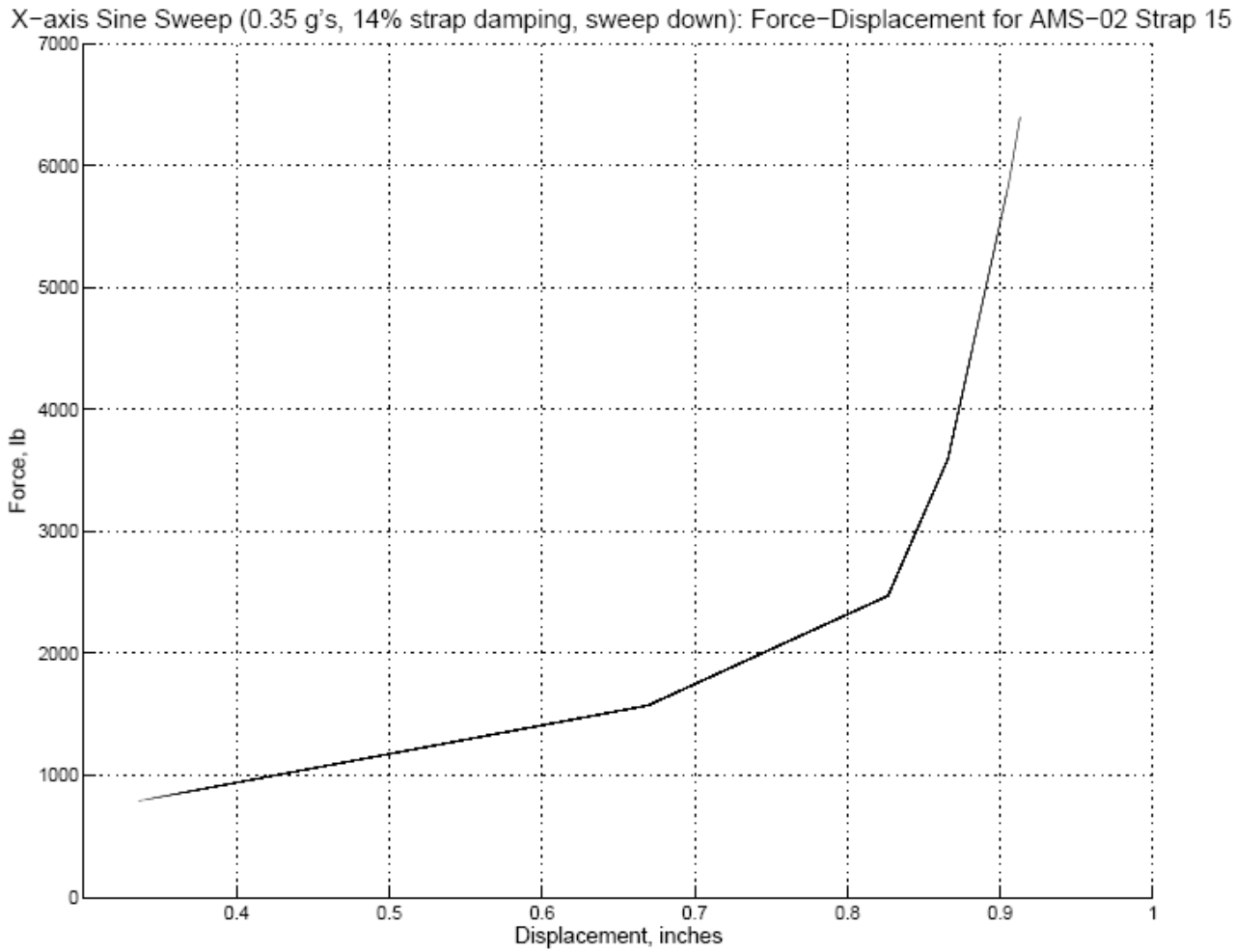

Figure 9-33 Strap 15 force-displacement curve for x-axis configuration with 0.35 g sweep down

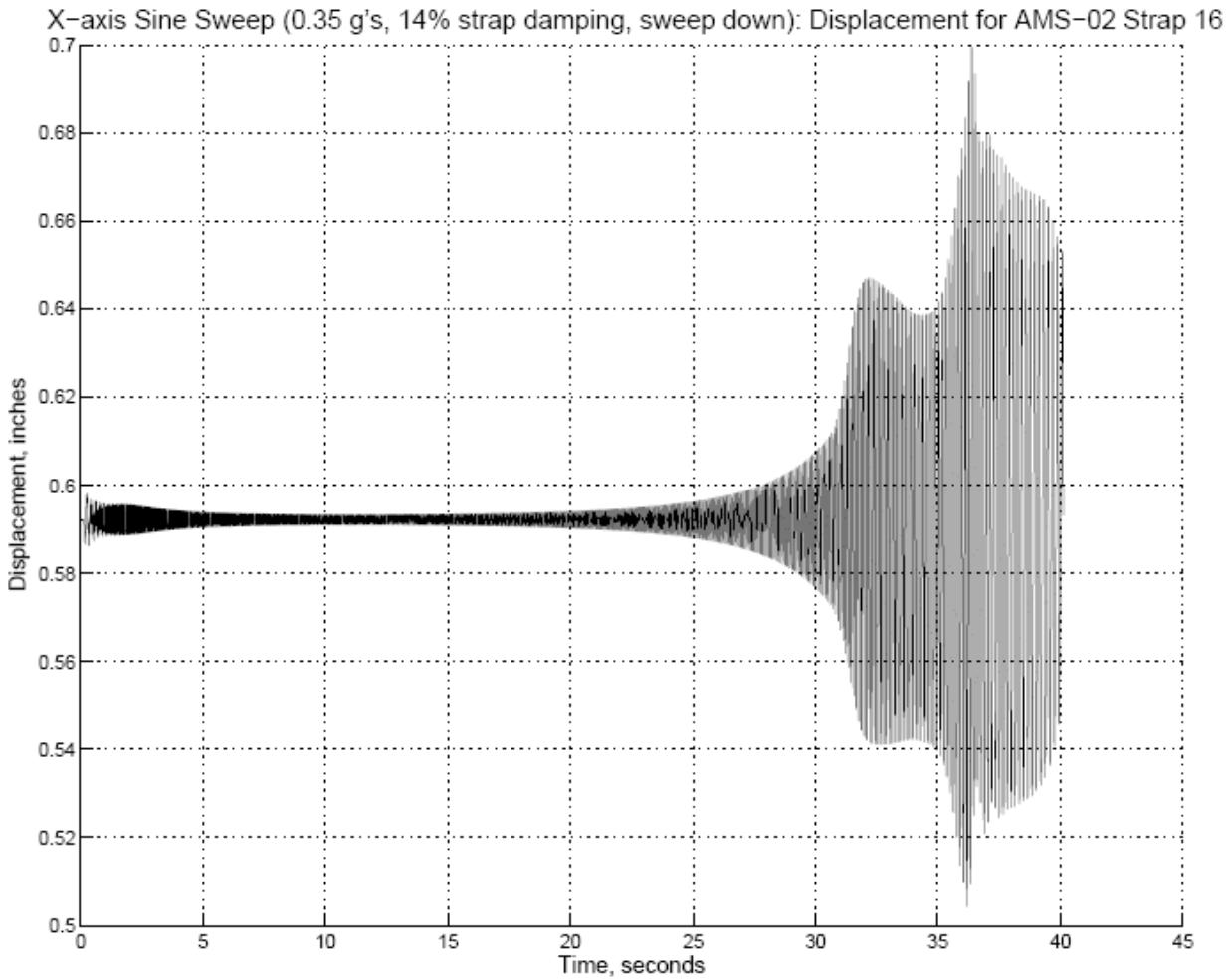

Figure 9-34 Strap 16 displacement response for x-axis configuration with 0.35 g sweep down

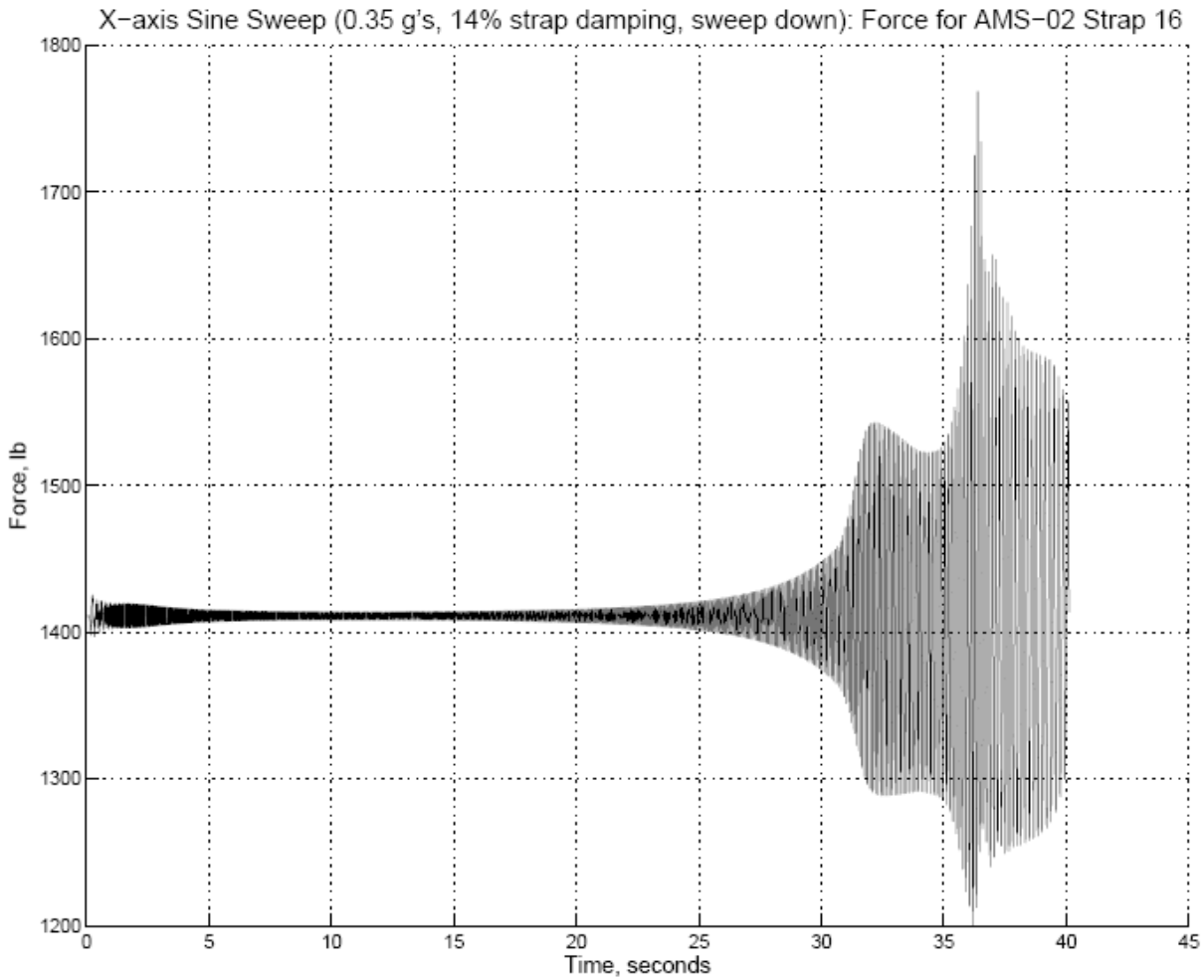

Figure 9-35 Strap 16 force response for x-axis configuration with 0.35 g sweep down

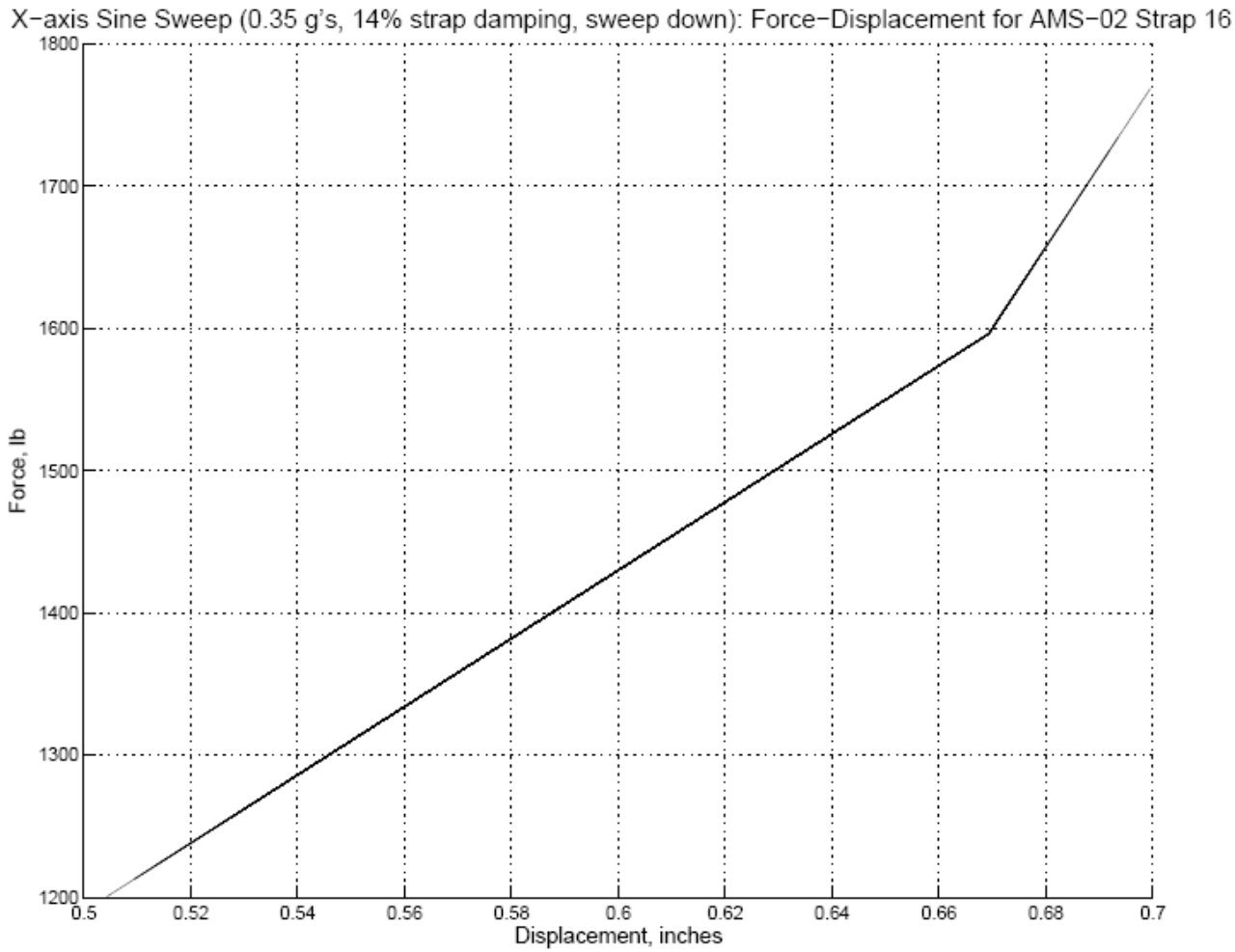

Figure 9-36 Strap 16 force-displacement curve for x-axis configuration with 0.35 g sweep down

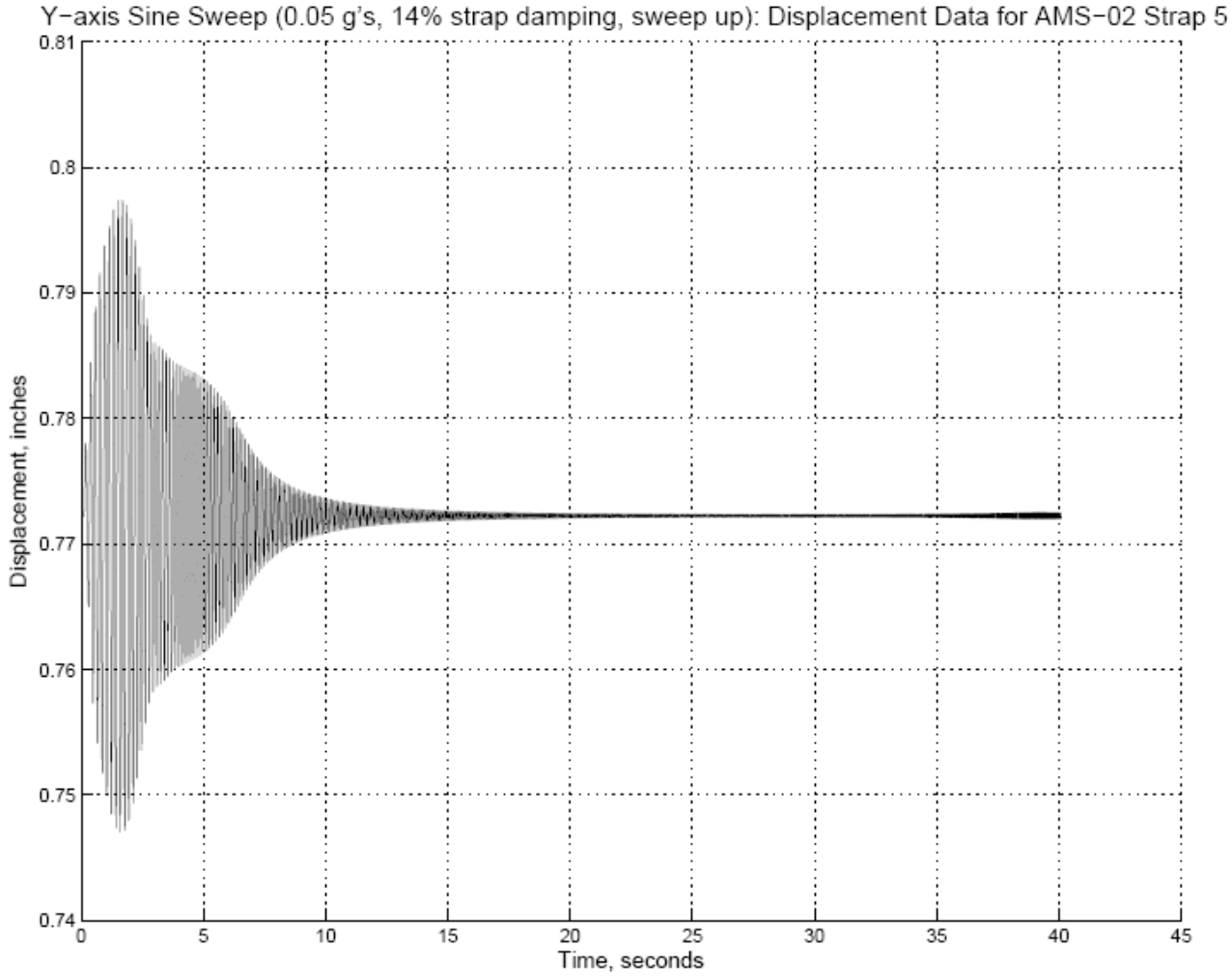

Figure 9-37 Strap 5 displacement response for y-axis configuration with 0.05 g sweep up

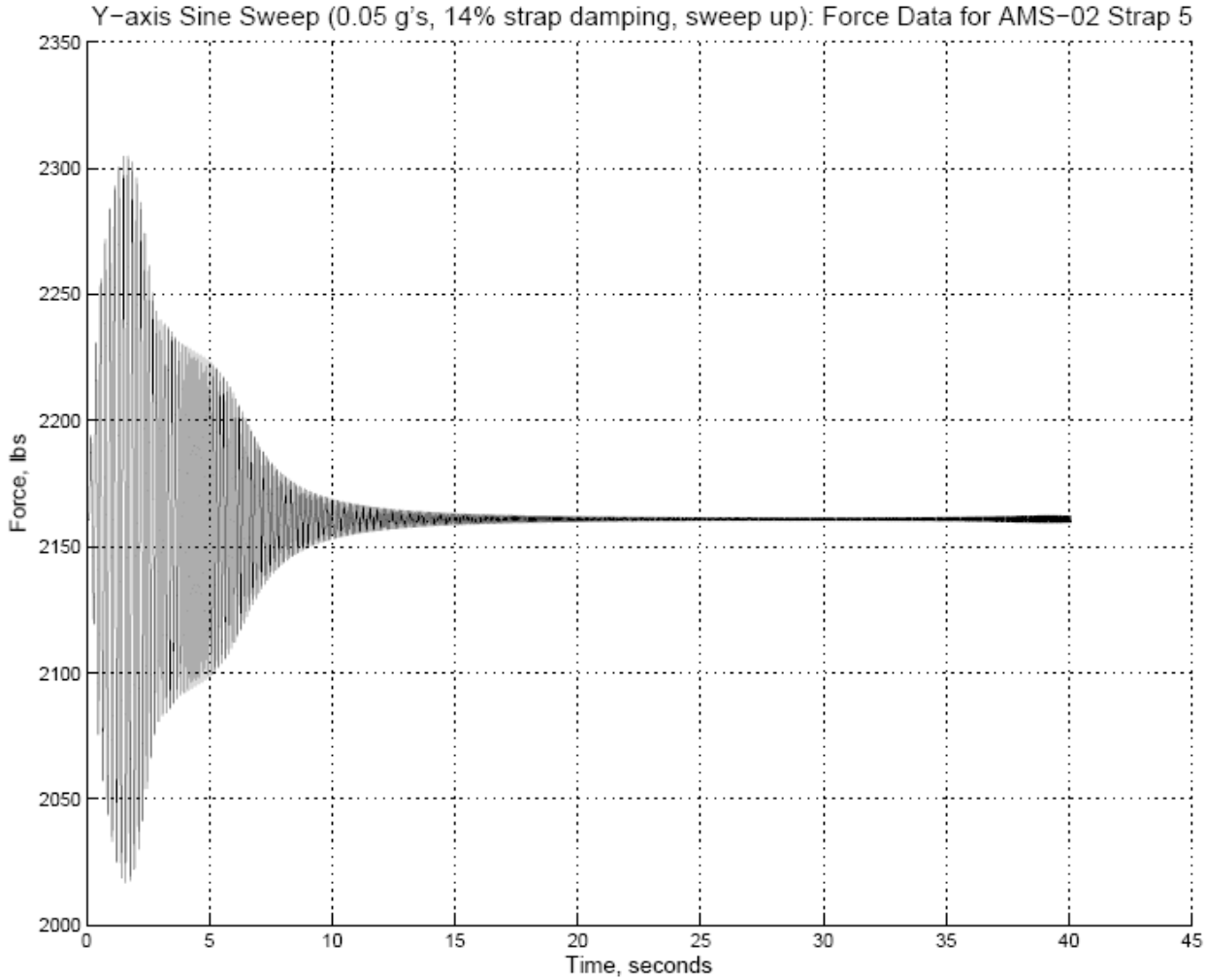

Figure 9-38 Strap 5 force response for y-axis configuration with 0.05 g sweep up

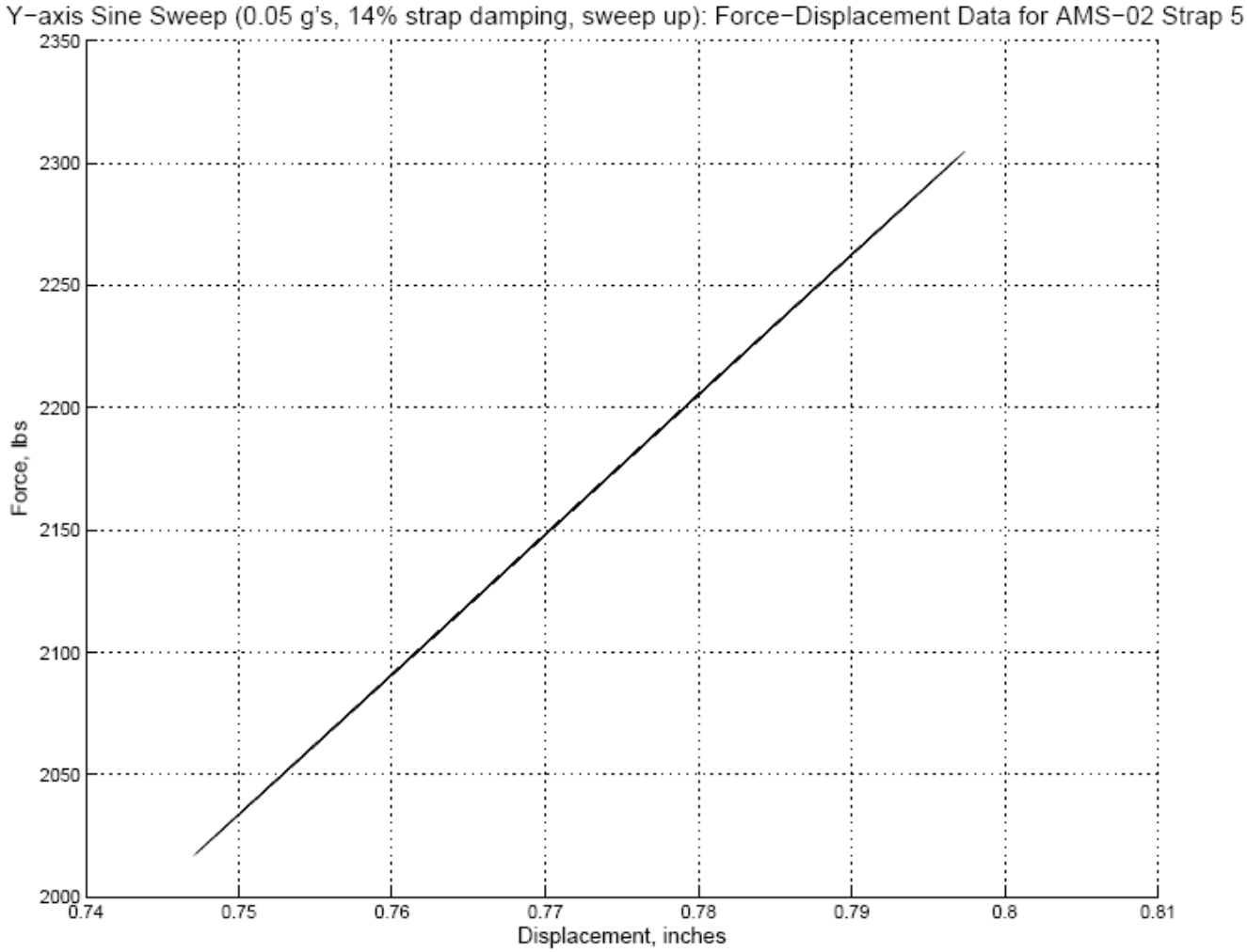

Figure 9-39 Strap 5 force-displacement curve for y-axis configuration with 0.05 g sweep up

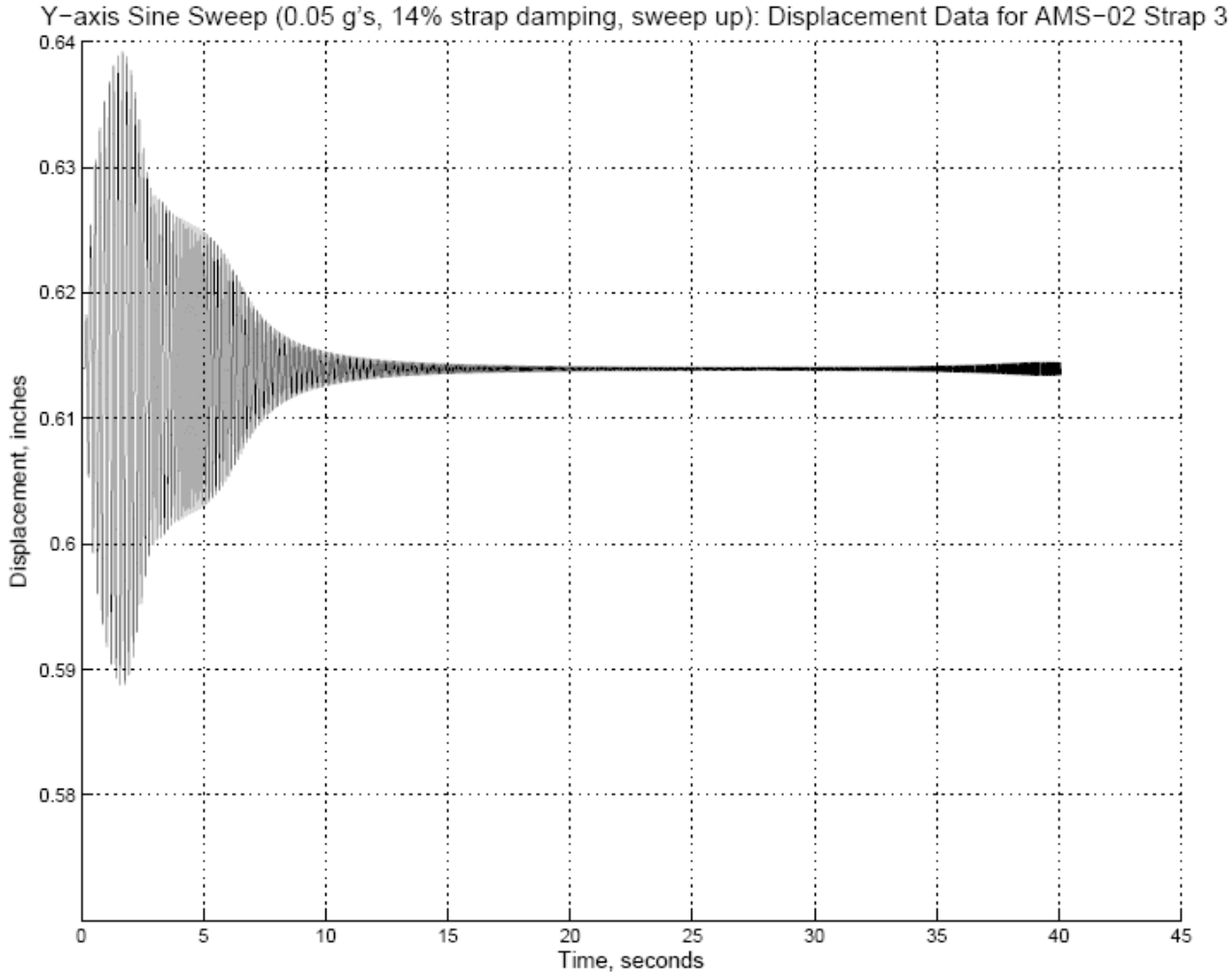

Figure 9-40 Strap 3 displacement response for y-axis configuration with 0.05 g sweep up

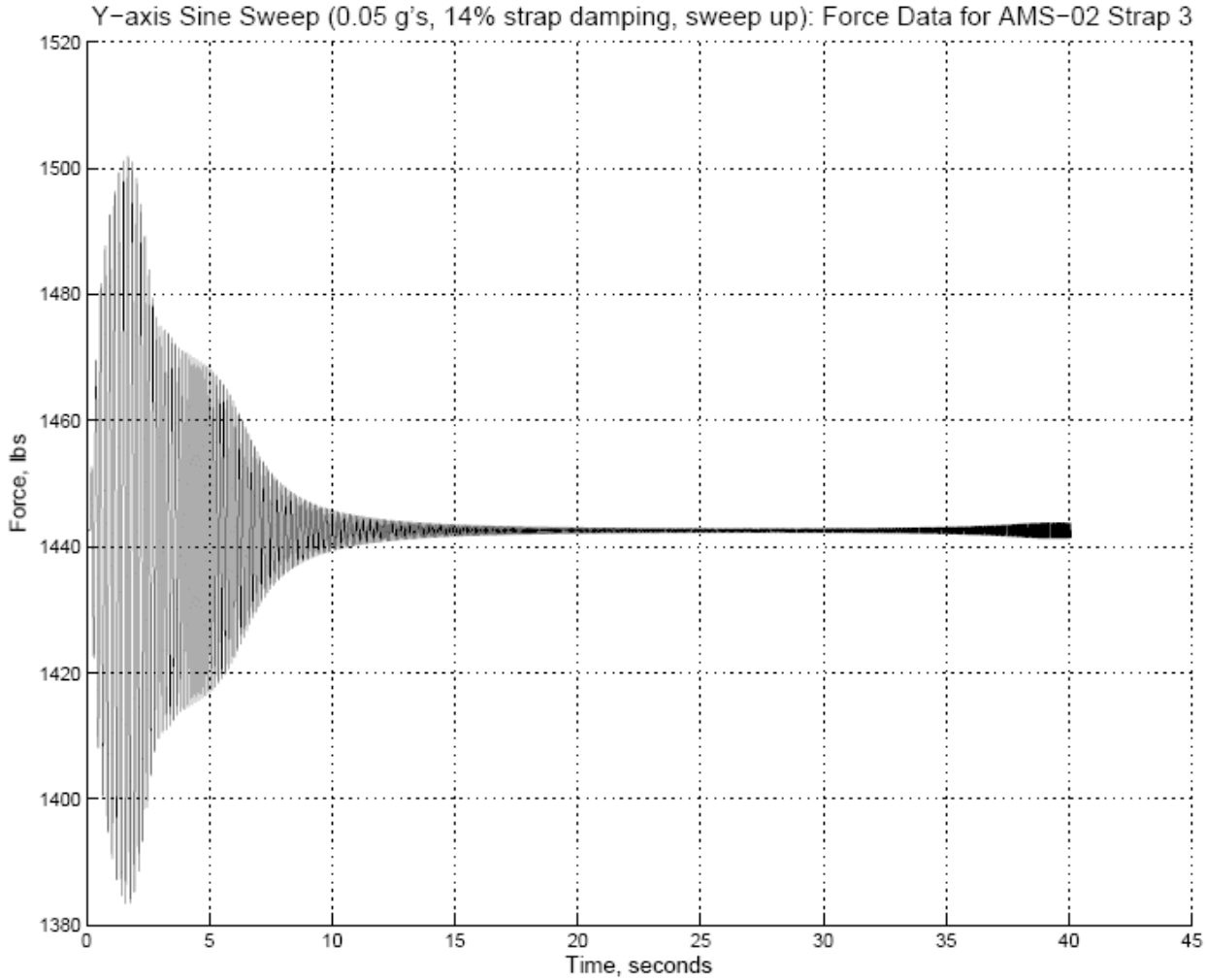

Figure 9-41 Strap 3 force response for y-axis configuration with 0.05 g sweep up

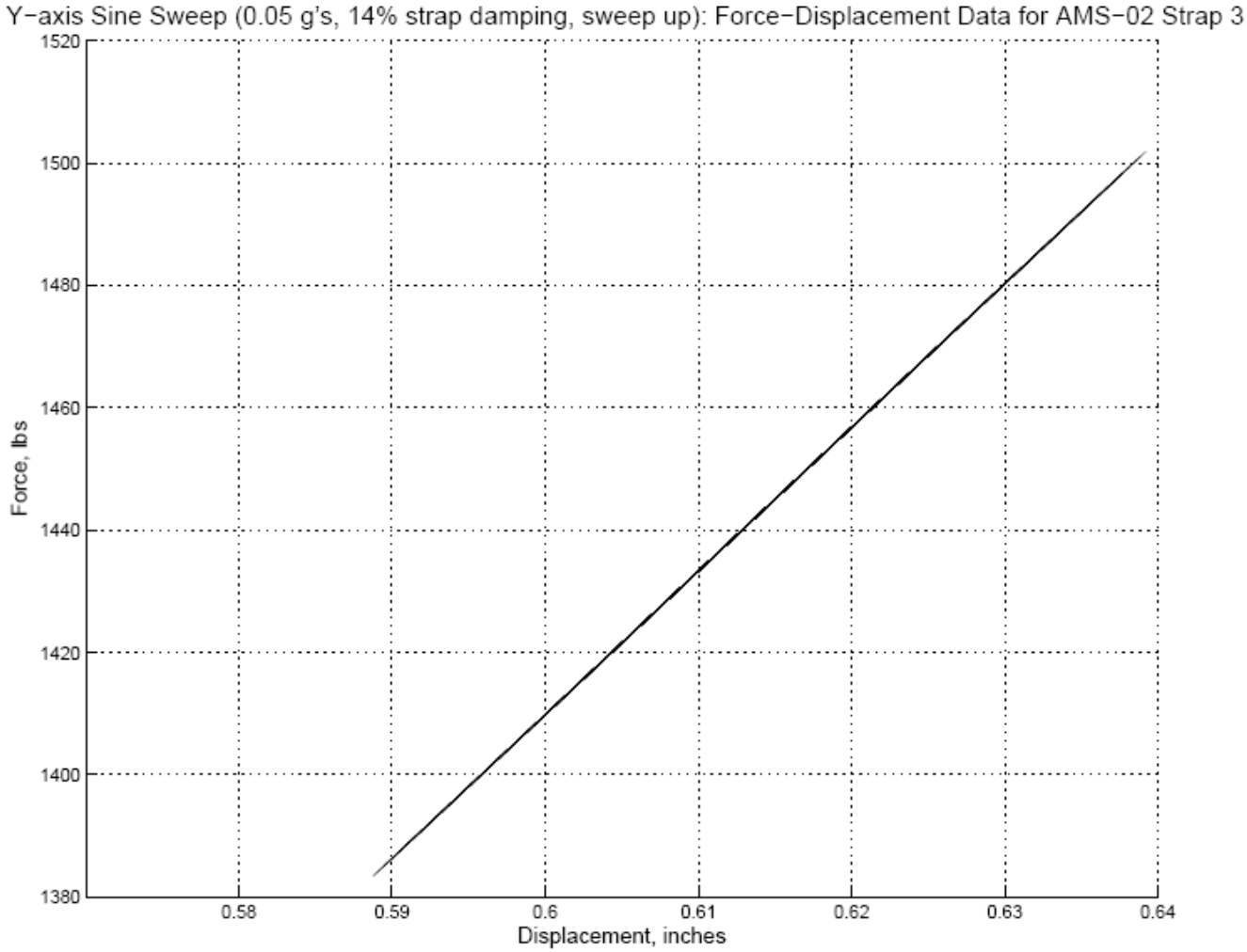

Figure 9-42 Strap 3 force-displacement curve for y-axis configuration with 0.05 g sweep up

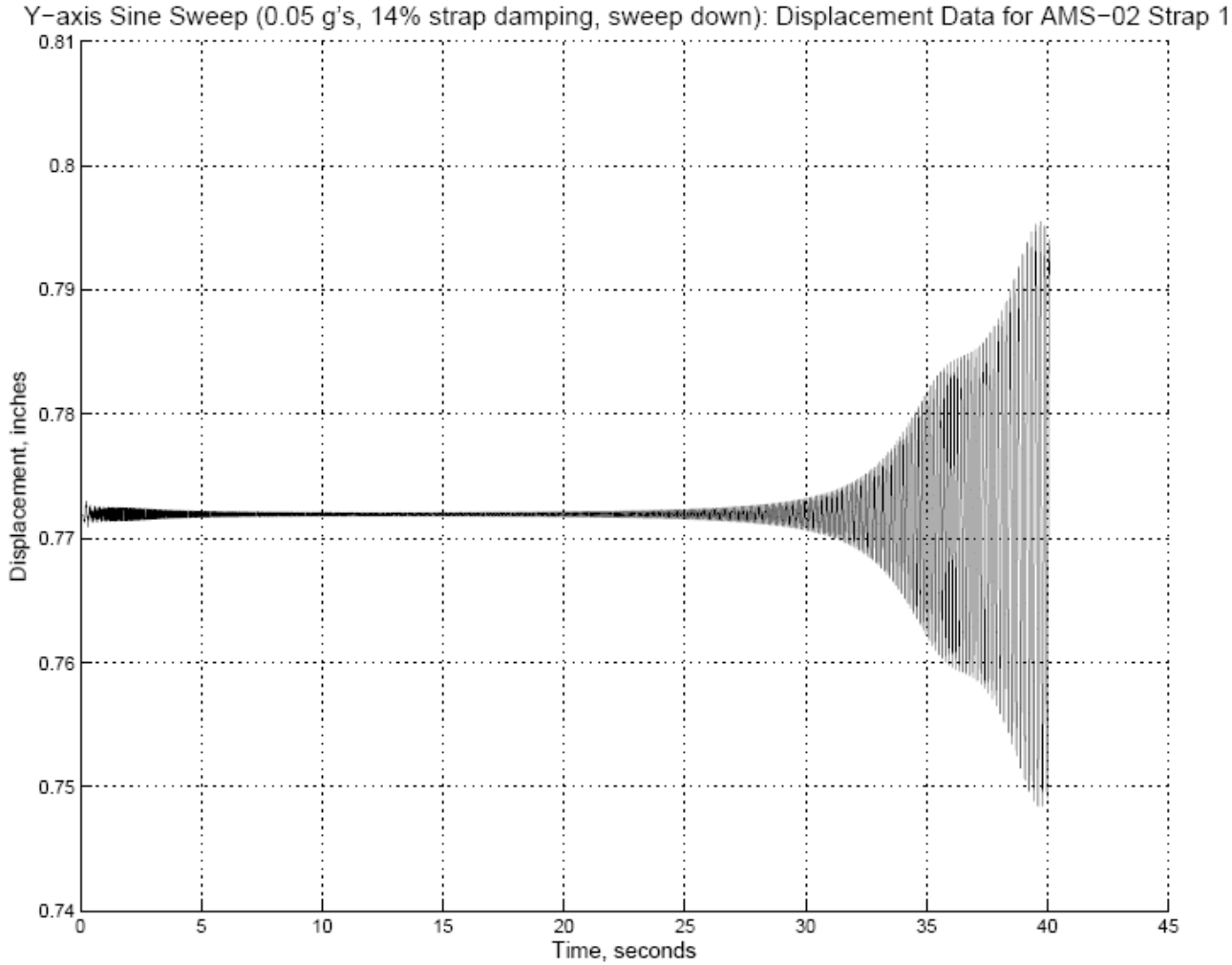

Figure 9-43 Strap 1 displacement response for y-axis configuration with 0.05 g sweep down

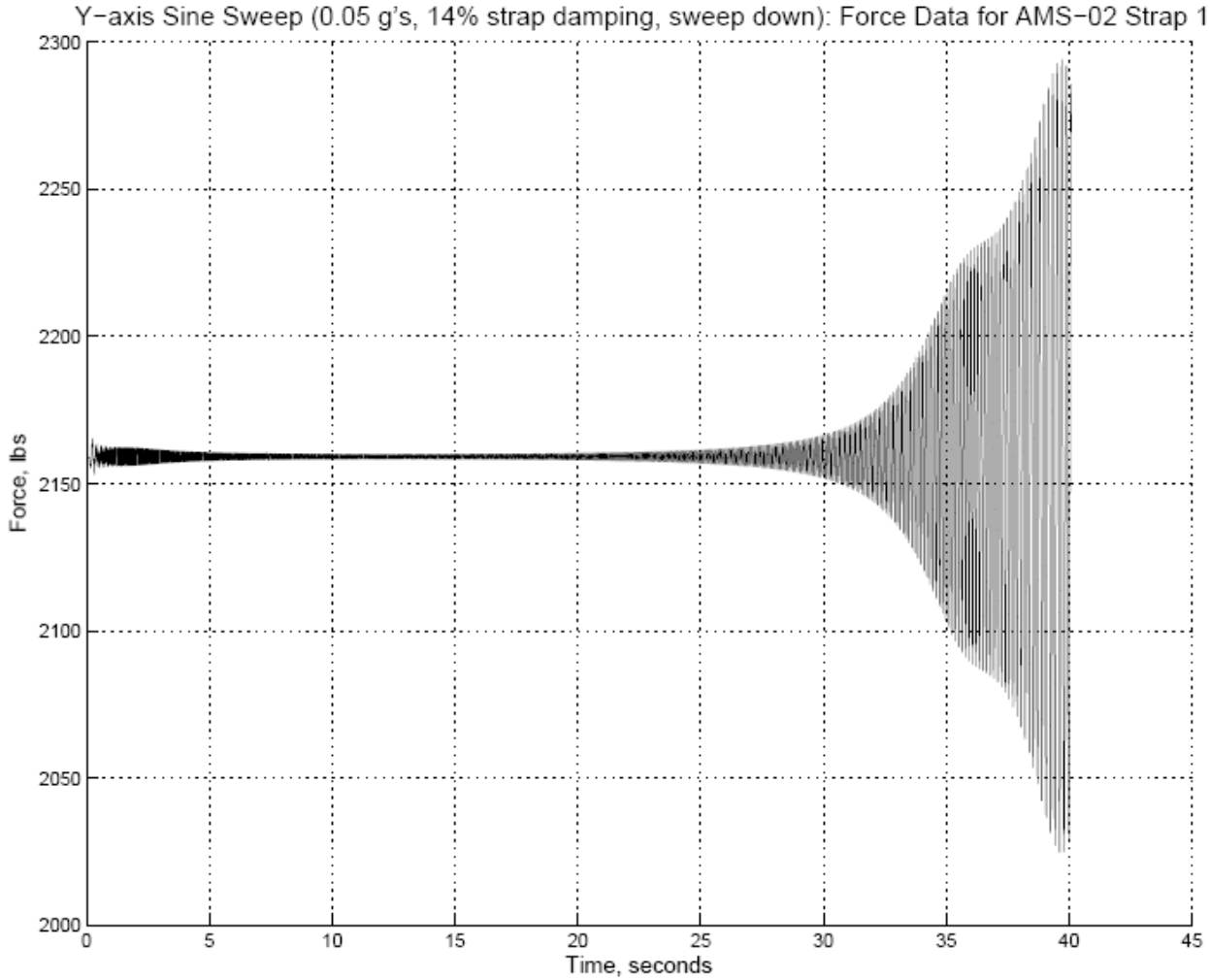

Figure 9-44 Strap 1 force response for y-axis configuration with 0.05 g sweep down

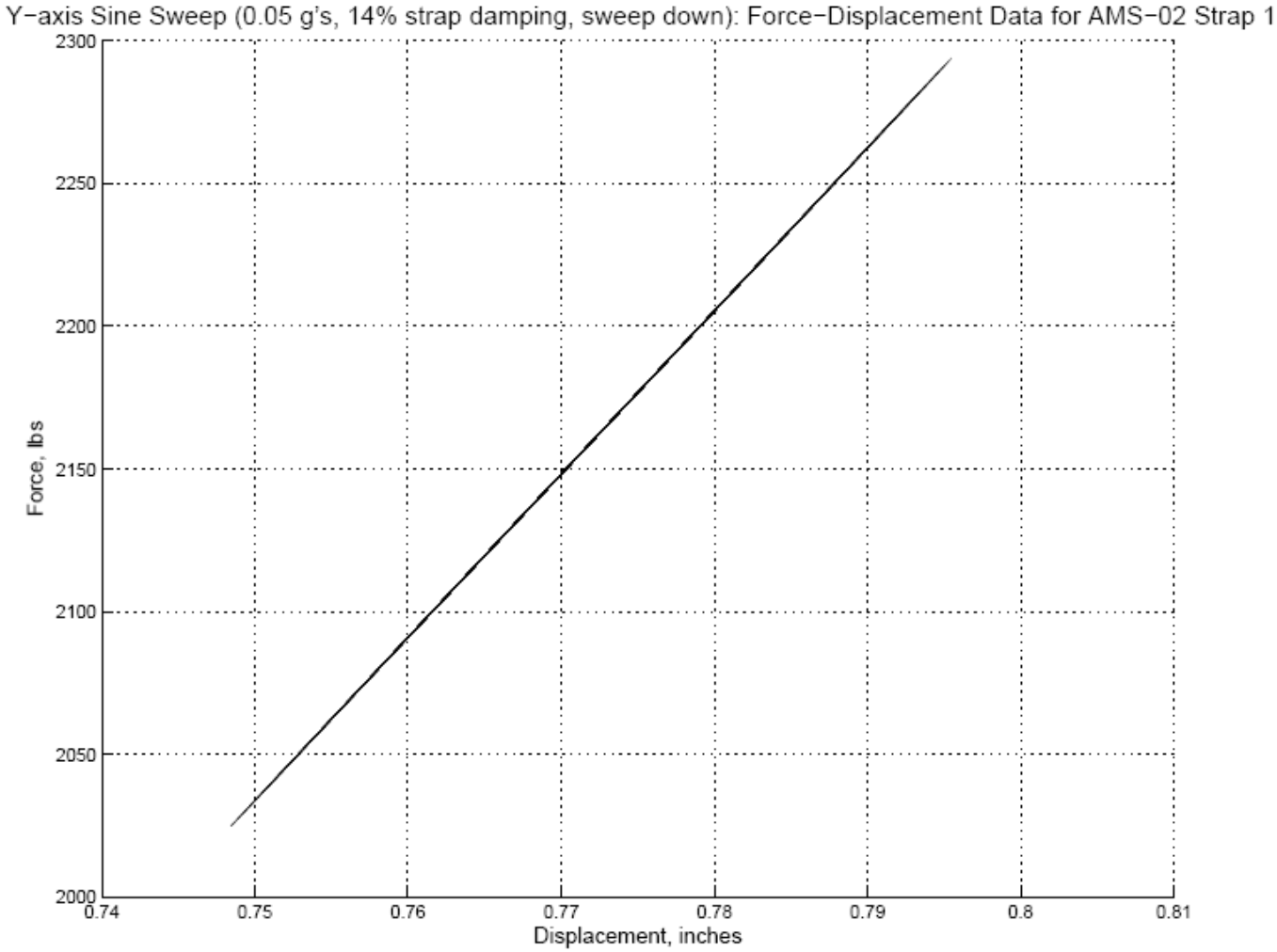

Figure 9-45 Strap 1 force-displacement curve for y-axis configuration with 0.05 g sweep down

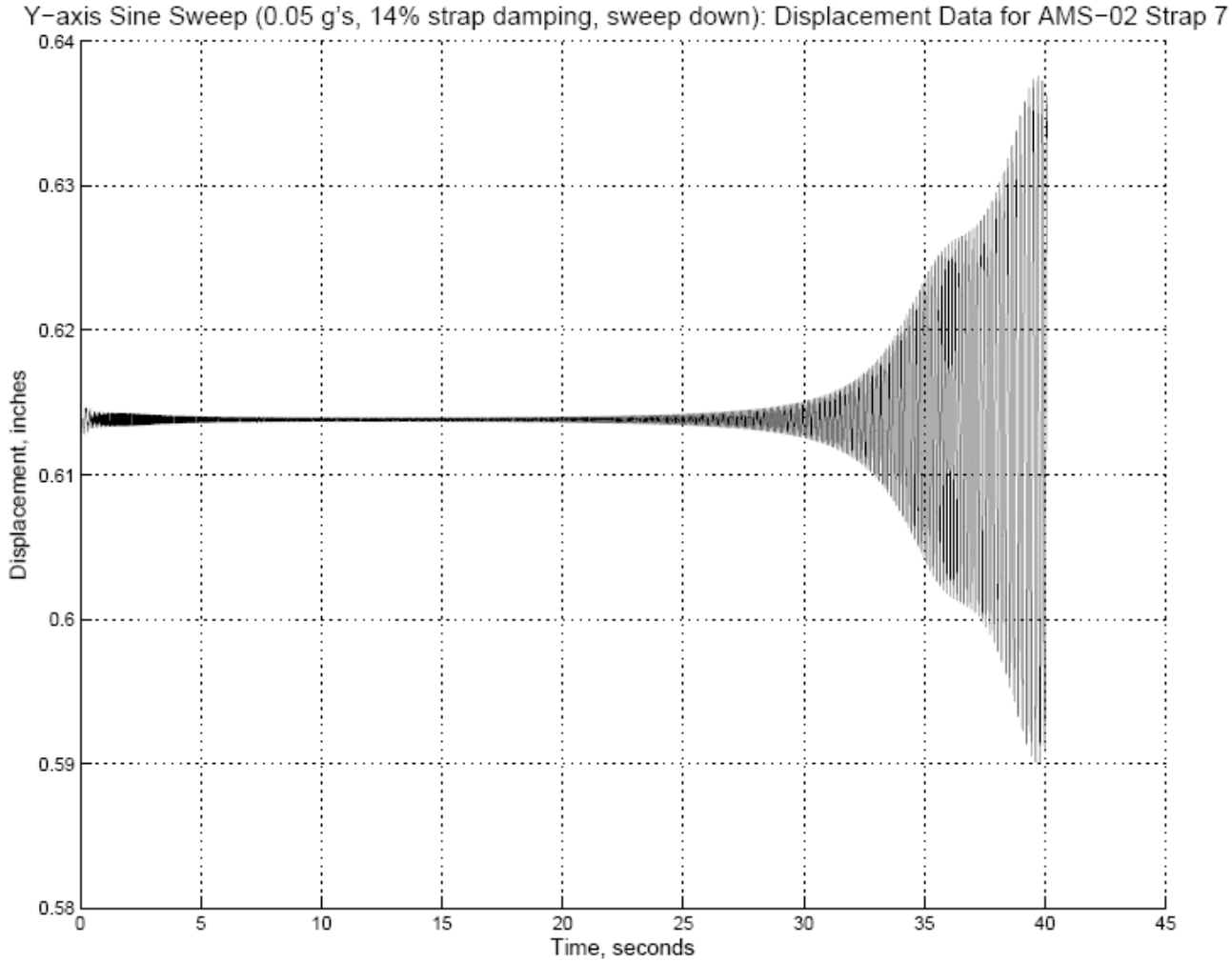

Figure 9-46 Strap 7 displacement response for y-axis configuration with 0.05 g sweep down

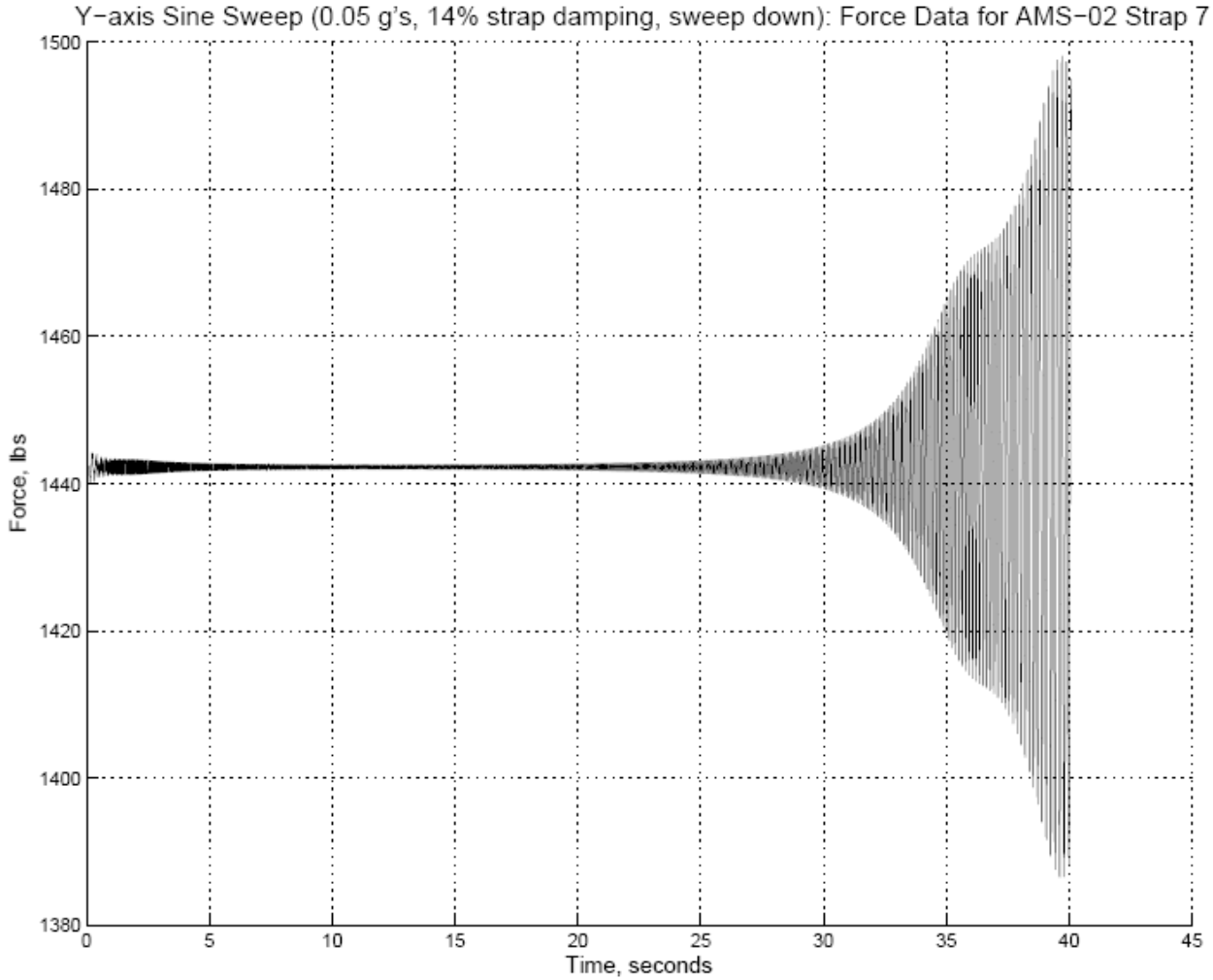

Figure 9-47 Strap 7 force response for y-axis configuration with 0.05 g sweep down

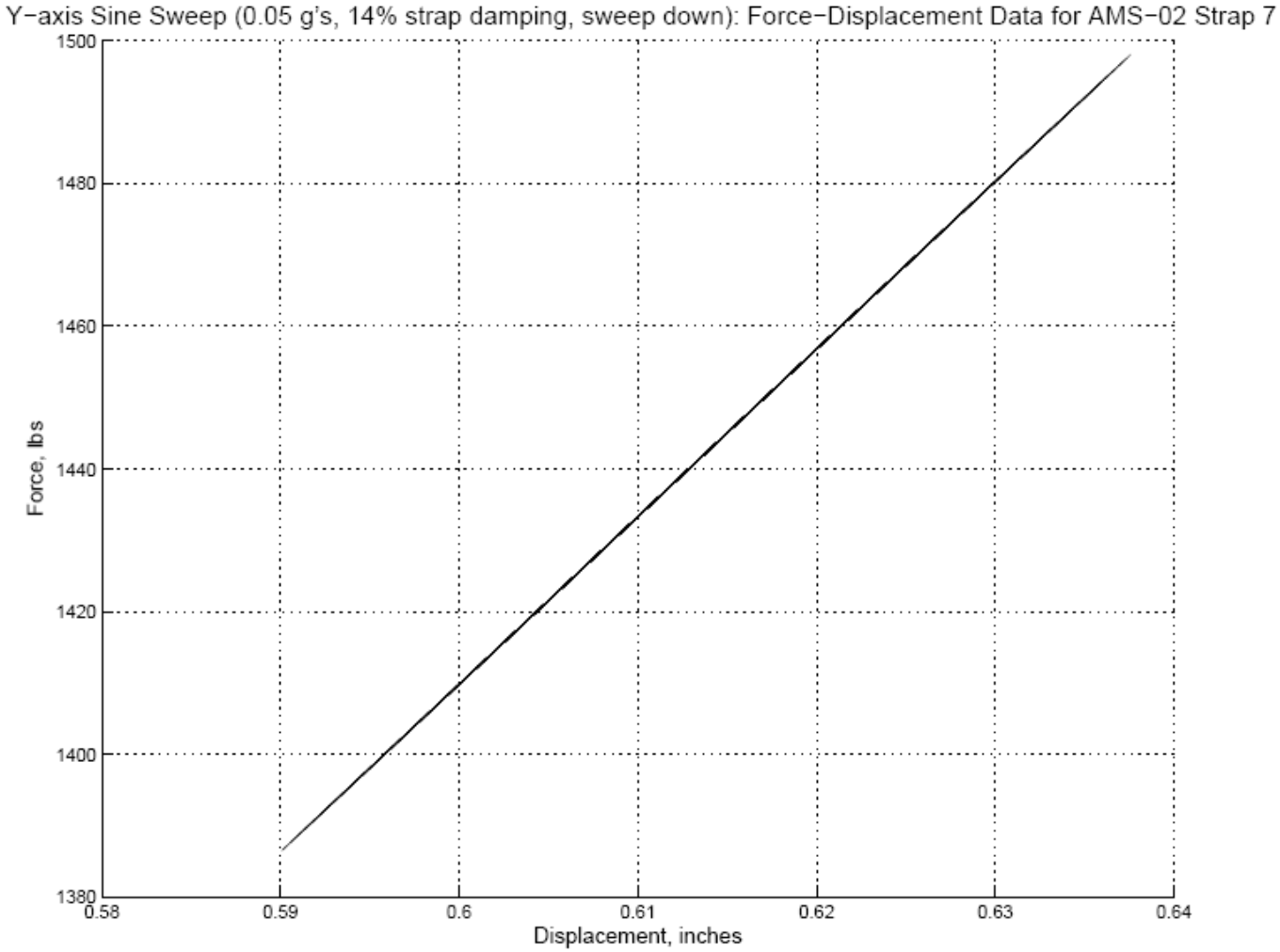

Figure 9-48 Strap 7 force-displacement curve for y-axis configuration with 0.05 g sweep down

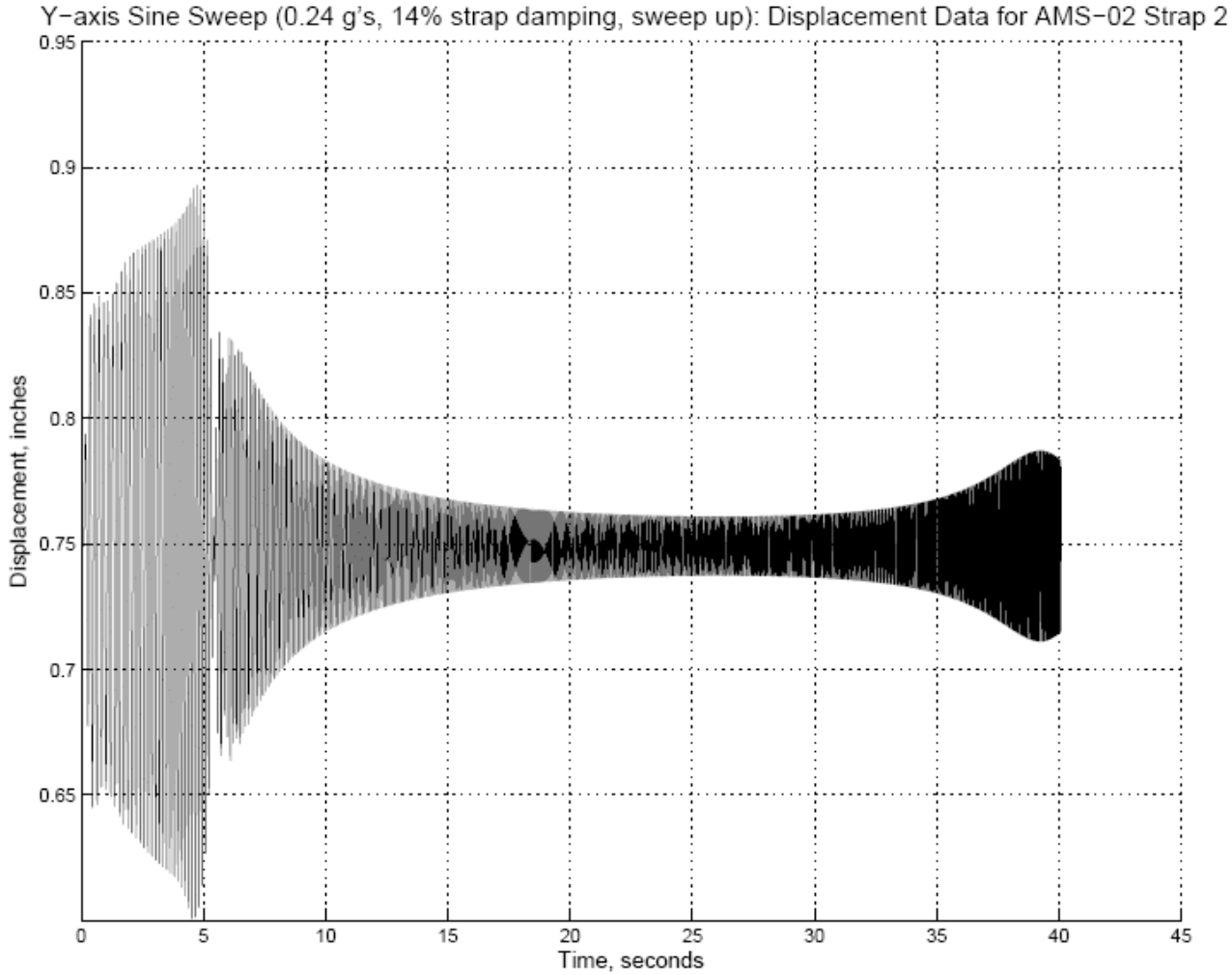

Figure 9-49 Strap 2 displacement response for y-axis configuration with 0.24 g sweep up

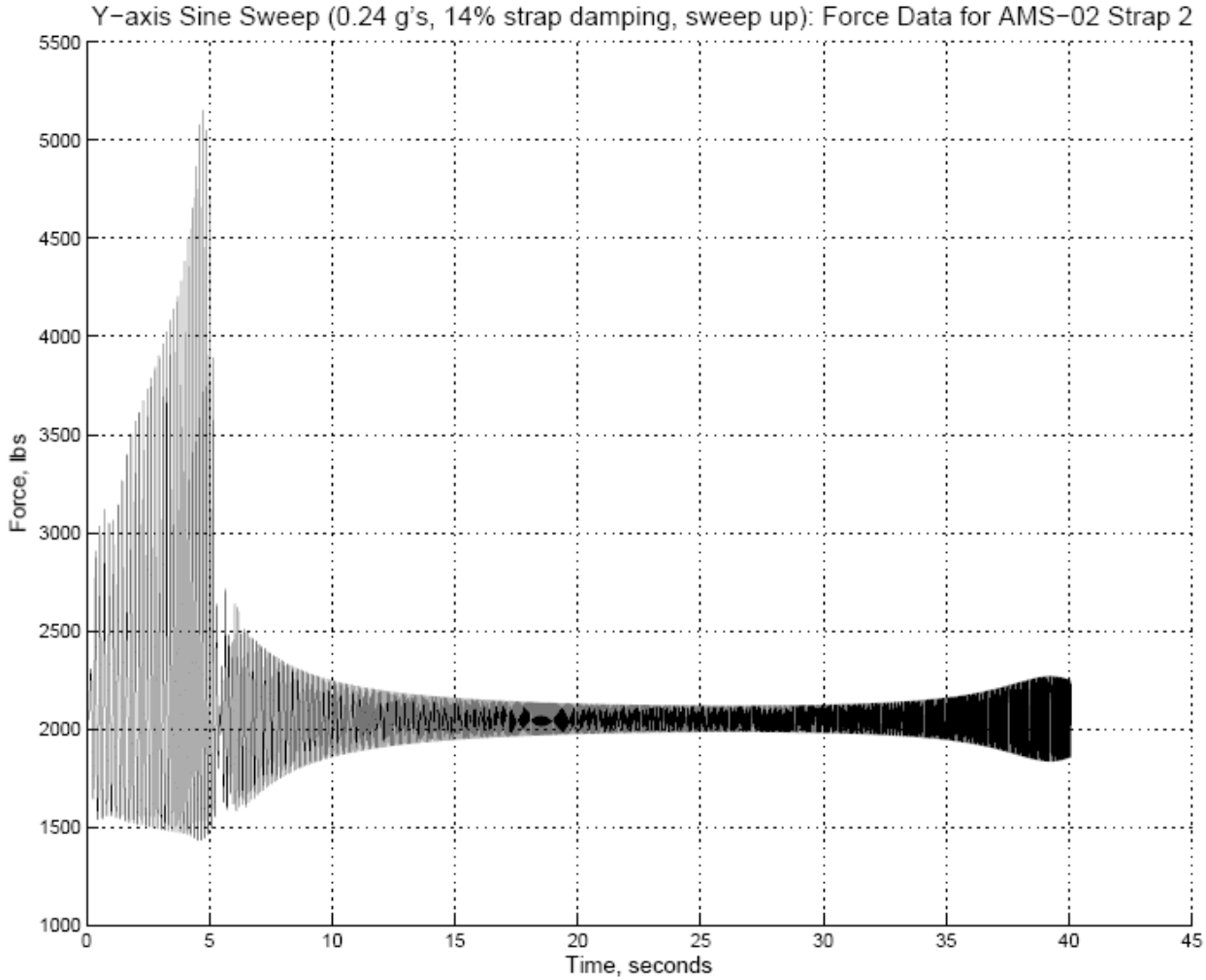

Figure 9-50 Strap 2 force response for y-axis configuration with 0.24 g sweep up

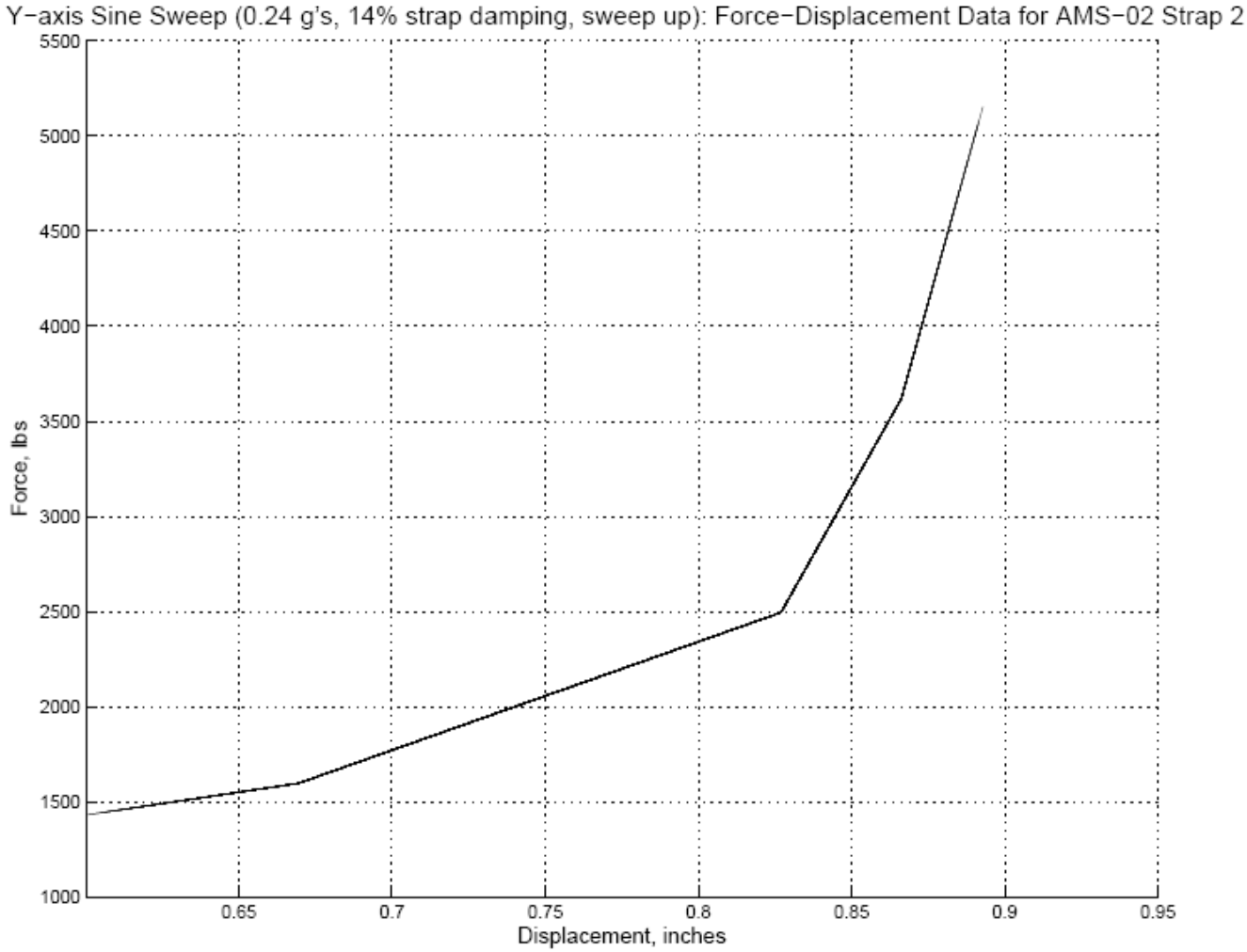

Figure 9-51 Strap 2 force-displacement curve for y-axis configuration with 0.24 g sweep up

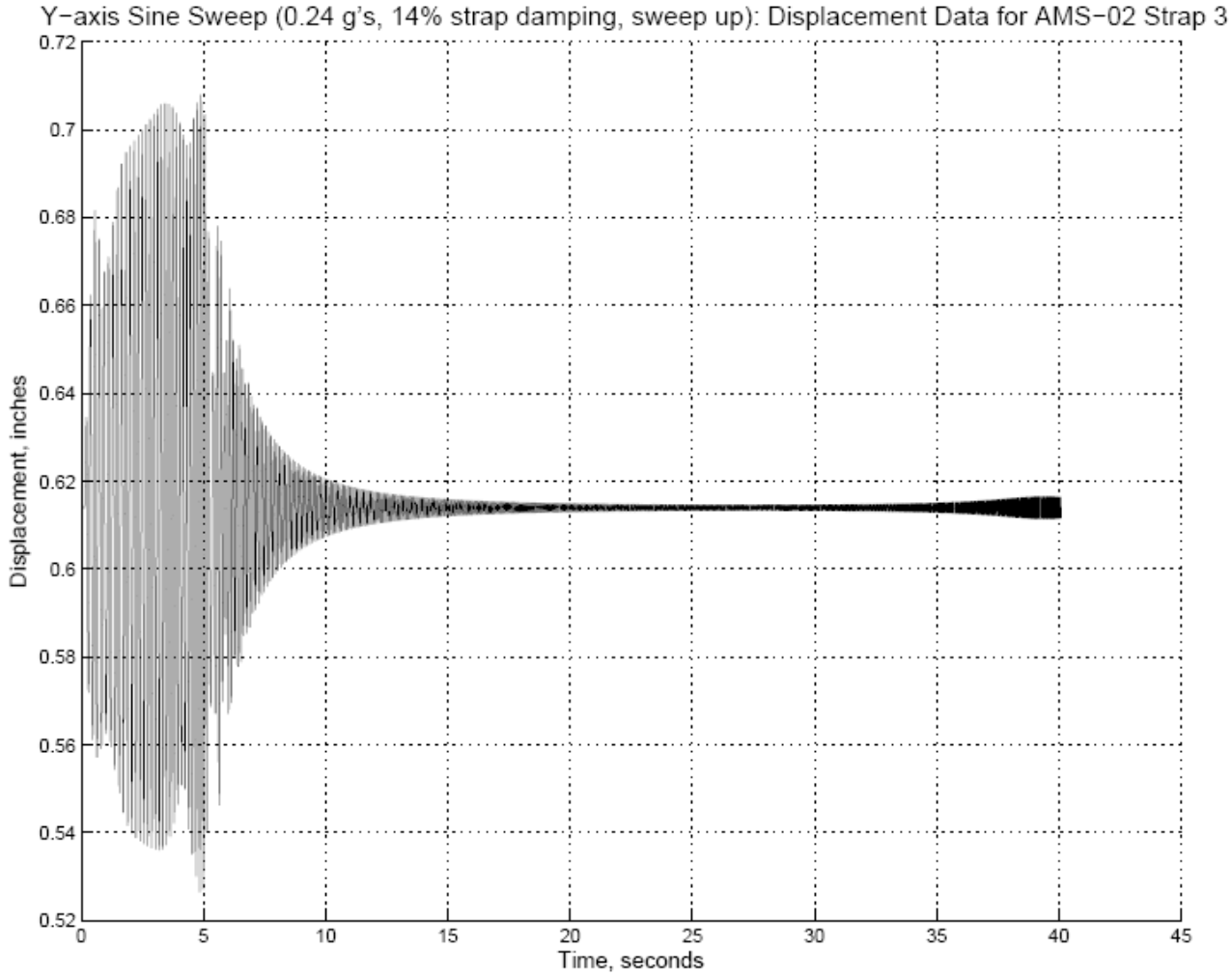

Figure 9-52 Strap 3 displacement response for y-axis configuration with 0.24 g sweep up

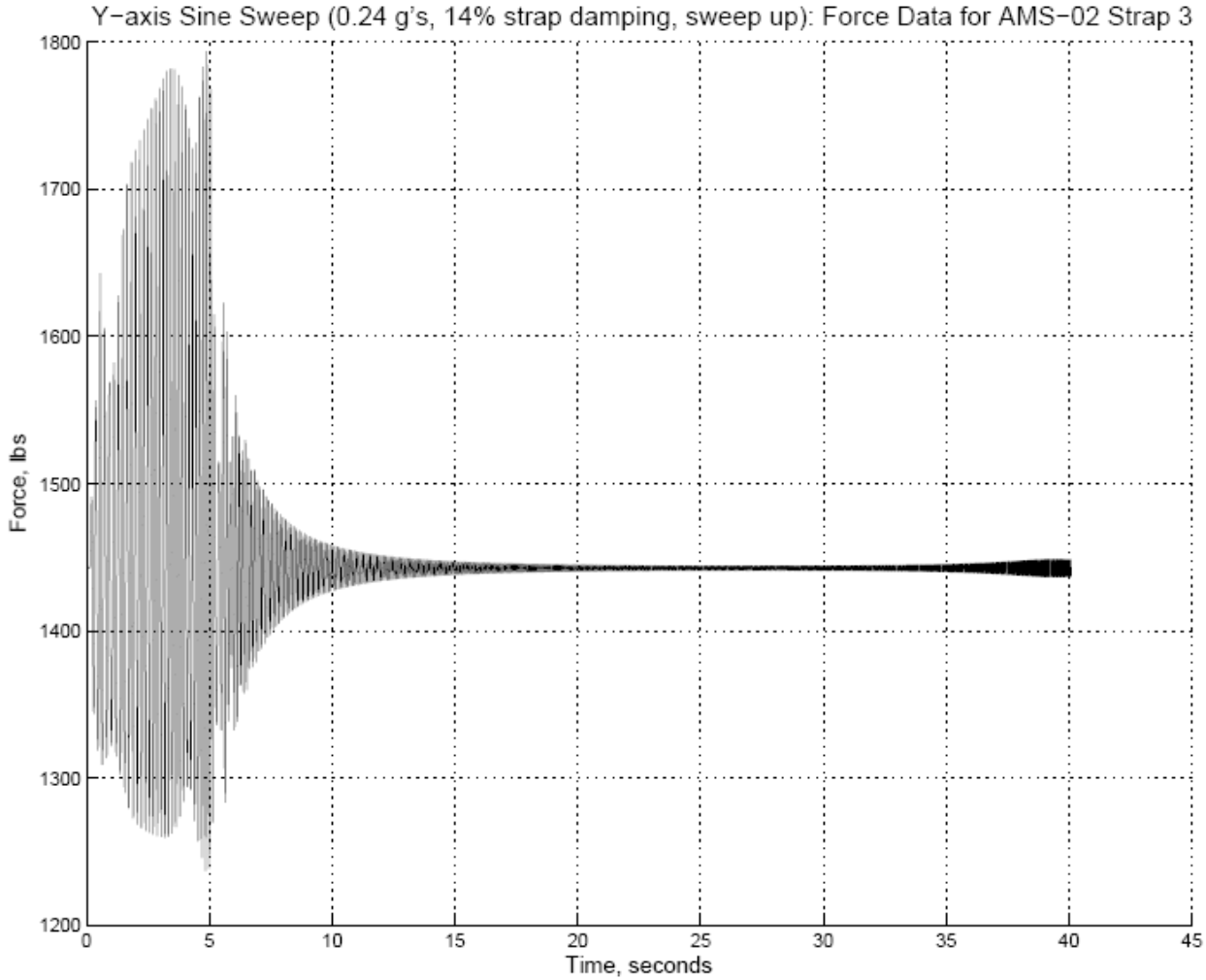

Figure 9-53 Strap 3 force response for y-axis configuration with 0.24 g sweep up

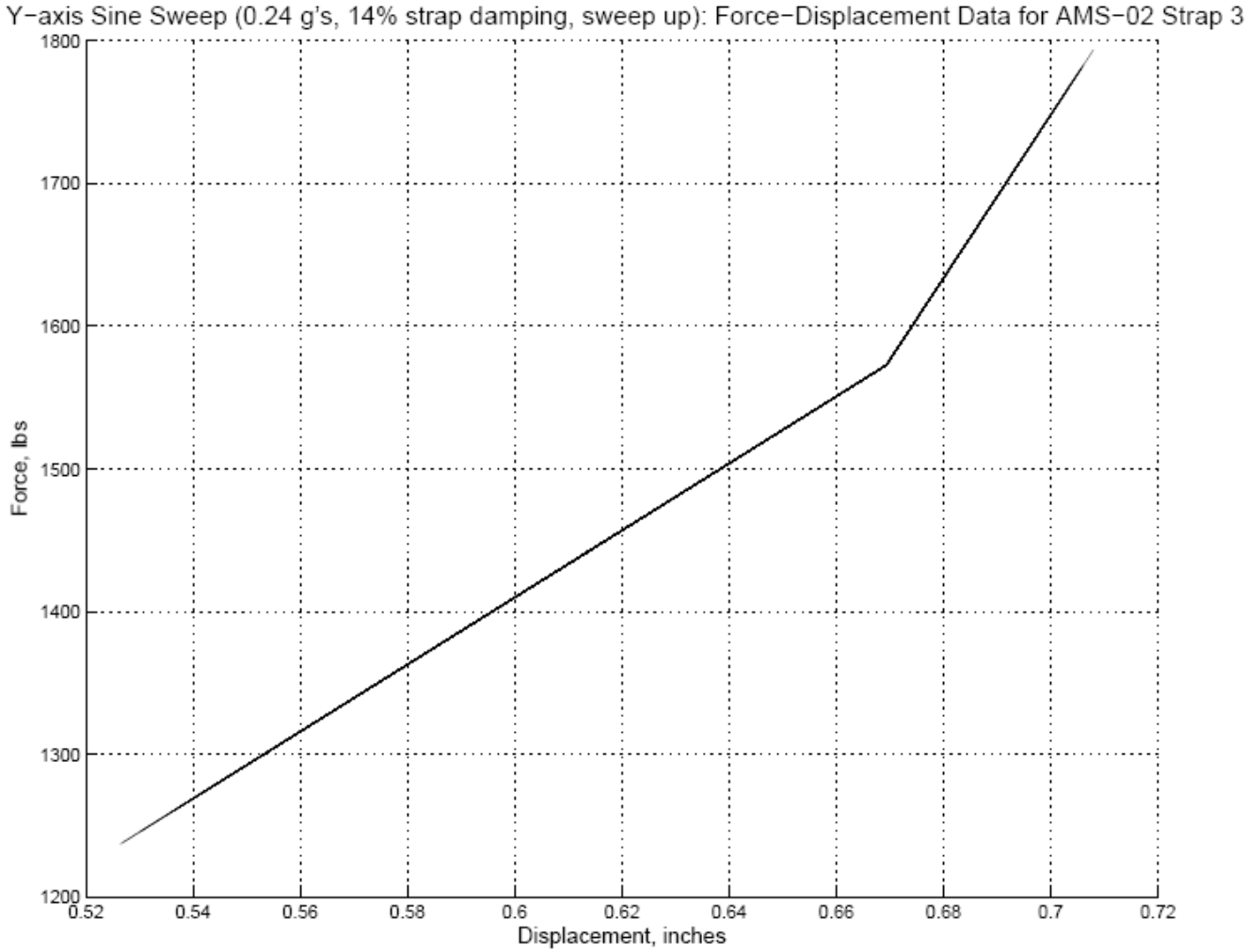

Figure 9-54 Strap 3 force-displacement curve for y-axis configuration with 0.24 g sweep up

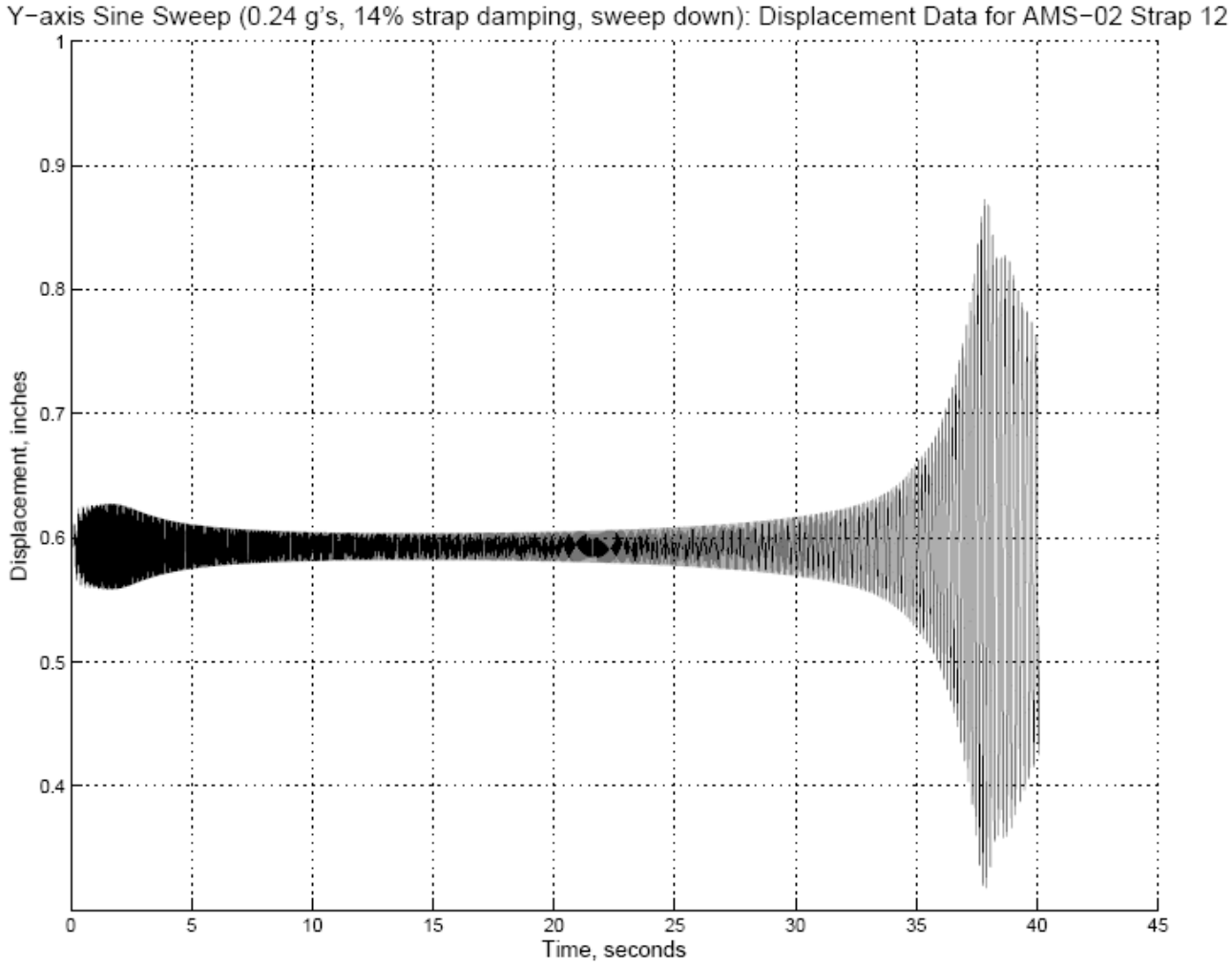

Figure 9-55 Strap 12 displacement response for y-axis configuration with 0.24 g sweep down

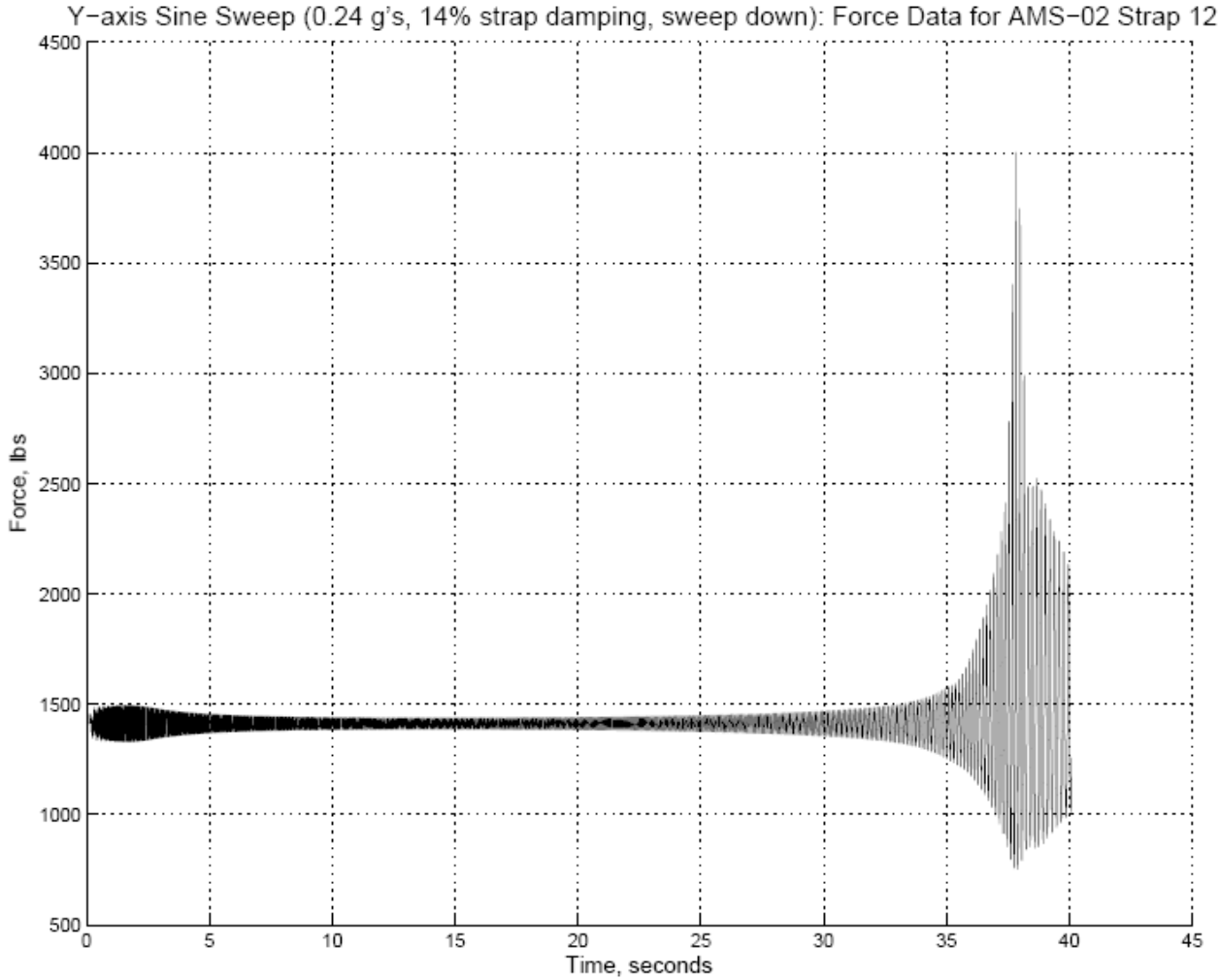

Figure 9-56 Strap 12 force response for y-axis configuration with 0.24 g sweep down

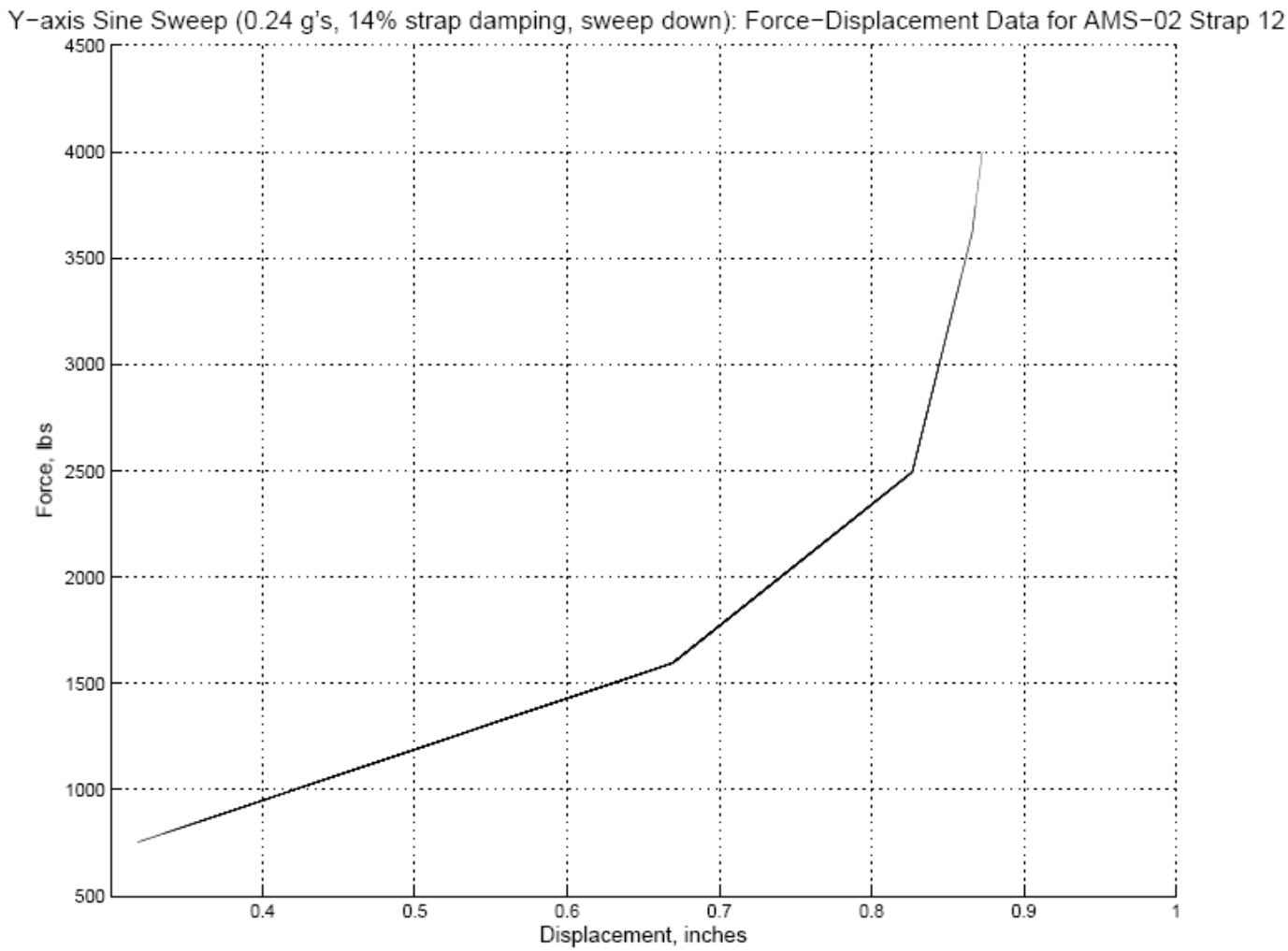

Figure 9-57 Strap 12 force-displacement curve for y-axis configuration with 0.24 g sweep down

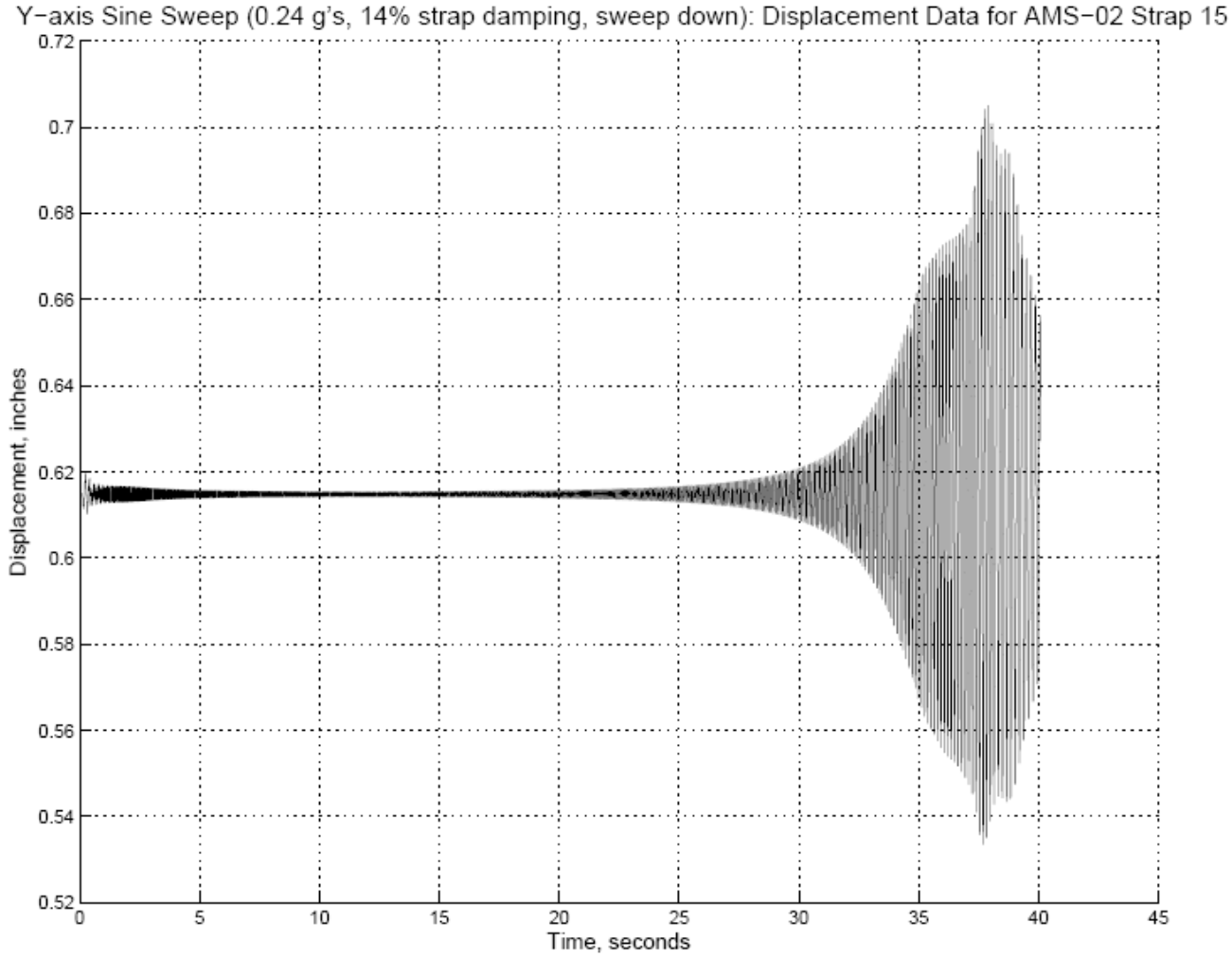

Figure 9-58 Strap 15 displacement response for y-axis configuration with 0.24 g sweep down

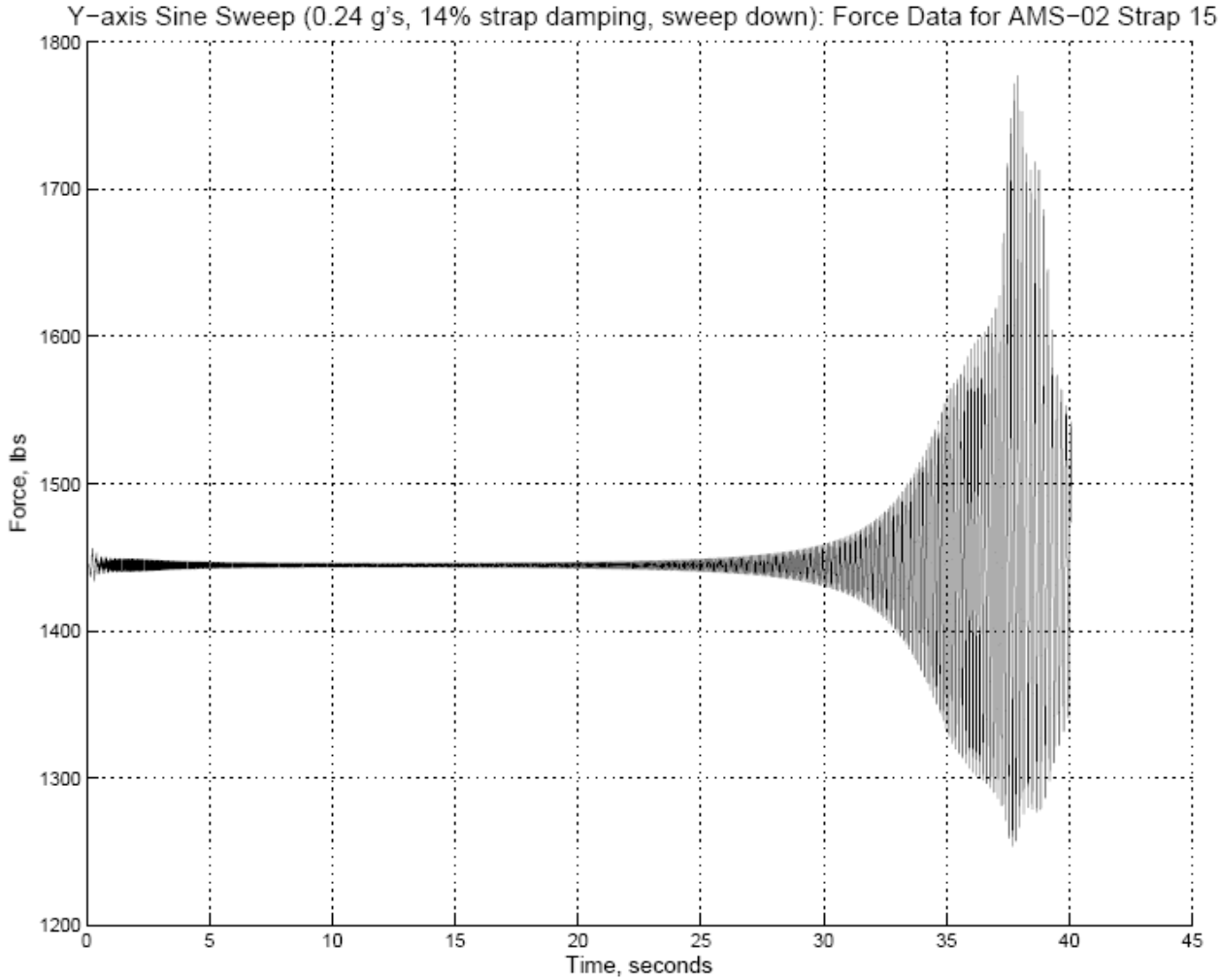

Figure 9-59 Strap 15 force response for y-axis configuration with 0.24 g sweep down

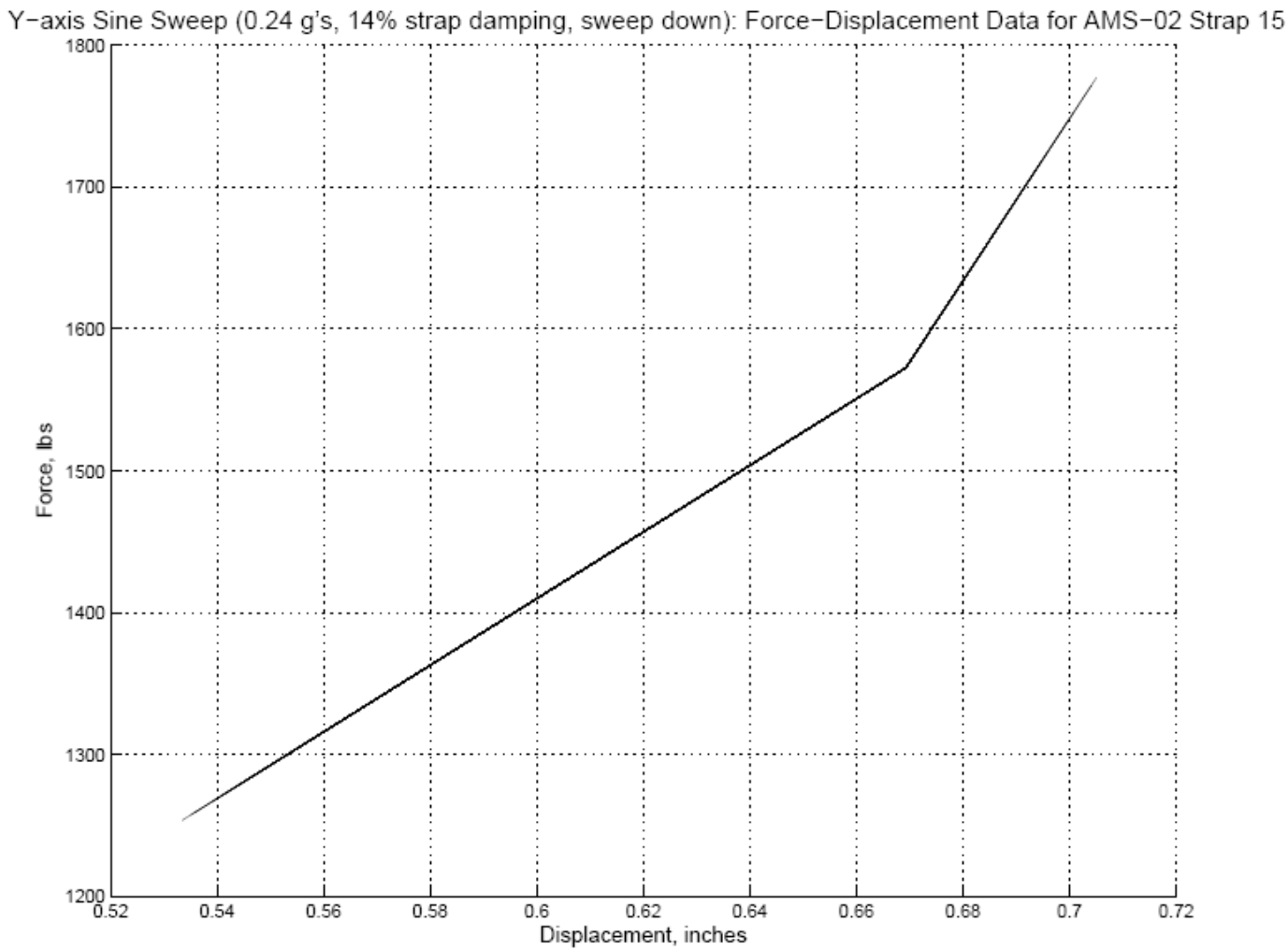

Figure 9-60 Strap 15 force-displacement curve for y-axis configuration with 0.24 g sweep down

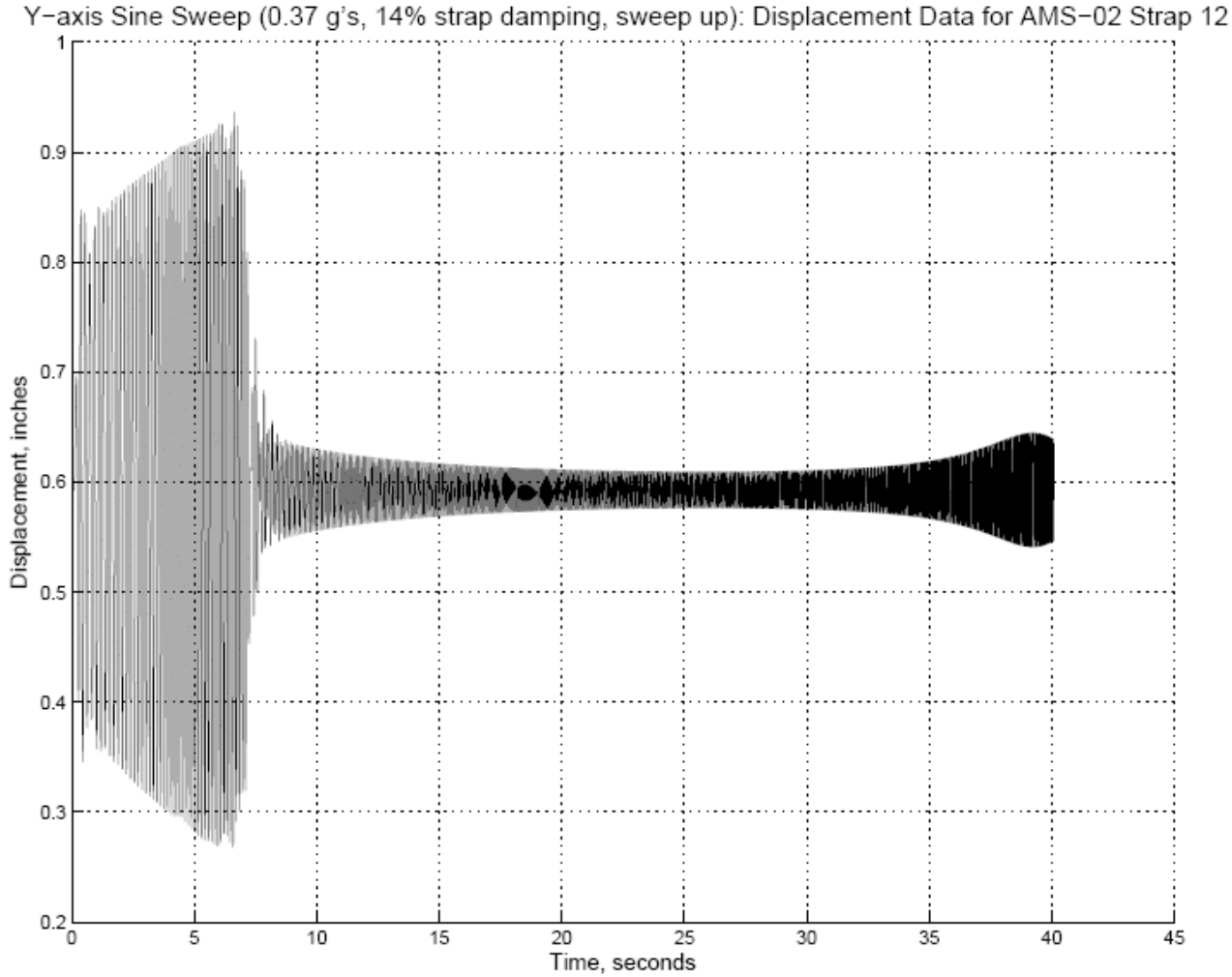

Figure 9-61 Strap 12 displacement response for y-axis configuration with 0.37 g sweep up

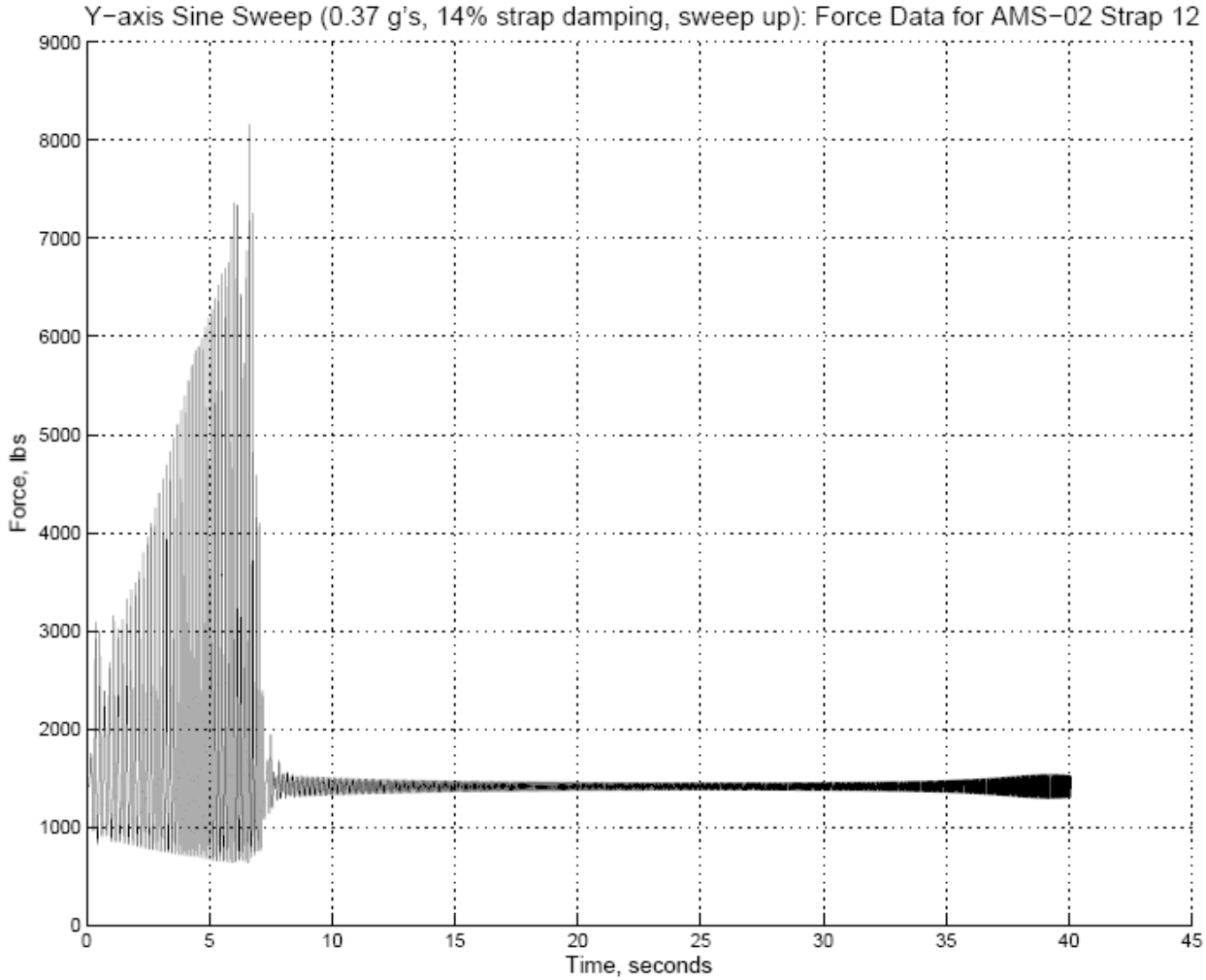

Figure 9-62 Strap 12 force response for y-axis configuration with 0.37 g sweep up

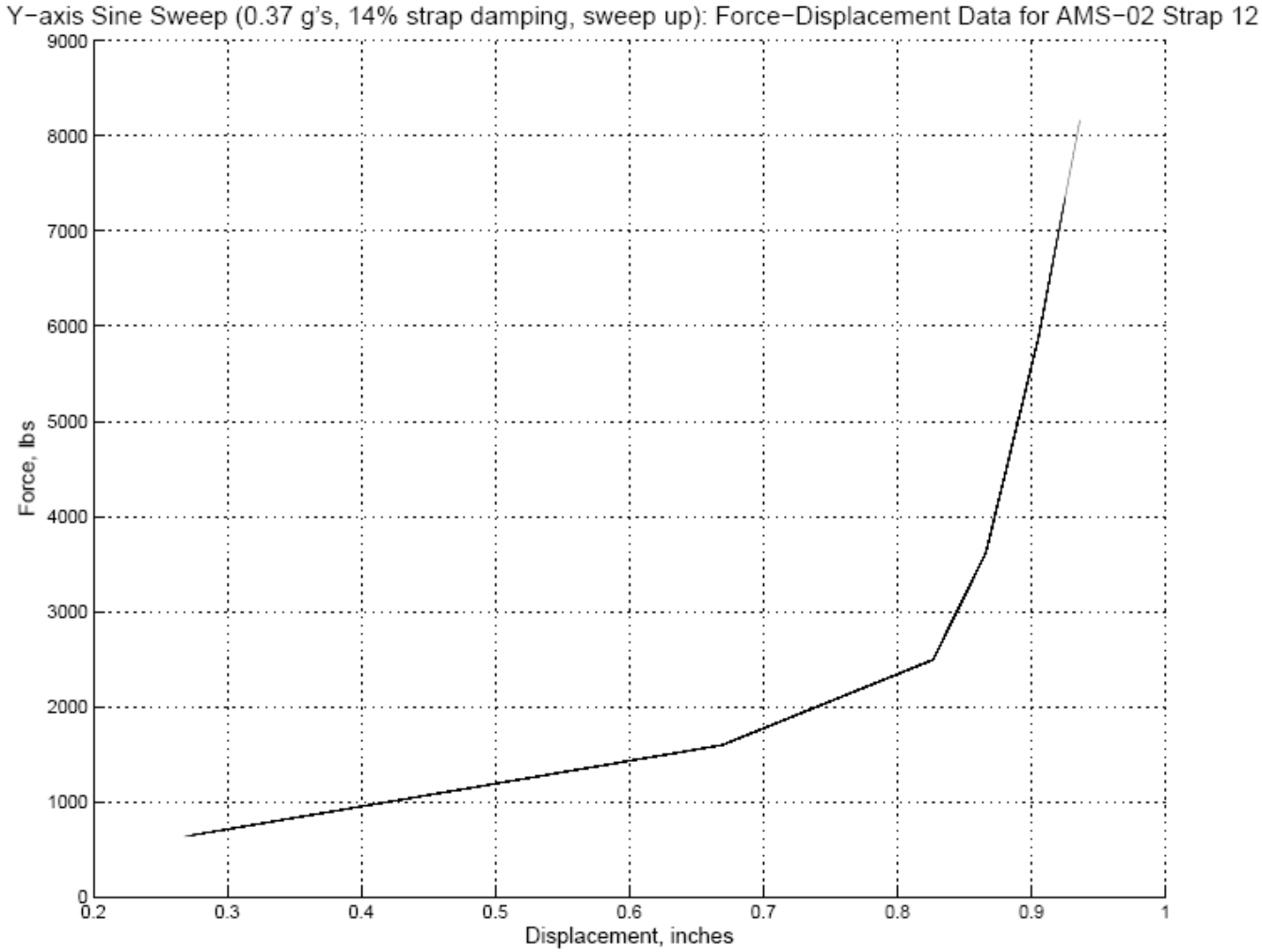

Figure 9-63 Strap 12 force-displacement curve for y-axis configuration with 0.37 g sweep up

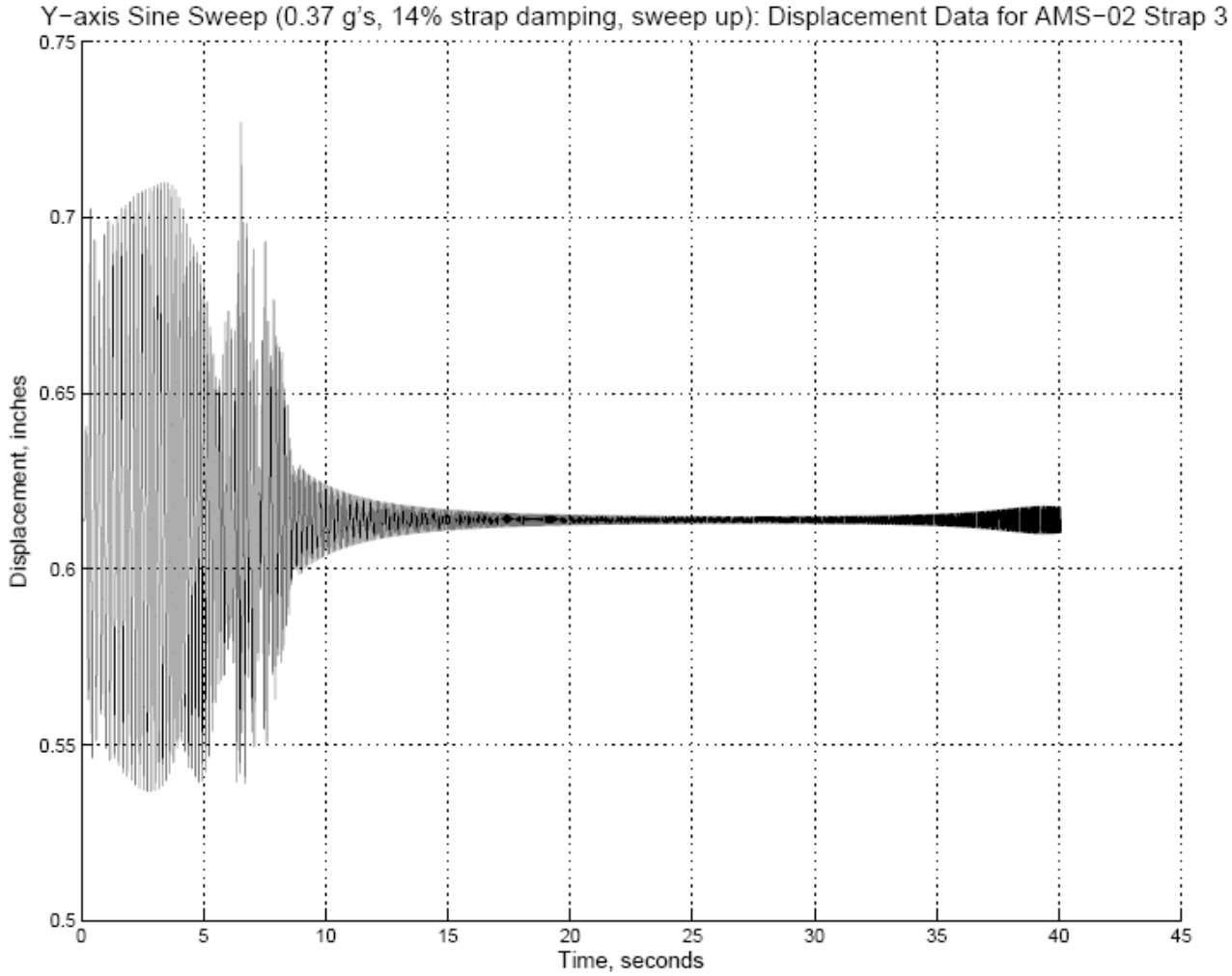

Figure 9-64 Strap 3 displacement response for y-axis configuration with 0.37 g sweep up

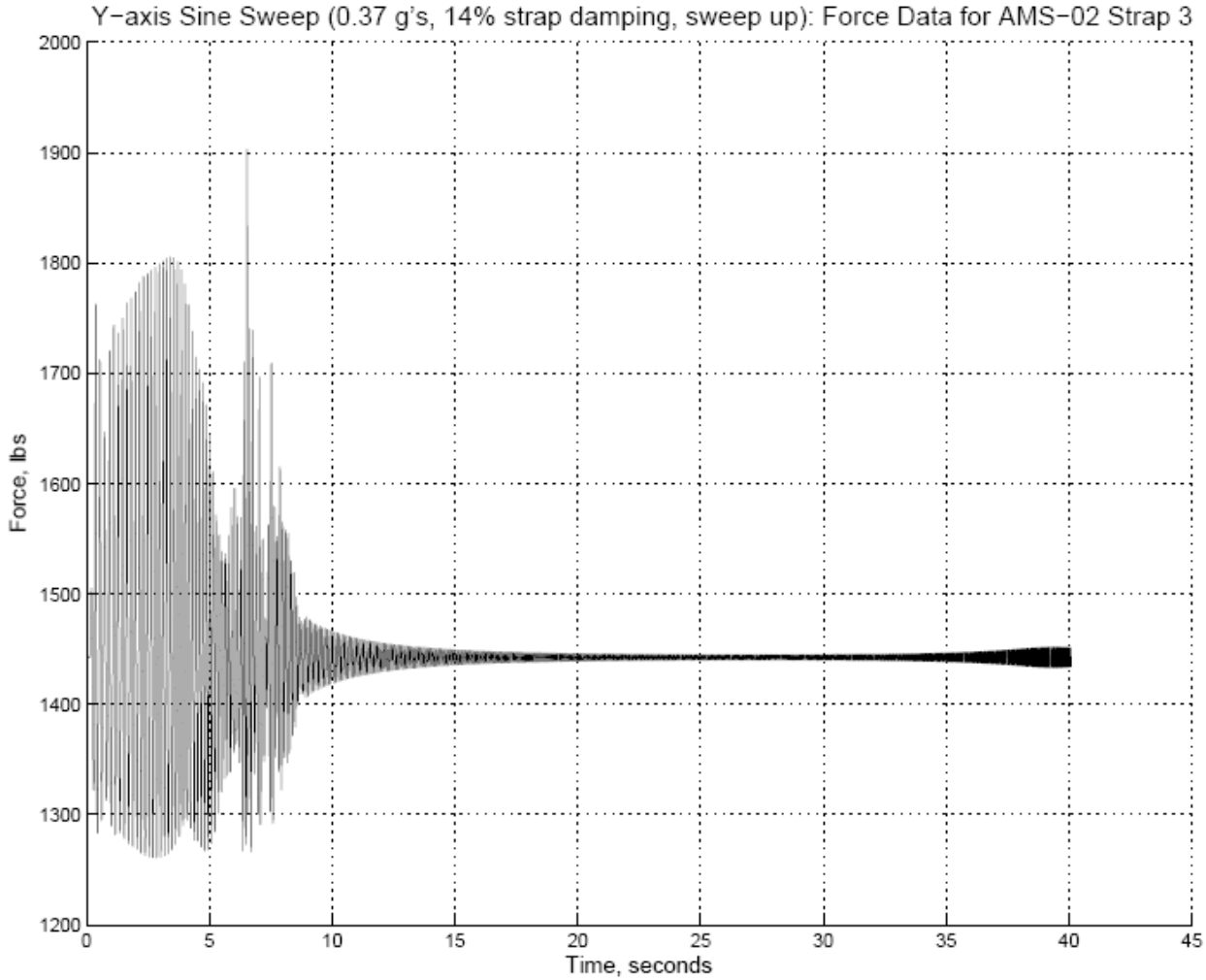

Figure 9-65 Strap 3 force response for y-axis configuration with 0.37 g sweep up

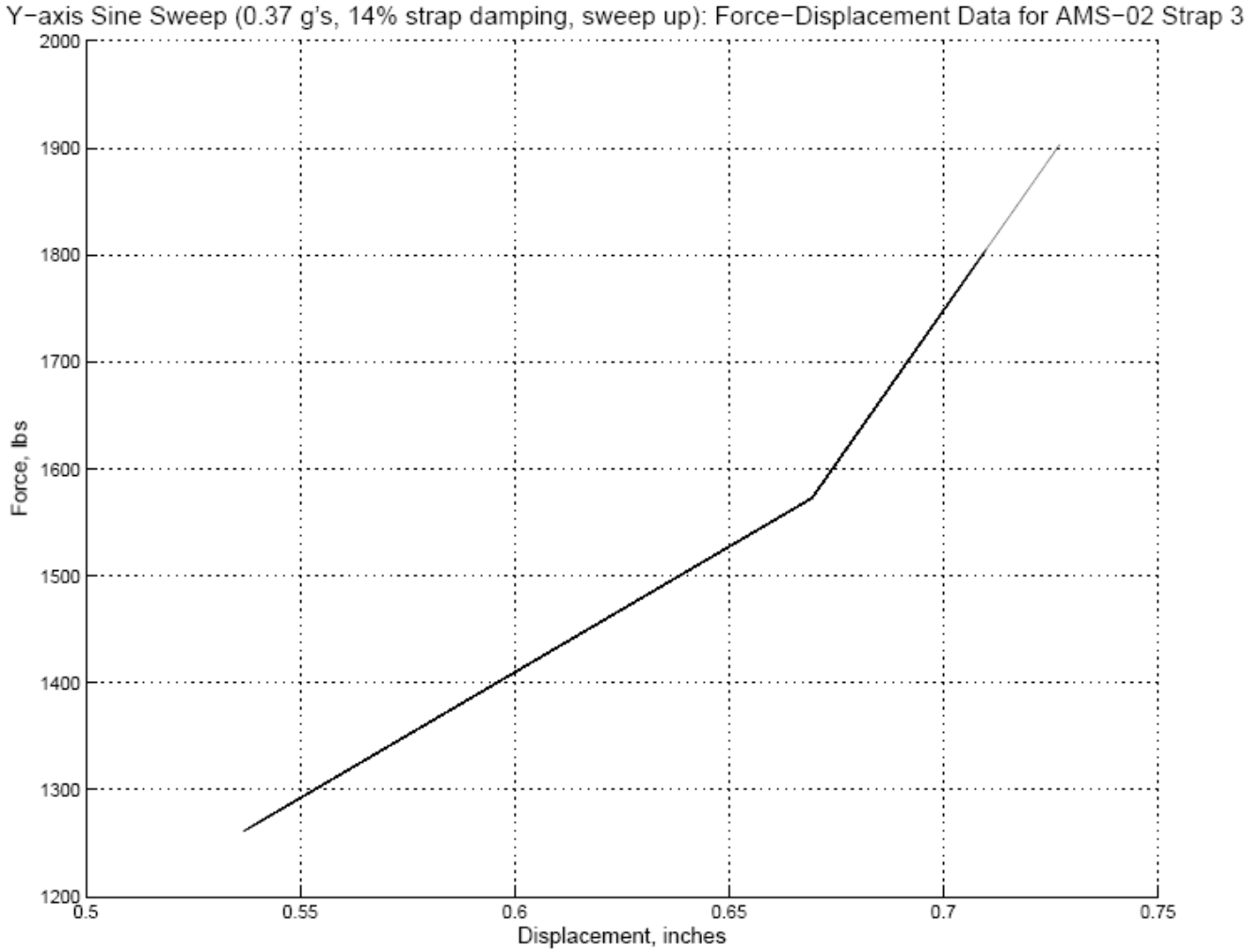

Figure 9-66 Strap 3 force-displacement curve for y-axis configuration with 0.37 g sweep up

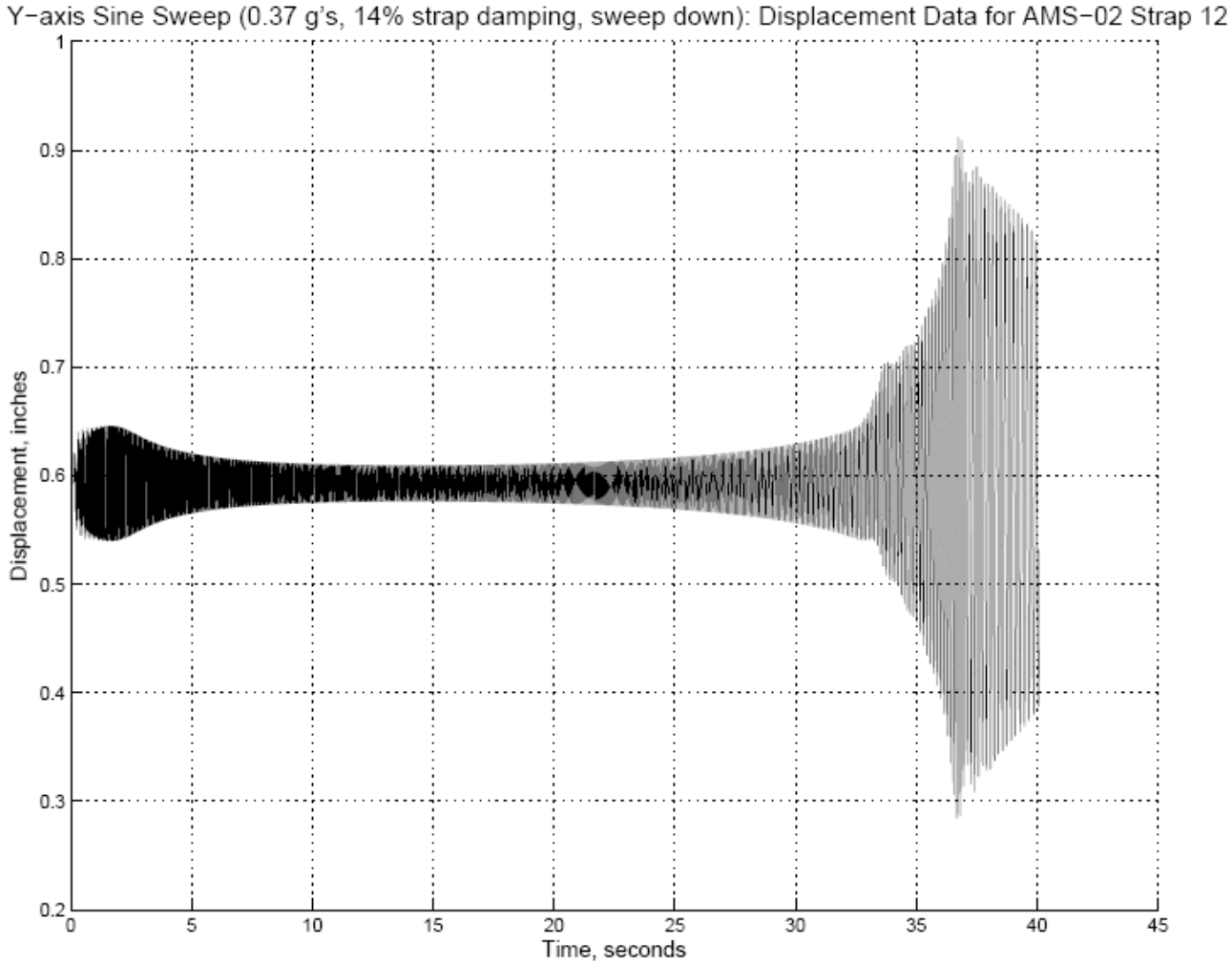

Figure 9-67 Strap 12 displacement response for y-axis configuration with 0.37 g sweep down

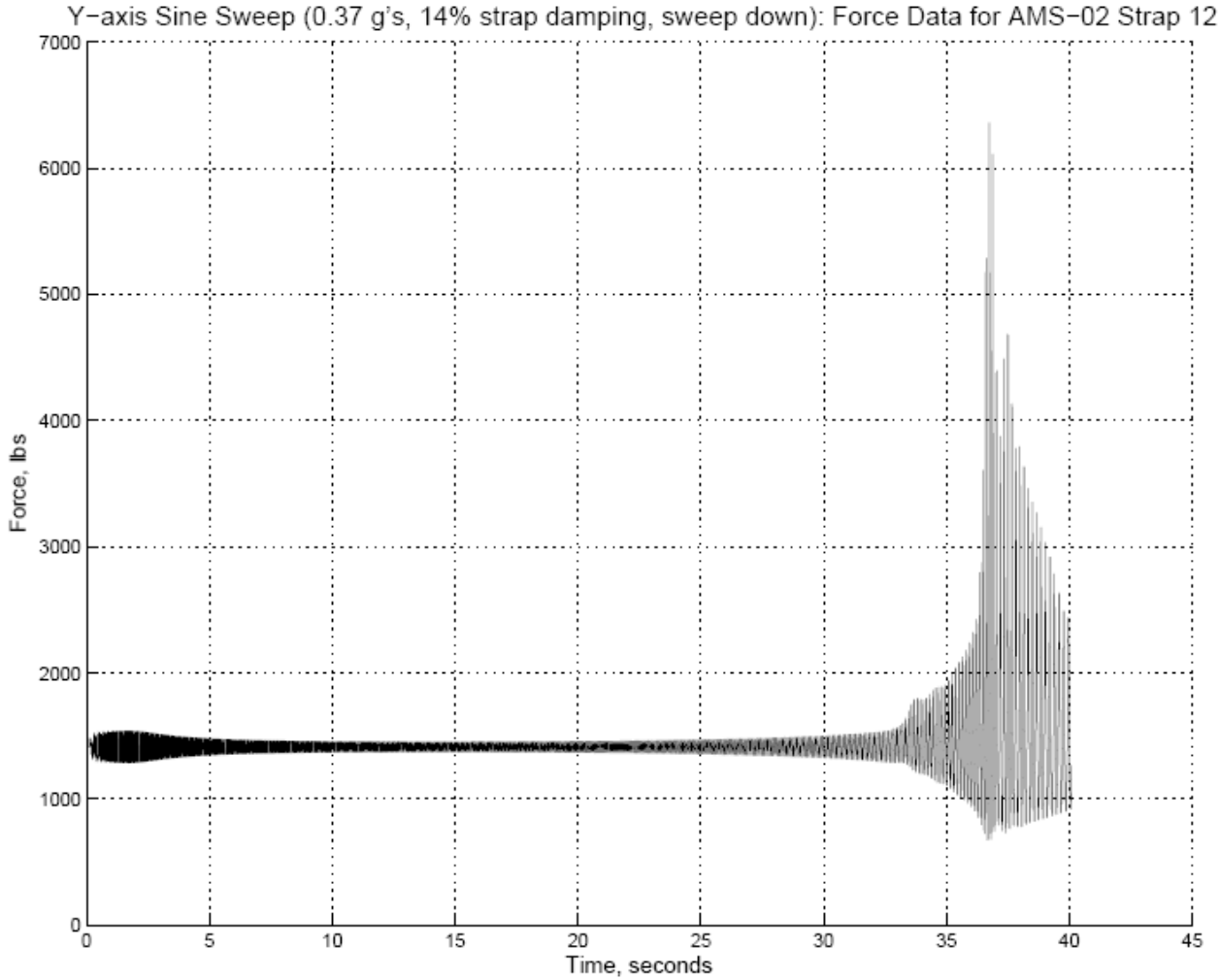

Figure 9-68 Strap 12 force response for y-axis configuration with 0.37 g sweep down

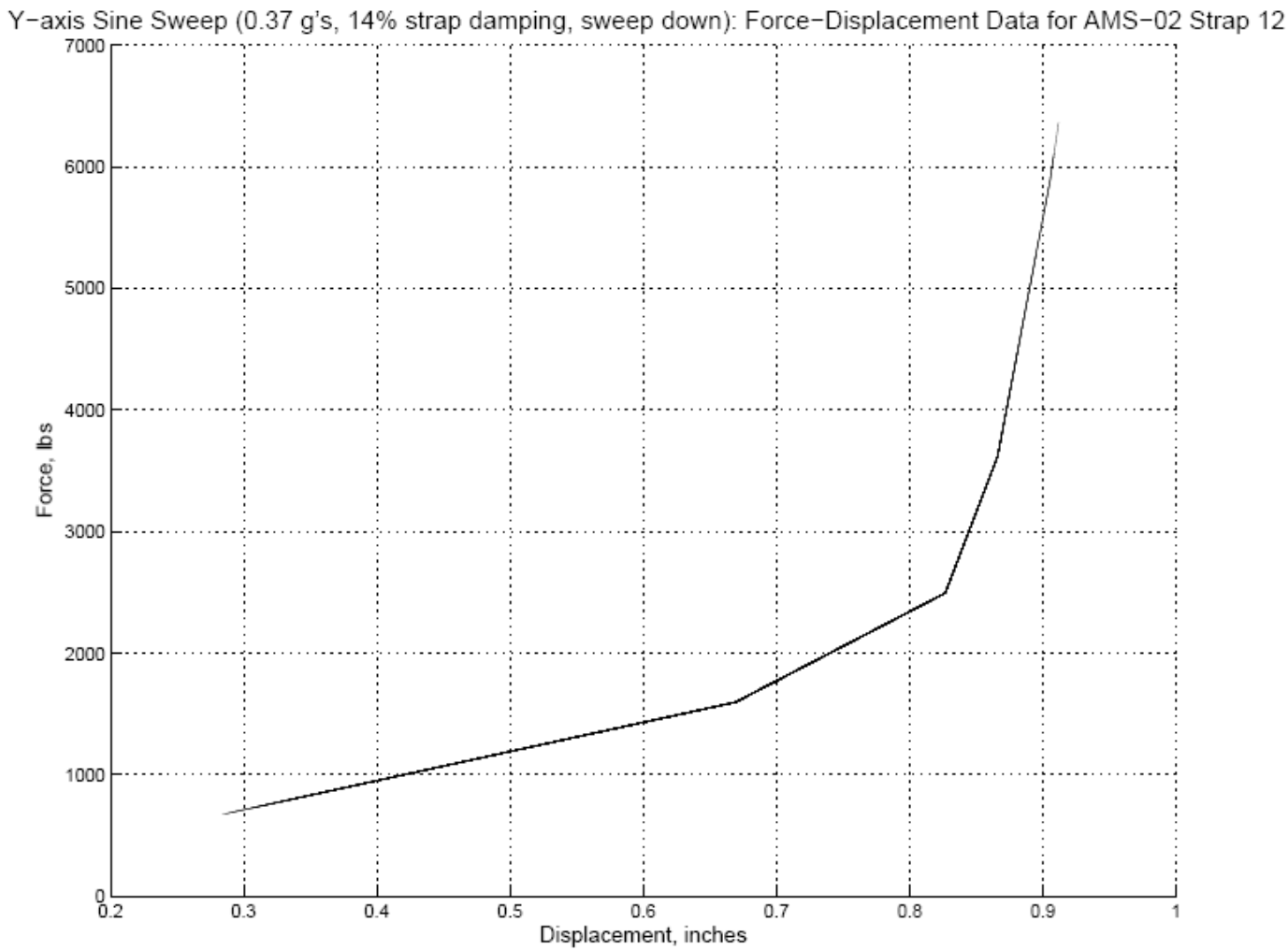

Figure 9-69 Strap 12 force-displacement curve for y-axis configuration with 0.37 g sweep down

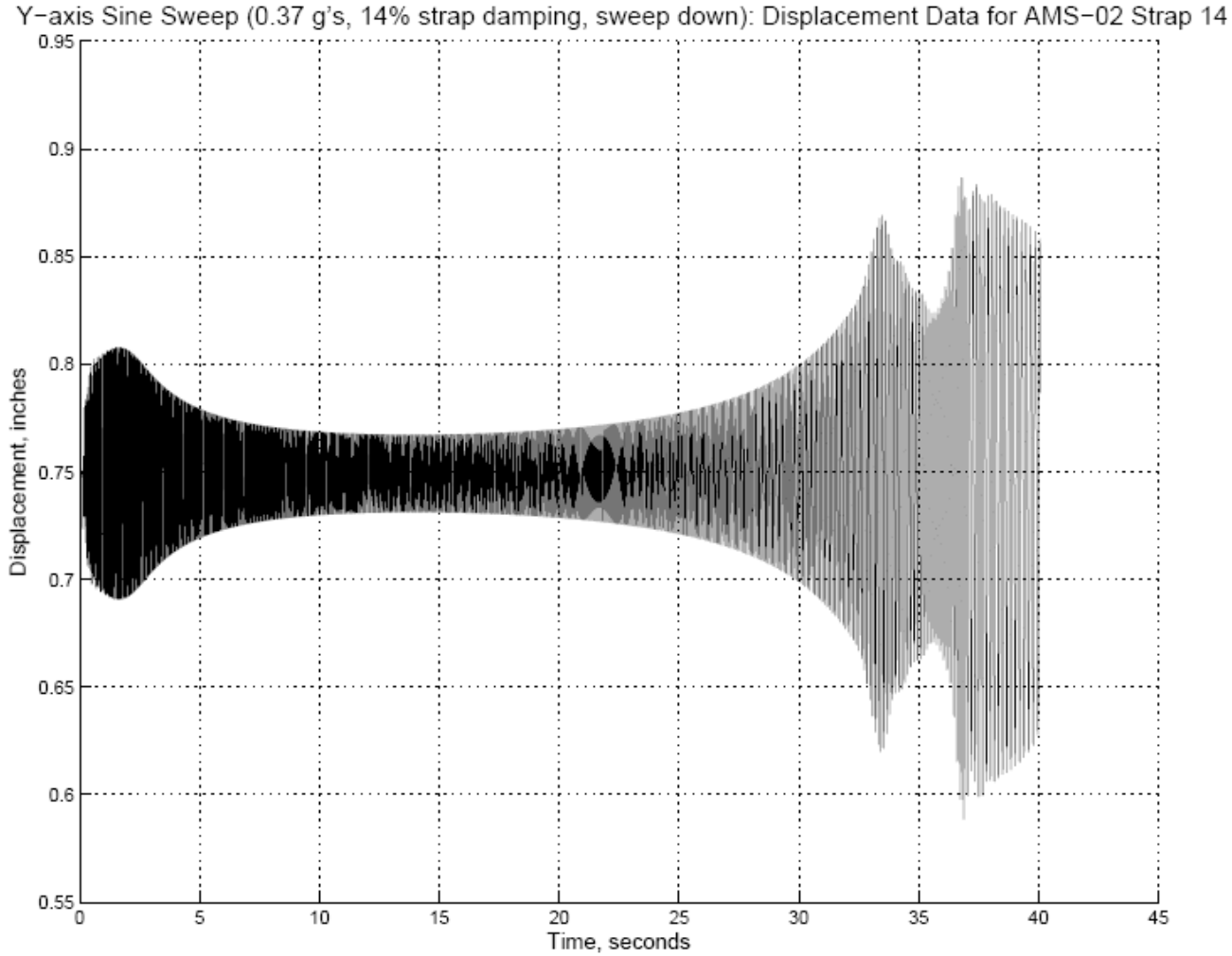

Figure 9-70 Strap 14 displacement response for y-axis configuration with 0.37 g sweep down

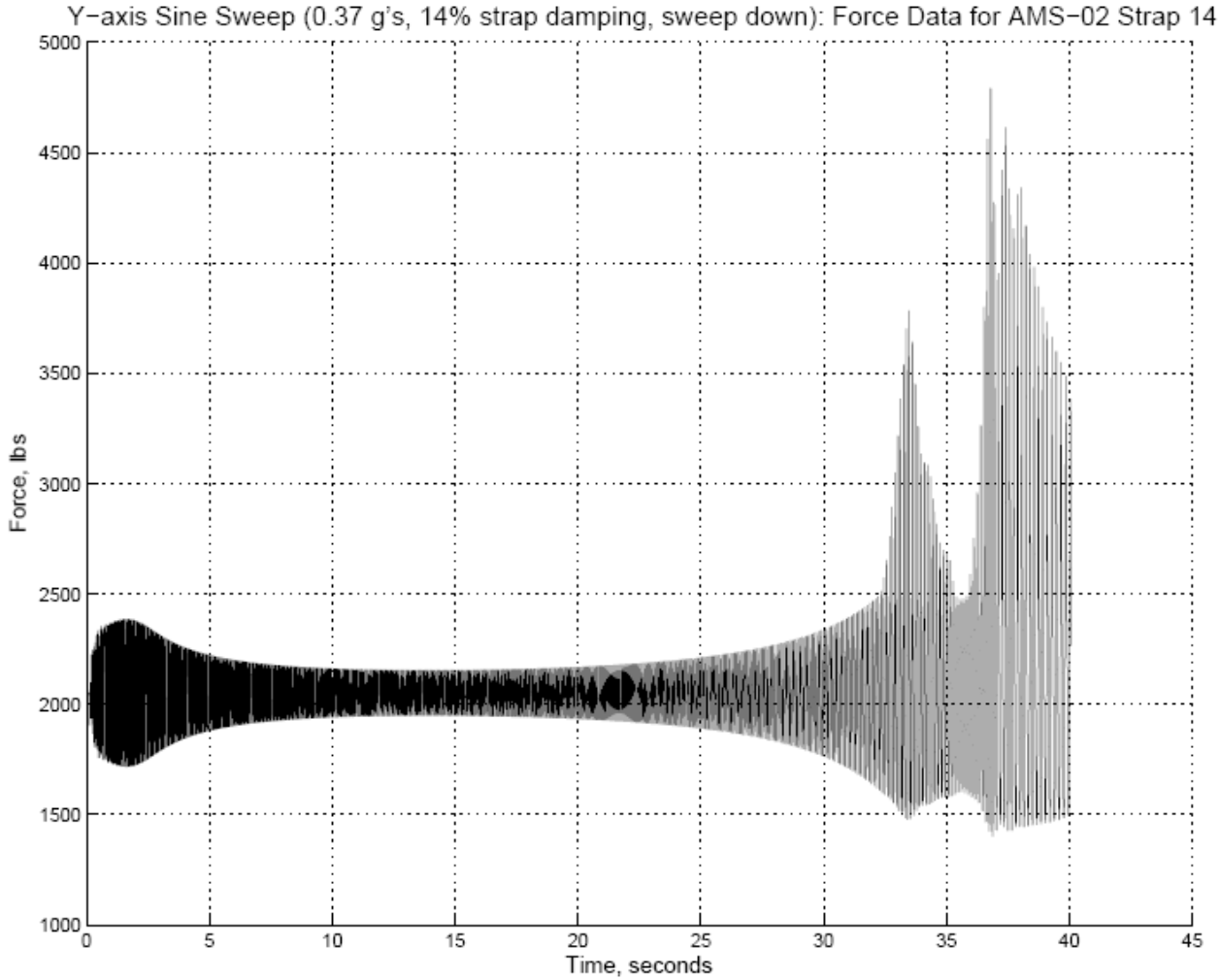

Figure 9-71 Strap 14 force response for y-axis configuration with 0.37 g sweep down

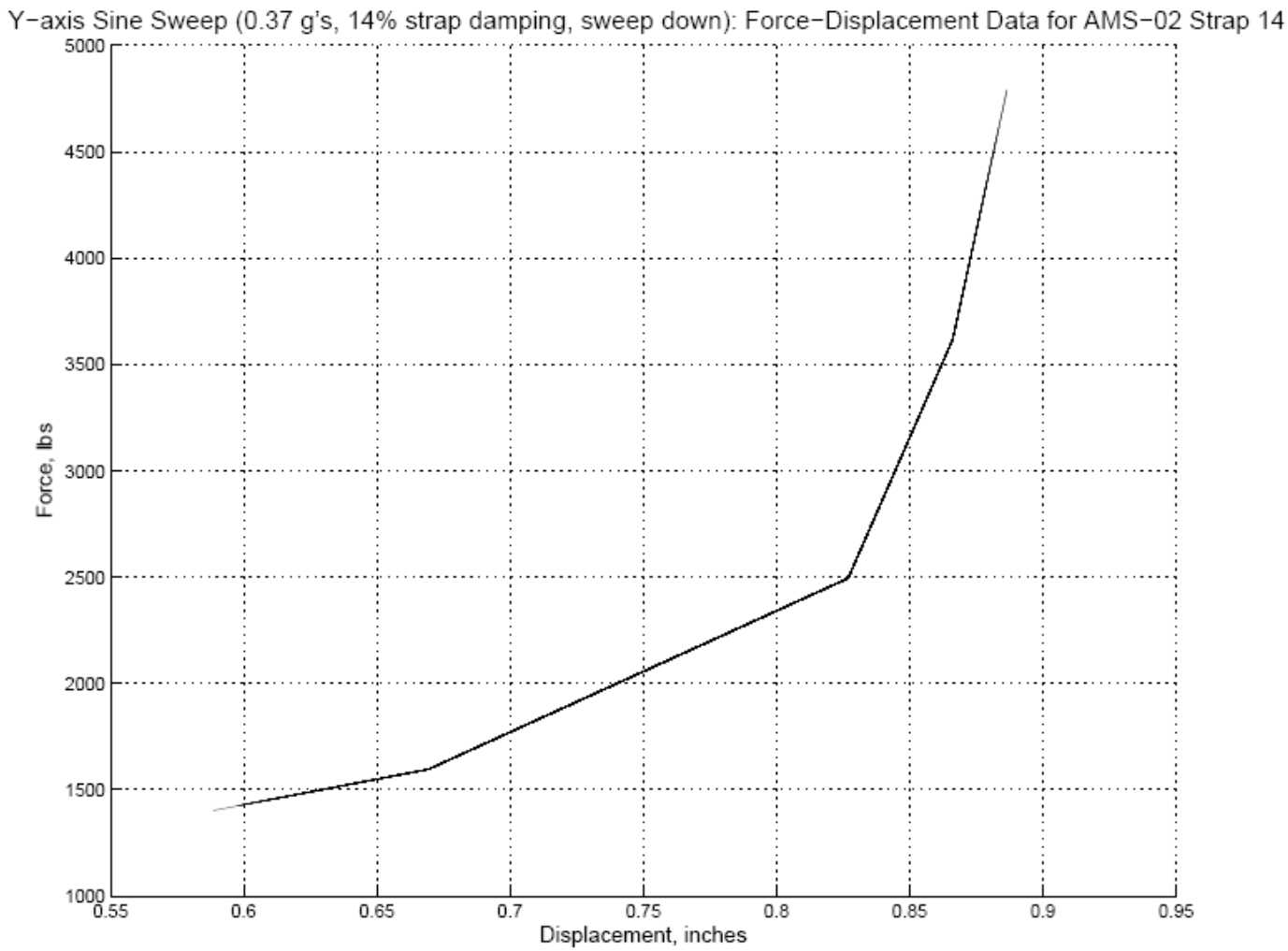

Figure 9-72 Strap 14 force-displacement curve for y-axis configuration with 0.37 g sweep down

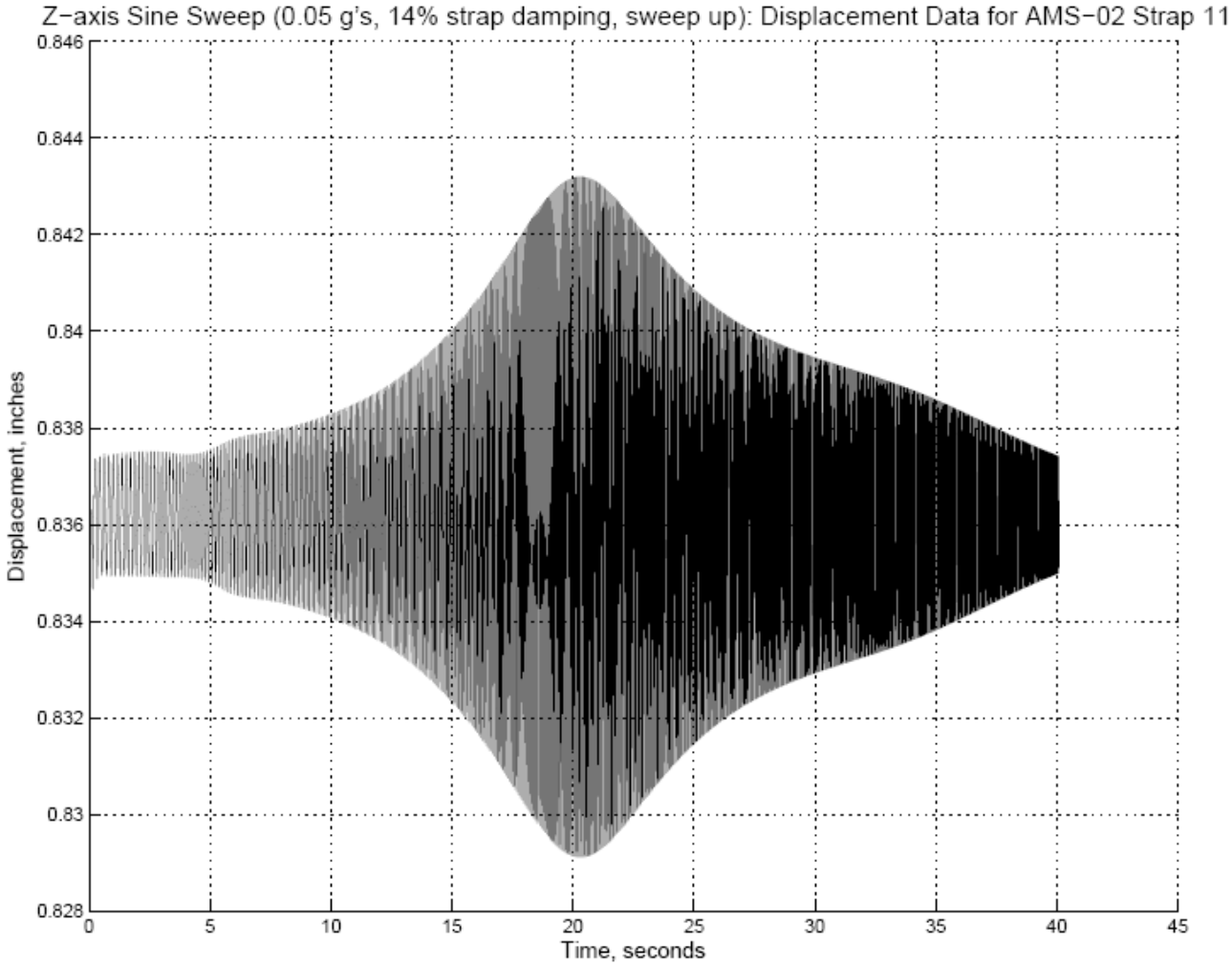

Figure 9-73 Strap 11 displacement response for z-axis configuration with 0.05 g sweep up

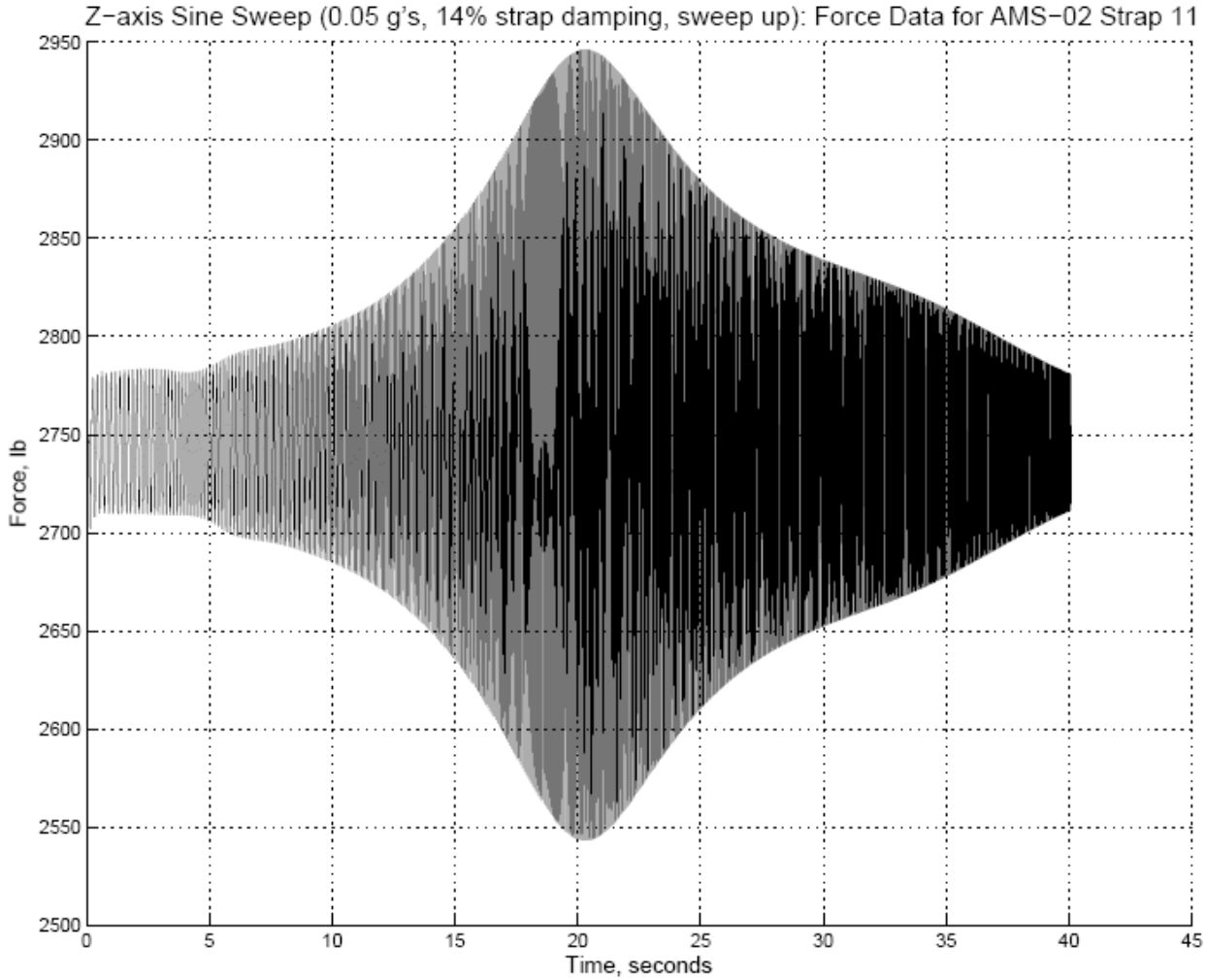

Figure 9-74 Strap 11 force response for z-axis configuration with 0.05 g sweep up

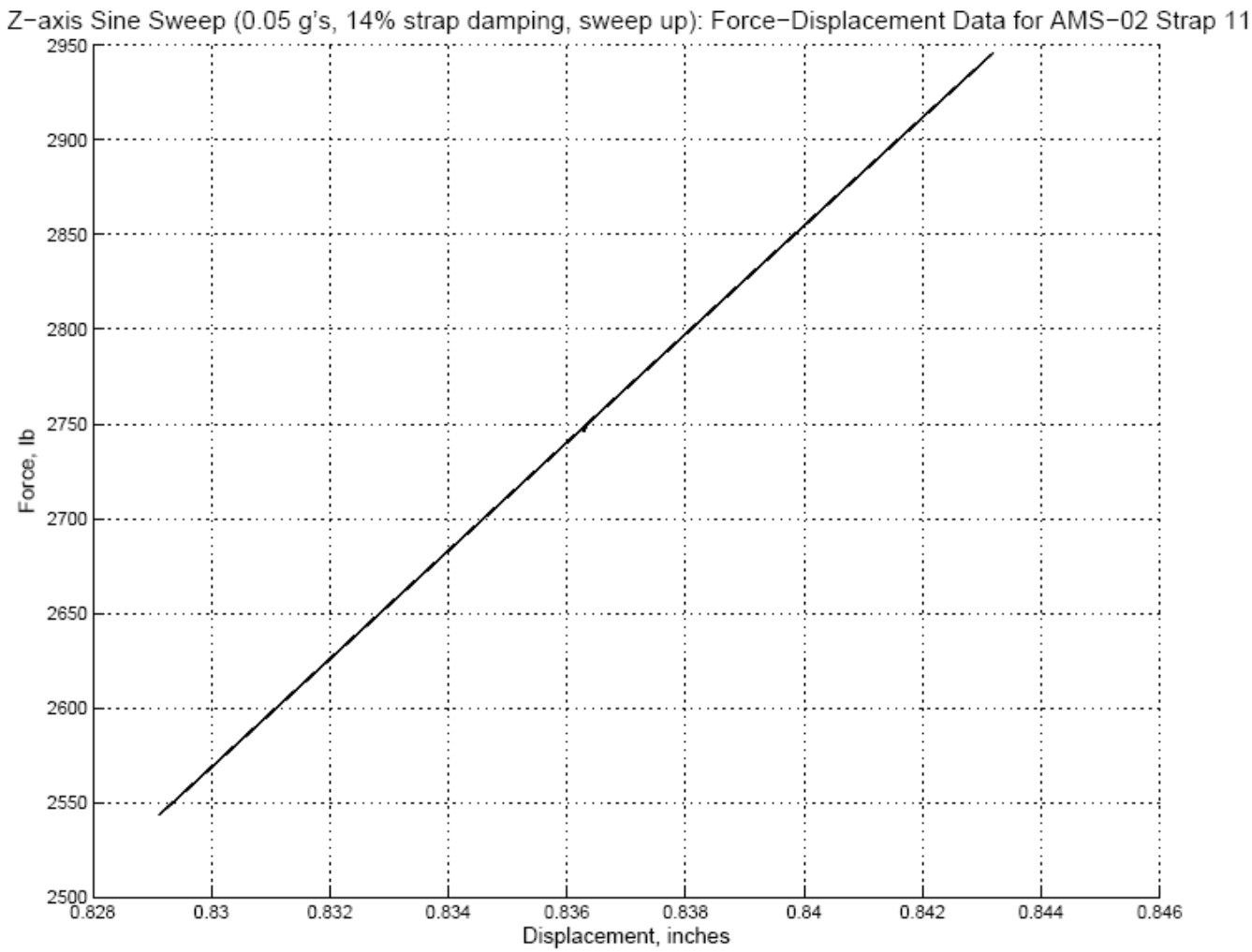

Figure 9-75 Strap 11 force-displacement curve for z-axis configuration with 0.05 g sweep up

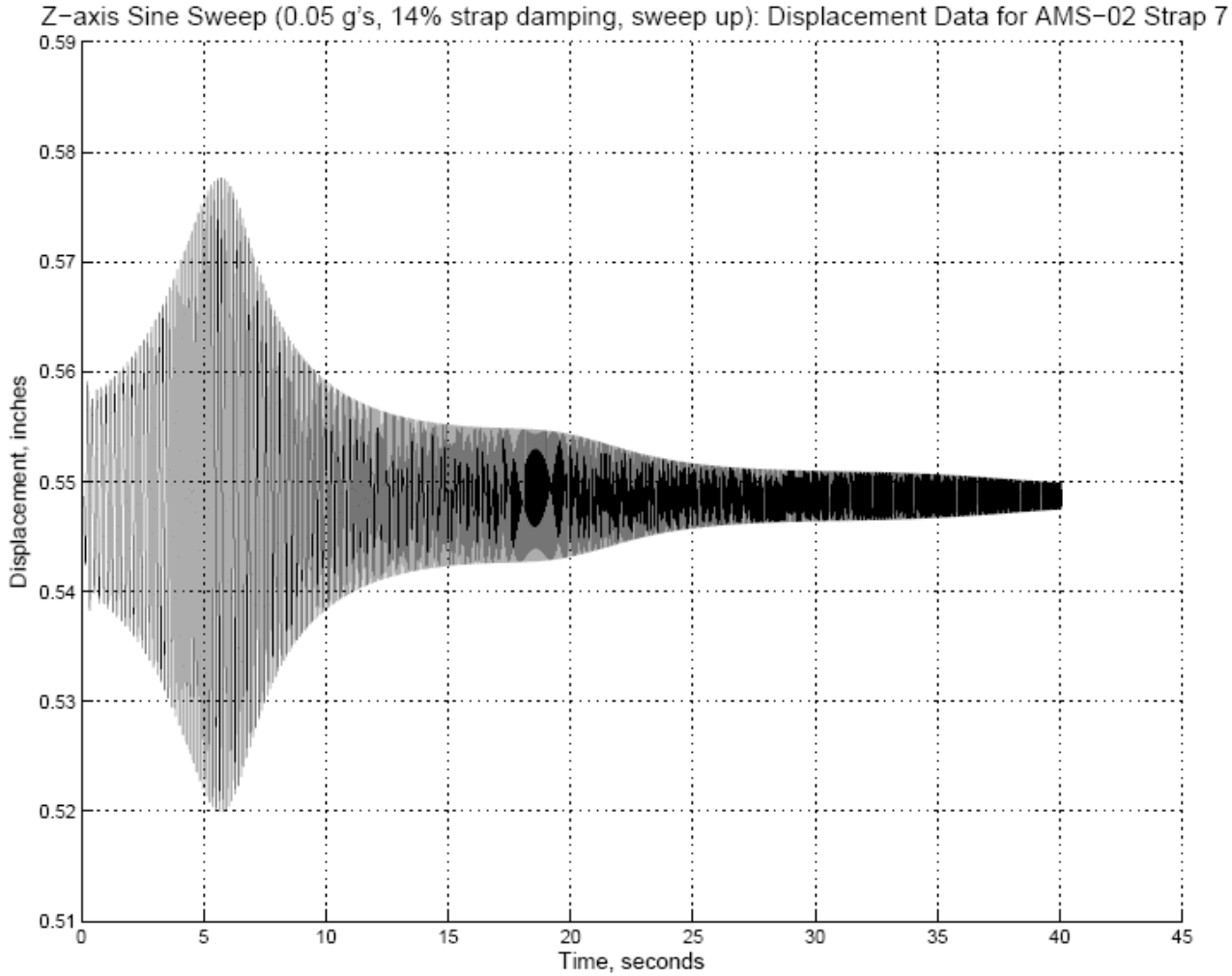

Figure 9-76 Strap 7 displacement response for z-axis configuration with 0.05 g sweep up

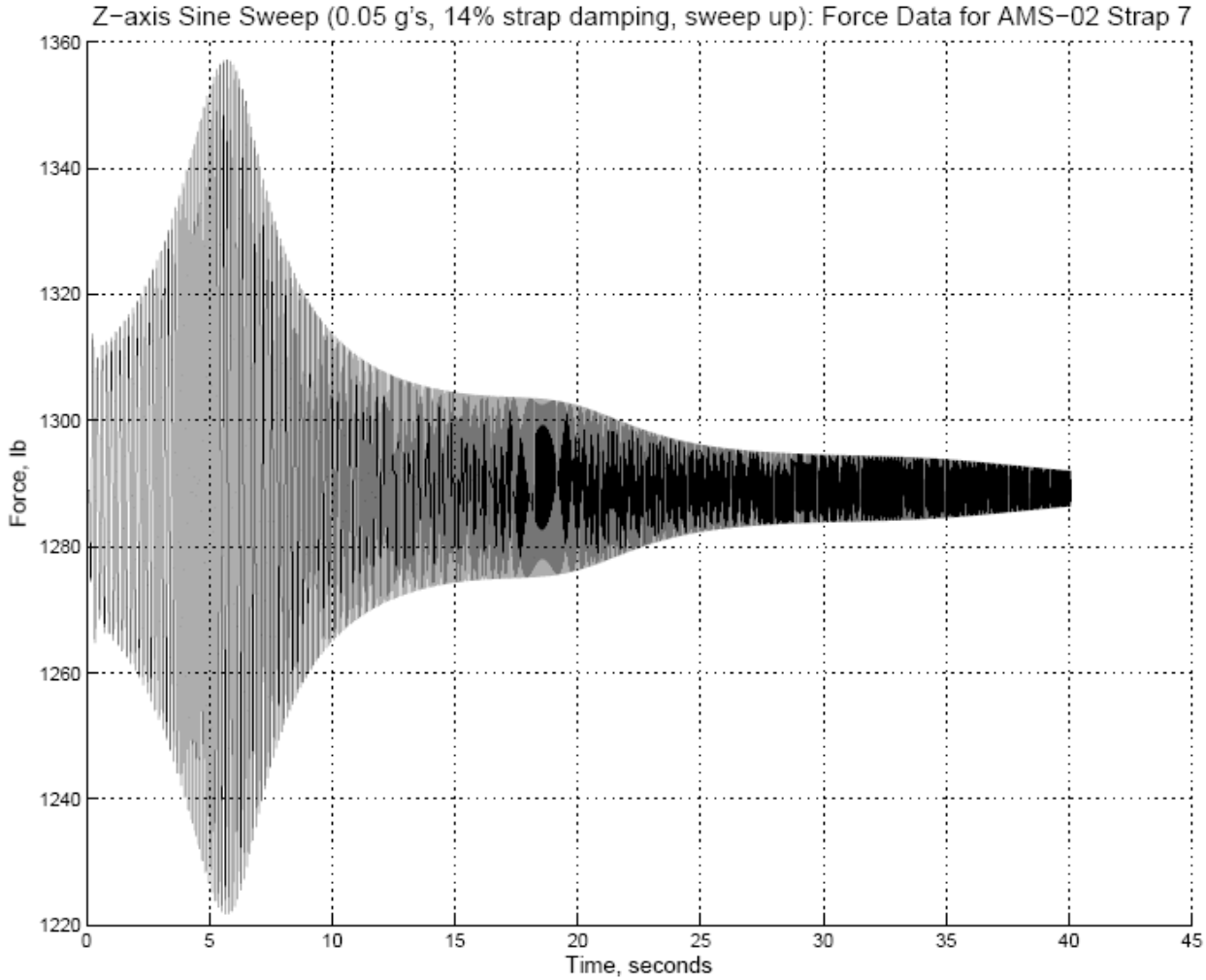

Figure 9-77 Strap 7 force response for z-axis configuration with 0.05 g sweep up

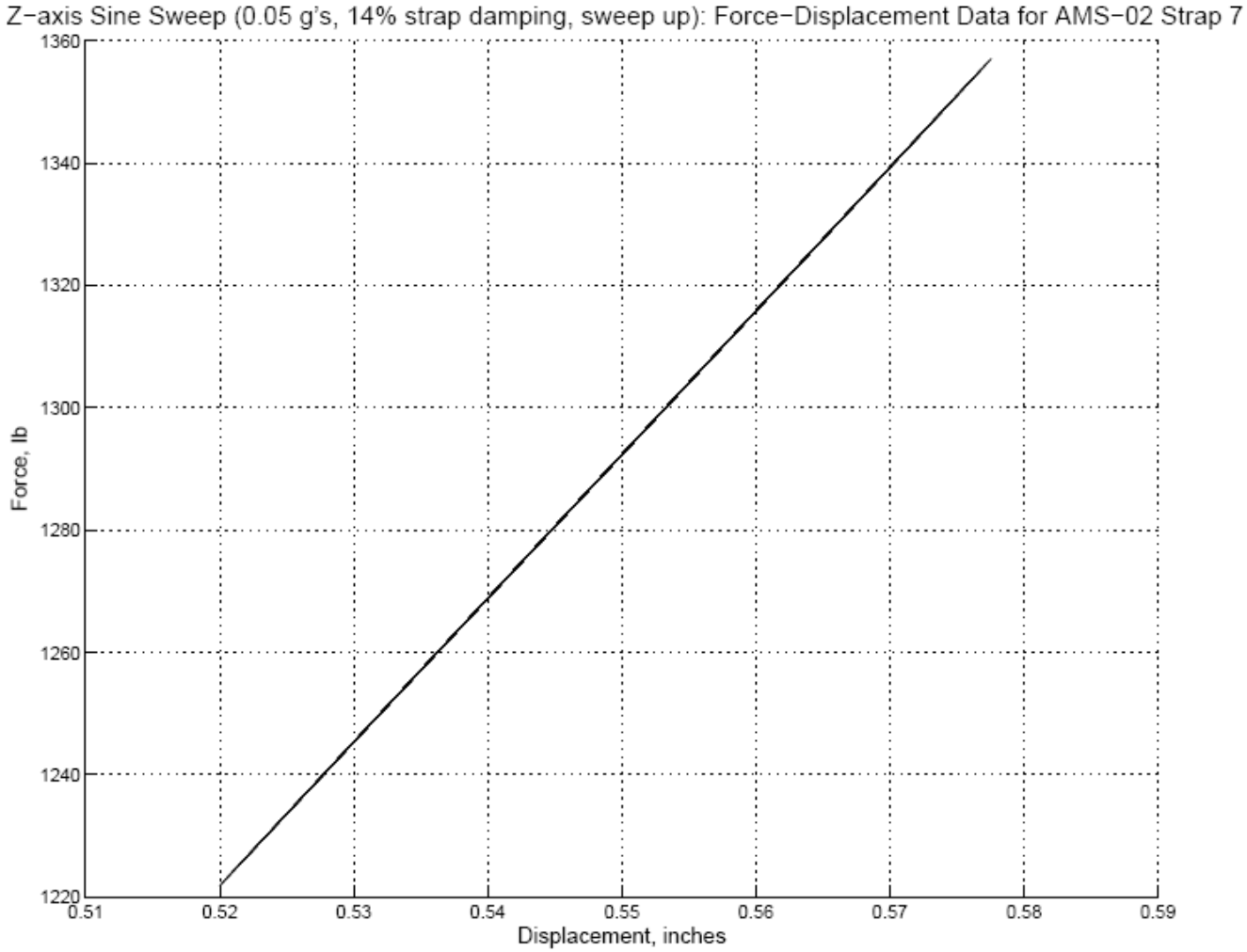

Figure 9-78 Strap 7 force-displacement curve for z-axis configuration with 0.05 g sweep up

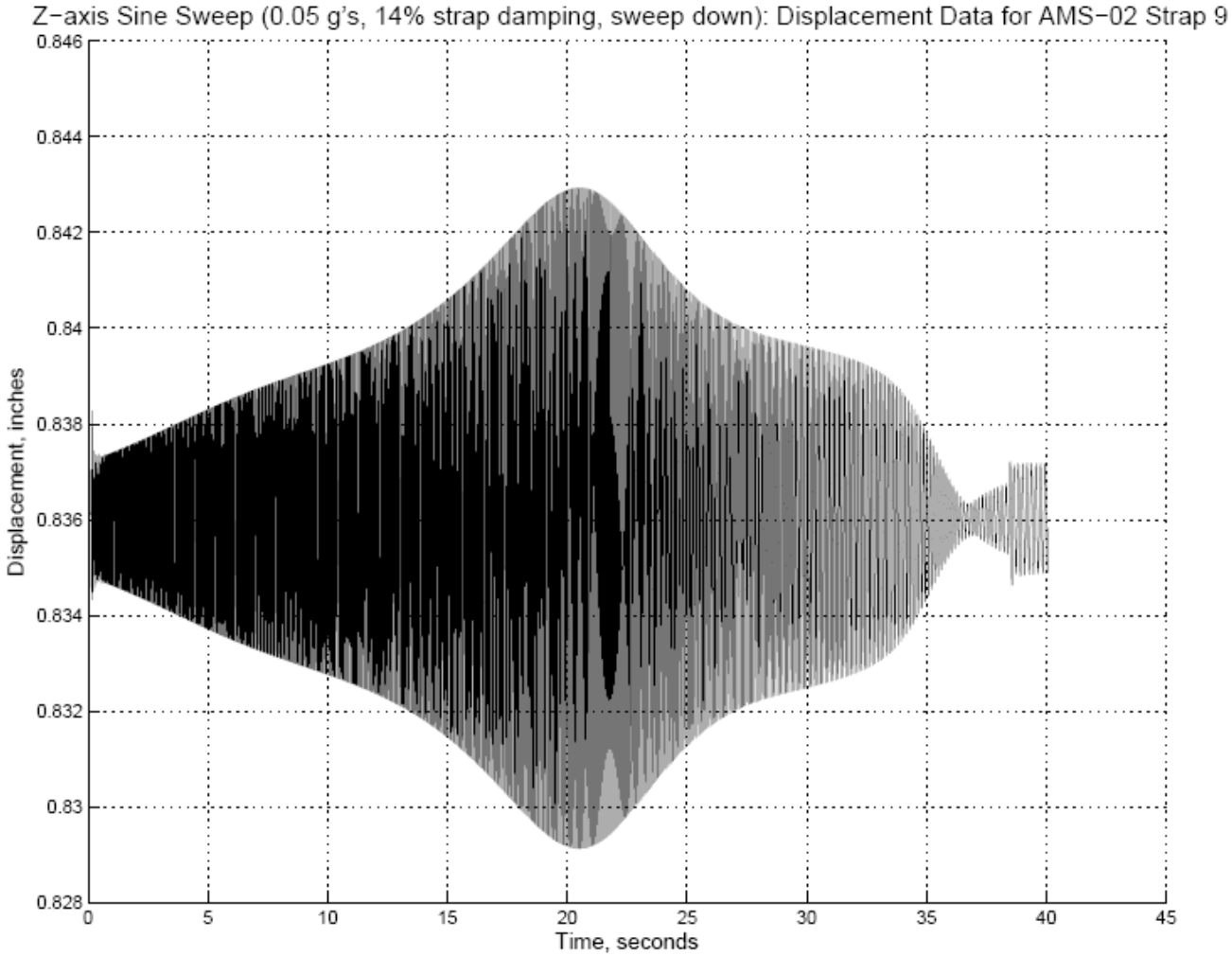

Figure 9-79 Strap 9 displacement response for z-axis configuration with 0.05 g sweep down

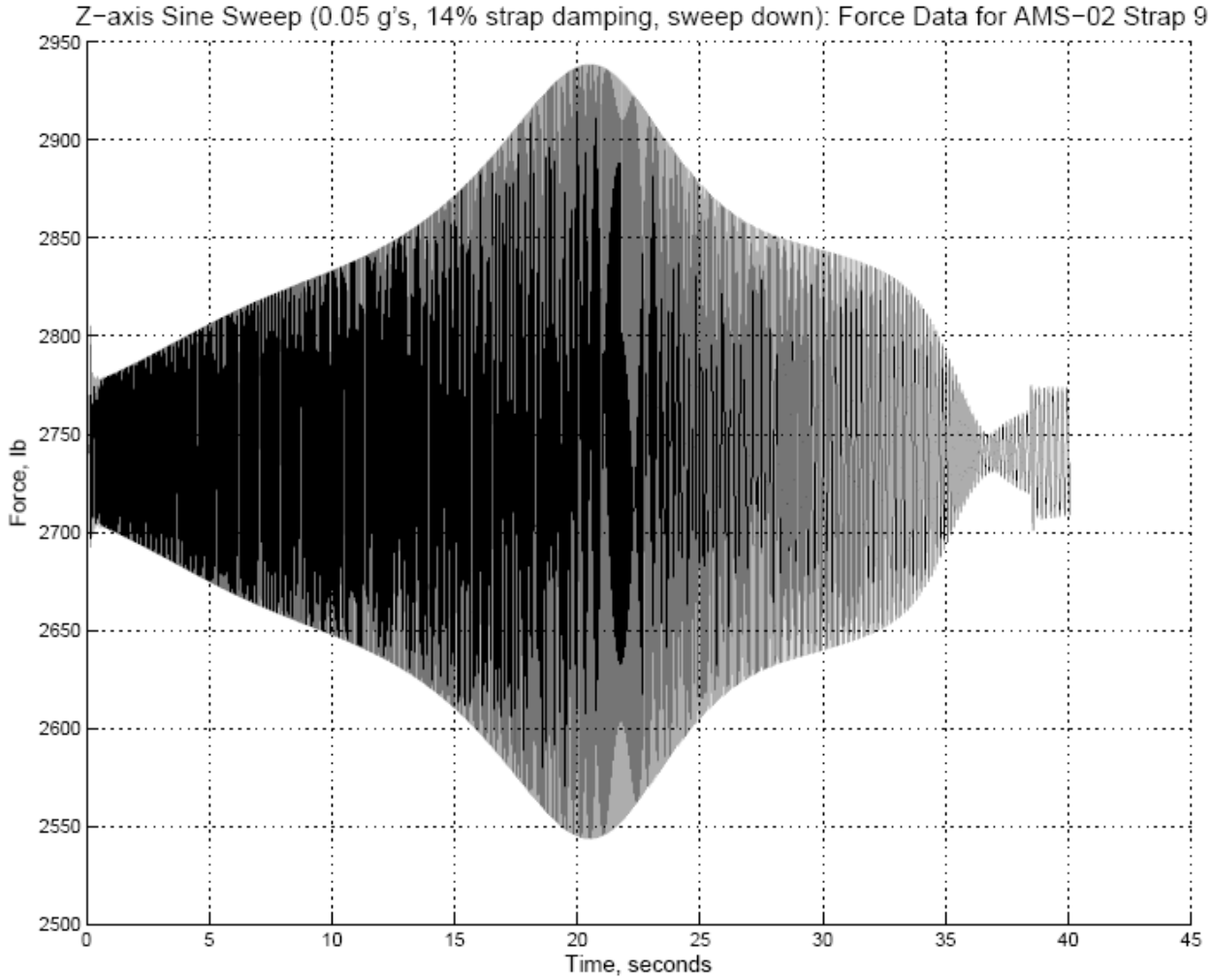

Figure 9-80 Strap 9 force response for z-axis configuration with 0.05 g sweep down

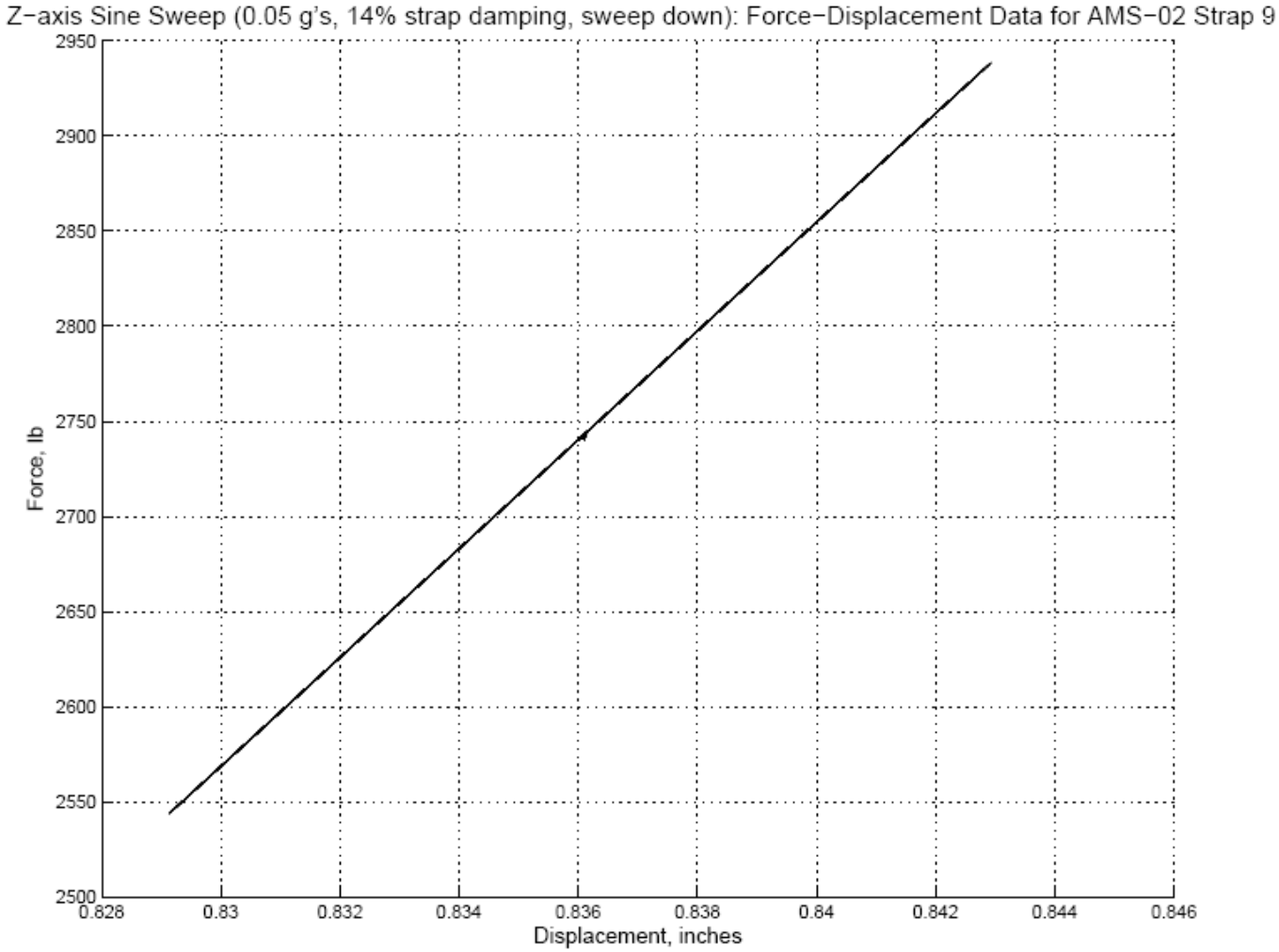

Figure 9-81 Strap 9 force-displacement curve for z-axis configuration with 0.05 g sweep down

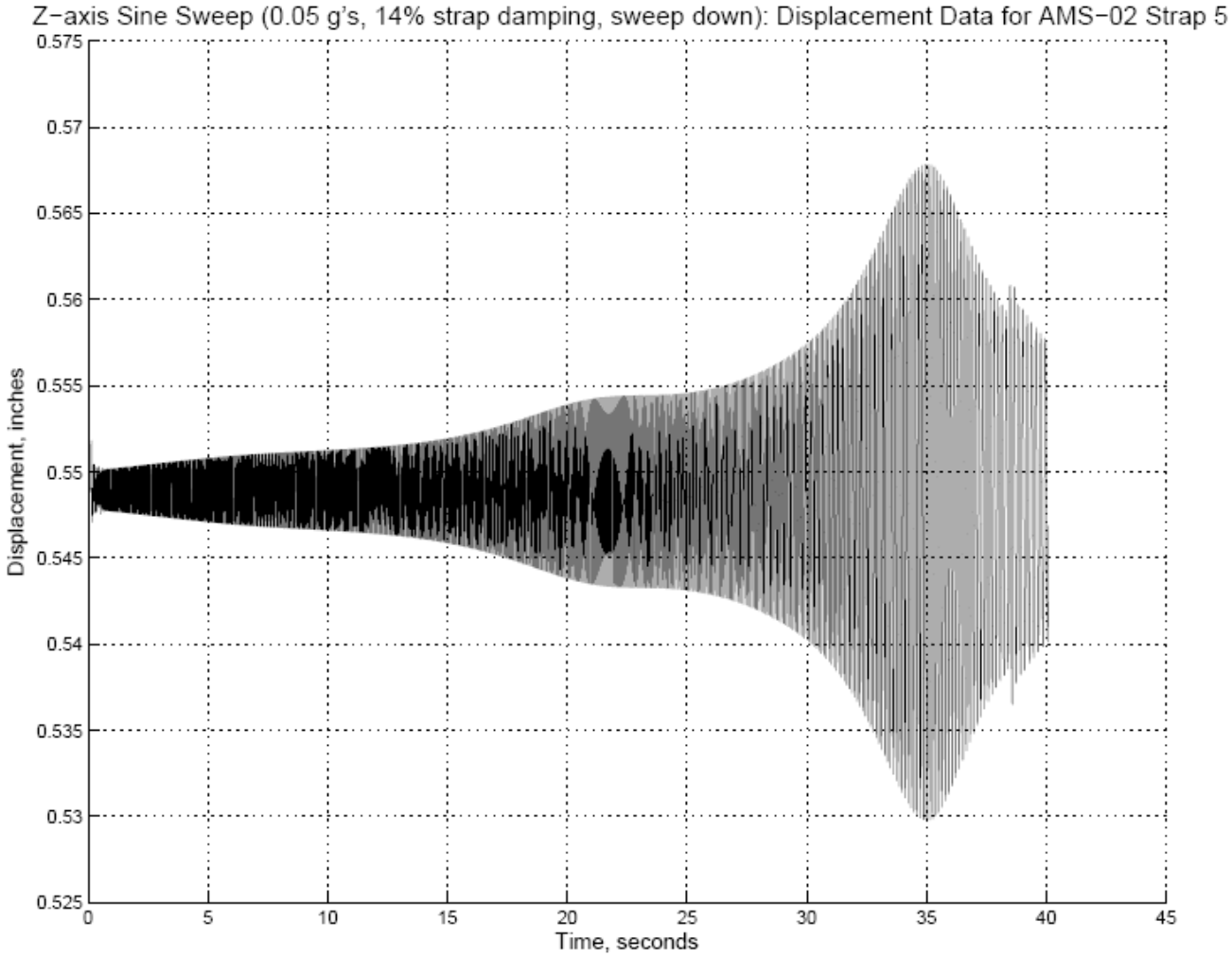

Figure 9-82 Strap 5 displacement response for z-axis configuration with 0.05 g sweep down

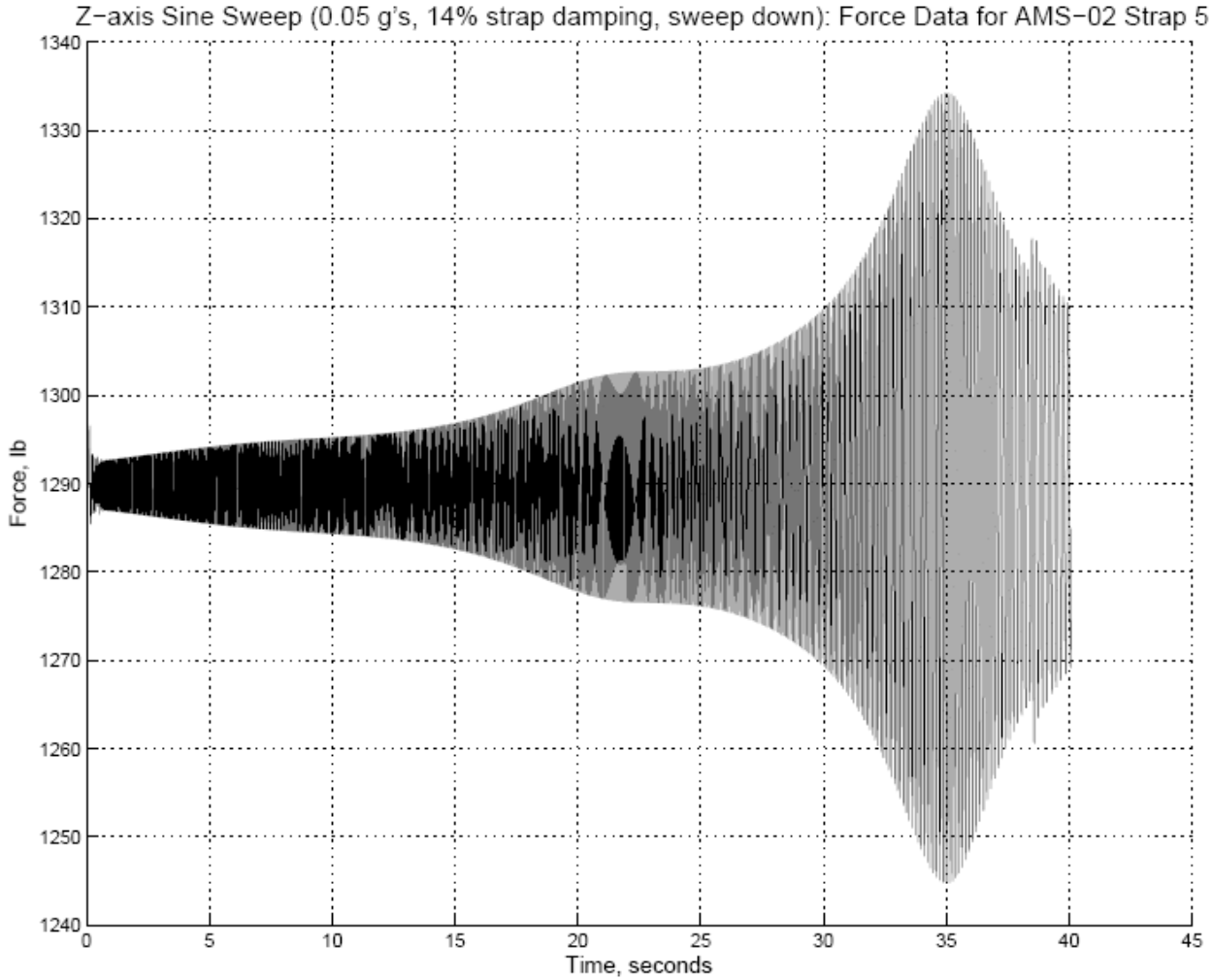

Figure 9-83 Strap 5 force response for z-axis configuration with 0.05 g sweep down

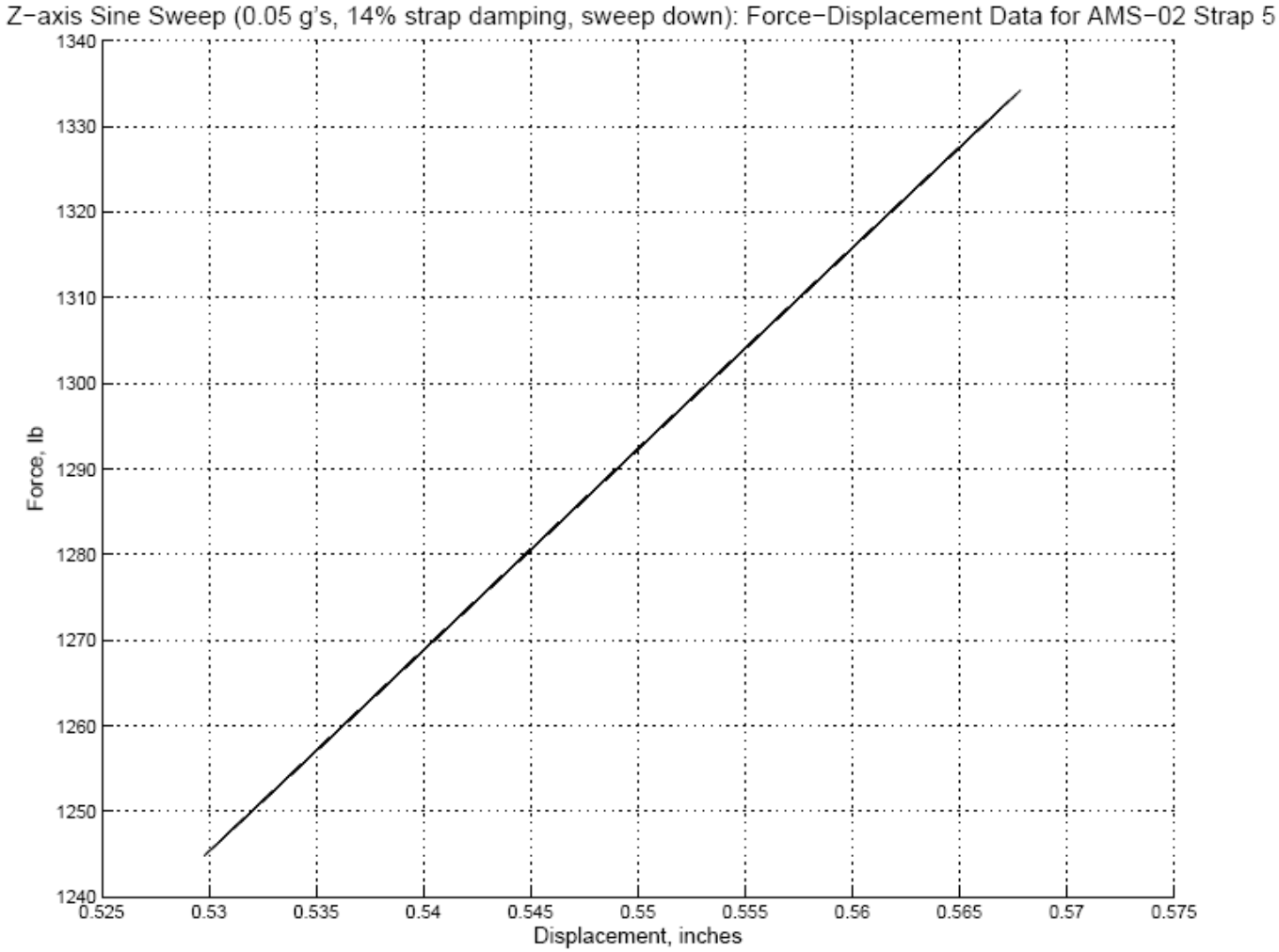

Figure 9-84 Strap 5 force-displacement curve for z-axis configuration with 0.05 g sweep down

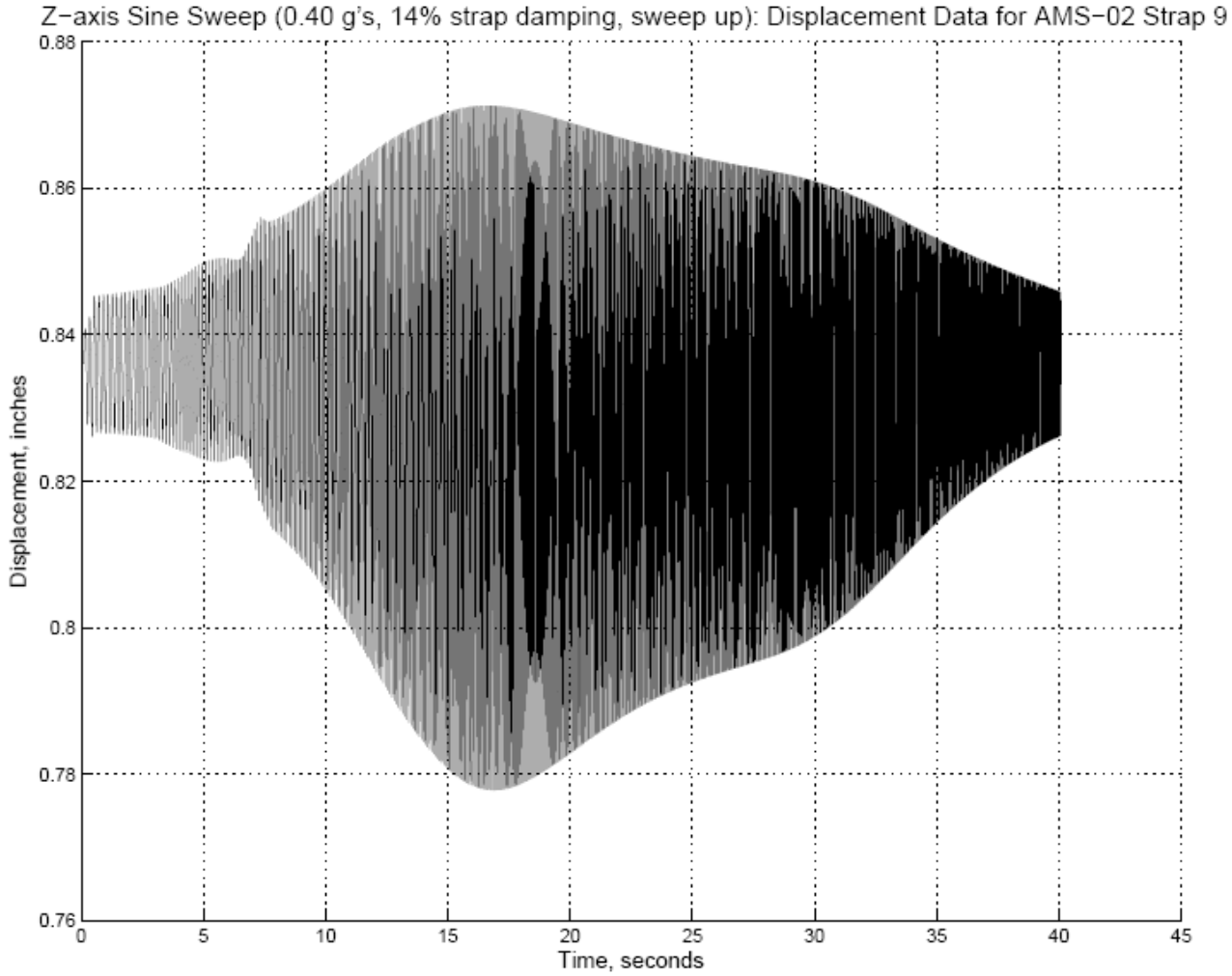

Figure 9-85 Strap 9 displacement response for z-axis configuration with 0.40 g sweep up

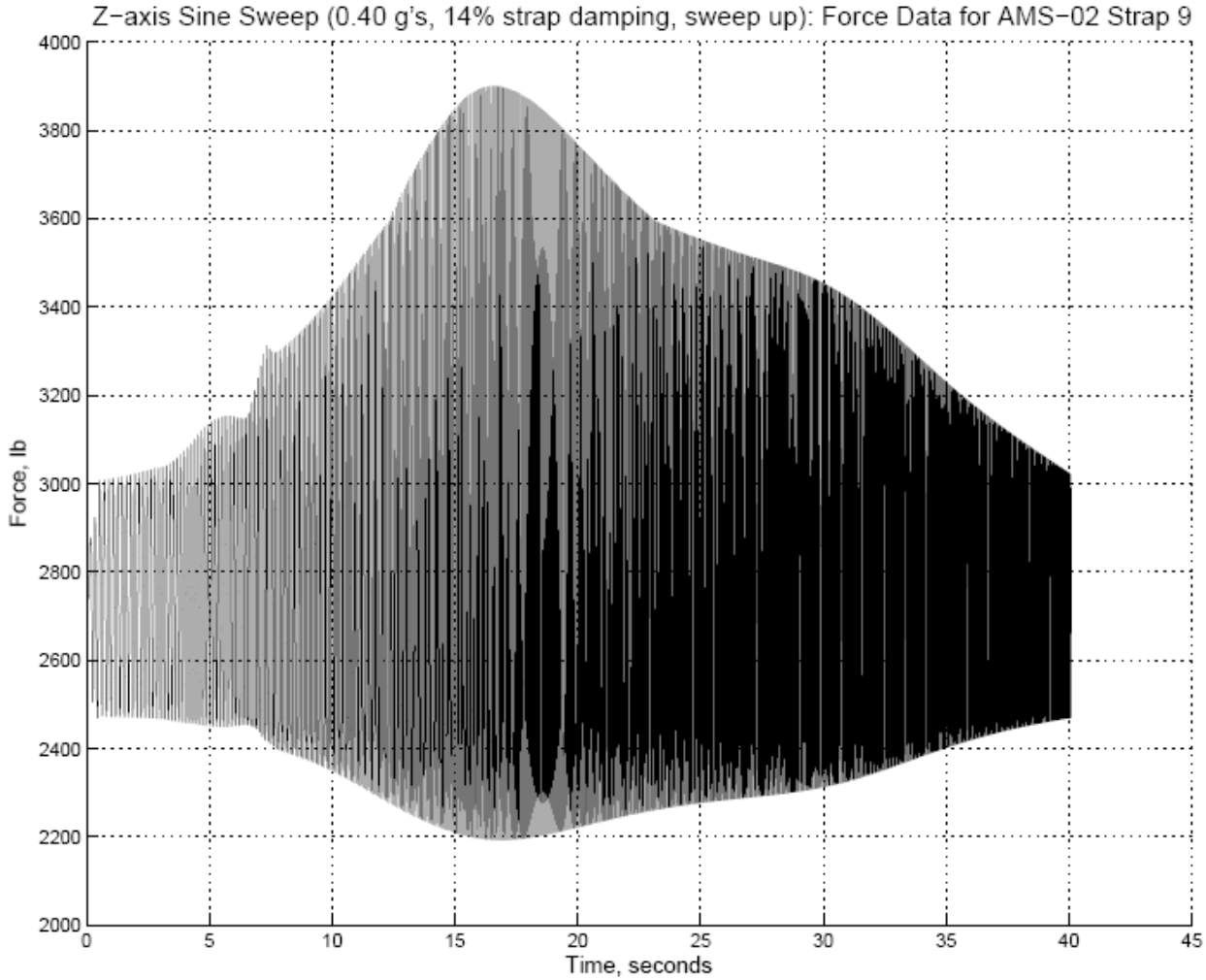

Figure 9-86 Strap 9 force response for z-axis configuration with 0.40 g sweep up

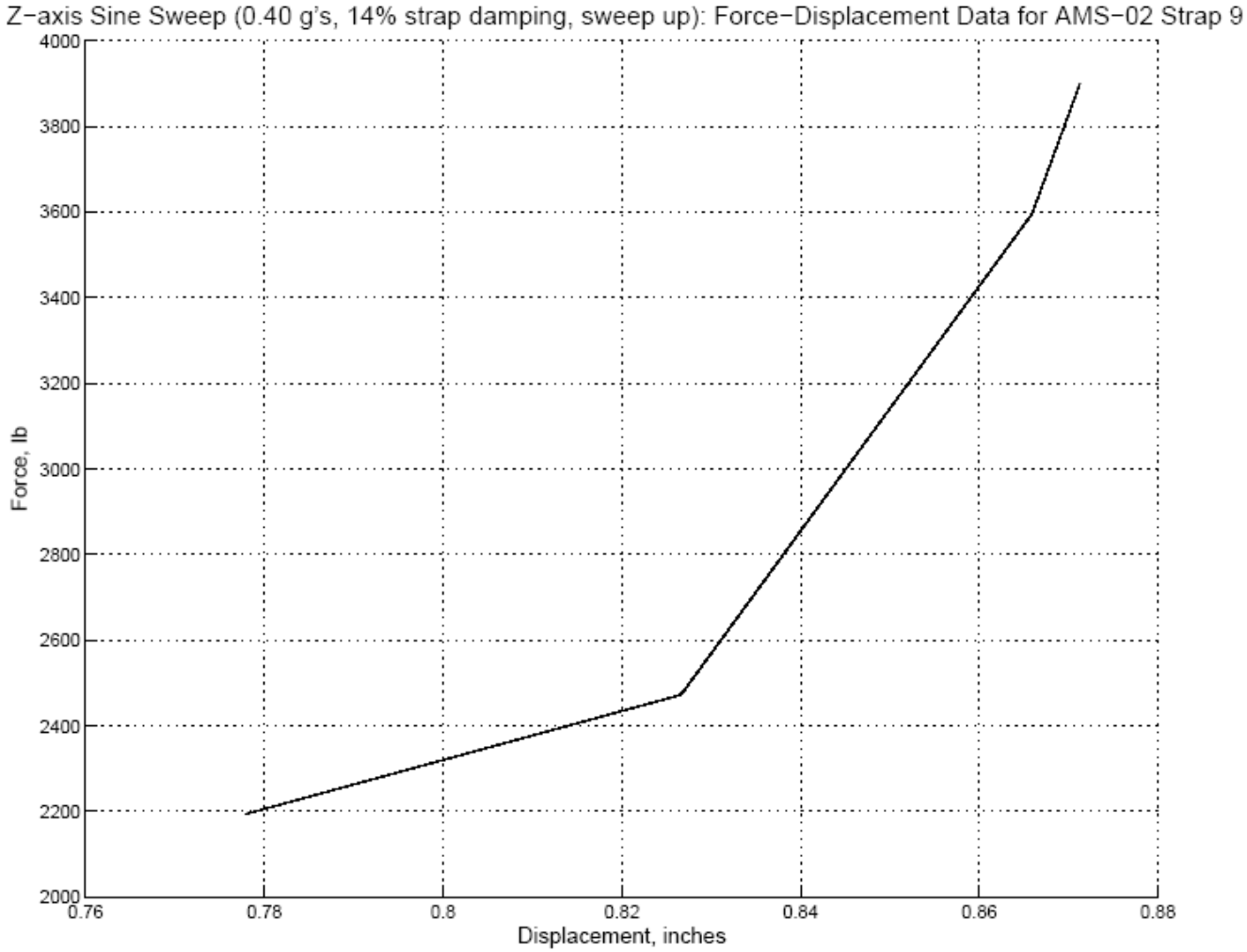

Figure 9-87 Strap 9 force-displacement curve for z-axis configuration with 0.40 g sweep up

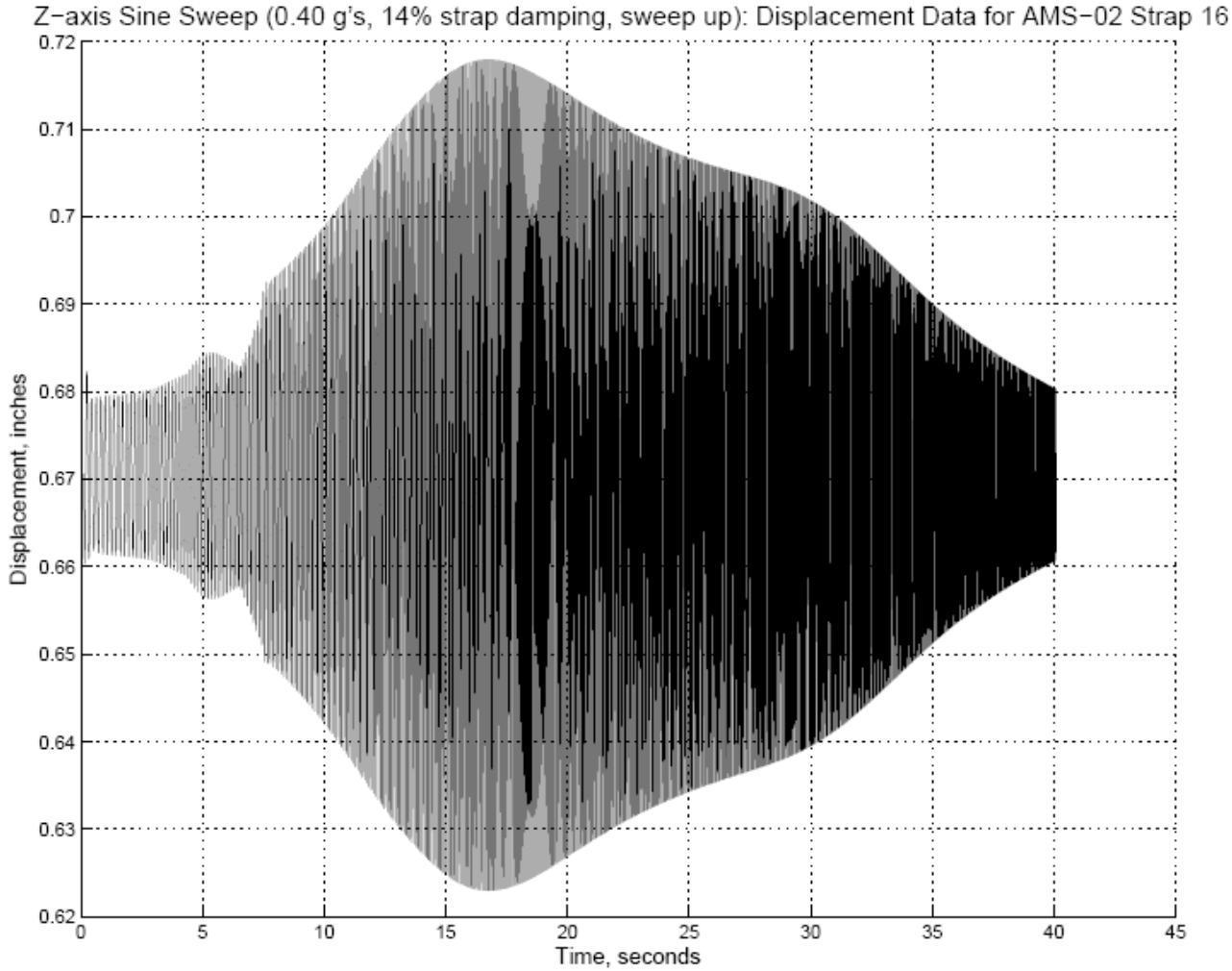

Figure 9-88 Strap 16 displacement response for z-axis configuration with 0.40 g sweep up

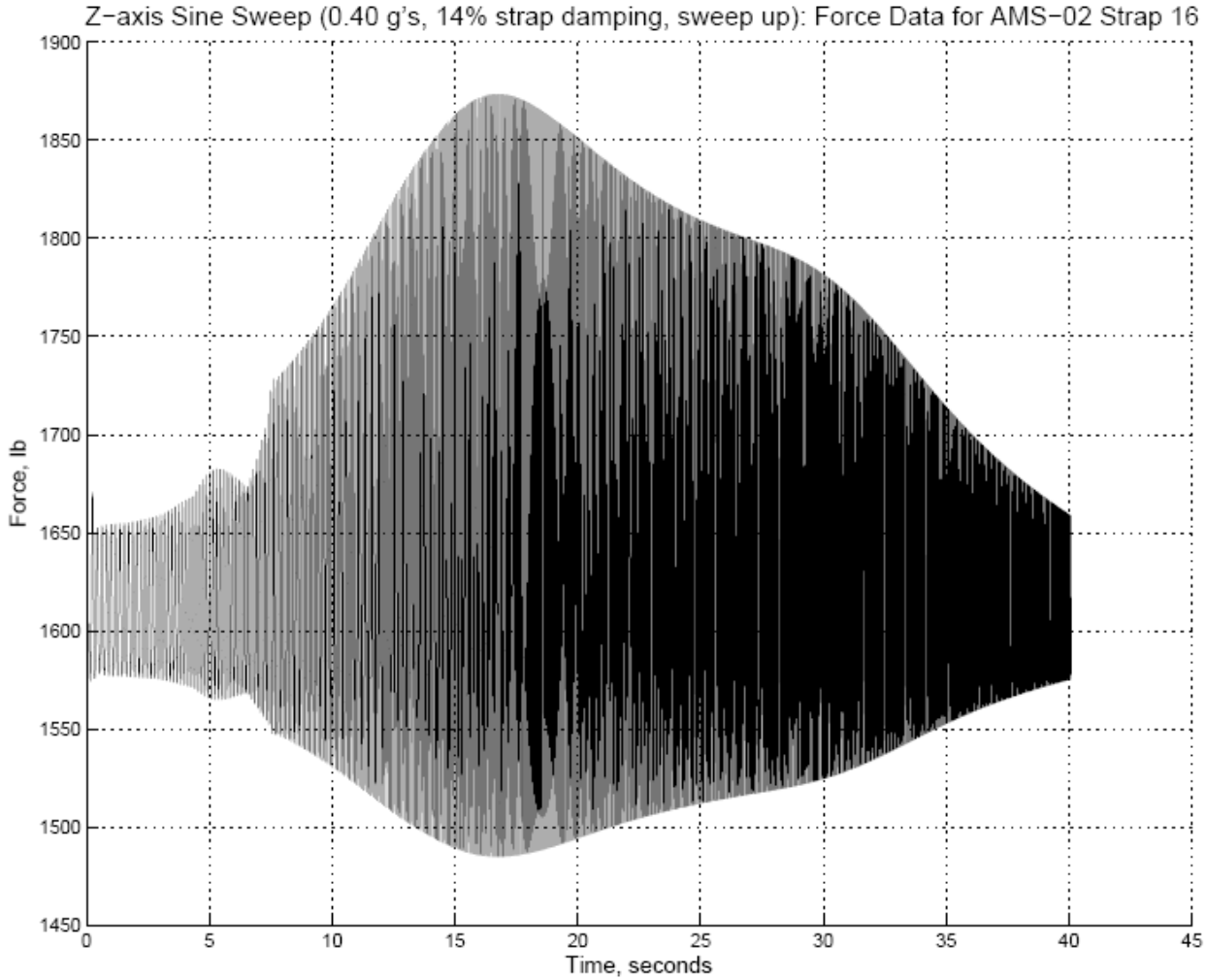

Figure 9-89 Strap 16 force response for z-axis configuration with 0.40 g sweep up

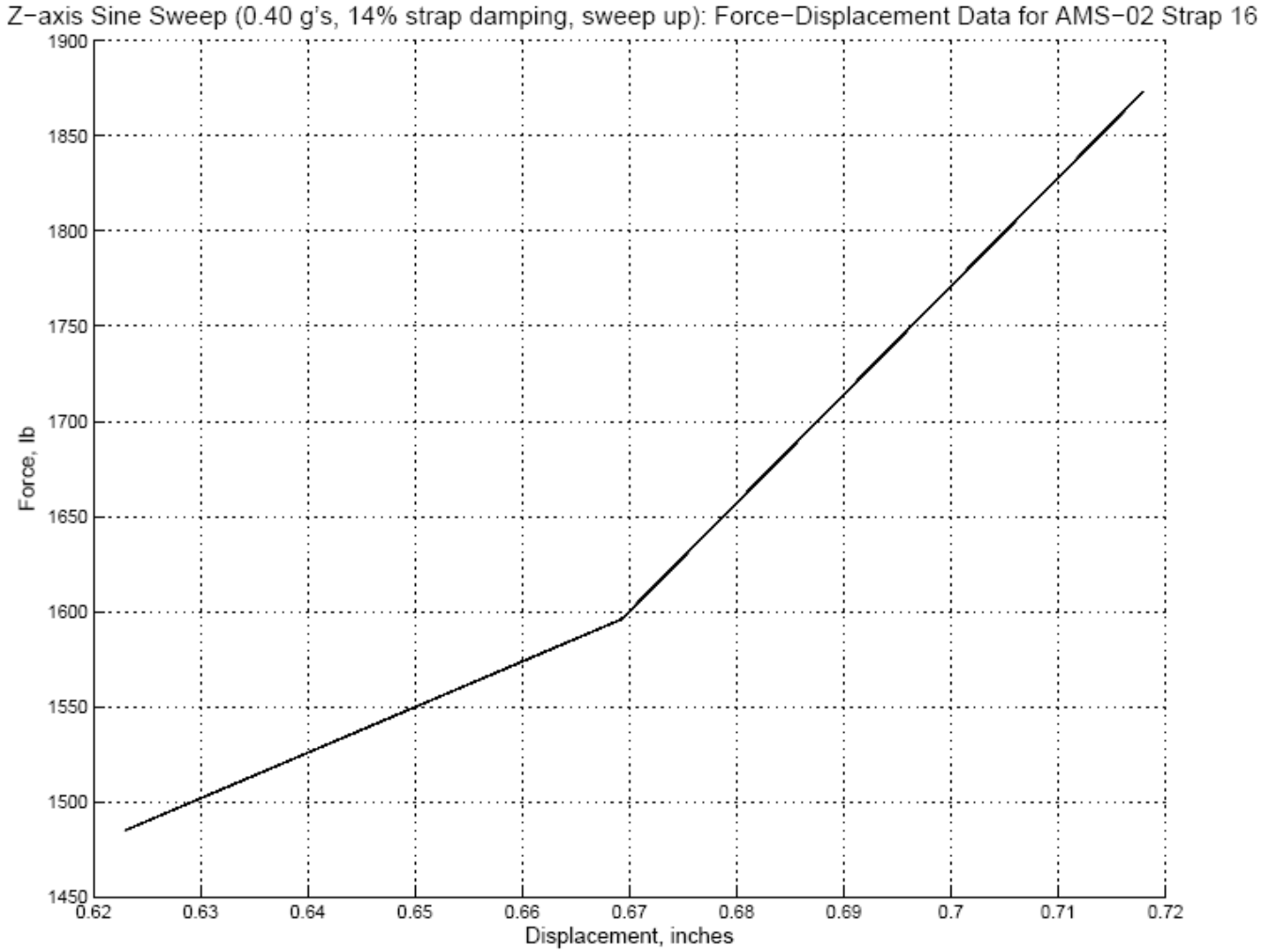

Figure 9-90 Strap 16 force-displacement curve for z-axis configuration with 0.40 g sweep up

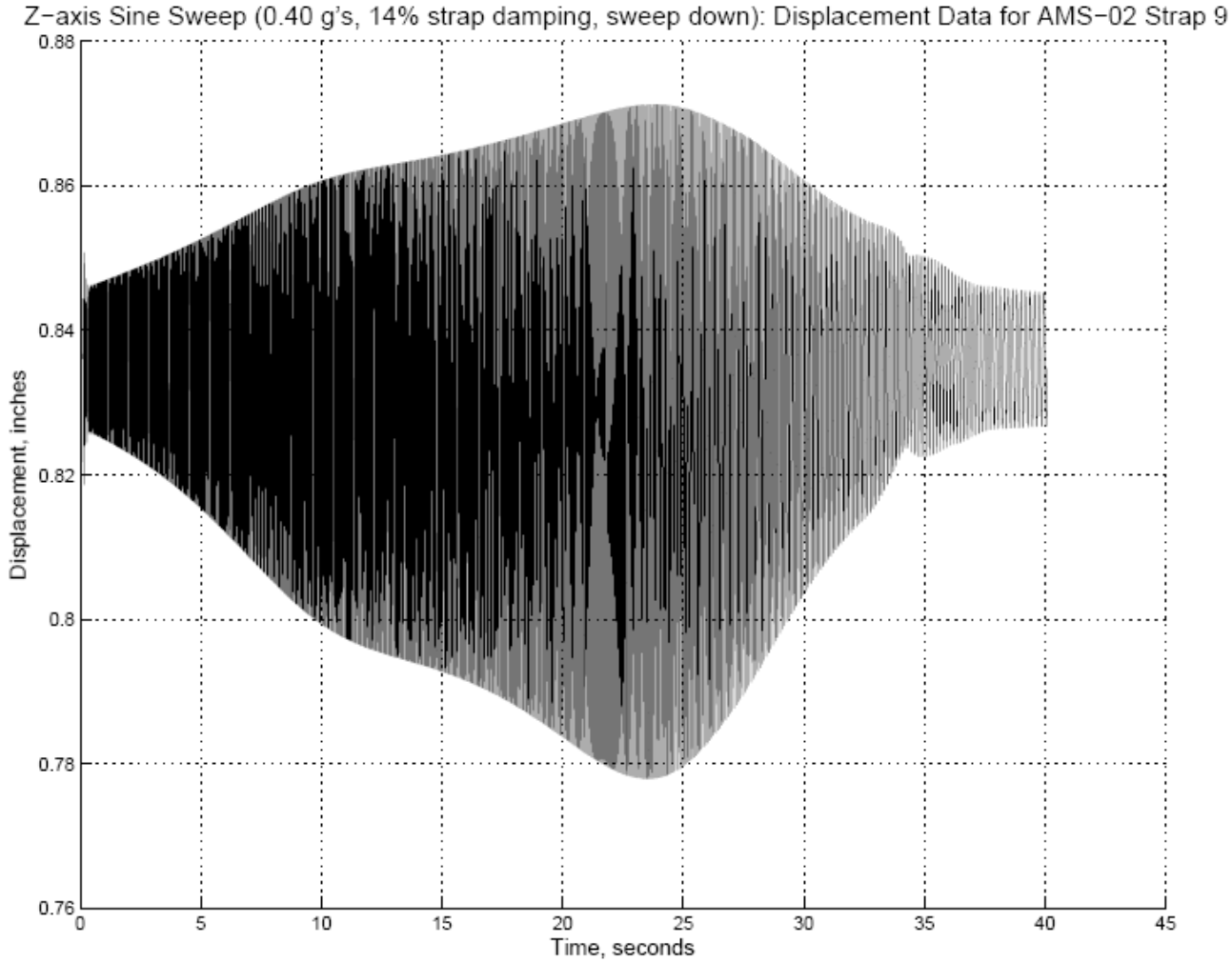

Figure 9-91 Strap 9 displacement response for z-axis configuration with 0.40 g sweep down

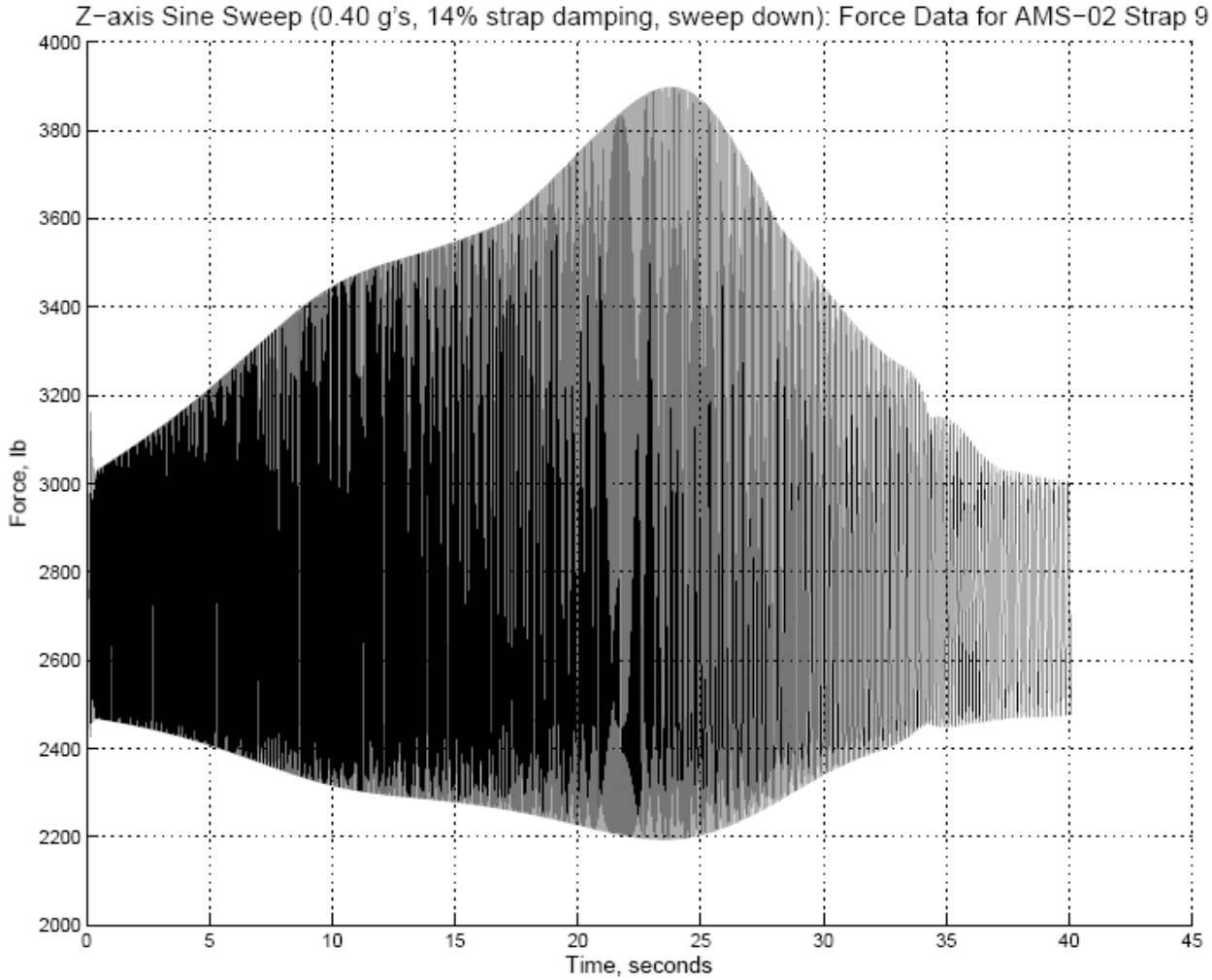

Figure 9-92 Strap 9 force response for z-axis configuration with 0.40 g sweep down

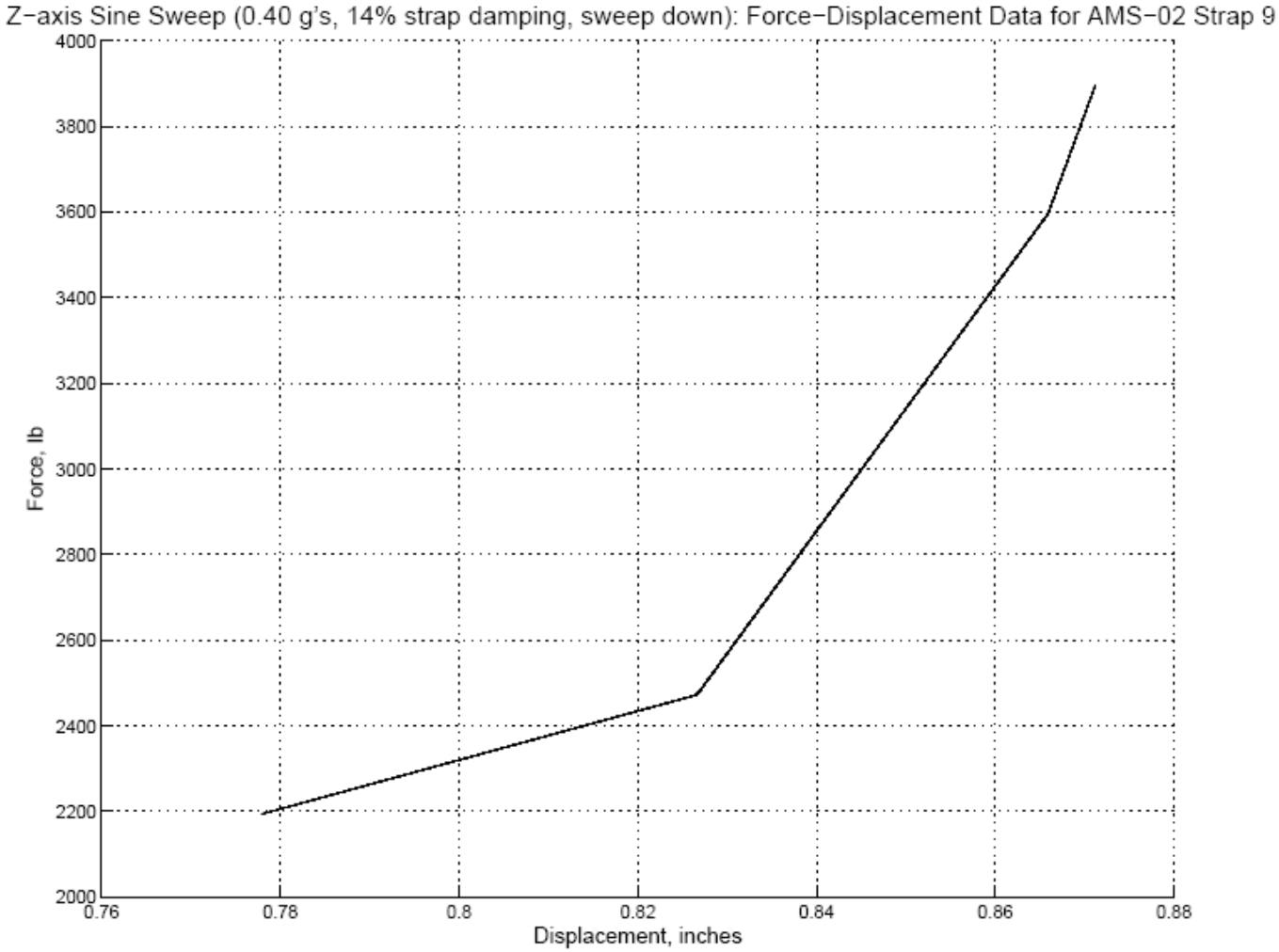

Figure 9-93 Strap 9 force-displacement curve for z-axis configuration with 0.40 g sweep down

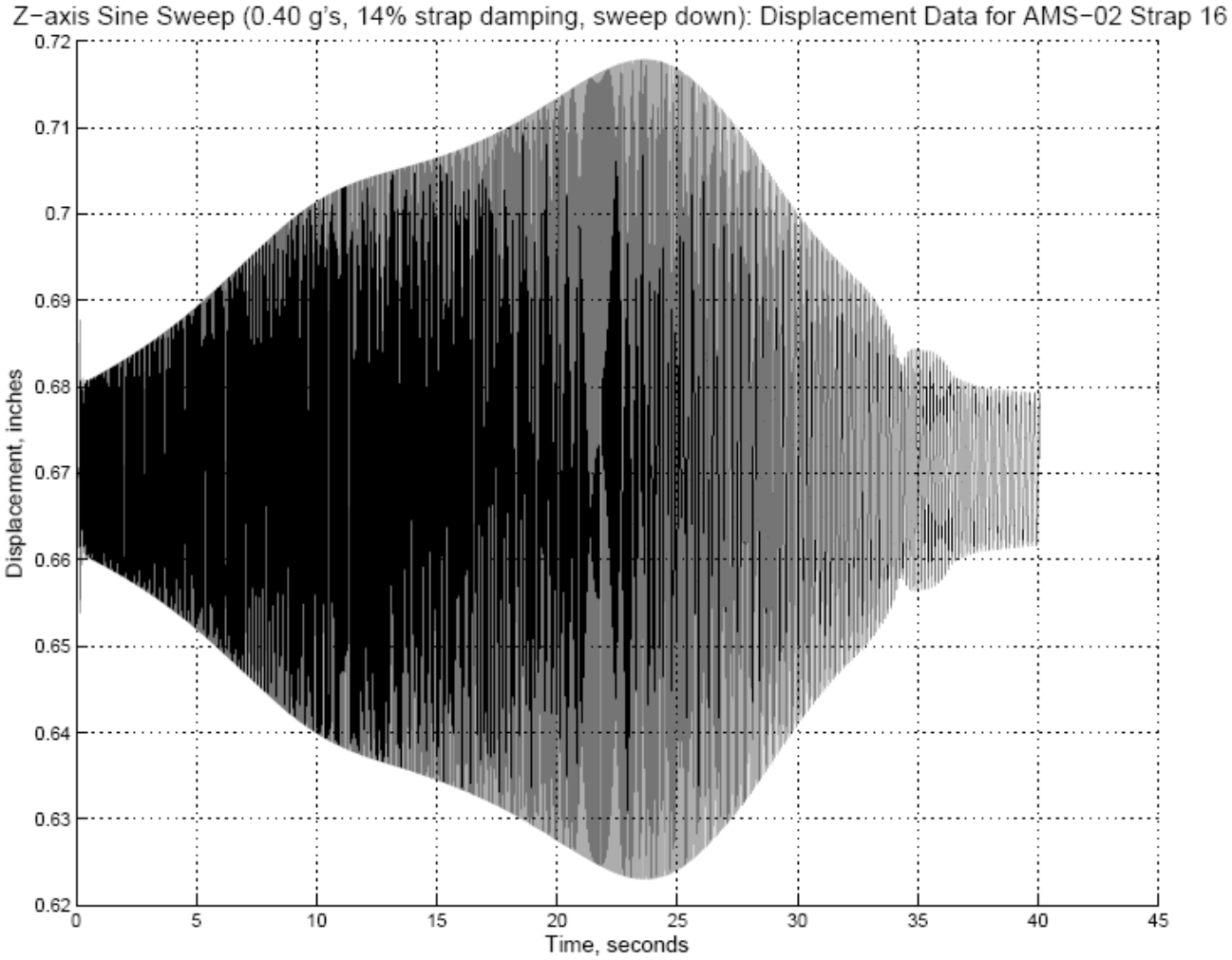

Figure 9-94 Strap 16 displacement response for z-axis configuration with 0.40 g sweep down

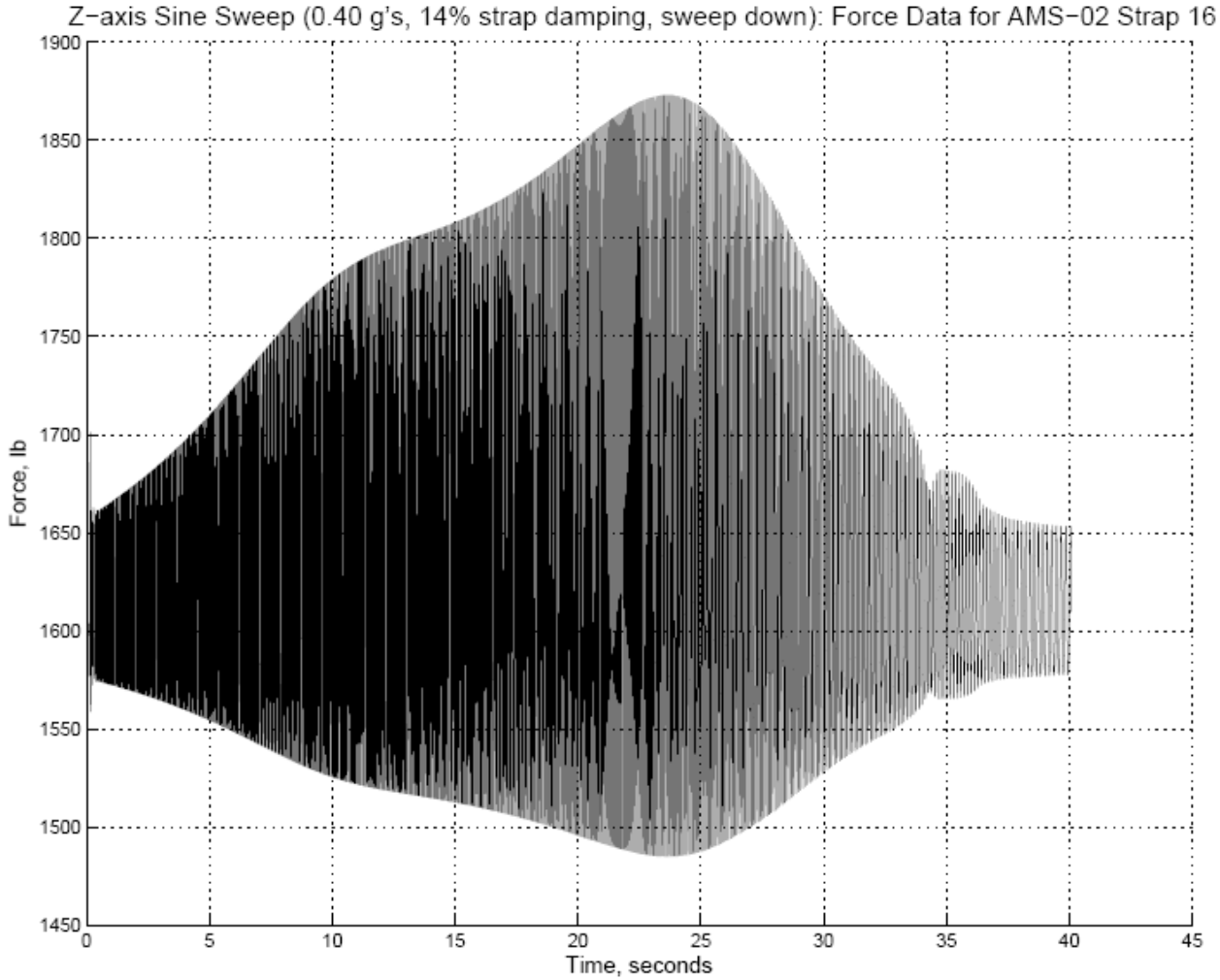

Figure 9-95 Strap 16 force response for z-axis configuration with 0.40 g sweep down

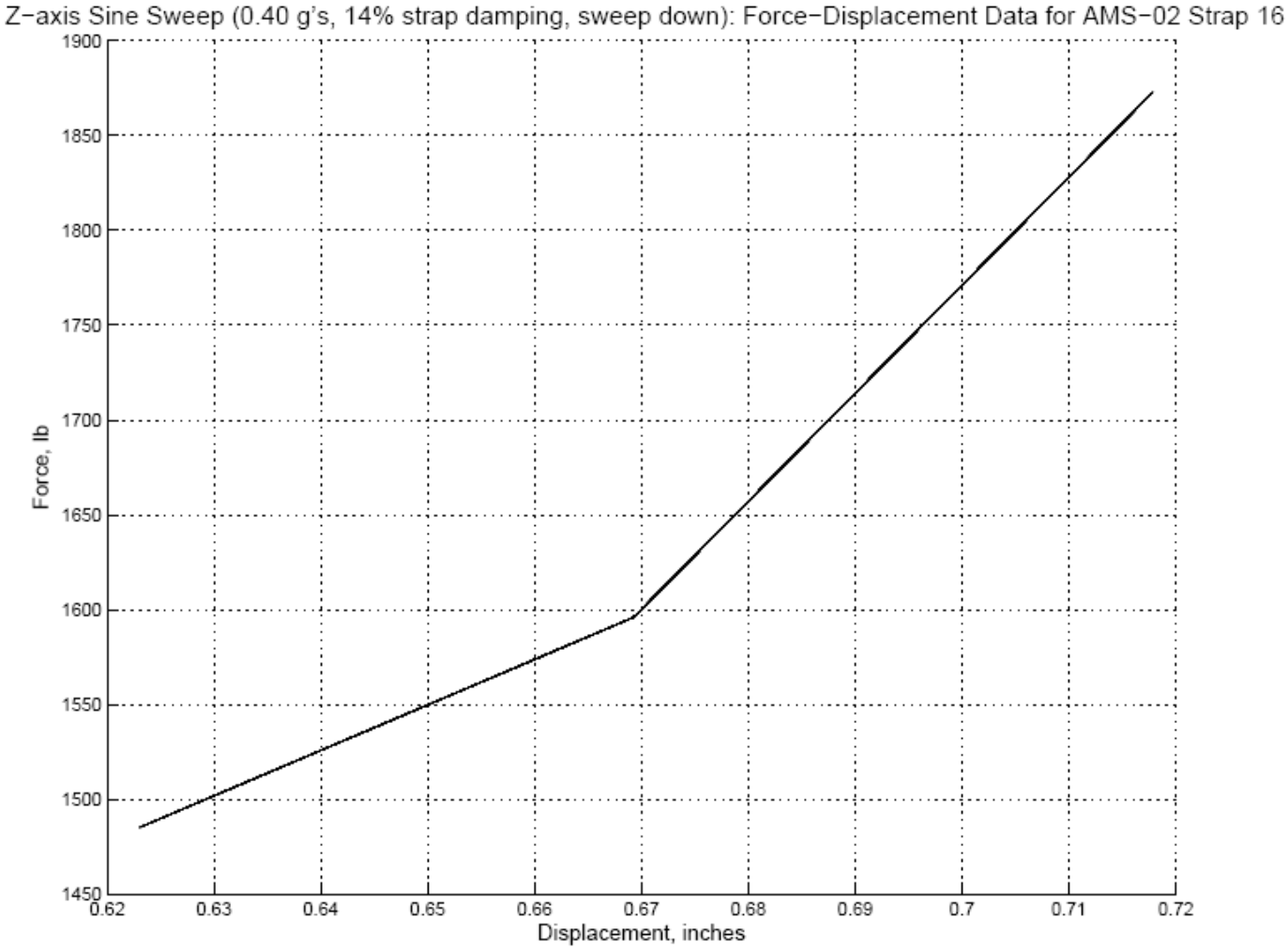

Figure 9-96 Strap 16 force-displacement curve for z-axis configuration with 0.40 g sweep down

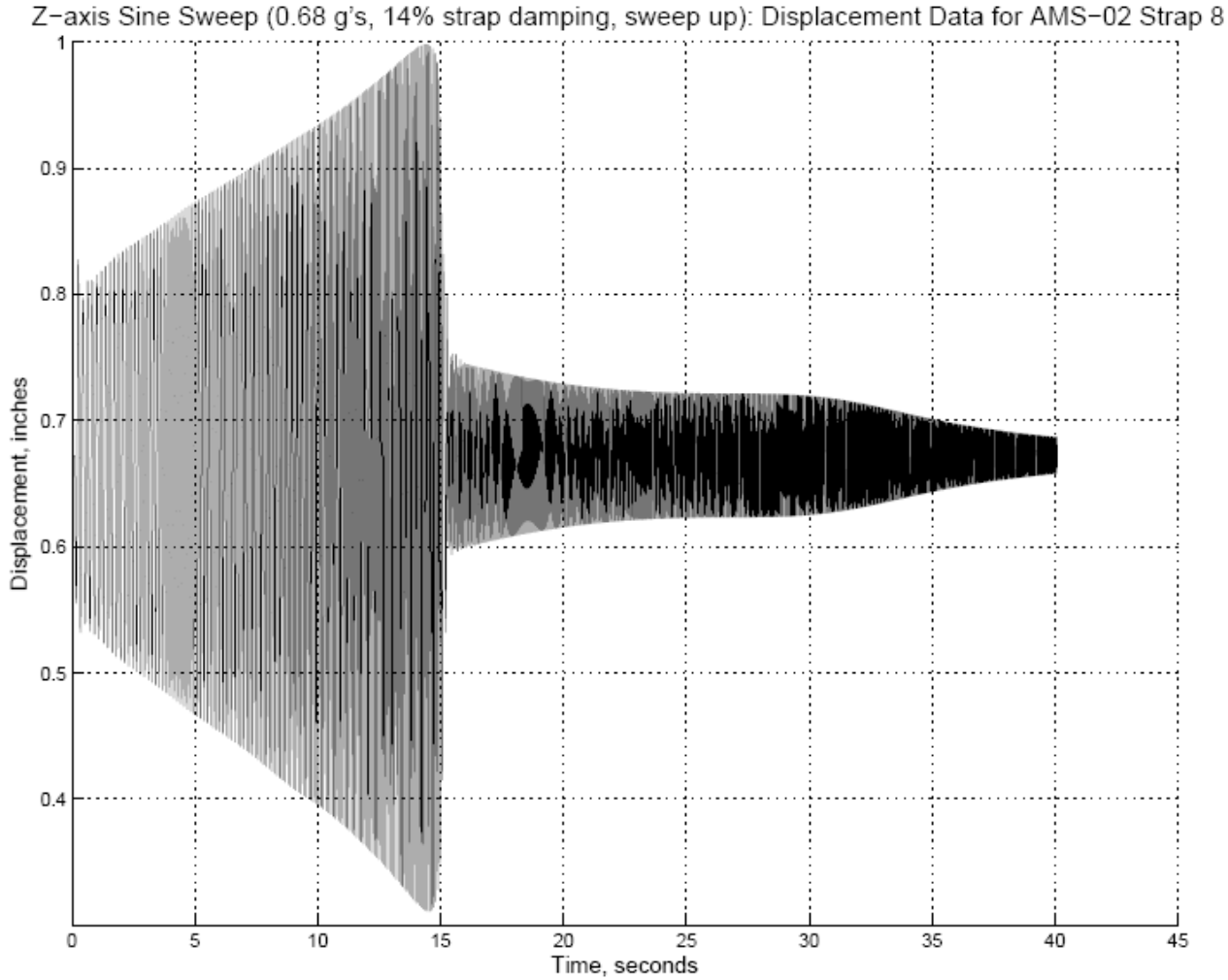

Figure 9-97 Strap 8 displacement response for z-axis configuration with 0.68 g sweep up

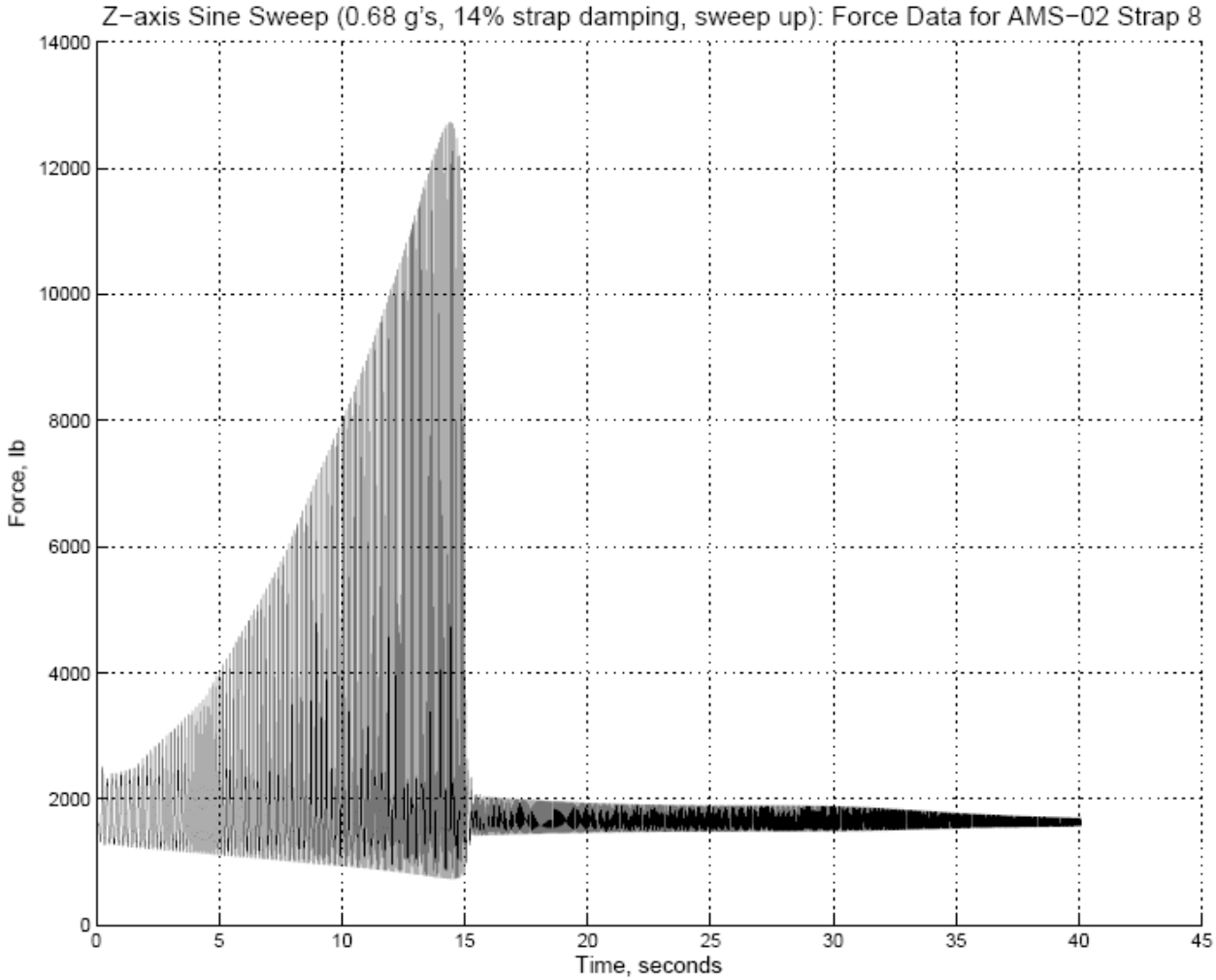

Figure 9-98 Strap 8 force response for z-axis configuration with 0.68 g sweep up

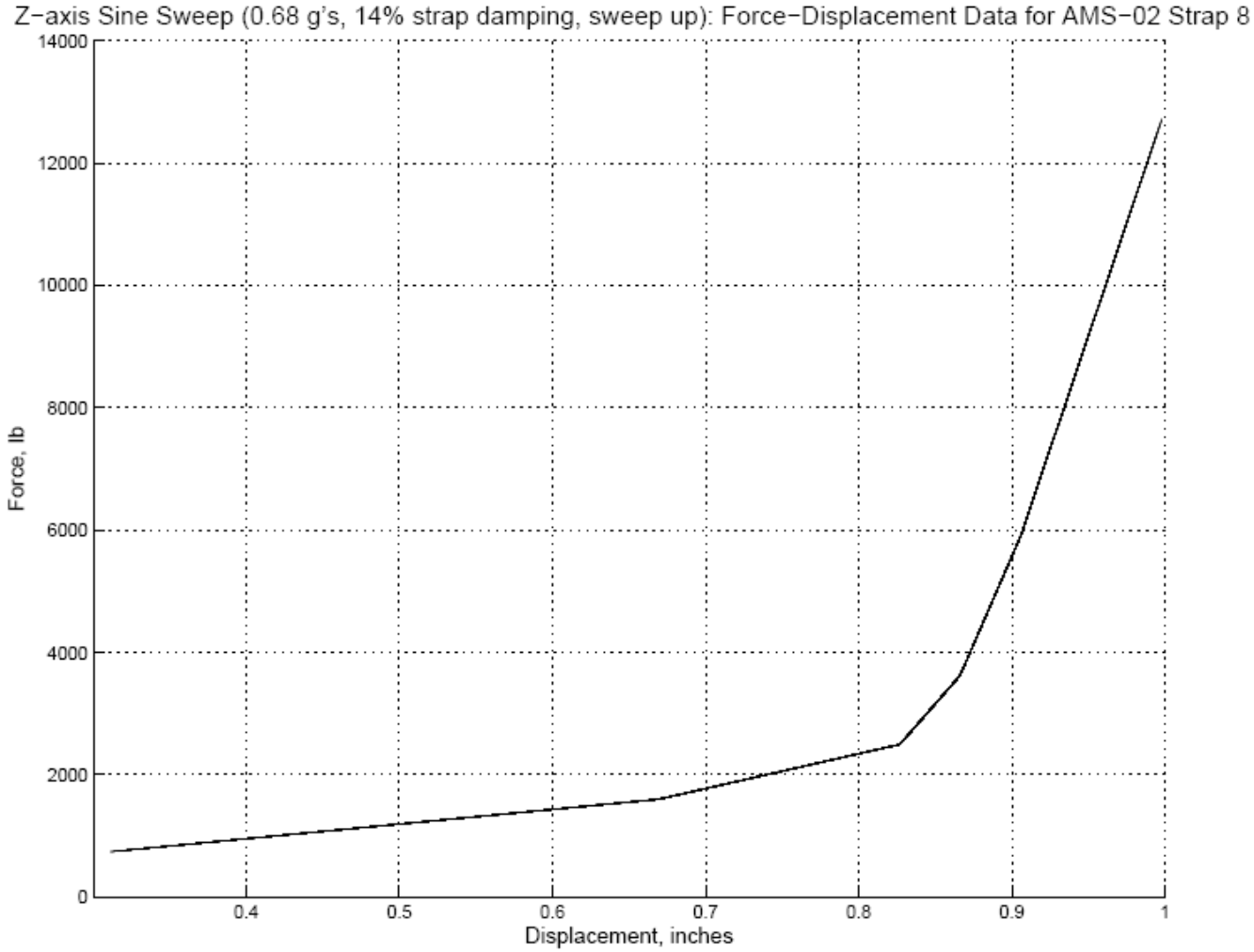

Figure 9-99 Strap 8 force-displacement curve for z-axis configuration with 0.68 g sweep up

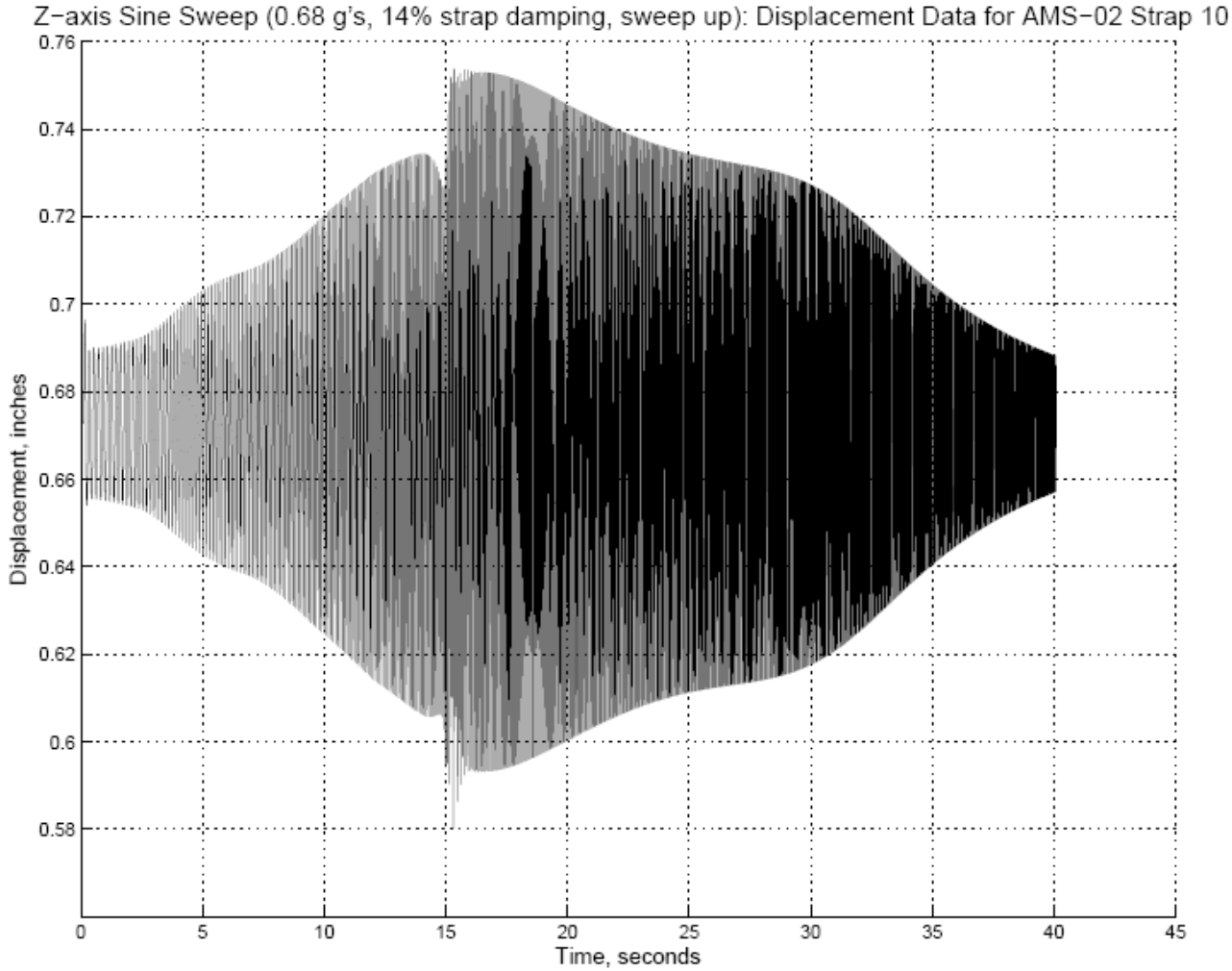

Figure 9-100 Strap 10 displacement response for z-axis configuration with 0.68 g sweep up

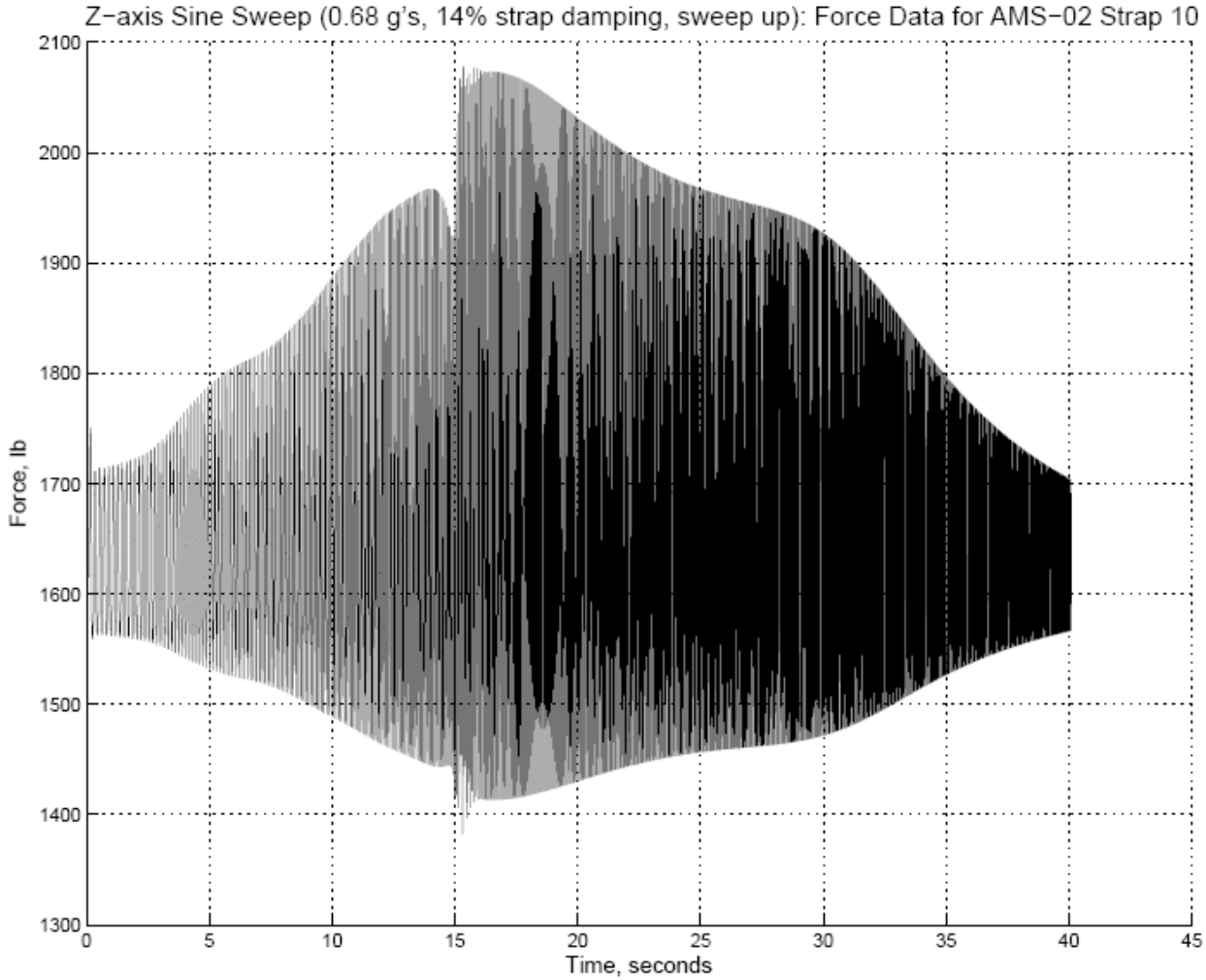

Figure 9-101 Strap 10 force response for z-axis configuration with 0.68 g sweep up

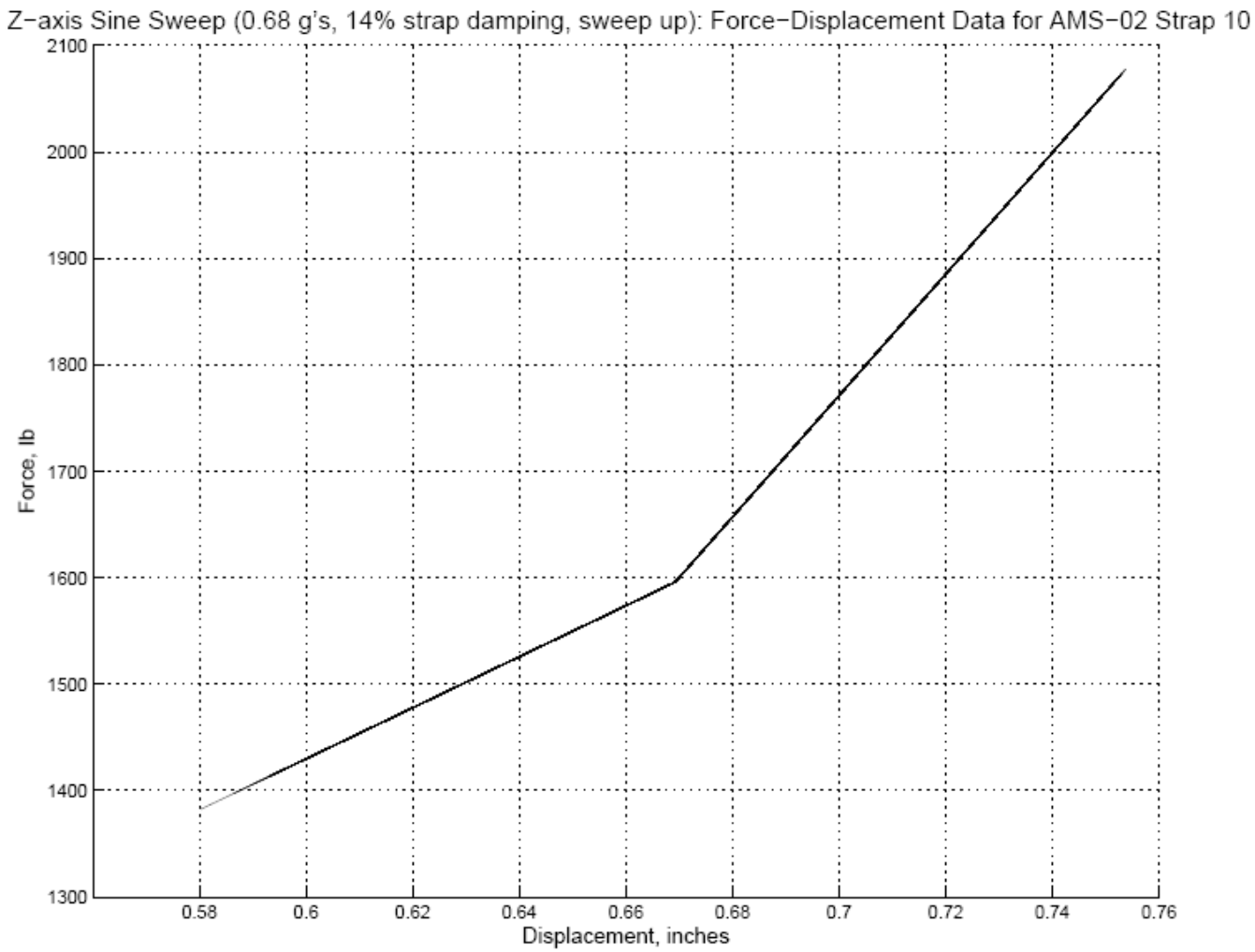

Figure 9-102 Strap 10 force-displacement curve for z-axis configuration with 0.68 g sweep up

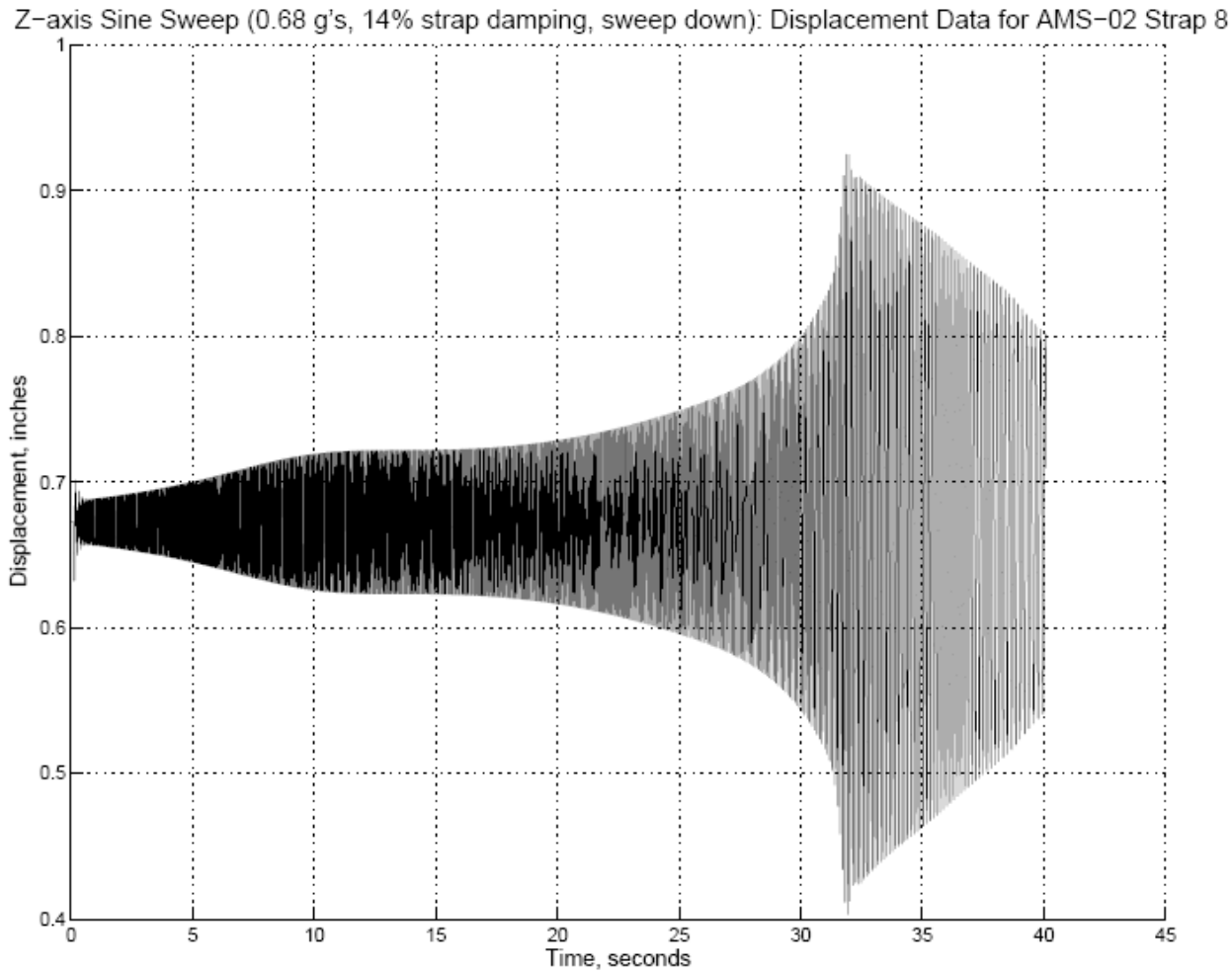

Figure 9-103 Strap 8 displacement response for z-axis configuration with 0.68 g sweep down

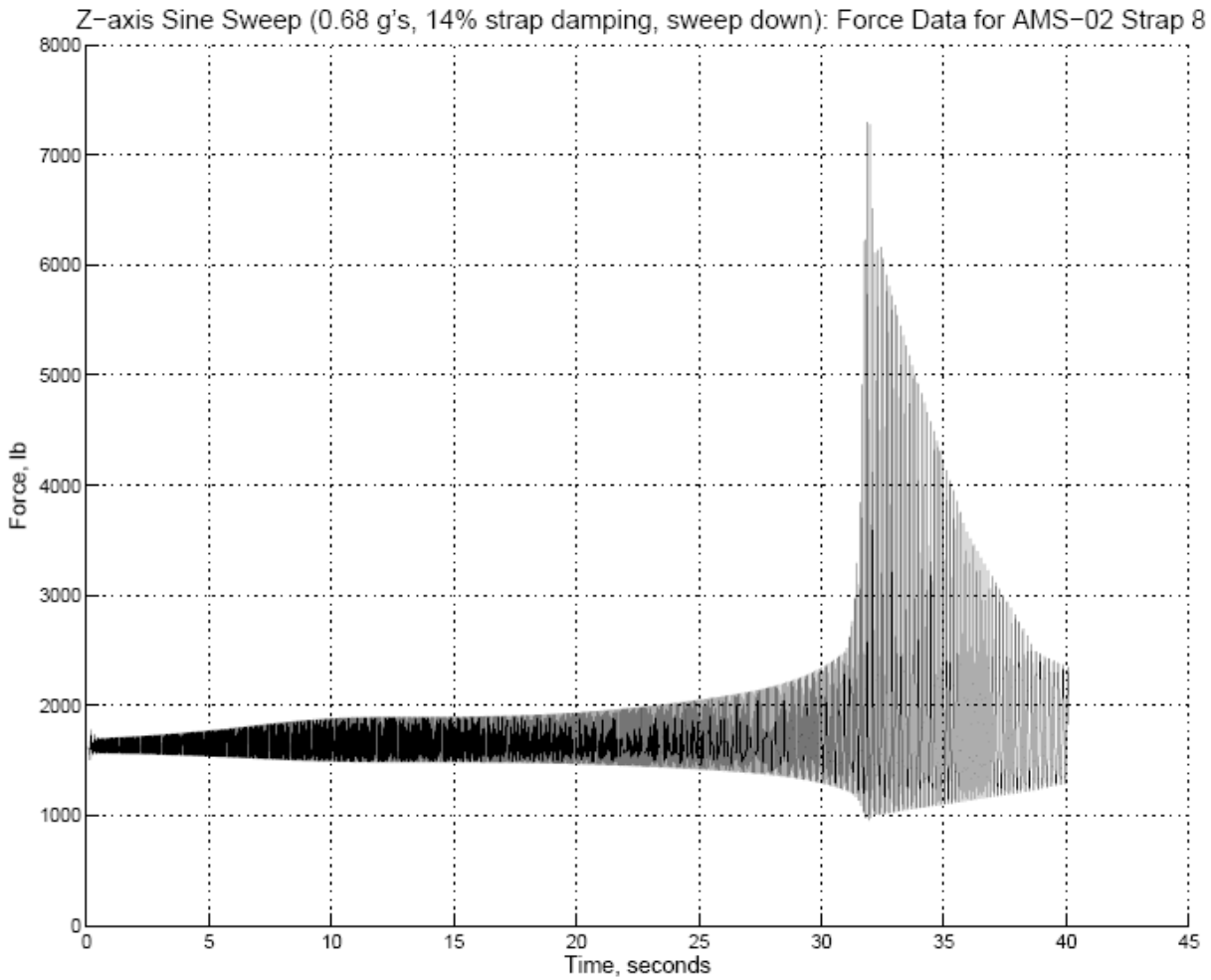

Figure 9-104 Strap 8 force response for z-axis configuration with 0.68 g sweep down

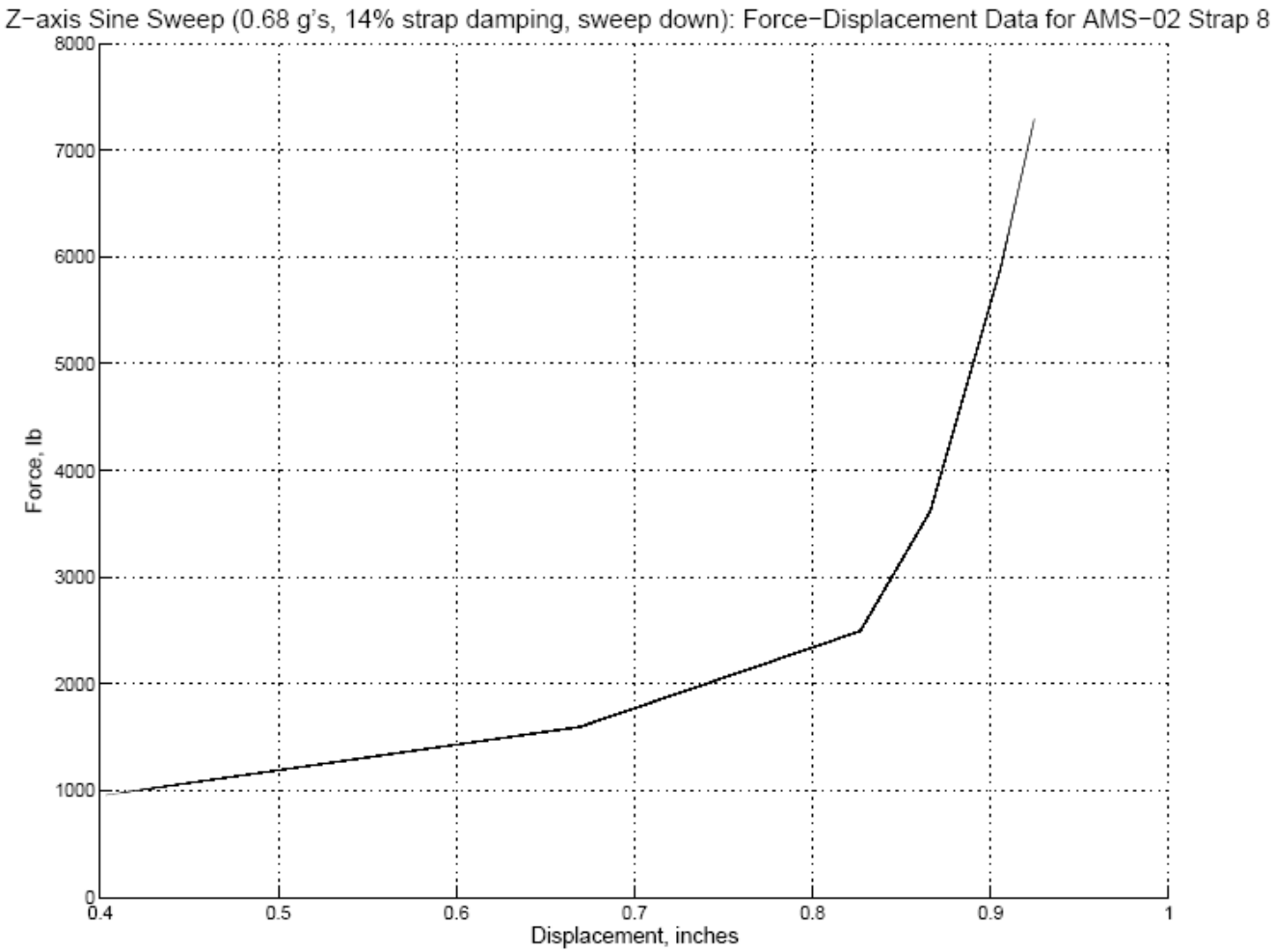

Figure 9-105 Strap 8 force-displacement curve for z-axis configuration with 0.68 g sweep down

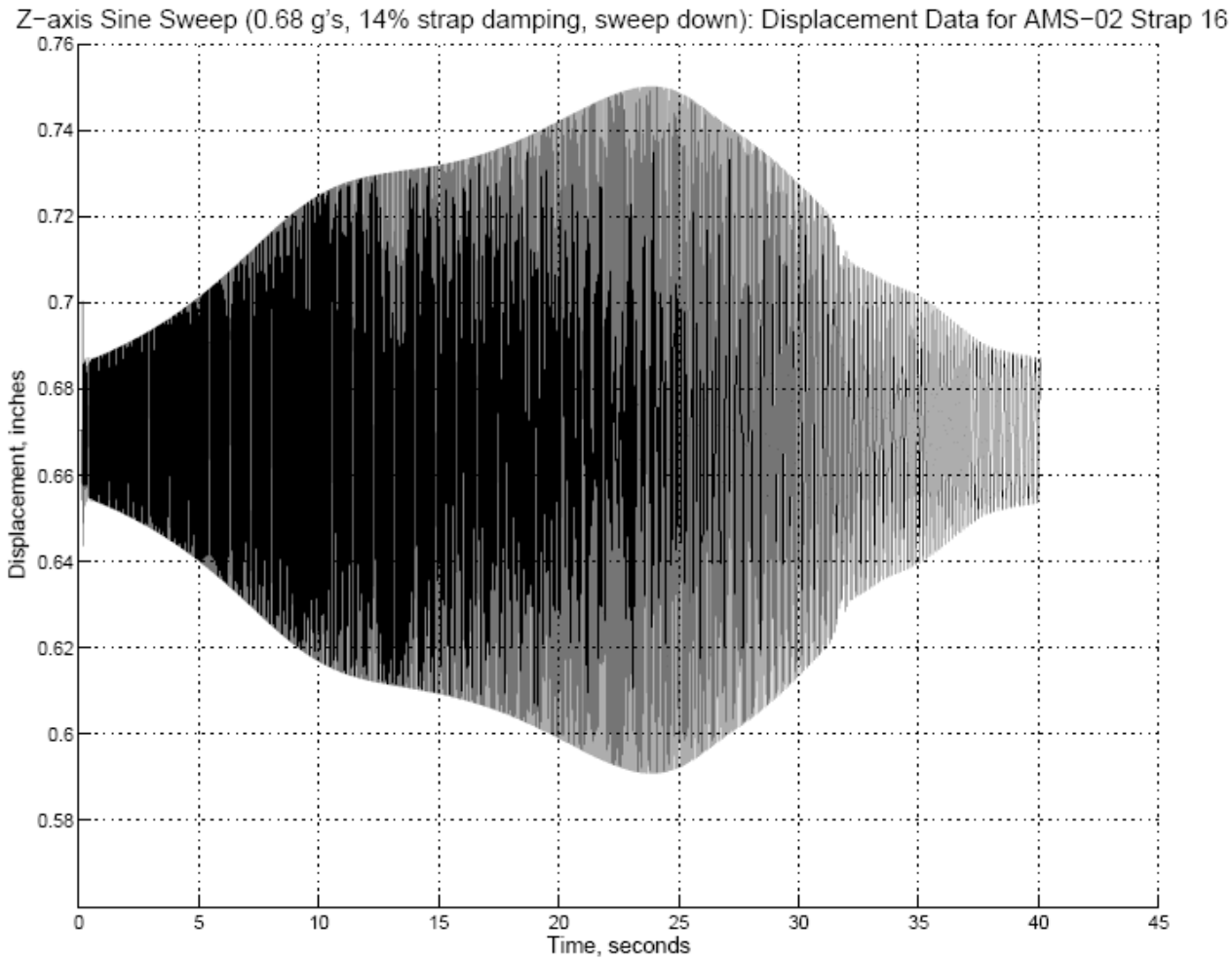

Figure 9-106 Strap 16 displacement response for z-axis configuration with 0.68 g sweep down

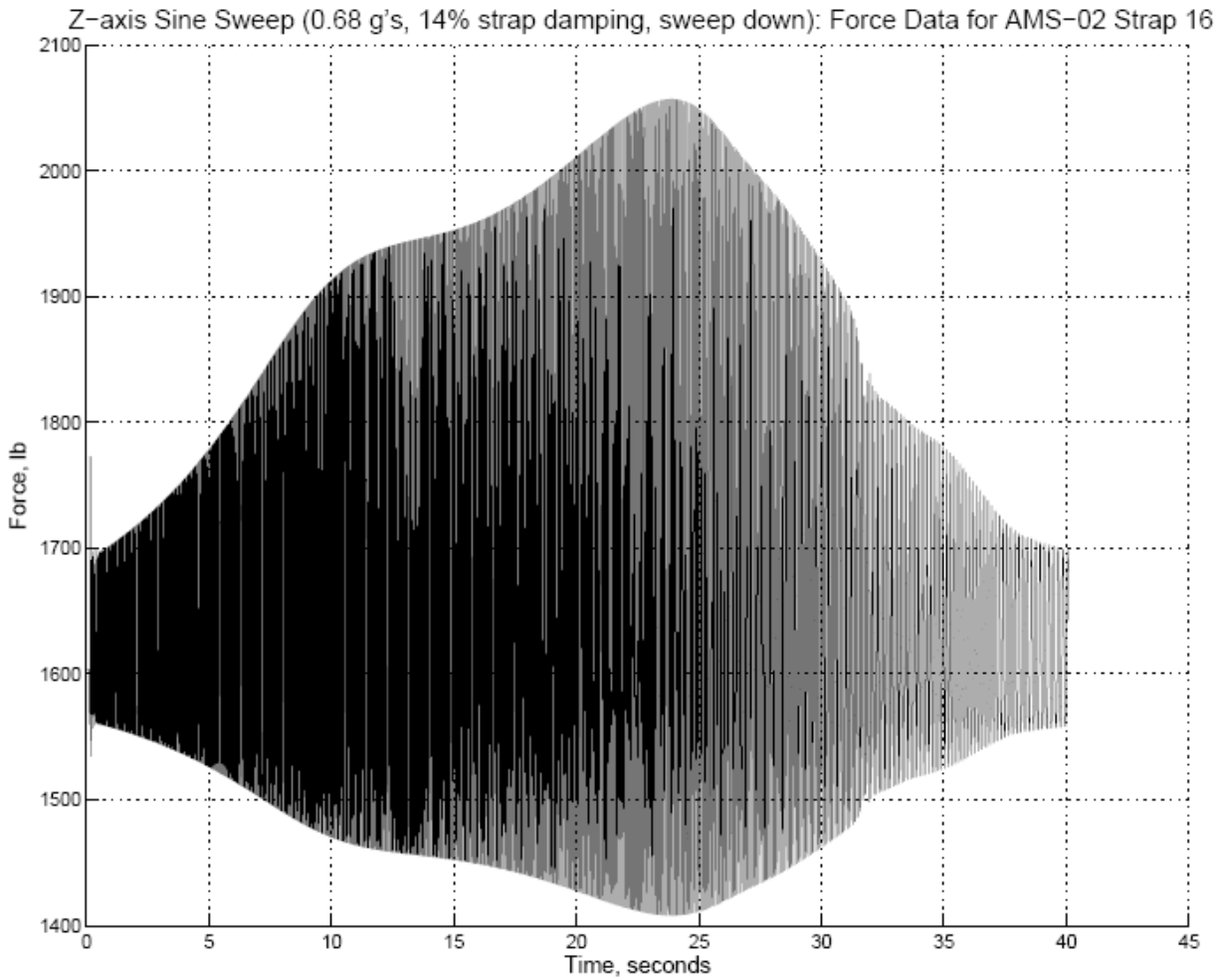

Figure 9-107 Strap 16 force response for z-axis configuration with 0.68 g sweep down

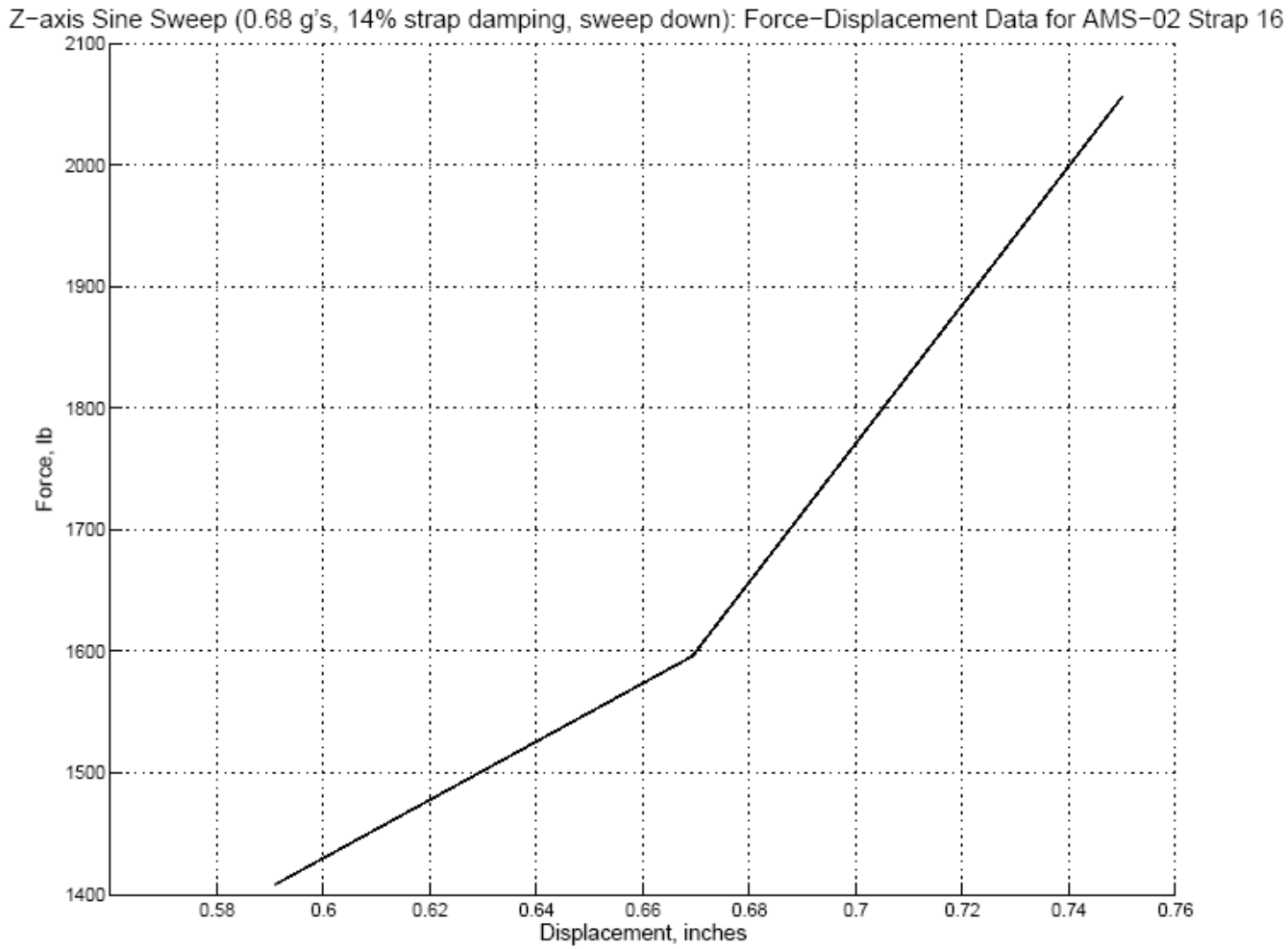

Figure 9-108 Strap force-displacement curve for z-axis configuration with 0.68 g sweep down

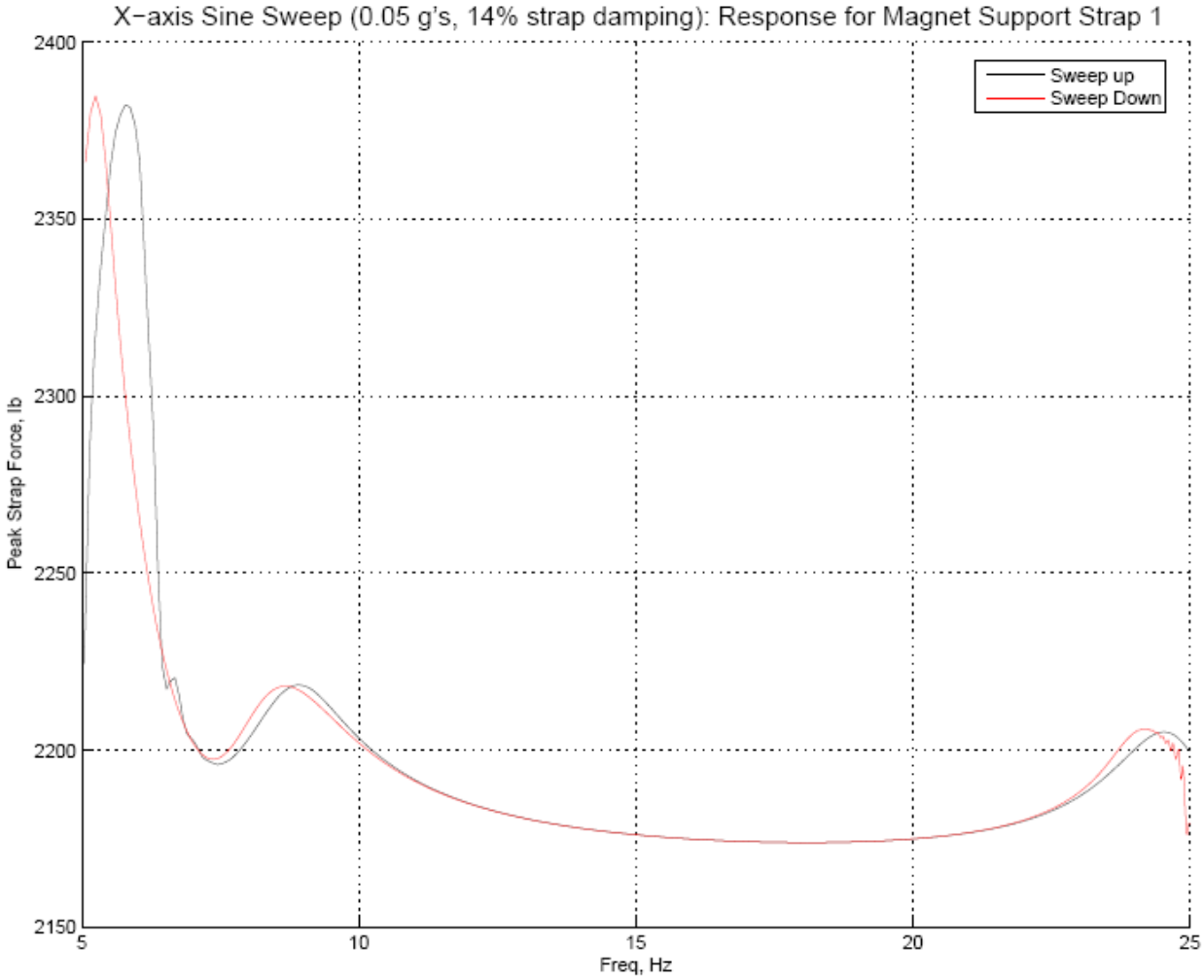

Figure 9-109 Strap 1 frequency response envelope for x-axis 0.05 g excitation

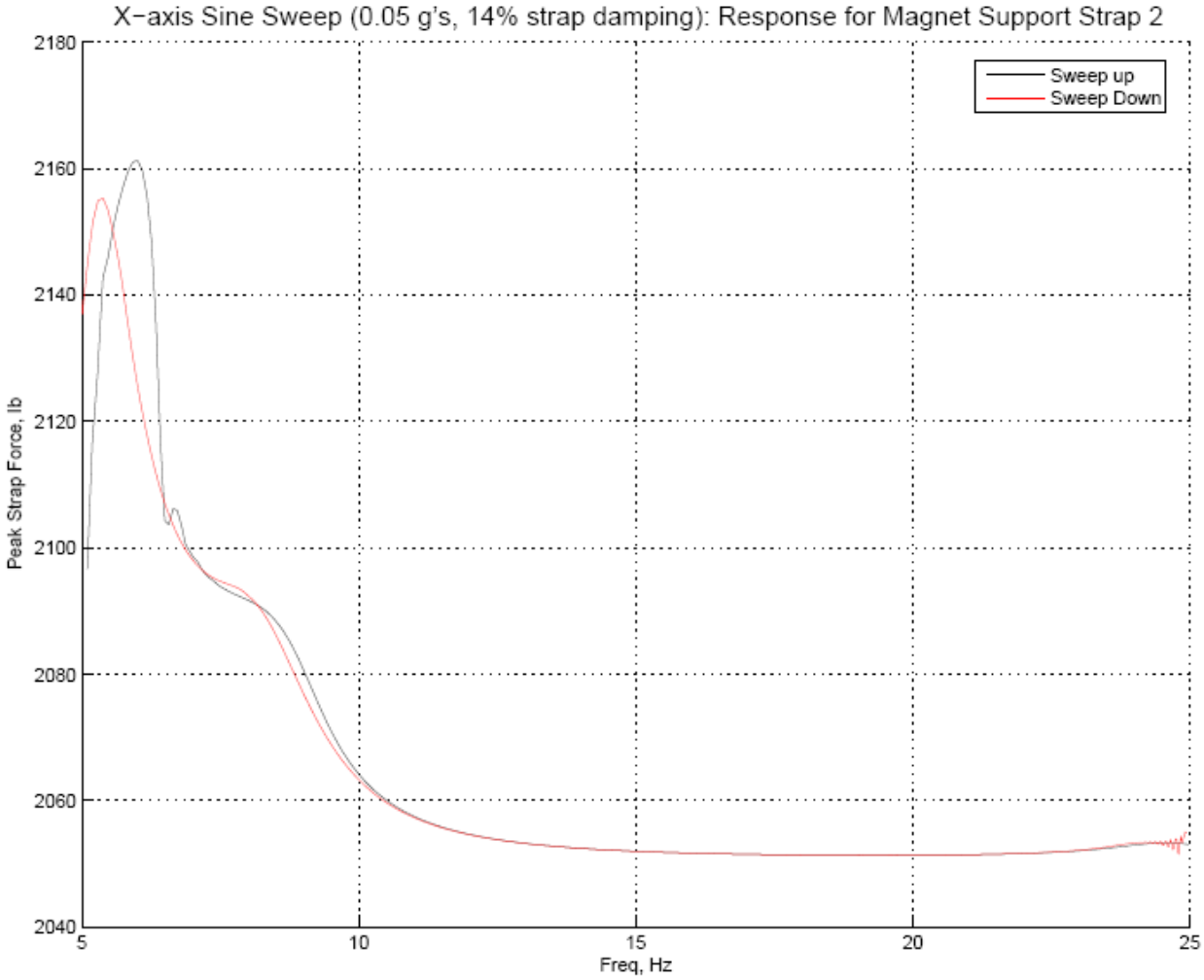

Figure 9-110 Strap 2 frequency response envelope for x-axis 0.05 g excitation

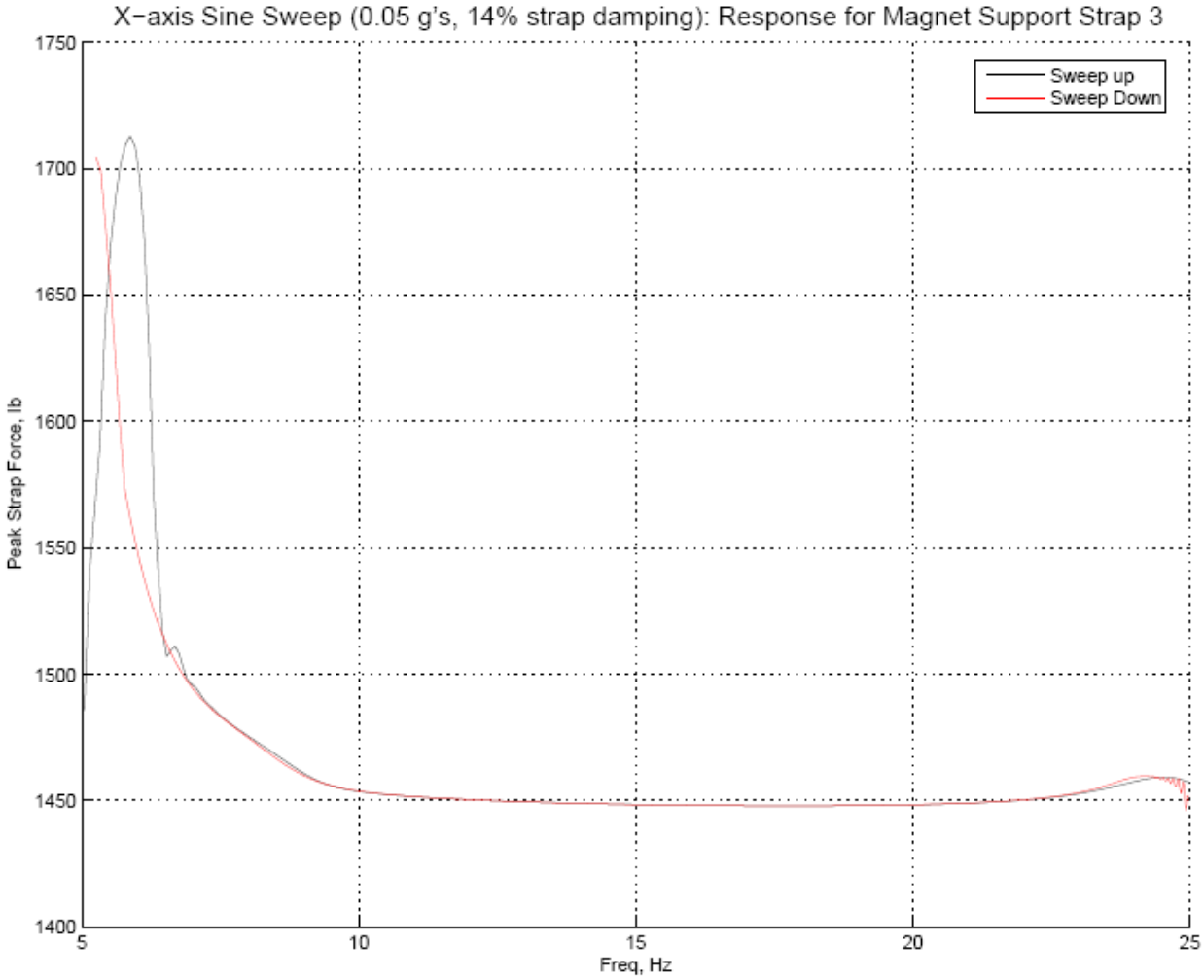

Figure 9-111 Strap 3 frequency response envelope for x-axis 0.05 g excitation

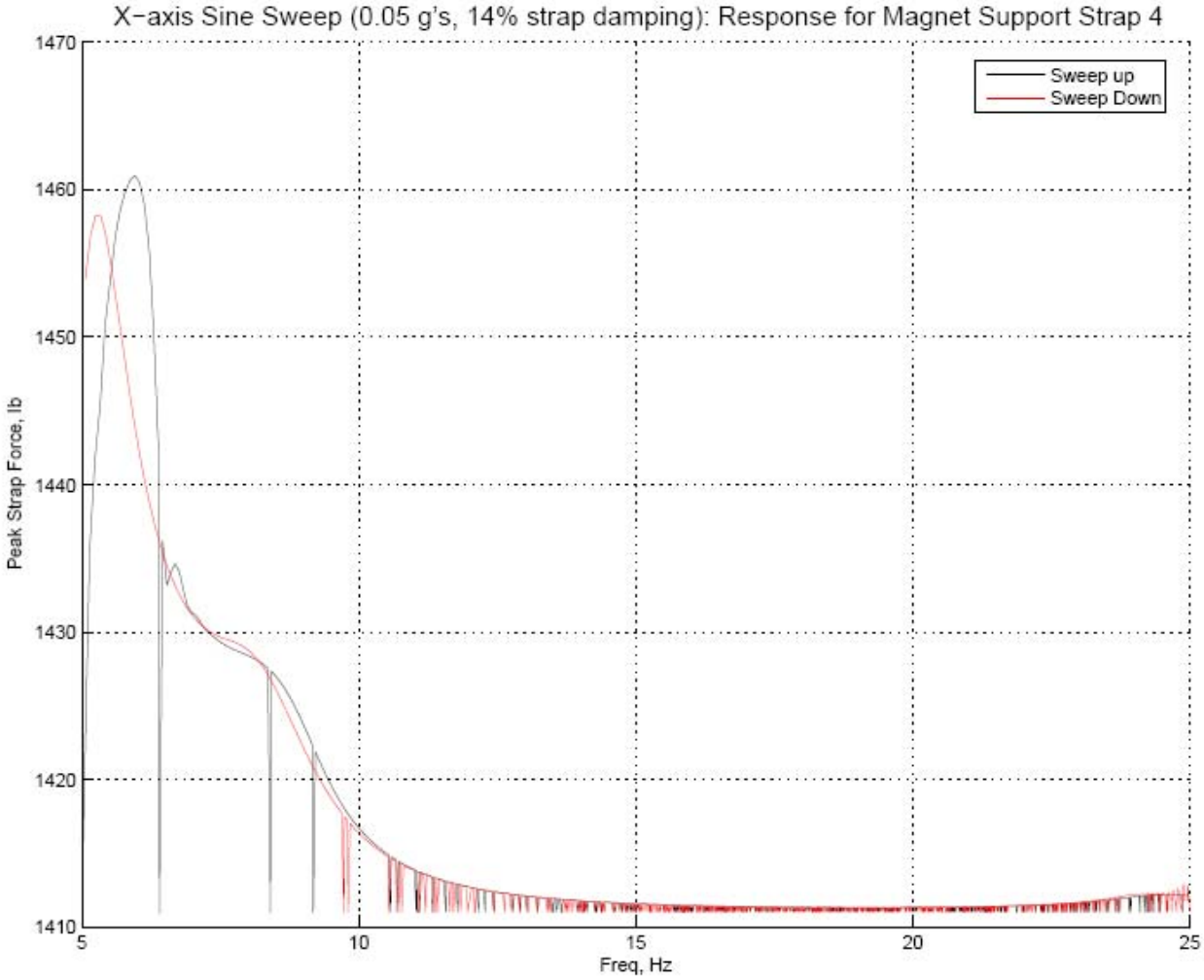

Figure 9-112 Strap 4 frequency response envelope for x-axis 0.05 g excitation

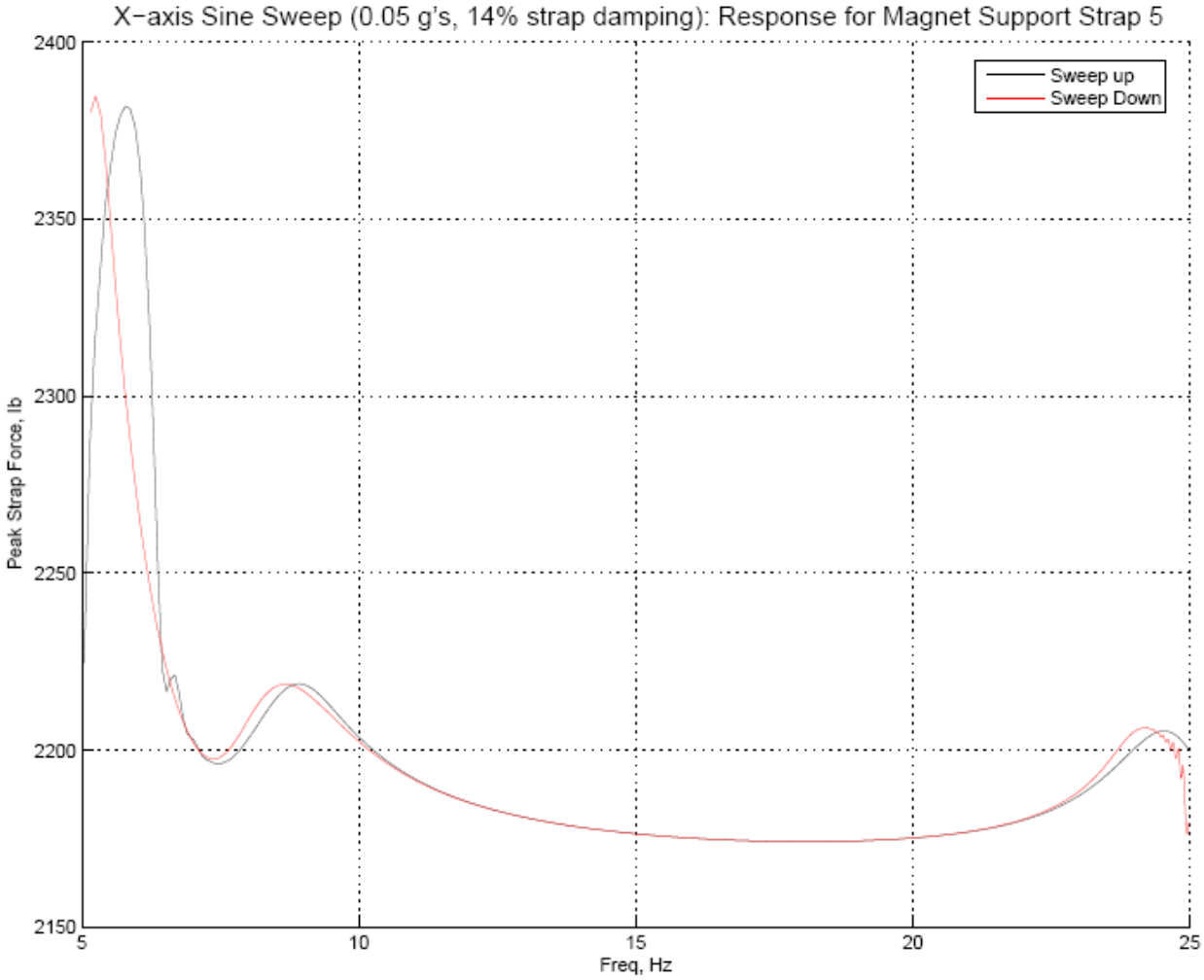

Figure 9-113 Strap 5 frequency response envelope for x-axis 0.05 g excitation

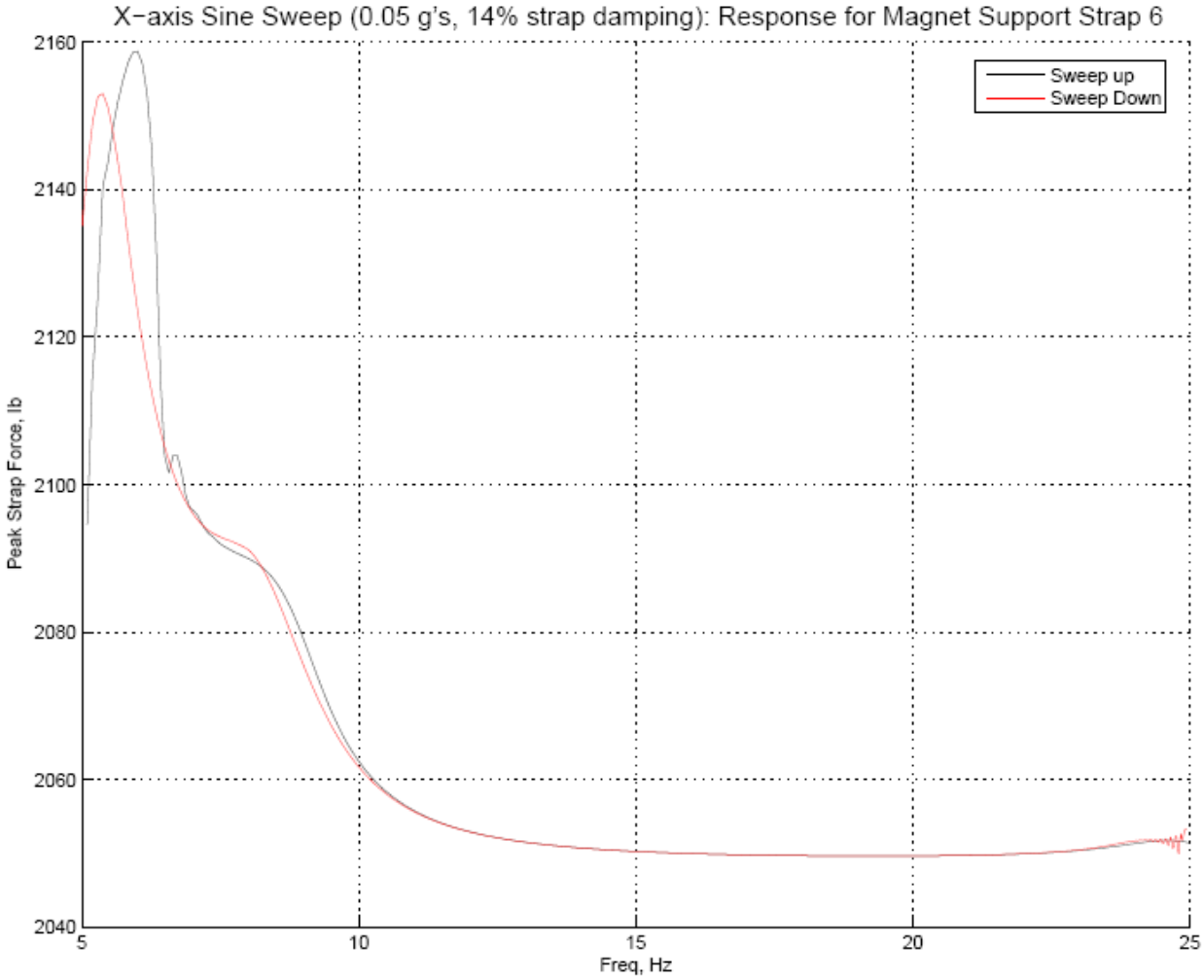

Figure 9-114 Strap 6 frequency response envelope for x-axis 0.05 g excitation

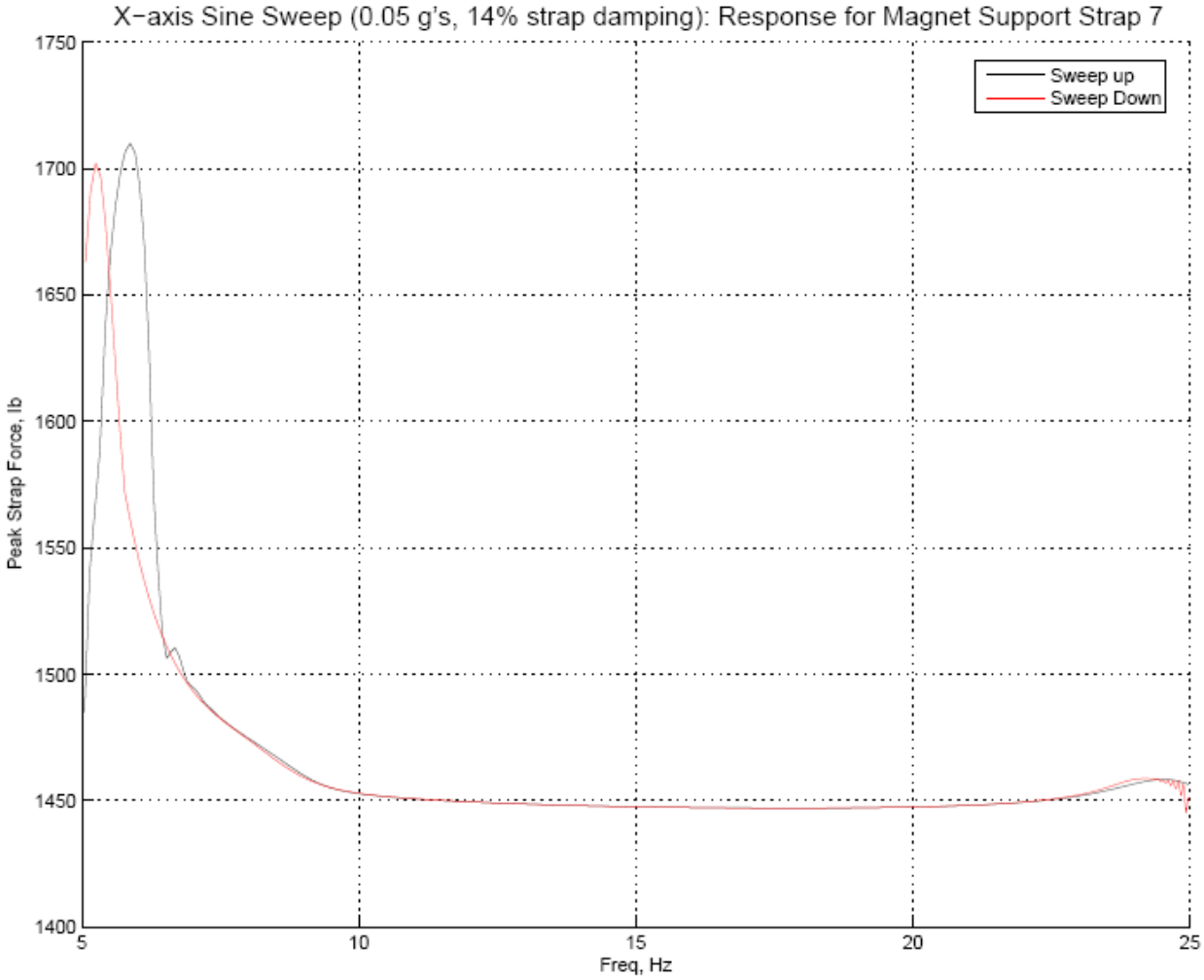

Figure 9-115 Strap 7 frequency response envelope for x-axis 0.05 g excitation

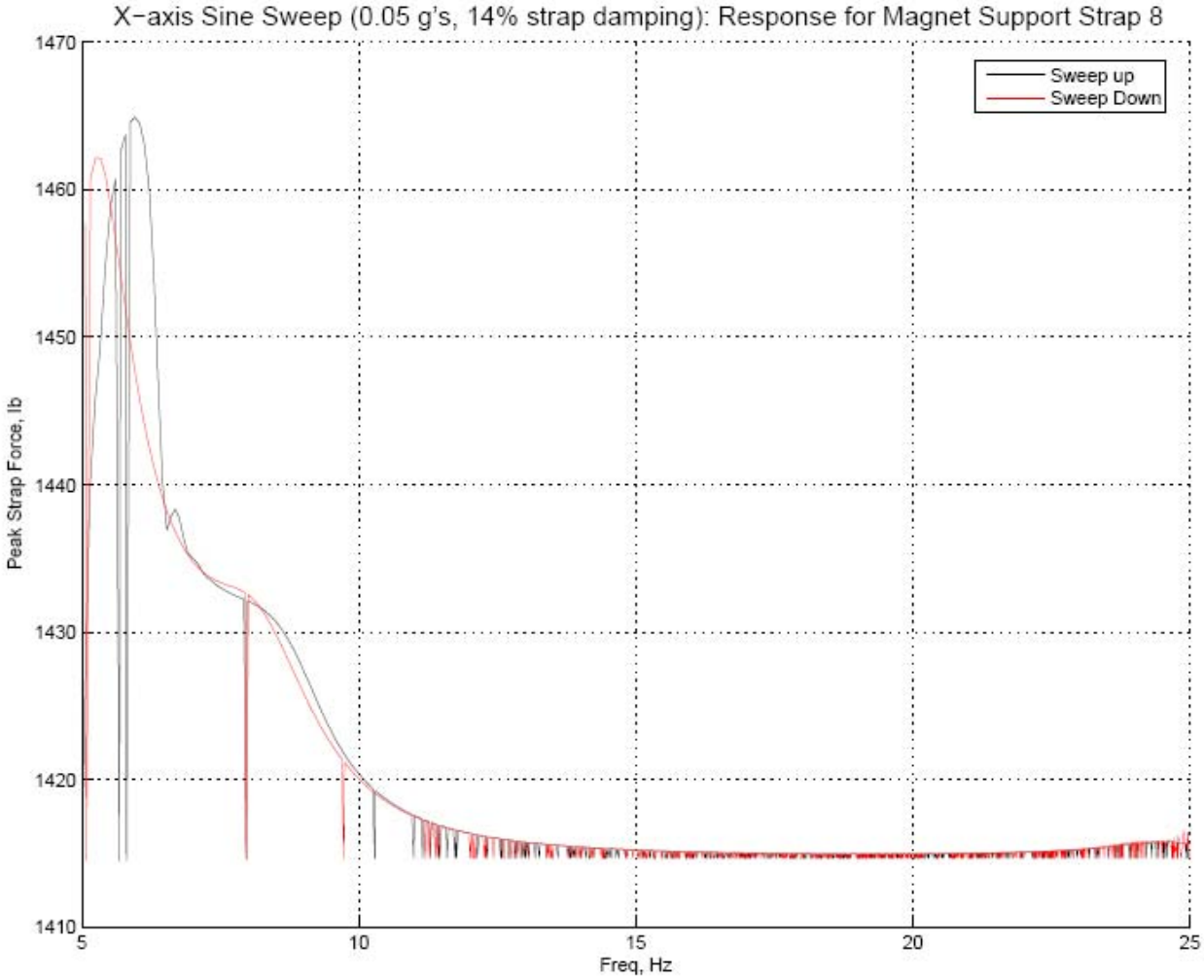

Figure 9-116 Strap 8 frequency response envelope for x-axis 0.05 g excitation

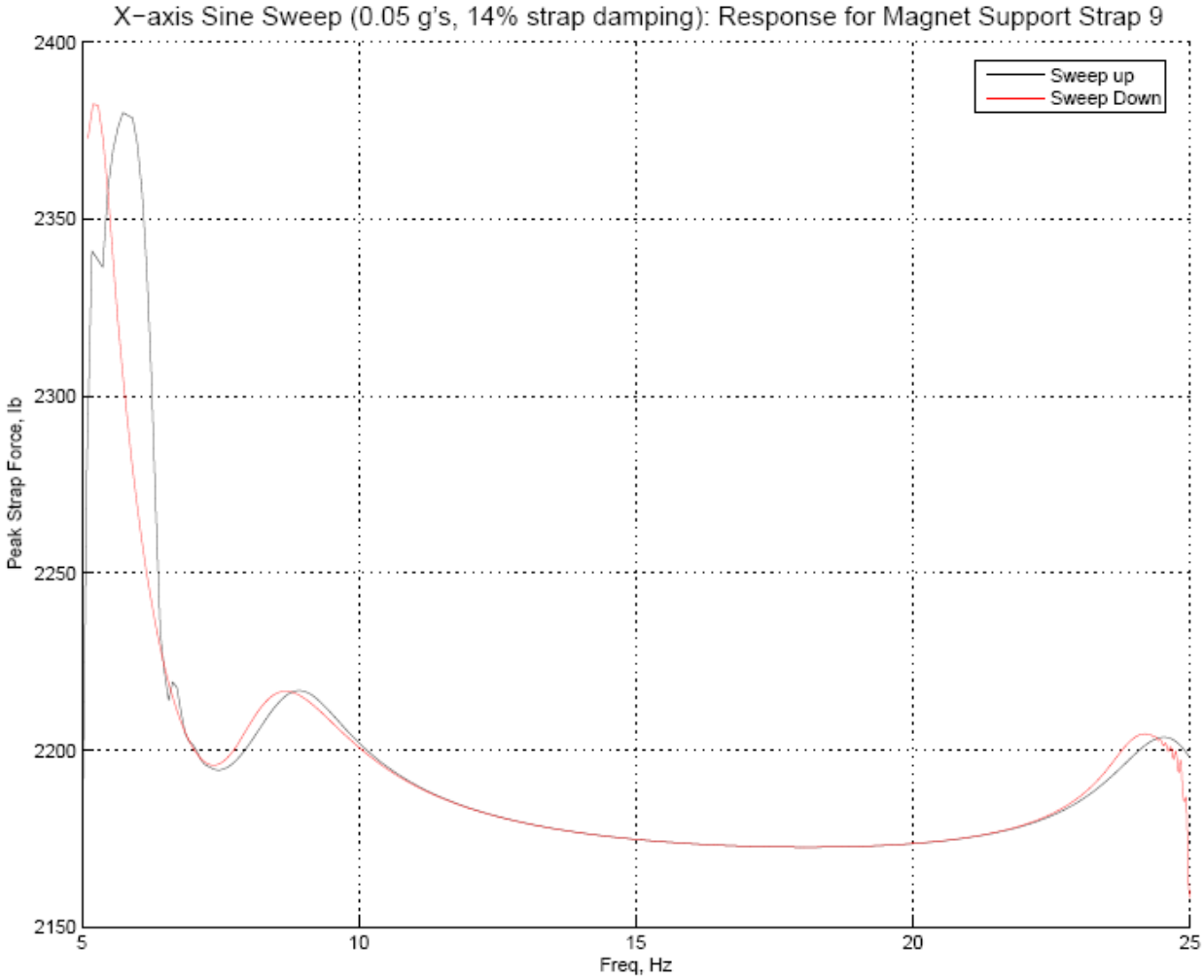

Figure 9-117 Strap 9 frequency response envelope for x-axis 0.05 g excitation